RADIO ECHO STUDIES OF POLAR GLACIER BEDS

by

Gordon Kenneth Andrew Oswald

A Dissertation submitted for the degree of Doctor of Philosophy at the University of Cambridge.

Clare Hall,

Cambridge.

29.May.1975

CONTENTS

PREFACE

The work on which this dissertation is based was carried out at the Scott Polar Research Institute, with the guidance of Dr.S.Evans as Supervisor, between October 1971 and May 1975.

All experimental work, reviews, discussion, and figures are, unless otherwise stated, the original work of the author. The thesis does not exceed 80,000 words, and has not been submitted for a degree at any other University.

Two periods of field work were carried out, the first during the Austral summer of 1971/72 as part of a series of radio echo surveys of the Antarctic ice cap, under the joint auspices of SPRI and the U.S. National Science Foundation. The second expedition took place during the summer of 1973, to Devon Island, where detailed investigations of the radio echo behaviour were performed.

I am indebted to the Natural Environment Research Council, which provided a maintenance grant covering the first three years of this research, and to the Director of SPRI, Dr.G.deQ.Robin, for financial support during the fourth year, as well as for use of the facilities of the Institute.

Introduction.

This thesis is an attempt to bridge the gap existing between the theory and practice of radio echo sounding of glaciers, in connection with the interpretation of the observed behaviour of echoes from the base of the ice.

The theory of reflections of electromagnetic waves from rough surfaces has been dealt with, in this specific connection, by C.H.Harrison(1972), and M.V.Berry (1973), and we shall draw heavily on their results.

Our intention is, however, in the light of experimental analysis of echoes, to distil from their general mathematical discussions a more physical understanding of the processes from which the echo behaviour results. We hope in this way to describe the echo in situations where the overlapping of different physical regimes makes rigorous mathematical analysis difficult, and to form a link between analytical results for limiting cases, and numerical solutions for intermediate cases. For the latter, we shall make extensive use of the results of E.N.Bramley and M.Young (1967).

It is possible to deduce some characteristics of the lower boundary of the ice with only qualitative information concerning the form and behaviour of the received echoes. Several conclusions have been drawn concerning the state of the base of the East Antarctic ice sheet, without benefit of quantitative records of the echo. These are the most important geophysical results obtained in the course of this work. However, very much more information is available, with appropriate adaptations of the basic echo sounding apparatus.

The uses of this information are to be found in academic geophysics, prospecting, climatology, paleo-climatology, and

predictive speculation. It is extremely expensive to obtain, and we hope to provide a manageable analysis, applicable to real field situations, and requiring a minimum of technological sophistication.

CHAPTER 1 The State of the Art: a review of existing techniques for sub-glacial investigations

(1.1) Introduction

The penetration of radio waves through a polar ice sheet, and their reflection from its lower boundary, was first postulated by W. R. Piggott, as the cause of a regular interference observed in the course of radar studies of the ionosphere, being carried out at the Royal Society Base, Halley Bay. (Evans, 1966)

It was quickly demonstrated that radio-frequency electro-magnetic waves could penetrate great thicknesses of ice. Since then, the technique of radio echo sounding has been used in many cold regions, to measure the depth of ice sheets, and to investigate the large-scale features of the sub-ice surface. The records of expeditions to both polar regions, and to many mountain glaciers have revealed ice up to more than four thousand metres in thickness, covering mountains, trenches, plateaux and plains. Ice shelves, where the ice floats on water, have been distinguished, and crevassing, ice rises, and ice streams are delineated. (Evans, Gudmansen, Swithinbank, Hattersley-Smith and Robin, (1969), Evans and Smith, (1970), Robin, Swithinbank and Smith, (1970), Evans and Robin, (1972), and others).

Attention was concentrated, in these studies, on the accuracy with which the time delay of the echo could be used to indicate the depth of the ice.

However, the reflections are not without an internal structure, and some aspects of their behaviour are of interest, independently of their application to depth measurement.

The structure depends on the inter-action of the waves with the reflecting surface. The form of the echo is capable of throwing light both on the composition of the sub-glacial material, and on the small-scale form of the interface.

The present work deals with this capability, and with the adaptation of present methods of extracting such information. The basic equipment has been described in detail by Evans and Smith (1969), and the interpretation of the results has been discussed by Robin, Evans and Bailey (1969), Harrison (1971) and others.

The theoretical treatment of reflections from rough surfaces has roots both in work relating specifically to radar, (Beckmann and Spizzichino (1963)), and to the study of the ionosphere (Booker, Ratcliffe and Shinn (1950), Bramley and Young (1967)). Further work relating to ice depth sounding has been done by Harrison (1972) and Berry (1973). Their aim has been to provide a general theory, covering all foreseeable experimental situations, and as wide as possible a range of reflecting surfaces.

We shall use our experience in the field to narrow down the range of theoretical discussion, and to develop further the argument in relevant directions. We hope to provide an algorithm whereby the observed characteristics of the echoes may be translated into statistical or particular characteristics of the reflecting interface. We believe that such information will be of value in discussions both of the past and present form of the ice sheet, and of the geological make-up of the bedrock.

The remainder of this chapter will be devoted to a review of the existing techniques by which observations of sub-glacial conditions may be made. We shall examine their applicability to the investigation of the surface forming the lower boundary of the ice.

(1.2) Existing techniques

The direct examination of the material in and below the ice, by means of bore-holes, cannot be seriously considered, except in the role of providing 'ground truth' by which other observations may be checked. The cost, the slowness of the procedure, and the spot nature of results rule out the method for coverage of significant areas. We must therefore turn to indirect measurements.

The interface may be described separately in terms of the bulk properties of the over- and under-lying materials, and in terms of the geometrical form of the surface. In general, the two are dealt with by different kinds of technique.

The bulk properties with which we may be concerned comprise; density, magnetic permeability, elasticity and electrical properties (permittivity and conductivity) of the ice and rock.

(1.2.1) Gravity measurements

A gravimeter measures relative values of the acceleration due to gravity, from the extension of a spring supporting a fixed mass. The local value of g is determined primarily by the altitude of the point of observation, and secondarily by the

local density distribution of the underlying rocks. The rock densities may be inferred by virtue of assumptions involving horizontal uniformity, and the existence of a finite number, of discrete strata.

In the case of a thick ice sheet, we know that the ice-rock interface is the closest material boundary to the observer, and that it involves a comparatively large density contrast (the density of ice being about 910 kg/m^3, whereas that for upper-crustal rocks averages about 2700 kg/m^3. Using the knowledge of surface elevation and ice thickness rendered by radio echo sounding and other sources, we may obtain, in areas of steady ice depth, a mean value for the density of the upper crust, weighted according to the relative proximity of the different layers.

Single observations of this type cannot resolve the strata, however, and cannot indicate the presence of comparatively thin layers overlying the basement. As an illustration, we consider the case of a layer, 500 metres thick, of sedimentary rock of density 2400 kg/m^3, overlying basement rocks of density 2900 kg/m^3. We assume that the slab is infinite in extent.

The associated gravity anomaly is calculated from the formula:

$$\Delta g = 2\pi\gamma\rho' H$$

where γ, the universal constant of gravitation, is equal to $6.7 \times 10^{-11} m^3 kg^{-1} sec^{-2}$

ρ' is the density contrast between the local rock and the average crustal density at the same elevation. In our case, the local density being 2400 kg/m^3, and the average being

2700 kg/m^3, ρ' = 300 kg/m^3.

H is the extent in depth of the upper layer, and here equals 500 metres.

Thus Δg = 6 x 10^{-5}m/sec^2, or 6 mgal.

The most accurate gravity stations in Antarctica are characterised by errors of ± 3-5 mgal (Grushinsky, 1970); on the ice sheet, uncertainties in the surface elevation and ice thickness may add errors of about ± 10 mgal. These figures are calculated by adaptation of Bentley's (1964) estimates, using updated estimates of the above uncertainties from Drewry's (1973) work on radio echo results.

Such a layer as that mentioned above would be at the limit of resolution of the gravimetric method. However, a systematic survey, consisting of close-spaced points, might shed light on the broad make-up of the sub-ice crust (Grushinsky and Lazarev, 1970).

(1.2.2.) Seismic dispersion studies

The velocity of propagation of seismic waves in a layer of finite depth is a function, not only of the elastic properties and density of the layer, but also of its thickness, and of the frequency of the wave. Though the latter effects are negligible for waves of length much smaller than the layer thickness, for the long period waves set up by earthquakes, the dispersion becomes significant.

This is the basis of so-called 'dispersion-wave studies', where the group velocities of seismic waves are measured for frequencies between .05 and .016 Hz (that is, for periods between

20 and 60 seconds). The seismic wave velocity is about 6 Km/sec, giving wavelengths between 120 and 360 km. The range of crustal thicknesses normally encountered runs from 10 km (typical of the sub-oceanic crust) to 50 km beneath the large continental shields. The dispersion of such waves, then, may be used to calculate the thickness of a crust whose composition is assumed. (Adams, 1970).

Seismic dispersion studies originally showed that the East Antarctic shield is typically continental, with a crustal thickness between 35 km (Evison and others, 1960), and 42 km (Adams, 1970). West Antarctica is found to be somewhat thinner at 25--30 km. This was the first positive evidence which confirmed the hypothesis that the Antarctic was made up of two distinct crustal blocks with different tectonic histories.

Attempts have been made to extend the method to resolve strata within the crust. Models including up to 6 discrete layers have been developed (Dewart and Toksöz, 1965), involving layers between 3 and 12 km thick. Adams, in reviewing these attempts (Adams, 1970), concludes that it is over-ambitious, without independent confirmation, to rely on the unique validity of any one solution. We shall accept that this technique is essentially one of low resolution, and not well adapted for local study of particular levels of the crust.

(1.2.3) Active seismology

In active seismic studies, an artificial explosion replaces the earthquake as the source of the seismic waves. The frequencies generated are much higher than those observed in

dispersion studies (between 10 and 500 Hz), and the crustal strata are no longer regarded as dispersive layers of finite thickness, but as homogeneous, non-dispersive media. Wave travel paths are calculated in the same way as in geometrical optics. Since the frequencies involved are much higher than in dispersion studies, the resolution attainable by active seismology is proportionately greater.

Deep seismic refraction shooting relies on the passage of waves horizontally through the crust, between two points on the surface, spaced apart by up to several hundred kilometres. Waves travelling in separate strata, with different velocities, arrive at the receiving station at different instants. When different groups have been identified, a model of the crustal structure is built up by fitting computed travel paths to the observed travel times. By this means, refraction shooting is claimed (Kosminskaya and Riznichenko, 1964) to be capable of resolving strata as thin as 3 km, using frequencies of about 10 Hz.

Though the detailed structure deduced may be questioned (Pakiser and Steinhart, 1964), the travel path of waves immediately below an ice sheet may be computed with some accuracy, knowing the depth of the ice. Thus the seismic wave velocity may be calculated reliably, which may indicate broadly the rock type involved. Changes in the type of rock should be apparent, and a widespread survey by this technique could be expected to reveal the broad distribution. The method, however, does not yield information on the nature of the sub-ice boundary itself.

Seismic reflection shooting, in contrast to refraction shooting, relies on the interaction of the transmitted waves with the interfaces between media with different acoustic impedances. We might expect this interaction to give rise to a similar infrastructure to the echoes as has been mentioned with respect to electromagnetic sounding. However, the technique is limited in this respect by several difficulties:

a) Signal-to-noise levels are generally low. Especially at high altitudes on the East Antarctic plateau, incoherent surface noise, excited by the shot, may persist for a second or more. The identification of echoes is itself a difficult problem (Bentley, 1964), and, under these conditions, a precise description of the received pulse is not possible.

b) Because of the inherent 'one-shot' nature of the method, overlapping echoes, from different parts of the reflecting surface are hard to distinguish. Numerical methods are not easily applicable: in general, the measurements are not amenable to statistical treatment.

c) The form of the reflected wave-fronts, and their angular spectrum, depends on the geometry of the reflecting interface, in the same way as do electromagnetic reflections. However, in order to obtain useful information about the interface, it must be possible to examine in detail the received pulse, knowing also the shape of the transmitted pulse as it travels into the ice. This shape is very uncertain, in the case of seismic sounding. It is not subject to direct control, but depends on the nature of the explosion, and on the coupling of the acoustic energy into the ice: a very inefficient process.

Bentley (1971) estimates an uncertainty of ± 60% in the acoustic energy generated by the shot, and that the duration of the radiated pulse is about 20 msec. The use of high-pass filters in the receiver, in order to reduce the noise level, further complicates the interpretation of the received pulse shape, and we conclude that, with so little initial information, detailed analysis is not worth while.

We shall see in Chapter 4 that knowledge of the pulse length is essential to any interpretation of the received power, and that interference effects necessitate the use of a mean level, rather than single spot values. (We are here drawing a direct analogy between seismic and electromagnetic pulse techniques). We conclude also, then, that little reliable information concerning the reflecting power of the sub-ice interface is available from this technique.

Some inferences have been drawn about conditions near the base of the ice, from seismic reflection studies. Bentley (1971) has described a low-amplitude reflection which has often been seen to precede that from bedrock proper, in seismic investigations of the Antarctic ice sheet. He hypothesises that this could represent a partially-reflecting interface between the upper ice, and a layer, either of ice at the pressure melting point, or of ice contaminated by moraine at some distance above the bed. Bentley deduces, from the 'reverberative, incoherent' character of the echo, that the latter cause was the more likely. The former would be expected to form a single, continuous surface, giving rise to a 'singular, impulsive' reflection. This is a study verymuch in the spirit of much of the present work, and one

which it will be of interest to examine.

We shall comment on Bentley's reasons for the above conclusion in the order in which he states them:

a) The observation of 'more than one amplitude maximum' in the echo traces is not evidence for an echo scattered from a 'rough' surface. It is more compatible with an undulating reflecting surface, to which more than one normal may be drawn through the point of observation.

b) Variations in the power of the echo over and above those allowed for by Bentley may be caused by the curvature of reflecting facets of an undulating surface. These will include augmentations of the apparent reflection coefficient.

c) Horizontal changes in the reflection coefficient are to be expected on the basis of this model of the surface.

d) Large dip angles of the surface, while not supporting the hypothesis of a velocity change due to the temperature gradient in the ice, neither lend weight to that of layers of morainal material. They suggest that the cause of the reflections may be some third, as yet unconsidered phenomenon. It is, however, possible that a surface undulating by a few meters might be caused by local variations in the basal heating due to friction and strain in the ice. The position of the reflecting layer, on the temperature model, would be extremely sensitive to the exact temperature profile at each point, since the velocity change occurs over a very small range of temperature (-0.1 to $-0.2^{\circ}C$). With a temperature gradient of $0.1^{\circ}C$ per 10 metres, it is only necessary for the temperature at the mean depth of the reflecting layer to vary by $0.1^{\circ}C$ to produce a shift in the vertical position of the layer of 10 metres.

Though it seems unlikely that a dip of 19°, as quoted by Bentley, could be produced by this means above an apparently flat bedrock surface, we emphasize that the temperature effect is not tied to flow lines in the ice, as is moraine, but may shift vertically, and smoothly from place to place, as a result of the local temperature profile. We also point out that where the base of the ice is at the pressure-melting point the local temperature structure may be affected by the distribution of actual melting zones as a result of the small-scale topography of the bedrock surface.

e) The reflection coefficient of a boundary caused by a temperature change will be dependent on the temperature gradient, and will be variable from region to region.

We believe that the quantitative value of measurements of the echoes is small, particularly since the signal-to-noise ratio is low (Bentley does not take this into account in his estimates of echo power, or comments on the coherence of the echoes). The above comments, rather than proving the opposite to Bentley's conclusion, demonstrate that no definite conclusion can be drawn. Paragraph (a) alone suggests to the author that a smooth, undulating surface would be closer to the truth than a rough, scattering surface.

(1.2.4) Magnetic surveying

In general, magnetic surveying suffers, for our purposes, from the same difficulties as does gravity surveying. The importance of accurate knowledge of altitude, of assumptions about the crustal structure, and the generally low resolution of the technique render it inapplicable to the detailed

investigations which we wish to consider. However, where abrupt changes in the crust involve magnetic materials, the method may yield important specific information which is especially useful in combination with the results of gravity, seismic, or electromagnetic surveys.

For example, Kogan and Morozov (1969) have described a magnetic survey performed along a traverse from Molodezhnaya Station to the Pole of Relative Inaccessibility. Among their general conclusions, they refer to changes in the character of the magnetic field variations, indicating changes in the nature of the crystalline basement. These are correlated with faulting revealed as a result of simultaneous seismic refraction shooting and the correspondence allows greater confidence to be placed in each set of results. Similar comparisons were used by Solov'yev and Kogan in their interpretations of observations on a 425 km traverse near Novolazarevskaya (1970).

Both of these studies illustrate the advantages of such combined surveys, each component of which suffers from difficulties of interpretation when seen in isolation.

(1.2.5) Electromagnetic sounding

The technique of radio echo sounding relies on the difference between the electrical properties of ice and those of rock. The relative permittivity of ice is approximately 3, whereas that of rock varies between 2 and 10. Fig. 1.1 shows the value of ϵ_r for various different types of rock, as given by Campbell and Ulrichs (1969), and by Keller (1966). The expected reflecting power is a function of the permittivities and conductivities involved, and is plotted in Fig. 1.2, as a

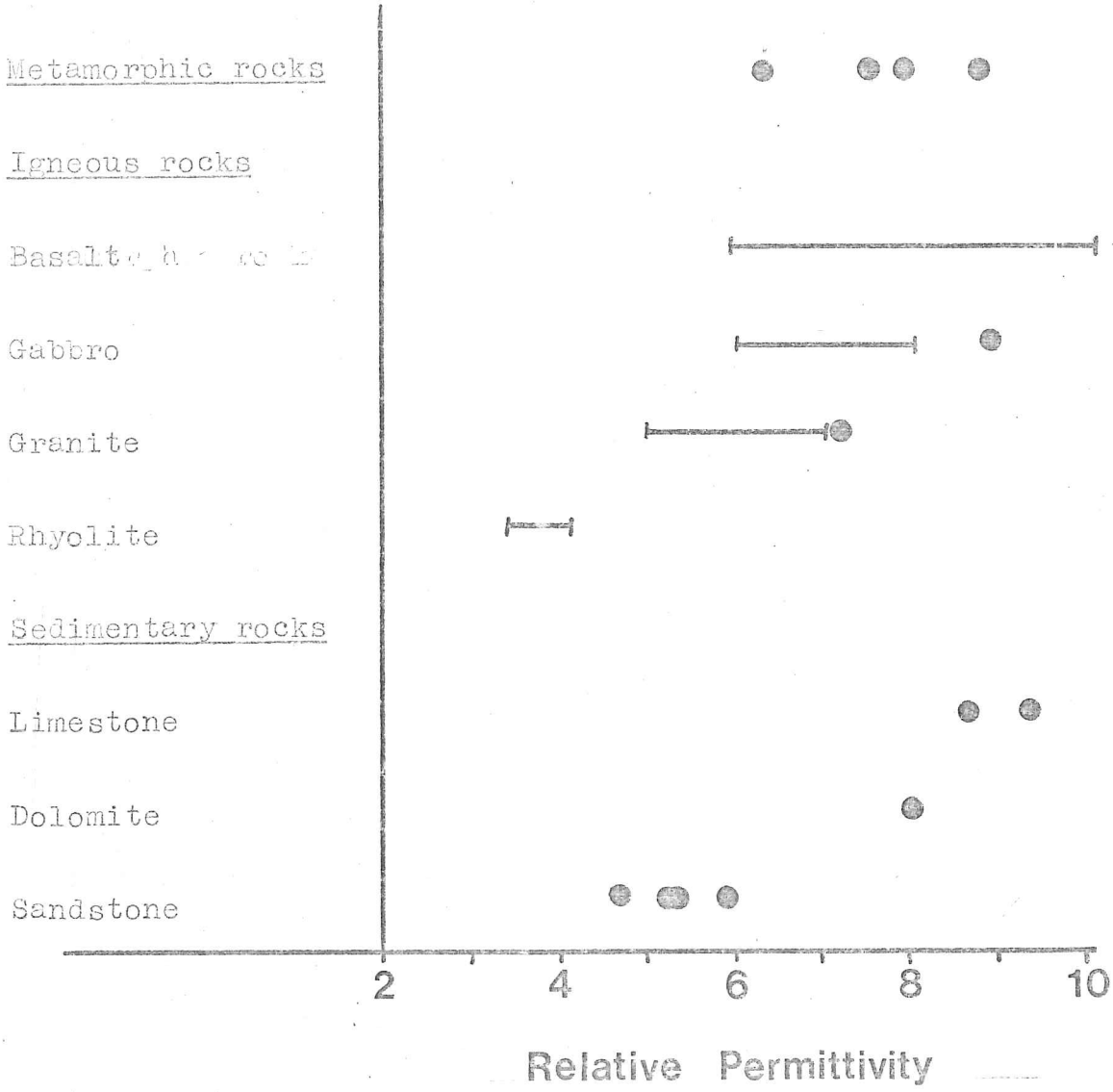

Fig.1.1 Values of relative permittivity for various rock types. The continuous ranges are derived from Campbell and Ulrichs (1969), and the point values from Keller (1966).

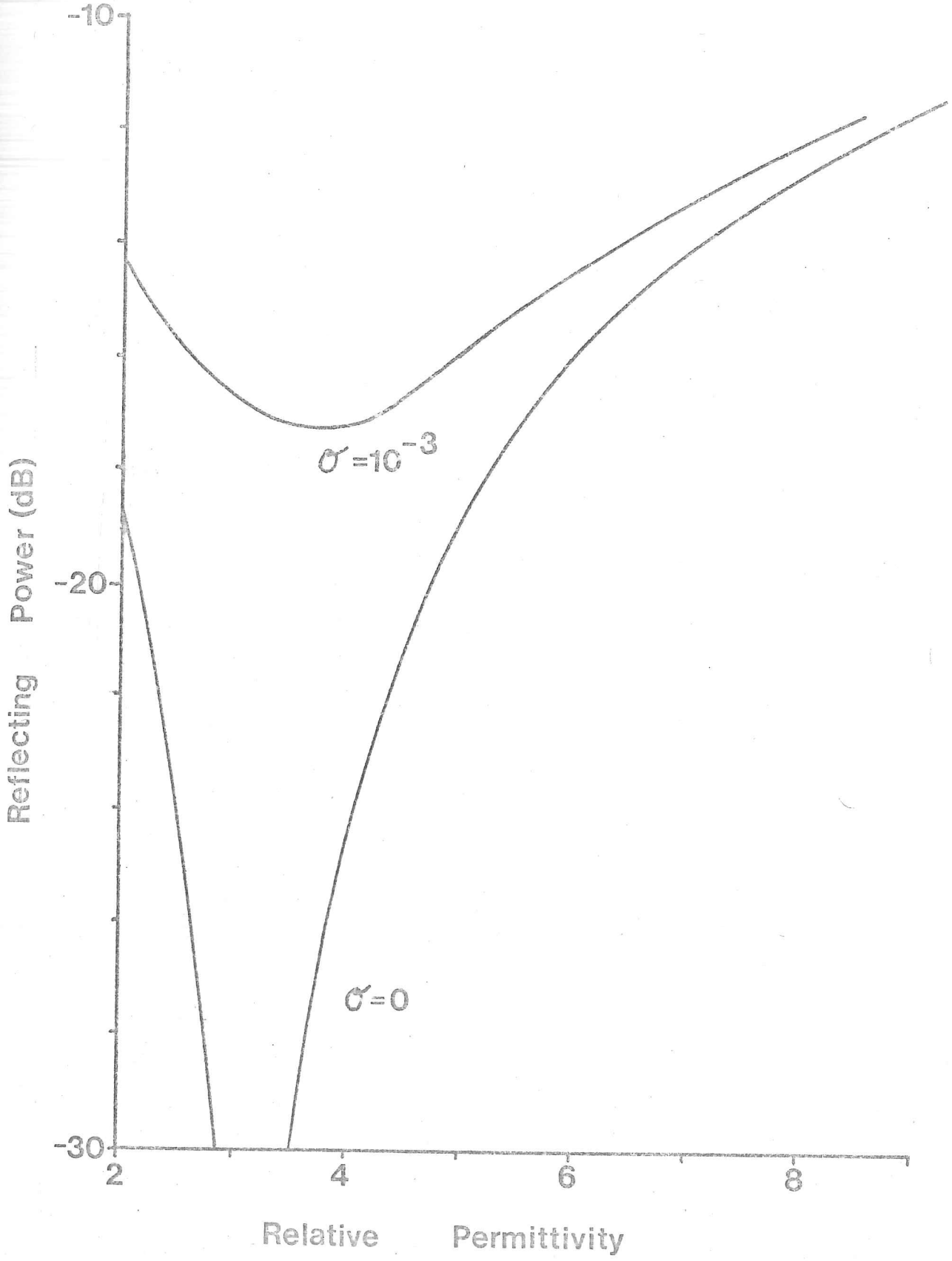

Fig. 1.2 The reflecting power of the ice-rock interface, expressed as a function of the rock permittivity, for rocks with conductivities of zero and 10^{-3} mho/metre.

function of ϵ_r, for rocks with conductivities of zero and 10^{-3}mho/m. A small range of volcanic rocks show permittivities lower than that of ice: excluding these, we expect the range of reflecting power to run from -10 to -25 dB.

Because of the nature of the rough surface under observation, the strength of the echo from a single pulse may not be representative of the reflecting power characterizing the materials which form the boundary. The two contributing causes are, where the observer is distant from the surface:

a) Interference between reflections from different facets of the rough surface. If the echo results from the addition of a sufficient number of elementary reflections, we may expect a Rayleigh distribution of echo amplitudes. Measuring the echo power in decibels, related to any fixed level of power, we expect a distribution given by:

$$p(P_t) = k.\exp(k[P_t - \bar{P}_t]).\exp(-\exp(k[P_t - \bar{P}_t]))$$

where P_t is the mean received power, measured in dB and K is Log $e^{(10)}$. It will be noted from Fig. 1.3, where the distribution is illustrated, that the maximum corresponds with the mean power. This effect will occur for the case of illumination by continuous waves.

b) The dispersal in time of pulsed reflections from different facets. We shall see in Chapter 4 that this effect may be allowed for by using a sufficiently long pulse length, since the effect is, of course, not seen in the case of continuous-wave illumination.

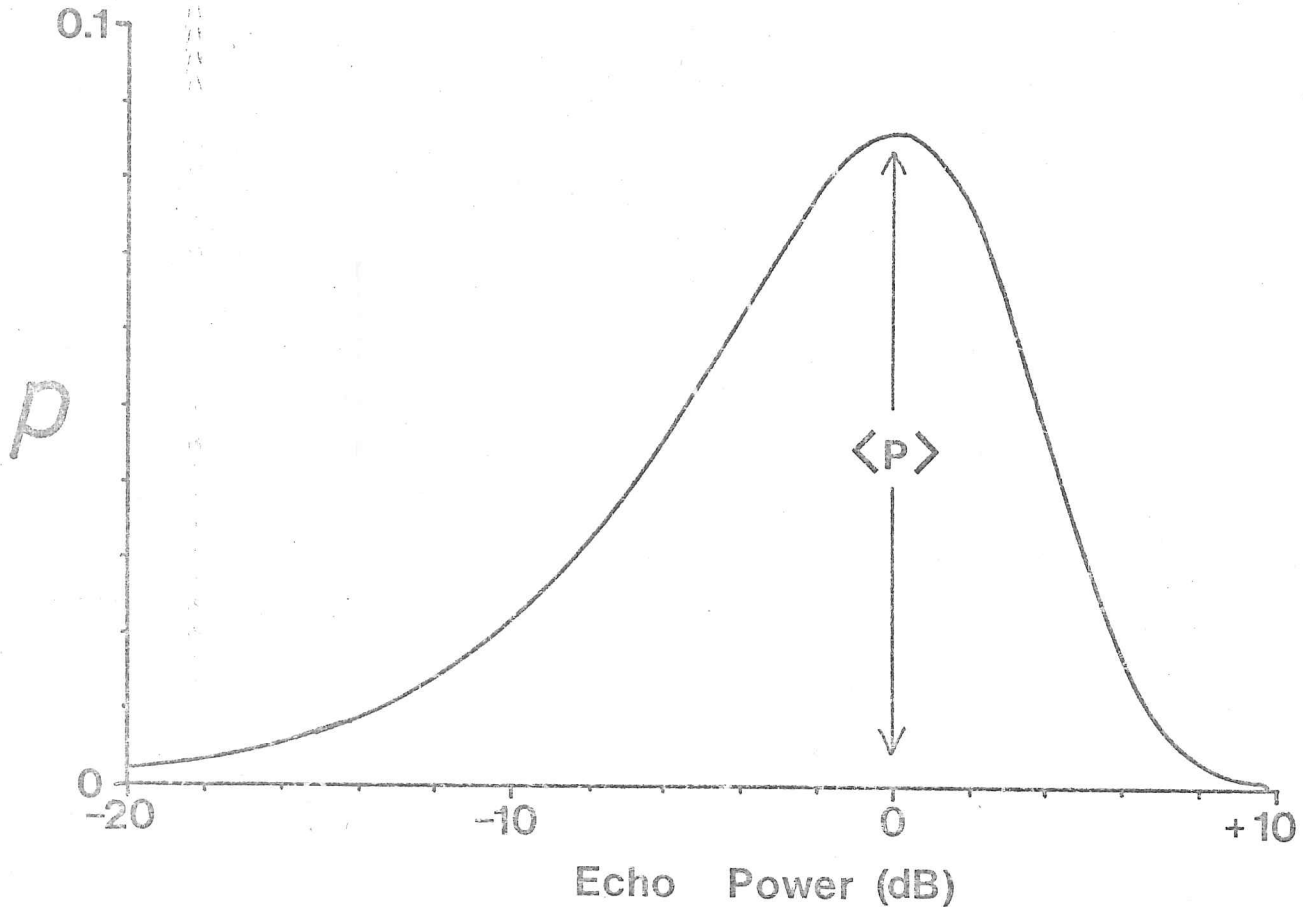

Fig.1.3 The distribution of echo power, measured in decibels referred to the mean level, to be expected in reflections from a random rough surface illuminated with continuous waves.

A systematic uncertainty is introduced in the measurement of the reflecting power by errors in estimates of the absorption of radio power in the ice. However, by using the aptitude of the technique for frequent, close-spaced observations, we may follow the variation of the average echo power and interpret observed changes according to their size, abruptness, and relation to other observed sub-glacial features. For a given change in the rock permittivity, the change in the reflecting power is given by:

$$\frac{\delta R}{R} = \frac{2\sqrt{\epsilon_i \epsilon_r}}{\epsilon_r - \epsilon_i} \cdot \left(\frac{\delta \epsilon_r}{\epsilon_r} \right)$$

where R is the reflecting power,

ϵ_r is the relative permittivity of rock,

ϵ_i is the relative permittivity of icw, and we neglect the effect of finite conductivity in either material. Taking $\epsilon_r = 6$, as for some forms of granite, and $\epsilon_i = 3.2$, we have:

$$\frac{\delta R}{R} \simeq 3 \frac{\delta \epsilon_r}{\epsilon_r}.$$

We may expect, in principle, to be able to detect a change of about 2 dB in the reflection coefficient, which corresponds with a change of 20% in the relative permittivity of the rock. In a thick ice sheet, we may expect such a change in the rock type to occur over a shorter distance than any significant change in the temperature structure, and therefore specific absorption, of the ice.

We mentioned in Section (1.2.3) that interpretation of the received pulse was impeded by a lack of knowledge of the shape of the transmitted pulse, in seismic sounding. In the case of electromagnetic sounding, the process of coupling of the transmitted signal into the body of the ice is understood in greater detail. Though the transition from snow to firn, and finally to solid ice may vary from place to place, the matching of the radio antenna may be checked and adjusted in situ. In the case of airborne radio echo sounding, the ice surface is not within the 'near field' of the antenna, and does not affect the pulse shape in this way. In all cases, continuous monitoring of the radar signals allows the transmitted pulse to be optimised, both in amplitude and shape.

Radio echo sounding has not been used for probing rock itself. Campbell and Ulrichs (1969) found that the absorption length (the length of path over which the power of a plane wave is attenuated by a factor of e) for various rocks lies between 1 and 10 wavelengths. The absorption length is not correlated with the relative permittivity. Using an average wavelength of 2 metres in the rock, for a frequency of 60 MHz, we deduce an attenuation of 10 dB after a penetration of between 4 and 40 metres. Given favourable conditions of ice depth, temperature, etc., we might expect a detectable reflection from, say, the lower boundary of a 50 metre layer of moraine. However, in practice, echoes from penetrable depths inside the bed would be obscured by the continuing echo from the upper interface.

We therefore expect the value of the technique to be restricted to studies of the interface itself, rather than of the bulk of the underlying material.

(1.3) Summary

With the exceptions of electromagnetic sounding and seismic reflection, the methods we have discussed relate to the bulk of the materials underlying the ice, rather than to the ice-rock interface itself. We have seen that seismic reflection shooting, though conceptually similar to radio echo sounding, and historically its precursor in the field, is not well adapted for our purpose of investigating the interface.

Our aim is to adapt the radio echo technique as a complement to other methods of geophysical exploration, in its capacity to observe and detect changes in the lower boundary of the ice mass.

The clearest example of its usefulness can be found in Chapter 3, where we consider changes in the echo character which are clearly visible in the original photographic records.

In most cases we cannot expect changes to be so obvious and must make quantitative and circumstantial studies in order to resolve different types of reflecting surface.

CHAPTER 2 ANTARCTIC FIELDWORK AND EQUIPMENT

(2.1) Fieldwork

An account of the work undertaken during the 1971/72 season of SPRI-NSF cooperative Antarctic radio echo sounding has been given by Evans, Drewry and Robin (1972). The equipment has been described by Evans and Smith (1969) and Smith (1971), and some refinements were mentioned in the fieldwork account.

The party consisted of Dr. S. Evans, D. J. Drewry, C. H. Harrison, M. Gorman, and the author, all of the Scott Polar Research Institute, and Dr. H. Decleir of the University of Ghent. The major object of the season's work was to obtain ice depth profiles over flight lines covering a large section of the East Antarctic ice cap (Fig. 2.1). The flights covered a total of 60,000 km, and depths were recorded over about 70% of this path length. A map has been published by the Scott Polar Research Institute (1974), as a result of this survey, showing ice surface and bedrock contours, and is reproduced in outline in Fig. 2.2. Perhaps the most striking feature of the map is a deep sub-glacial trench running from beneath the centre of outflow of ice near 75°S 120°E, in a North-Westerly direction towards the coast. Further mention of this feature will be made in Chapter 3. The subglacial topography of the Trans-Antarctic mountains was studied in detail by D. J. Drewry (1973), in his reconstruction of the geological history of Antarctica, and the ice surface contours were interpolated, using an elaborate statistical process, by D. Jenssen (University of Melbourne) and A. Clayton (SPRI).

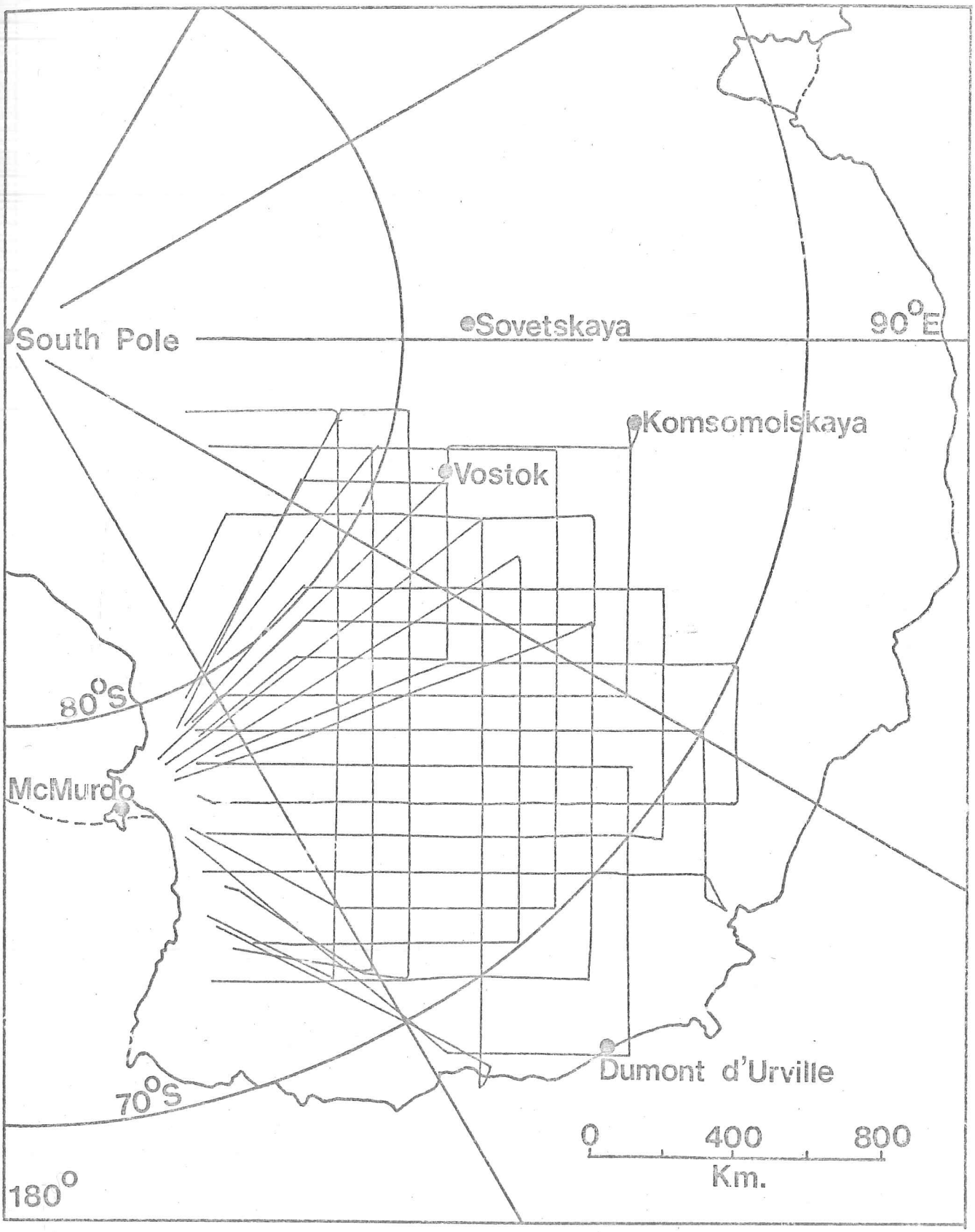

Fig.2.1 A map of flight lines covered during the 1971/72 season of Antarctic radio echo sounding.

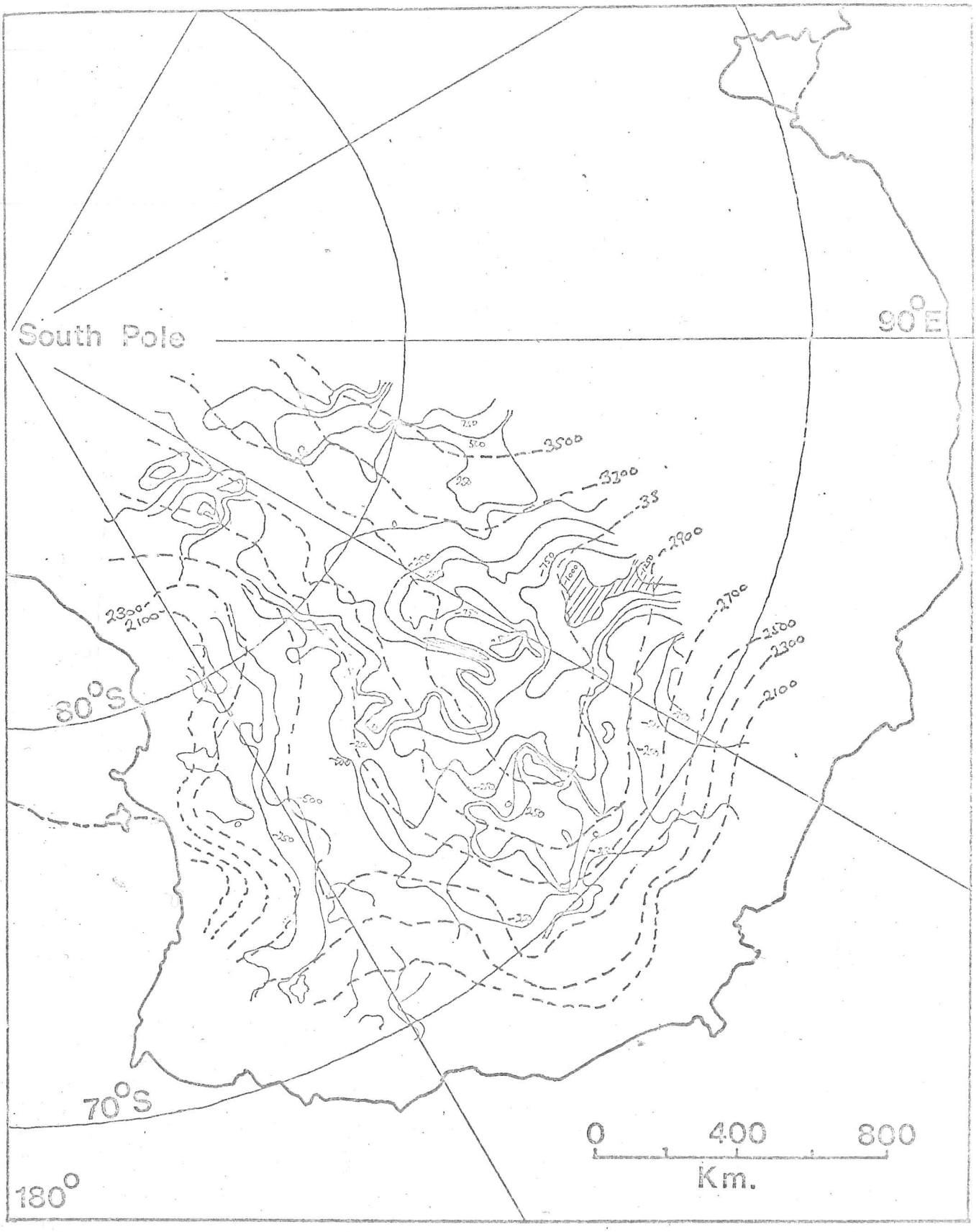

Fig.2.2 Outline of the SPRI map of Ice surface contours (dotted lines) and bedrock contours (continuous lines).

This work was carried out in collaboration with the International Antarctic Glaciological Project of Australia, France, USA and USSR, and is the third season of the SPRI-NSF cooperative programme.

The team were based at McMurdo Station, and completed over 150 hours of survey flights in US Navy C-130 (Hercules) 148320. Though mechanical faults had reduced the available time from the original estimate of 300 hours, the extension of flights to 10 hours' duration allowed the completion of the great majority of the proposed network.

The 16 flights completed were located to cover as evenly as possible the region of the East Antarctic Plateau between 90°E and 180°. The grid consisted of lines spaced at 100 km intervals. A square grid gives fairly good efficiency for conversion into contours, while maintaining a degree of redundancy which is necessary for checking the reliability of depth measurement and navigation data.

In previous seasons the aircraft had flown at a specified terrain clearance, relying on pressure altimeter readings for the measurement of surface elevations. Since accurate elevations were required by the IAGP, constant pressure altitude was maintained on these flights, using the radio echo apparatus to measure and record the depth of the surface below the constant pressure surface. As a result, the terrain clearance tended to exceed that adhered to previously, and on occasion, the bedrock echo was lost.

(2.2) Equipment

The main innovations in this season's work were:

a) Operation at a carrier frequency of 60 MHz, instead of 35 MHz. This allowed the use of an antenna array with more directional characteristics, giving greater gain, and therefore higher sensitivity in the vertical direction.

b) The new antenna, designed and built by the Laboratory of Electromagnetic Theory, Technical University of Denmark, whose impedance matching was carefully adjusted, and whose electromagnetic performance in the field was excellent. The antenna was mounted beneath the wing of the aircraft, and was subjected to severe stresses, owing to its position in the slip-stream, immediately behind the propellers. Some re-design was necessary, involving the replacement of struts in the supporting frame, and these mechanical problems were finally overcome, largely through the endurance of US Navy engineers, working under very adverse conditions.

c) The use of a logarithmic receiver characteristic. This meant an increase in the dynamic range of the receiver from about 12 dB to about 60 dB. The advantages of this were two: firstly, whereas in previous seasons it had been necessary to continuously monitor the received signal, and adjust the receiver sensitivity by means of input attenuators, in this case the dynamic range was sufficient to cater for all levels of received power encountered, and the attenuators were dispensed with. Secondly, the response of the receiver could be tailored to provide a suitable output to drive the oscilloscope-camera recording system. Though the desired result was never fully achieved, it was possible to go some way towards providing

a characteristic which would allow the clear photographic recording of all echoes, from the strong ice-surface reflection, through internal echoes from the ice, down to the weakest detectable bottom echoes.

Examples of the records are shown in Fig. 2.3. For the great majority of the sounding carried out in this season, the radar parameters were as follows:

The transmitted pulse was rectangular, with a duration of 1 μ sec., and rise- and fall-times of approximately 50 and 100 n sec. respectively.

The receiver bandwidth was 1 MHz, giving a noise factor of approximately 3 dB, and a total system performance approaching 170 dB.

The pulse repetition rate was 8.33 kHz, representing, at normal flying speed, about 80 pulses per metre.

The polar diagram of the antenna array gave a gain of +5dB in the vertical direction. This fell to 0 dB at approximately 25° to starboard and 15° to port, with respect to the vertical, but was approximately isotropic in the fore-aft plane (Harrison, 1972). Robin (in press) has calculated that the effect of refraction, as the waves enter the ice, is such as to cause a gradual increase in the gain up to the critical angle of about 38°, at which angle the transmitted energy flux, and the sensitivity are rapidly cut off. The same array was used for transmitting and receiving, using an automatic switch to isolate the two functions.

A schematic diagram of the equipment can be seen in Fig. 2.4.

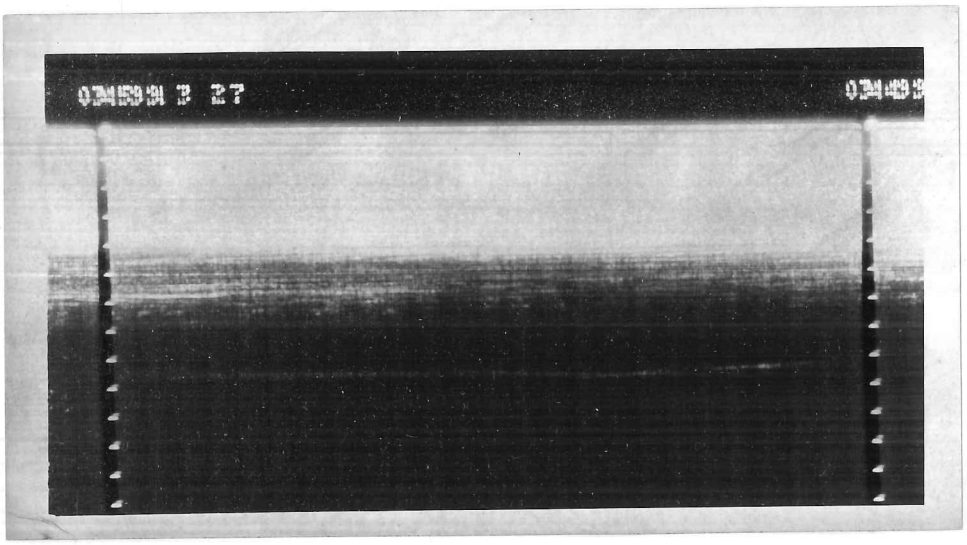

Fig.2.3a. A typical bedrock echo of low intensity.

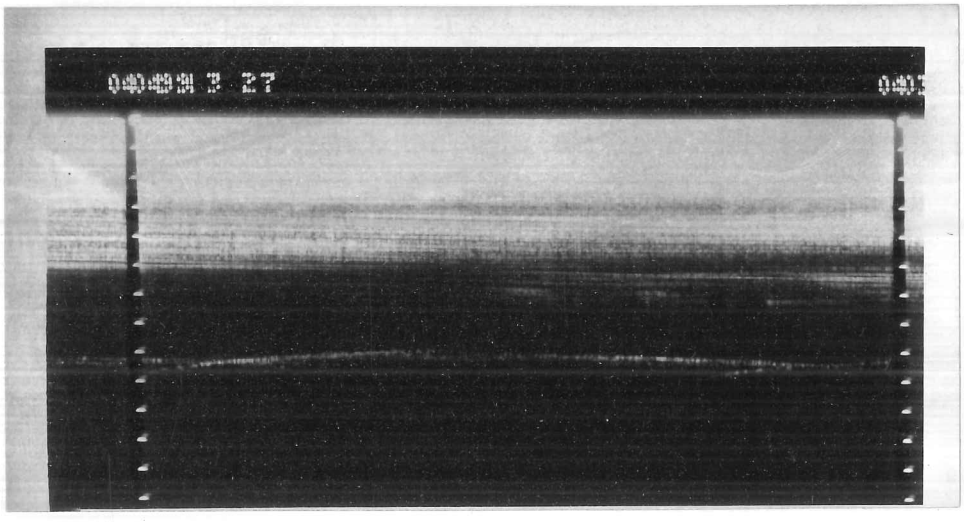

Fig.2.3b. Illustrating a bedrock echo of 'medium strength'.

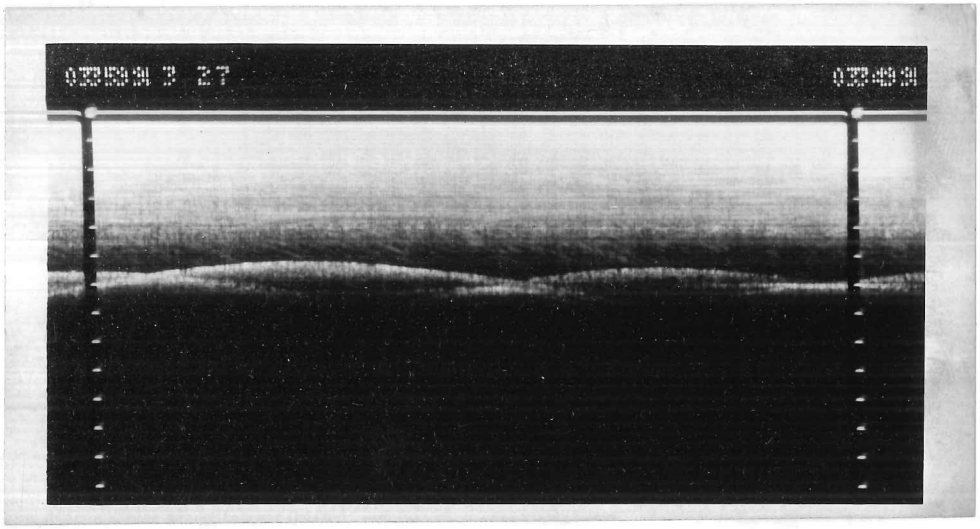

Fig.2.3c. Illustrating a bedrock echo of high strength.

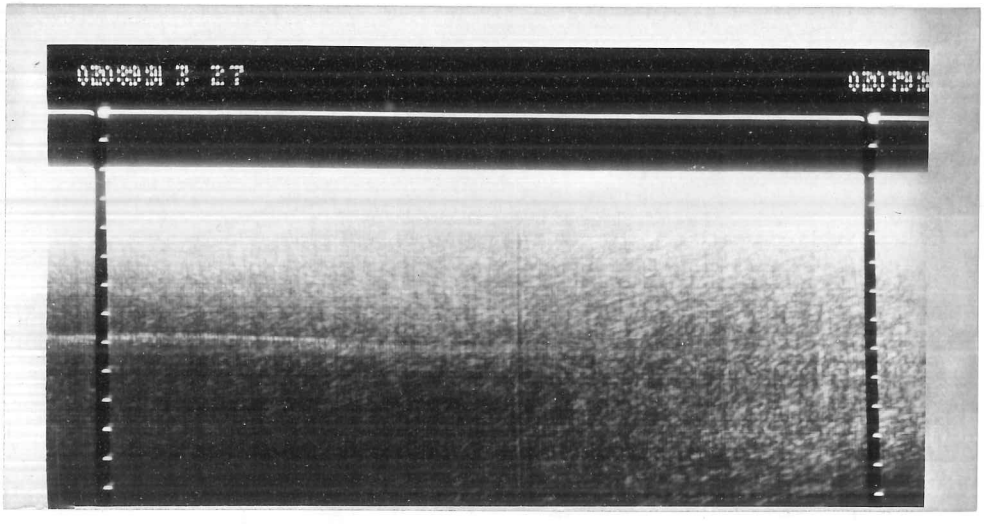

Fig.2.3d. The bedrock echo obscured by scatter from a heavily-crevassed surface.

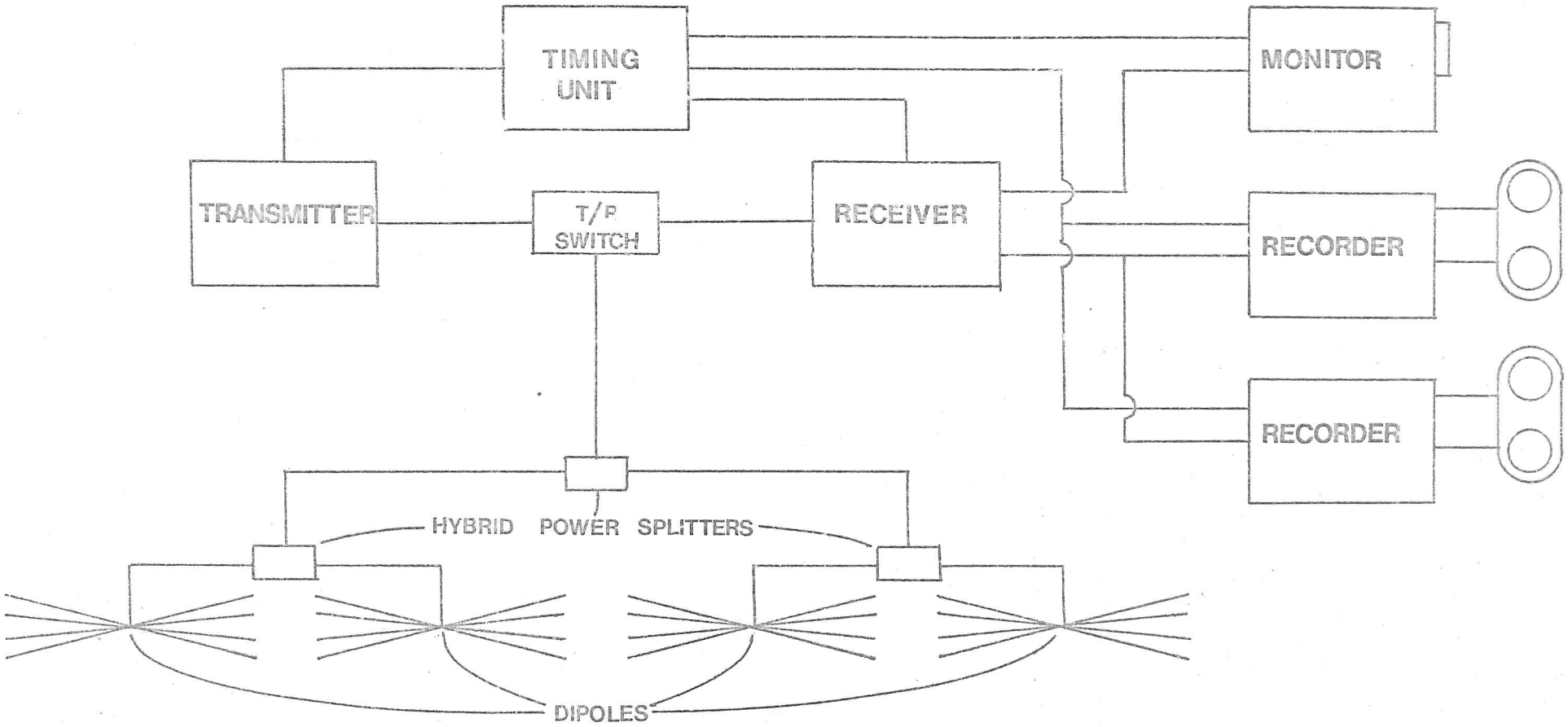

Fig.2.4 Schematic diagram of the SPRI radio echo sounder used for the 1971/72 Antarctic survey.

(2.3) The recording system

It was realised early in the field season that, though no built-in provision was made for the recording of echo strengths, or of the shape of the received pulse, much information might be retreived from the photographic records, whose intensity was dependent on the strength of the signals involved. This is potentially a fruitful added dimension to the recording system, and we shall examine it in detail from this point of view. Unfortunately, those few direct recordings of the signal envelope which were made do not constitute an adequate calibration of the system, and since this was, at the time, very much a secondary aspect of the survey, many problems were left to be solved by retrospective analysis.

In order to estimate the value of the recorded echo-strength information, we investigate the characteristics of the components of the receiving and recording equipment, whose non-linearities were in part designed, inpart anticipated and accepted, and in part random uncertainties.

(2.3.1) The Antenna

The antenna and transmit-receive switch were responsible for little non-linearity in the system characteristic. Though the latter is, as a whole, a highly non-linear device, consisting of a network of diodes and lumped 1/4-wave transmission lines, its action is to divide signals, according to their strength, between two linear paths. At the levels of signal encountered, the interaction of the non-linear region of its response with the received signals was negligible.

The initial stages of the receiver consisted of linear pre- and filter-amplifiers. These both operated on the r.f. signal, and determined the noise level and bandwidth of the receiver. Their contribution to the non-linearity of the system is also negligible.

(2.3.2) The logarithmic amplifier and video amplifier

The first non-linear stage of the receiver consisted of an amplifier with a logarithmic characteristic, designed by Dr. S. Evans. The circuit used six integrated amplifiers whose r.f. signal paths were cascaded, and whose rectified current outputs were added. The principle of operation is that, as each successive stage saturates with increasing input signal strength, the gain at the summed, rectified current output falls by a factor equal to the gain of that stage. The result is a piecewise-linear simulation of a true logarithmic curve, and the circuit also performs the function of rectifying and smoothing the signal. The gain of each stage is approximately 10 dB, giving a maximum circuit gain of about 60 dB, and a dynamic range at the input (given the noise input of the pre-amplifier) of the same magnitude.

The current output was fed to a stabilising and level-shifting amplifier, which gave the final form of the output as a positive-going voltage signal, with a stabilised base level. This circuit was perhaps more complex than was necessary, and it was later observed that the 'stabilised' base level in fact exhibited an exponential 'droop' in voltage, when the circuit was subjected to a high duty cycle. This was not noticeable to the naked eye, on examination of the output monitor, but, as we shall see later, the great sensitivity of the recording process

at low signal levels exaggerated the effect. The complex stabilising network was subsequently replaced by a simple d.c. amplifier.

This stage was also used to introduce a further compression of the dynamic range of received signals. A simple diode function generator decreased the sensitivity above the point of operation set up by the noise output of the logarithmic amplifier. The final output gave a mean level of approximately 1 volt corresponding to the receiver noise, increasing to a maximum of about 6 volts when saturated by a large input signal. The full characteristic is shown in Fig.25.

It is appropriate to mention here a problem which is not apparent under the conditions of airborne radio echo sounding, but which requires some consideration for over-snow work. This refers to the limitations of the performance of the transmit-receive switch, and of the receiver under overload. When the transmitter pulse arrives at the switch, it is directed to the antenna array, and isolated from the receiver input, by the action of the switch. However, the isolation is not complete, and a break-through signal, about 40 dB below the transmitted pulse, penetrates to the receiver. This is still a very high level of input (about 125 dB above the noise level), and the receiver exhibited a 'dead time' of between 2 and 3 μsec. The inability to receive echoes within this interval was not important during this season's work, since the aircraft flew at a minimum terrain clearance of 1000 metres. However, for work on the surface it would preclude the detection of echoes from depths of less than 170-250 metres.

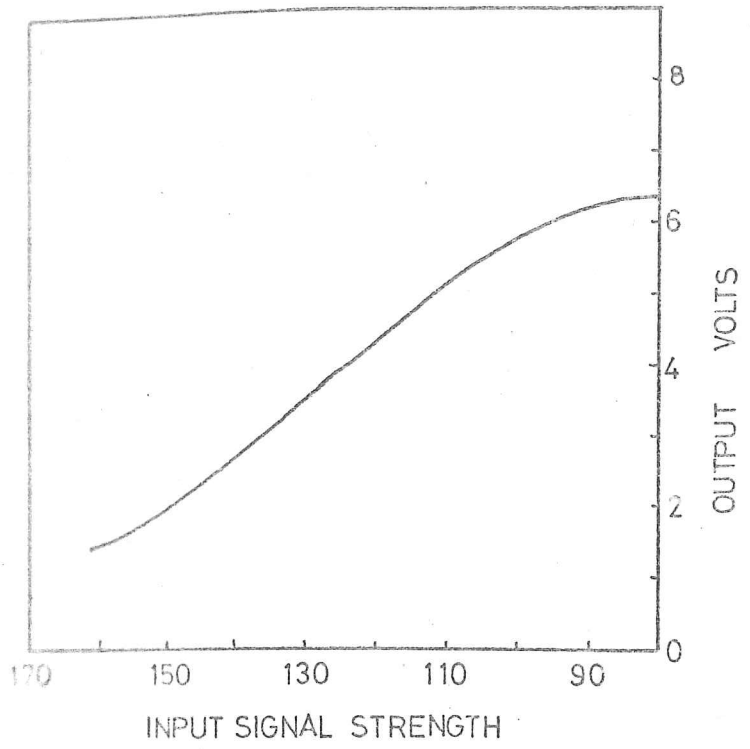

Fig. 4.3 Characteristic of complete receiver unit.

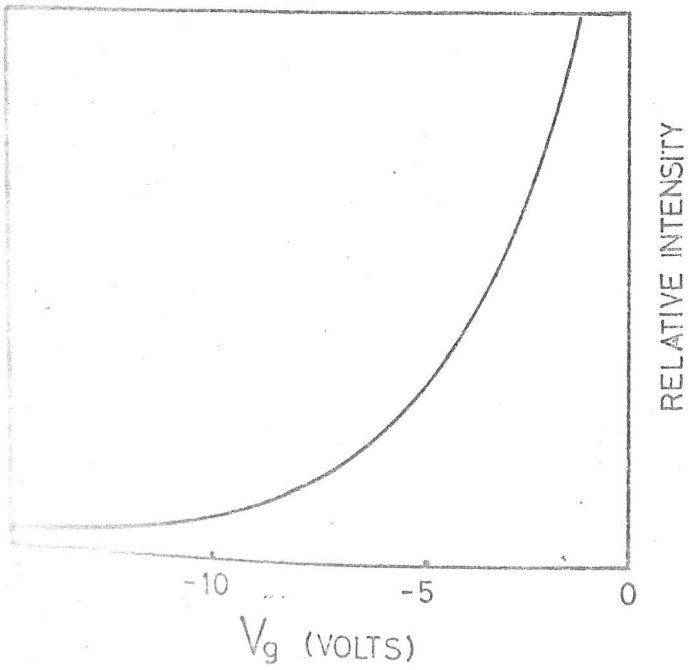

Intensity characteristic of c.r.t., showing
intensity vs. control-grid-to-cathode

(2.3.3) The optical and photographic systems

The output signal from the receiver (positive-going d.c., or 'video' signal) is fed to the intensity - modulating grid of a cathode ray tube. This is held at a steady base level by a Zener diode, and the receiver signal is superimposed.

We expect the intensity of the c.r.t. spot to vary with the grid voltage according to Child's law:

$$I \propto (V_g)^{3/2}$$

This is borne out approximately in observations at the higher levels of brightness. We can see from Fig.2.6 that this law is not followed accurately at lower levels, where the intensity would be expected to cut off at $V_g = -10$ volts (with respect to the cathode). The anomaly is due to the finite spacing of the wires forming the grid, and the analytic form of the dependence of I on V_g is not known in the operating region of -17 to -10 volts. We may expect I to approach zero asymptotically with decreasing V_g, approximating an exponential curve and counteracting to some extent the characteristic of the logamp.

The c.r.t. sweep, in the x-axis, is initiated simultaneously with, or at some well-defined delay after, the triggering of the transmitter. The resulting trace displays the variation of received signal strength as a function of delay time.

The greatest problem in relating the observed intensity at any point of the screen to the received power at any one instant arises from the phenomenon of halation. The 'spot' is not in fact a singular point on the face of the c.r.t., but the finite visible maximum of a distribution of intensity. At any

instant the intensity radiated by any small area of the screen is non-zero and depends on the position and intensity of the maximum. Summing over a period, during which the maximum changes both in position and intensity, the integrated light emanating from the element is a convoluted function of the history of the 'spot', dominated, of course, by any time where the spot coincided with the element. This effect is transmitted, not only along the linear trace, but, in the case of a raster scan, from one horizontal trace to every other. In the present system, a raster is not used, but the photgraphic recording technique simulates the effect.

The image of the linear trace is focused so as to fall across the width of 35-mm. recording film. As the film is moved, in a direction perpendicular to the trace axis, the spot performs effectively a continuous raster scan down its length. The resulting profile of received echoes is an approximation to the profile of the ice itself, but convoluted as a result of the broad radar beamwidth. The deconvolution has been dealt with by Harrison (1971). Though the eye is not seriously troubled by the general blurring of the image due to halation, in viewing the developed film, when objective measurements are made of the optical density, the effect is very troublesome. Fig.2.7 shows a length of test film, where the delayed transmitter pulse is attenuated by between 100 and 170 dB and used as a direct input to the receiver. Fig.2.8 is a sequence of traces produced on examination of four sections of this film using a scanning microdensitometer. The increase in width of the exposed area can be clearly seen, as the signal strength rises,

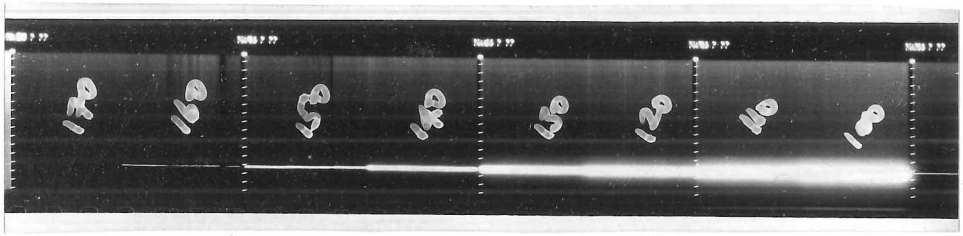

Fig. 2.7 Contact print of test film showing the response of the recording system to known pulse inputs. The signal strength is related to the transmitter pulse power. (~ dB)

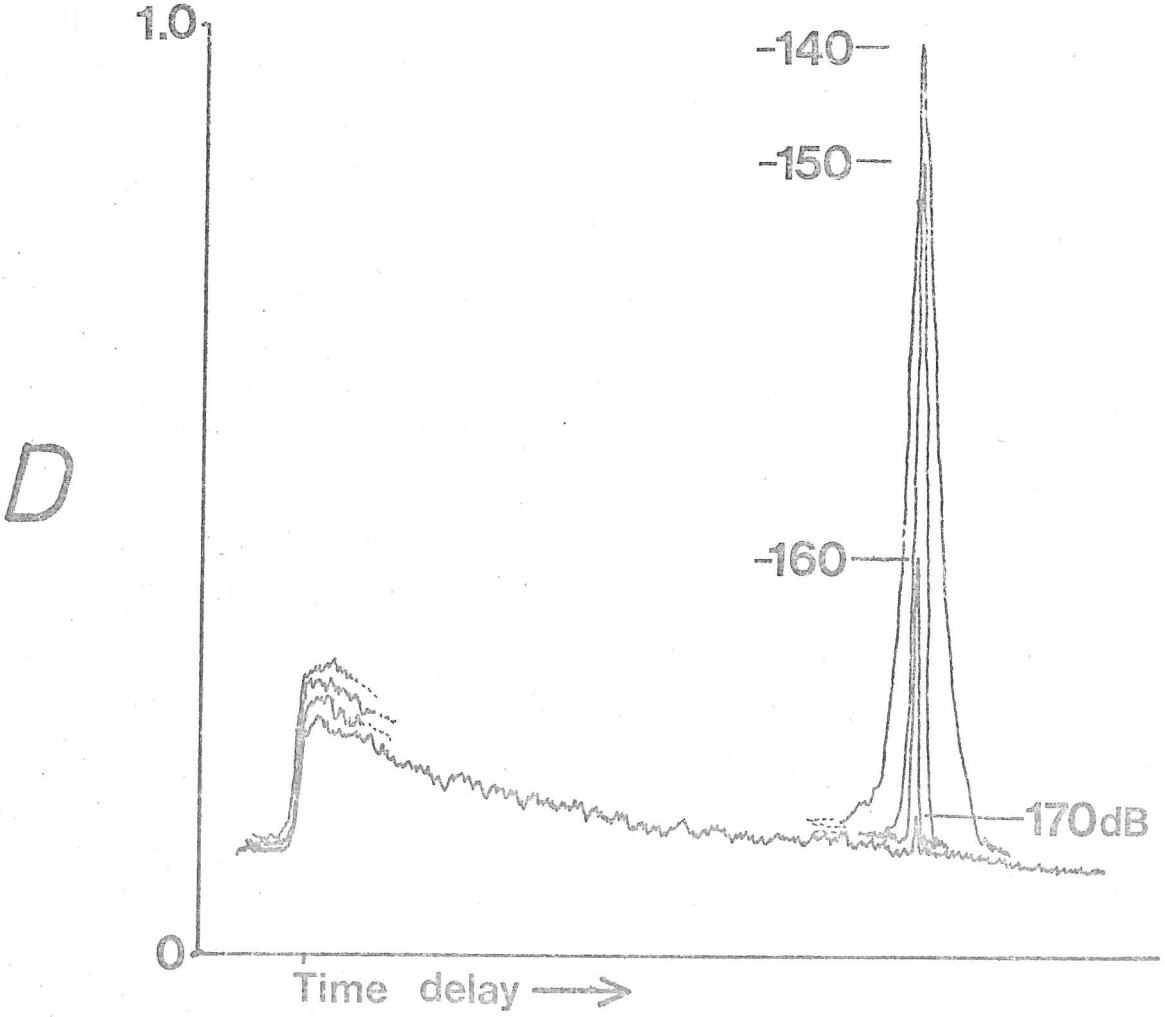

Fig.2.8 Microdensitometer traces of the first four sections of the test film shown in Fig.2.7.

as can the 'droop' of the background which we mentioned earlier.

The characteristics of the film and of the developer are also of critical importance in determining the optical density of the final record. Fig.2.9 shows the variation of the density with exposure, for a range of development times in the ratios 1:1.25:2 where the density is defined as:

$$D = \log_{10}(I_o/I_t)$$

where I_o is the light intensity incident on the film, and I_t the intensity transmitted. The abscissa in Fig.2.9 is the common logarithm of the exposure, measured in the standard unit of 'metre-candle-seconds'. (1 mcs = 1.6 J/m^2).

From measurements of the light transmitted through the recorded film, we have derived a parameter B, given by:

$$B = (I_o - I_t)/I_o$$

In Fig.2.10 we have plotted B as a function of the logarithm of the exposure, from the curves of Fig.2.9. These are proprietary examples for Kodak RAR 2492 recording film, which was used throughout this season's work.

From the traces of Fig.2.8, we derive the characteristic shown in Fig.2.11, relating the film blackening, B, to the input signal strength. The uncertainties in this characteristic resulting from possible variations in development are indicated by the dotted lines, It is unlikely that the lower line represents a possible situation, since the background level of density observed in the traces of Fig.2.8 indicates that the development in this instance was at the lower end of the range in Fig.2.9.

In order to allow for the effects of film development, the intensity of light transmitted through the film at the

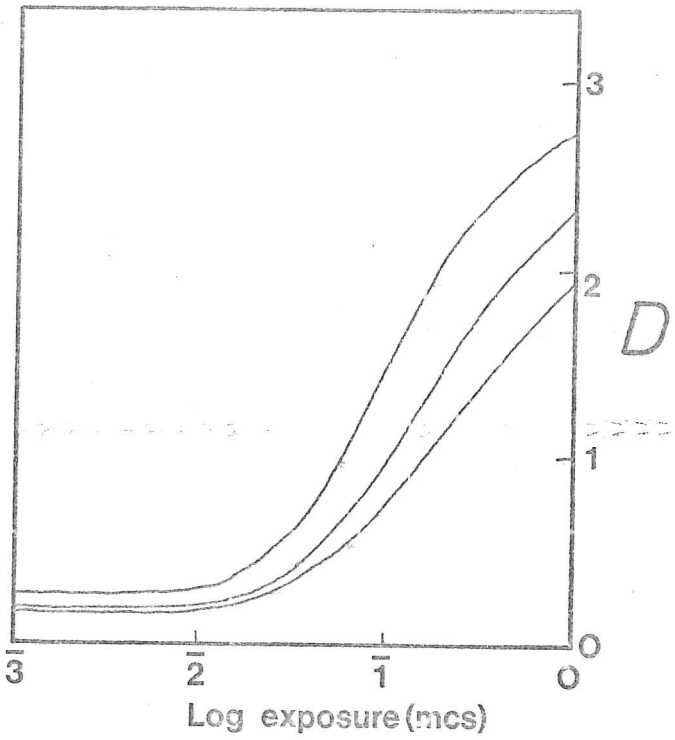

Fig.2.9 Variation of film density with exposure and development time for Kodak RAR 2492 recording film. The development times are in the ratio 1:1.25:2

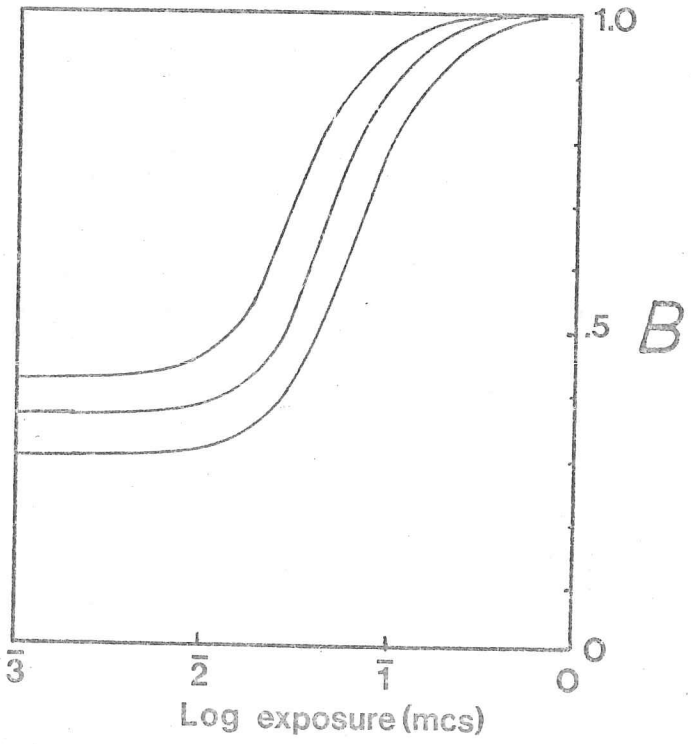

Fig.2.10 Variation of the parameter B with exposure, for the same film and development times as in Fig.2.9.

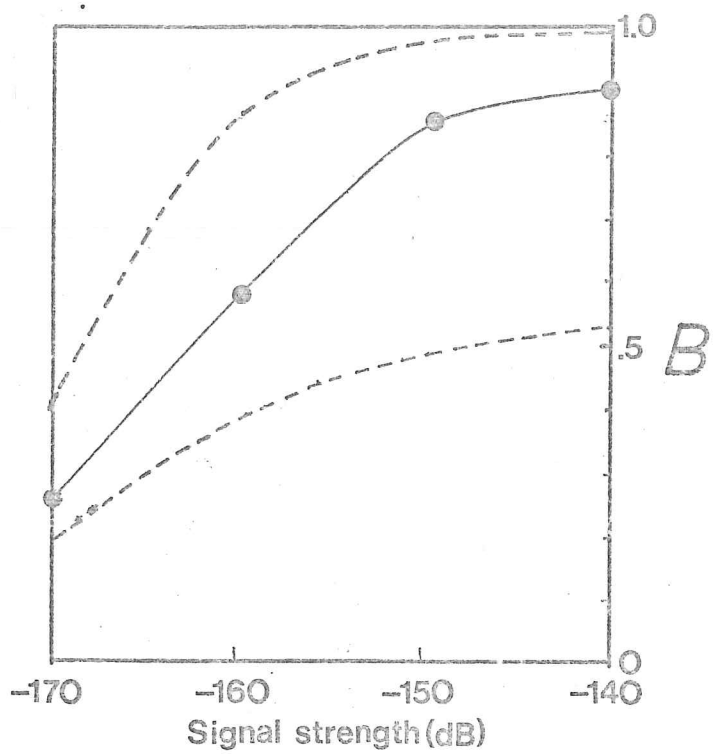

Fig.2.11 Variation of B with signal strength input to the radio echo receiver.

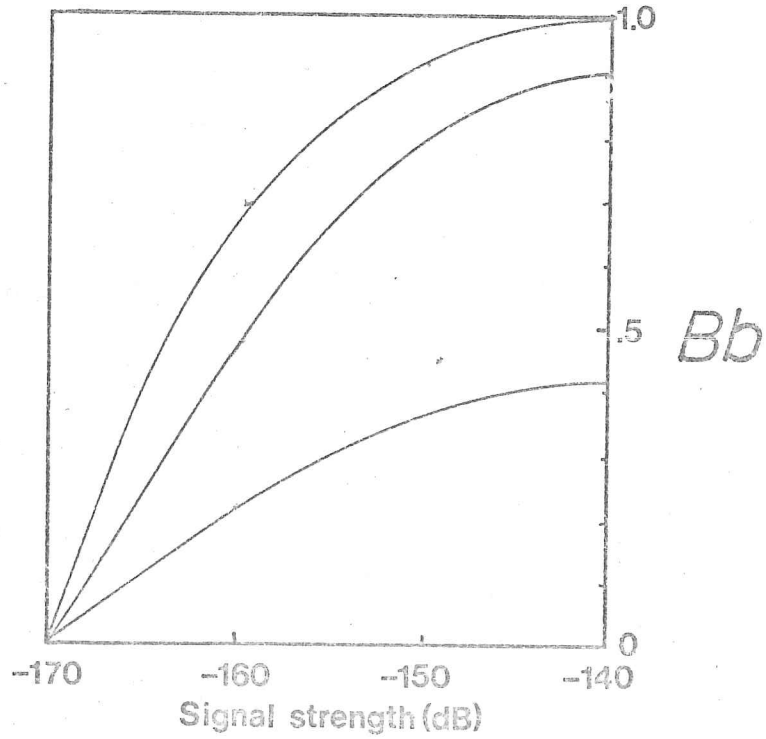

Fig.2.12 Variation of Bb with input signal strength. We take the dotted line as a reasonable simple representation of the characteristic.

position of the bedrock echo may be compared with the local background level. The parameter Bb, representing the blackening due to the bedrock echo alone, is related to the total blackening and to that due to the film base and background signal, B_1, by the formula:

$$1-Bb = \frac{(1-B)}{(1-B_1)}$$

In Fig.2.12, Bb is plotted as a function of signal strength, for the three cases shown in Fig.2.11. Once again, we consider that the lower curve does not represent a real case, and we shall approximate the final characteristic of Bb vs. echo strength by a straight line between the points (-170,0) and (-140,1). The uncertainties due to the vagaries of development, and convolution due to halation of the c.r.t. spot, are such that we shall not attempt to draw detailed quantitative conclusions from echo strengths measured in this way, but may rely on qualitative comparisons.

(2.4) Densitometry

The foregoing argument leads us to the conclusion that, for lack of preparation and understanding in the field, the information carried in the degree of blackening of the record film cannot be interpreted quantitatively. This does not imply, however, that the film density is useless as an indicator of signal strength. We may make qualitative comparisons between different echoes on the same film, and may attempt to allow for differences in development between films by comparison of the densities produced by similar signals.

Fig. 2.14 shows a microdensitometer scan of the recording film close to the location where the photograph in Fig.2.13 was taken of the 'A-scope' monitor display. The initial high, sharp peak corresponds to the sweep initiation, the depressed black dot in the photograph. As we have intimated, the background 'droop', though clearly visible in the scan, is not detectable by eye in the A-scope trace. The considerable peaks A,B,C in the scan correspond to small peaks in the end of the visible echo in the photograph, confirming that much of the dynamic range of the film density is occupied by the first 20-30 dB of the receiver's range.

Though these two figures illustrate the similarity between the microdensitometer output and the original signal as shown by the monitor screen, the instrument is not applicable to a large-scale survey of film densities, mainly because of the quantity of redundant data produced, the physical inconvenience of existing equipment, and the slowness of the procedure.

Several different automatic scanning systems were considered for the proposed survey, apart from the above instrument, the most promising being flying-spot scanners, and stationary arrays of semiconductor photodiodes. Though each of these systems had much to recommend it, it was decided that the cost and time involved in developing such a system was not justified, in view of the lack of precision of the results we might expect.

Accepting the limitations imposed by non-standard development, drooping background intensities, and halated spot images, it was decided that a simple manually-operated system would provide the necessary flexibility for a qualitative

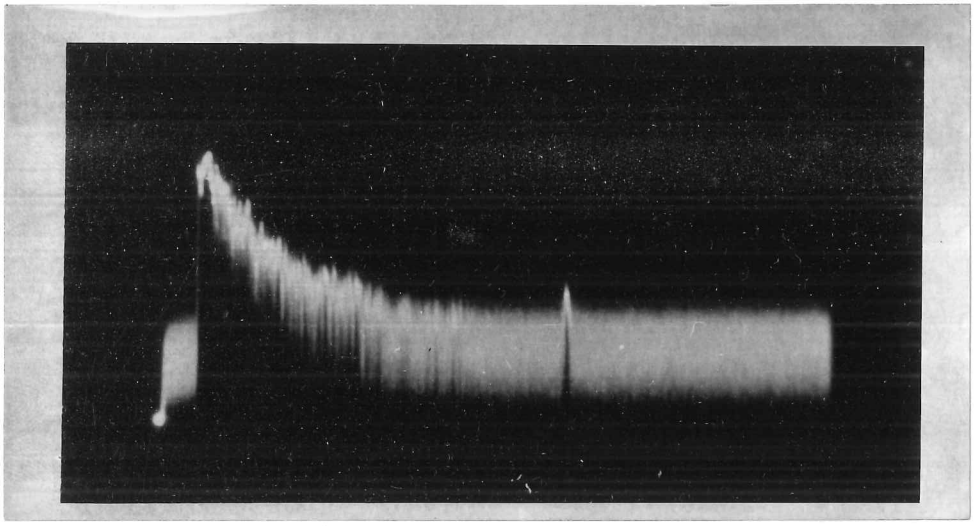

Fig.2.13 An A-scope photograph showing a fairly strong echo from bedrock. The sweep duration is 60 seconds, and the echo from a depth of 3 km.

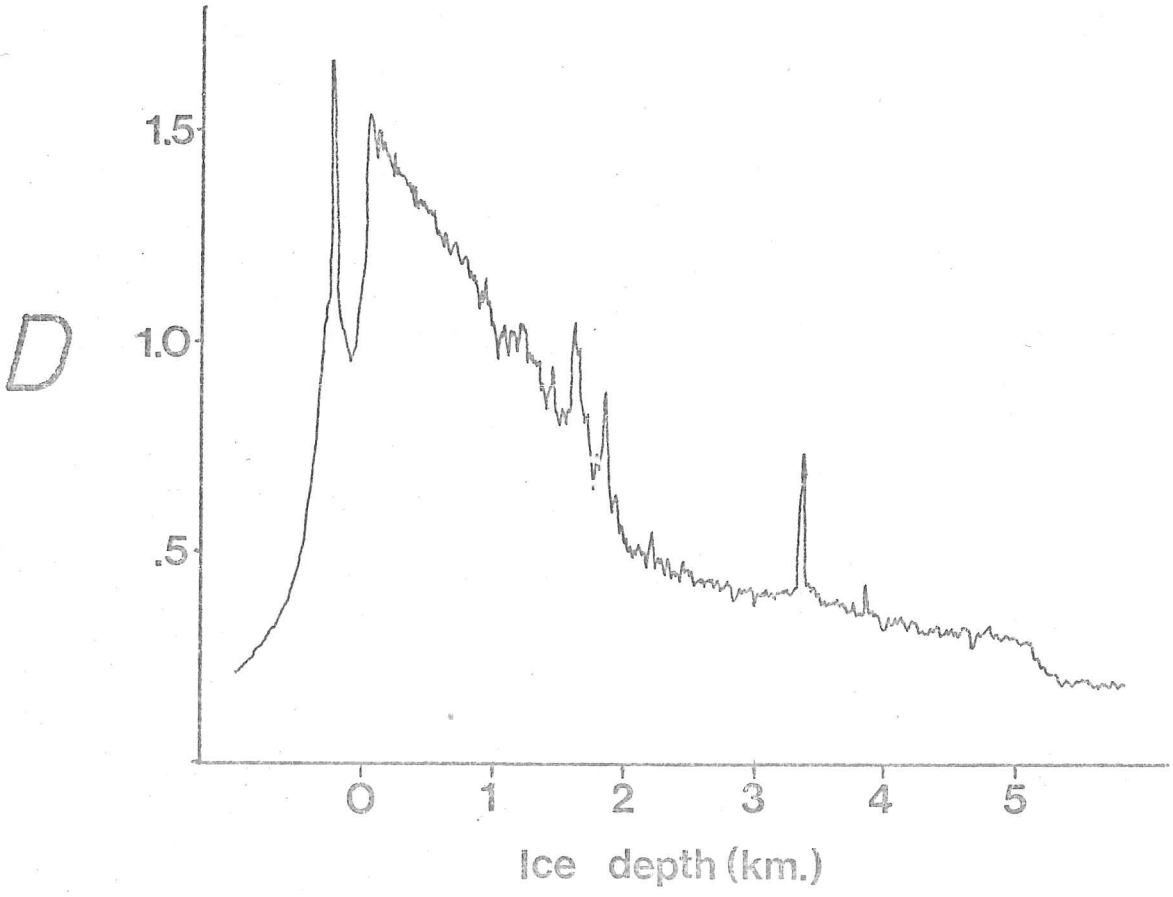

Fig.2.14 Densitometer trace from a location close to the position of the A-scope photograph shown in Fig.2.13

investigation of the echo strengths. A simple photodiode was used to scan the intensity of a back-projected image of the film. Little redundancy of information resulted since it was possible accurately to select the point of measurement, thus avoiding the need for intermediate analysis.

The photodiode was connected, via an amplifier and digital voltmeter, to a teletype, on which the readings of intensity were recorded.

The cost of the apparatus was minimal, and though the process of taking readings was comparatively slow, very little time was wasted on setting up the system. The circuit used is shown in Fig.2.15 and the combined photodiode and amplifier is shown in Fig.2.16, detached from the projection screen. The photodiode was mounted about .5 mm from the screen, and was masked to restrict its field of view to an area approximately 2 x.5 mm, orientated along the film, out of a total projection area of about 300 x 200 mm. The resolution in ice depth was similar to that of the film itself, and the larger aperture in the horizontal dimension allowing some averaging over the echo fading.

The results of the survey will be presented in the following chapter. As we have indicated, it is restricted to a qualitative description of the variations of echo character and strength. These problems, associated with the retrieval of information on the echo strength, would not have arisen had regular and frequent recordings been made of the signal envelope. Though a small number of such recordings were made, this was insufficient for them to be of use for the large-scale survey. Subsequent

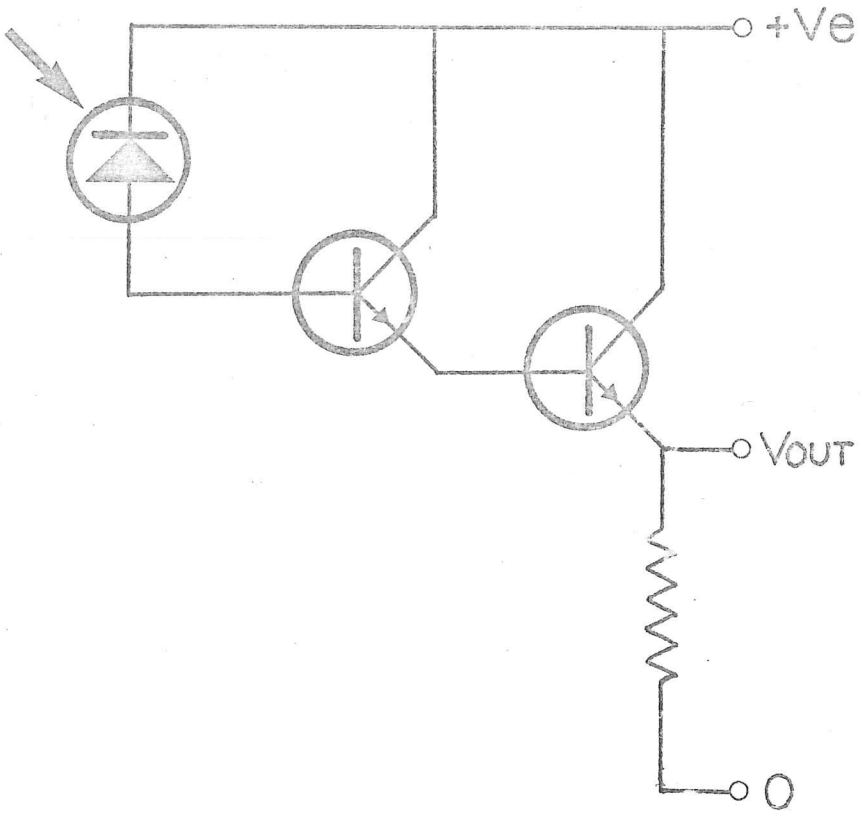

Fig.2.15 Circuit diagram of the photo-detector used to examine the optical densities of radio echo record films.

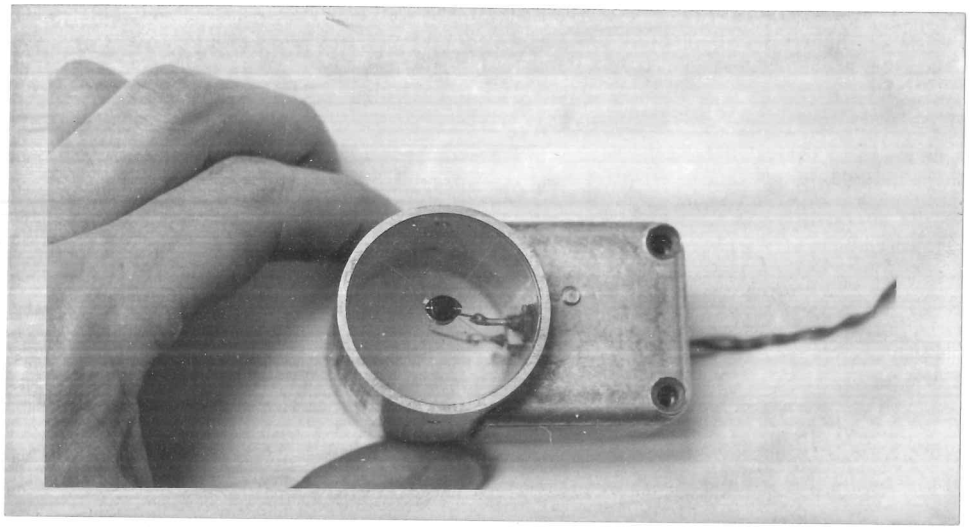

Fig.2.16. The combined detector and amplifier. The 'window' of the detector is formed by the semicircular masks on the front perspex panel.

work has been aimed at obtaining such quantitative information, in sufficient quantity for genuine statistical analysis.

CHAPTER 3 Section 1 : Interpretation of intensity-modulated records

In Chapter 2, the form of the intensity-modulated (often referred to as 'z-mod') records was described, and discussed in terms of the equipment used to produce and analyse them. Little reference was made to any results obtained, or any evaluation of the recording technique as such, beyond circumstantial difficulties. These are the subject of the present chapter, where we will examine the results of attempts to recover information concerning the strength and variation of the echoes, in addition to the depth information for which the technique is so well suited.

We have, in fact, in the records, a variable (the optical density of the film), which is a function of the received signal strength. We must discover how much information can be retrieved, bearing in mind from Chapter 2 that the function in question is neither single-valued, nor of well-defined shape. We must also discover what this can tell us about the state of things at the base of the ice.

Using the photodiode scanner mentioned in Chapter 2, the light intensity of the projected image of the film could be measured at any point. For this investigation, the intensity corresponding to the bottom echo was compared with that appearing immediately above it. Using the latter measurement as a standard, it was intended to allow as simply as possible for variations between the brightness levels of the different c.r.t.'s used, which would have a spurious effect on the measured intensity of the bottom echo. Where there is added exposure of the film at

this point due to high-angle surface scatter, or to internal reflections from the ice, (for example in crevassed regions, or in regions of thin, cold ice), errors will be introduced. (See Fig. 2.3d) However, the occurence of such scatter echoes, and of internal reflections down to the bedrock, is very infrequent in the high regions of the Antarctic Plateau with which we shall be dealing.

The output current of the photodiode was proportional to the intensity of the image of the recorded film at the point of observation, and was converted to a figure for signal strength as indicated in Chapter 2. A realistic calibration was taken to be a straight line, using fixed points at:

(background intensity; -170 dB signal)

(zero transmitted intensity; -140 dB signal).

Echoes were then divided into four groups, labelled qualitatively and defined roughly by the following inequalities: (see Figs. 2.3a, b, c)

class 1 (no echo) $P_r/P_t < -170$ dB

class 2 (weak echo) -170 dB $< P_r/P_t < -160$ dB

class 3 (medium echo) -160 dB $< P_r/P_t < -150$ dB

class 4 (strong echo) -150 dB $< P_r/P_t < -140$ dB

Remembering the uncertainties inherent in using any such calibration, the qualitative designations of these classes are more useful than their putative quantitative limits.

(3.1) Regional variation of echo strengths in East Antarctica

Records from seven flights were scanned in this way, readings being taken at intervals of one minute (equivalent to about 7 km) along the flight path. These covered the majority of the survey area. The figures derived were divided into the above classes and, with some averaging over distances of a few tens of kilometers, are mapped in Fig.3.1. A regional map (this is not an accurate contour map) shown in Fig.3.2 can be compared with maps of surface elevation, bedrock elevation, ice thickness or surface temperature (Figs.3.3,4,5,6).

The most obvious trend is a decrease of echo strength as one approached the coast. In the centre of the Plateau, the surface elevation is at its highest, and the ice is at its thickest and coldest. Though we might expect the great thickness to cause a reduction in the received power, this effect is over-ridden by that of the low temperature.

(3.1.1) Effect of Temperature and Depth of Ice

The absorption of radio waves in ice increases rapidly with increasing temperature. Laboratory measurements on 'pure' ice (Westphal, 1963) give the relation shown in Fig.3.7 for a frequency of 150 MHz. This relation has been found to give generally satisfactory results when compared with SPRI field data, and will be used as the standard for the remainder of this work. We have estimated values for the absorption over return paths through columns of ice of different depths and at different temperatures, to illustrate the relative effects:

(3.1) Regional variation of echo strengths in East Antarctica

Records from seven flights were scanned in this way, readings being taken at intervals of one minute (equivalent to about 7 km) along the flight path. These covered the majority of the survey area. The figures derived were divided into the above classes and, with some averaging over distances of a few tens of kilometers, are mapped in Fig.3.1. A regional map (this is not an accurate contour map) shown in Fig.3.2 can be compared with maps of surface elevation, bedrock elevation, ice thickness or surface temperature (Figs.3.3,4,5,6).

The most obvious trend is a decrease of echo strength as one approached the coast. In the centre of the Plateau, the surface elevation is at its highest, and the ice is at its thickest and coldest. Though we might expect the great thickness to cause a reduction in the received power, this effect is over-ridden by that of the low temperature.

(3.1.1) Effect of Temperature and Depth of Ice

The absorption of radio waves in ice increases rapidly with increasing temperature. Laboratory measurements on 'pure' ice (Westphal, 1963) give the relation shown in Fig.3.7 for a frequency of 150 MHz. This relation has been found to give generally satisfactory results when compared with SPRI field data, and will be used as the standard for the remainder of this work. We have estimated values for the absorption over return paths through columns of ice of different depths and at different temperatures, to illustrate the relative effects:

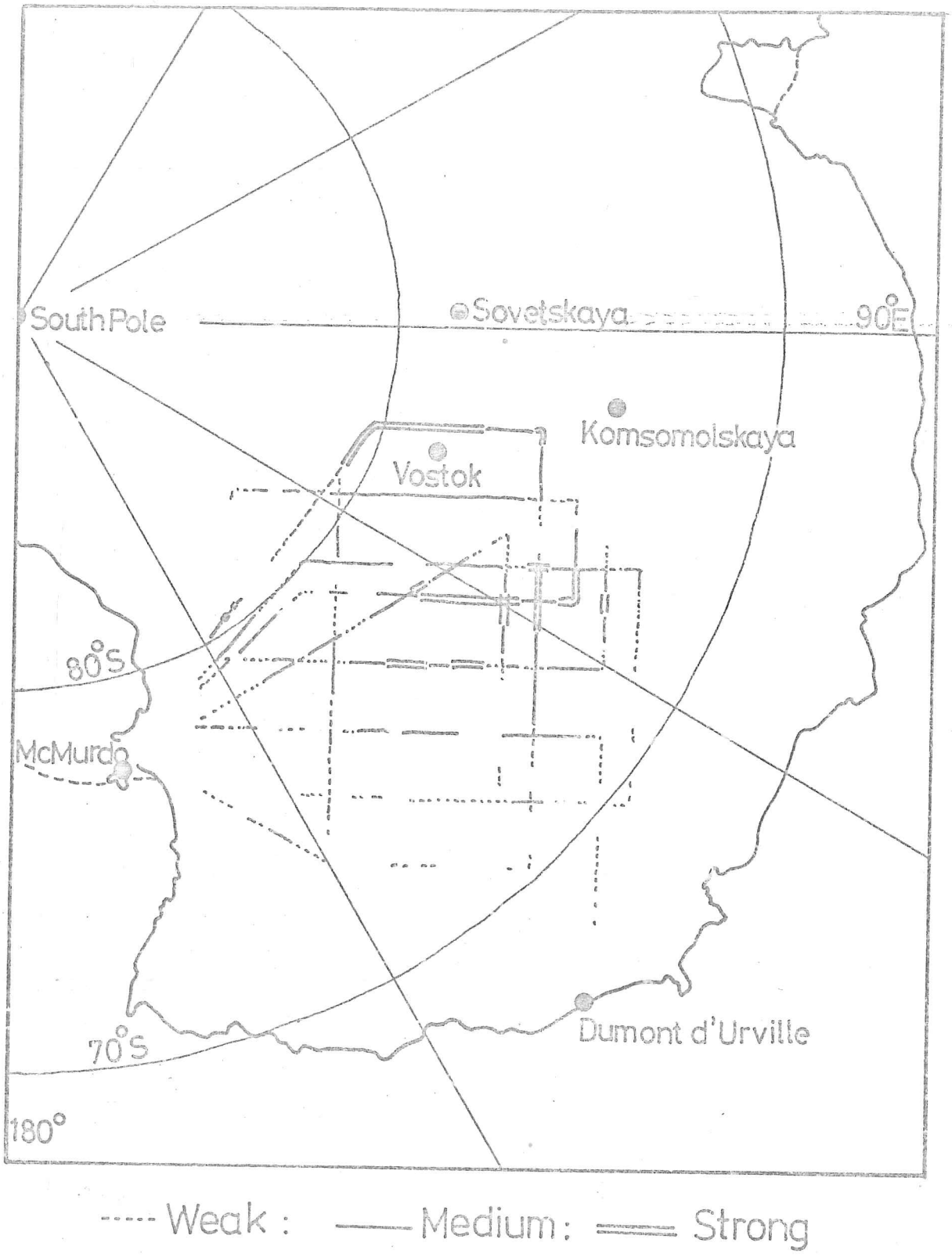

Fig.3.1. Map of relative echo intensities along radio echo flight lines.

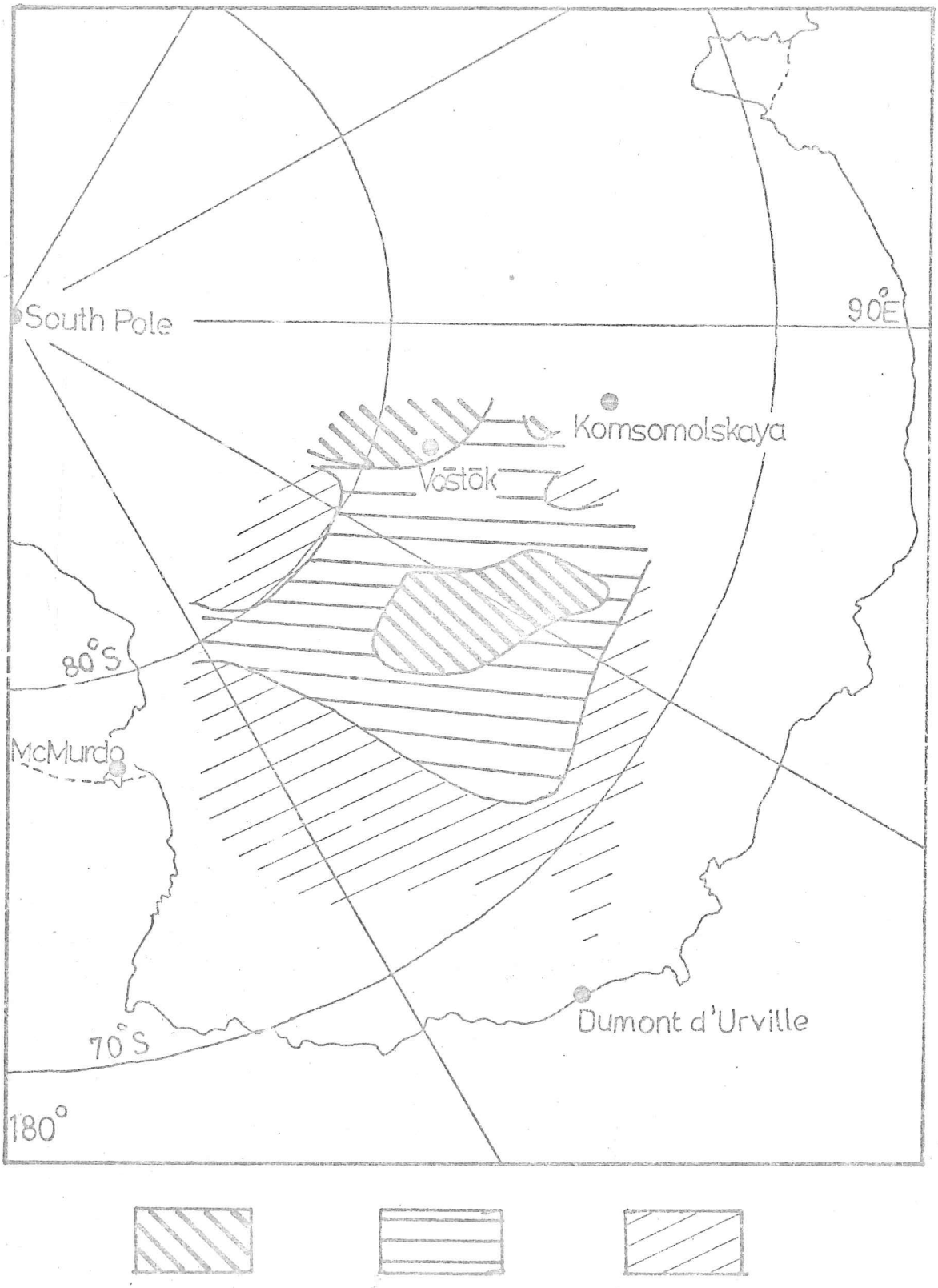

Fig.3.2 Regional mapping of relative echo strengths in East Antarctica.

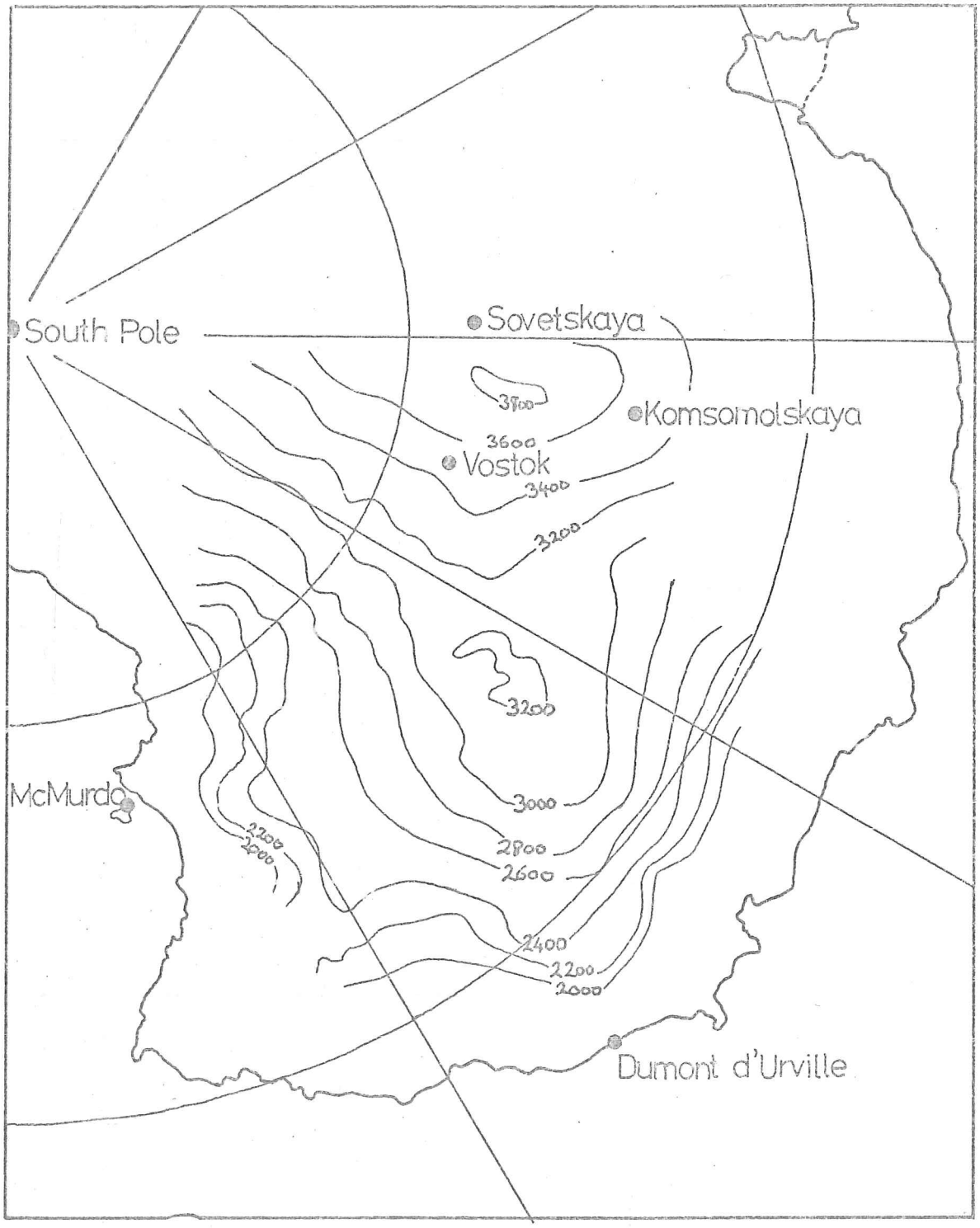

Fig.3.3 Map of surface elevations in East Antarctica (m.a.s.l), after SPRI (1974) publication.

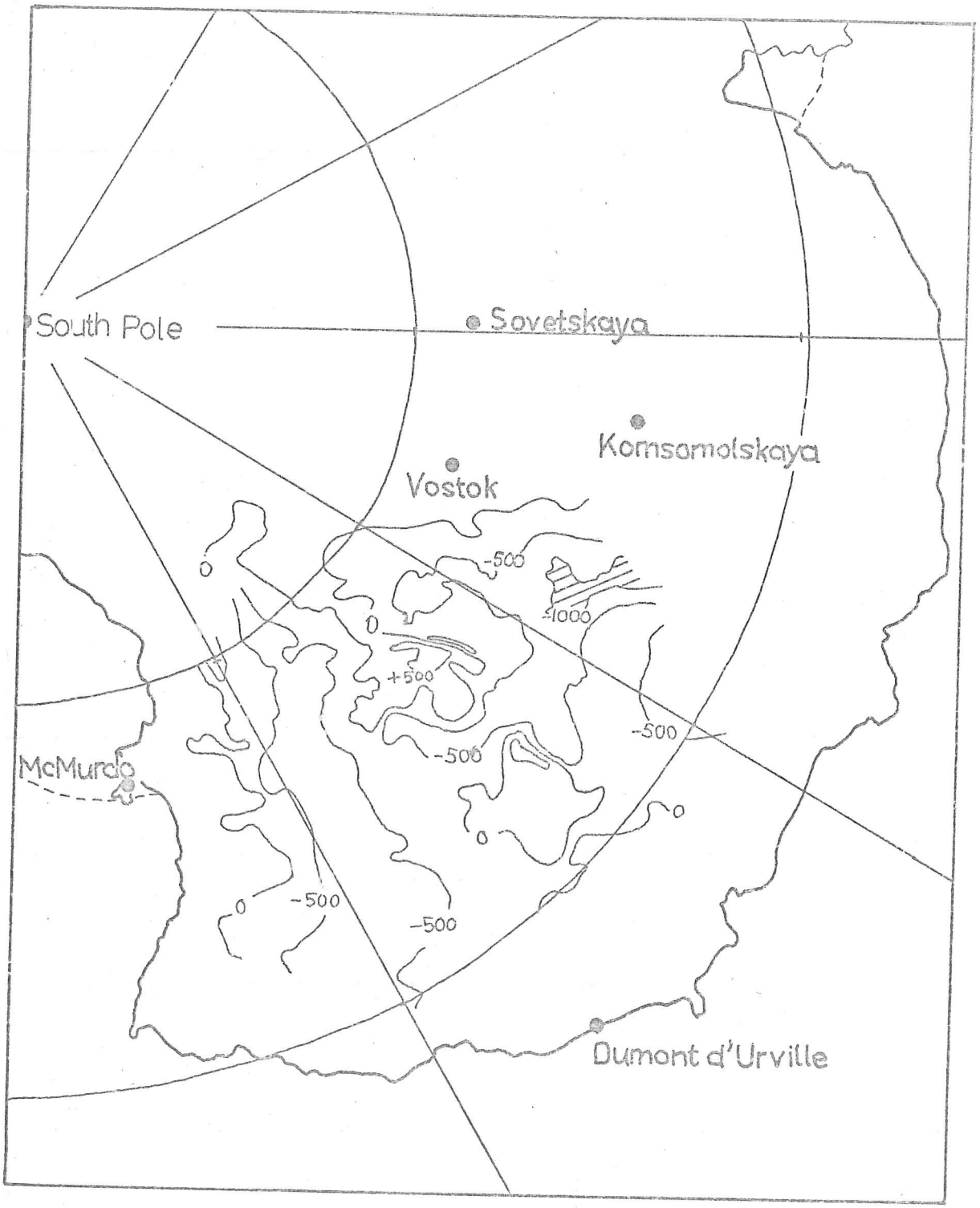

Fig.3.4. Bedrock elevations in East Antarctica (after SPRI 1974 publication) (metres above sea level).

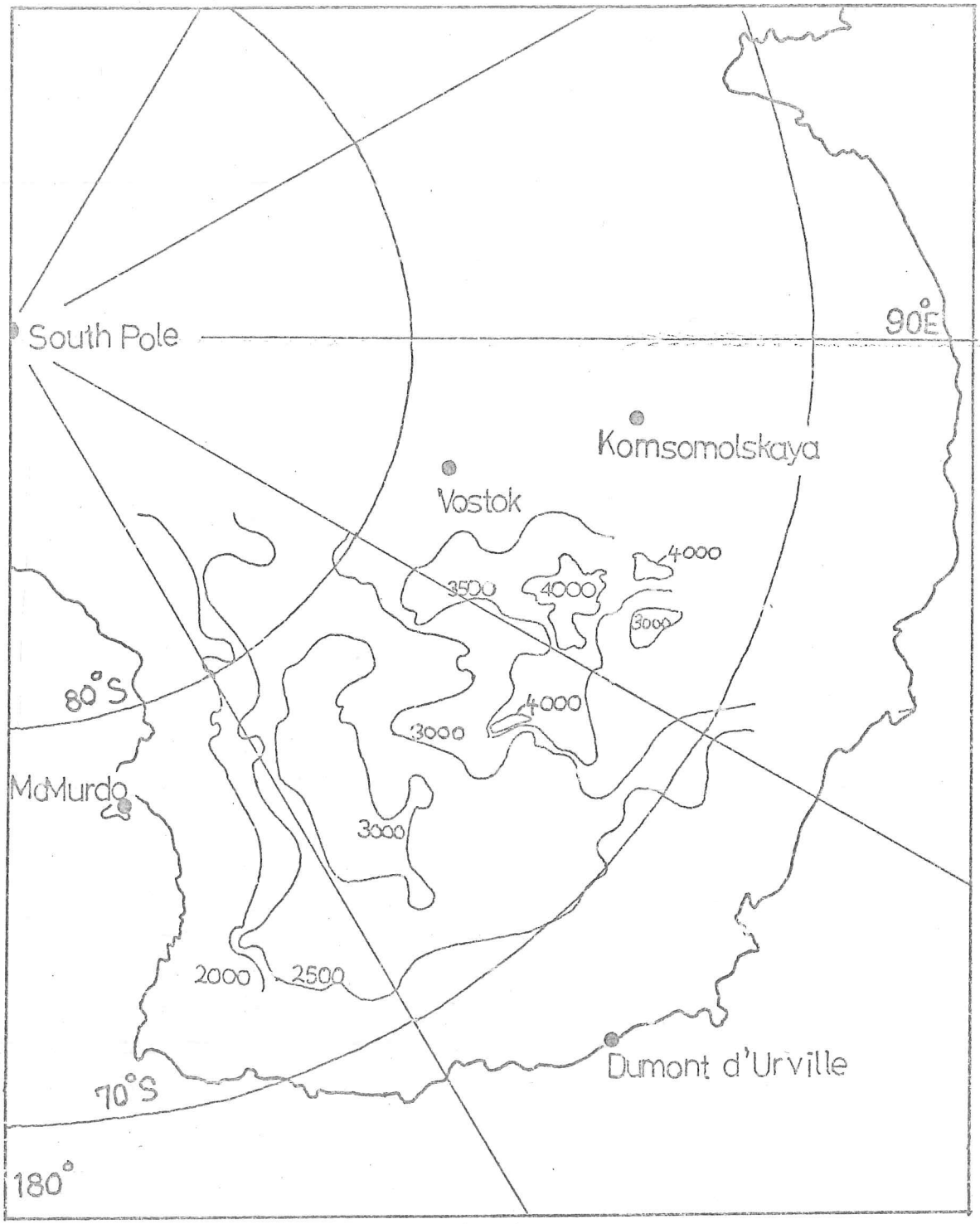

Fig.3.5. Ice thickness in East Antarctica (metres) after SPRI (1974) publication.

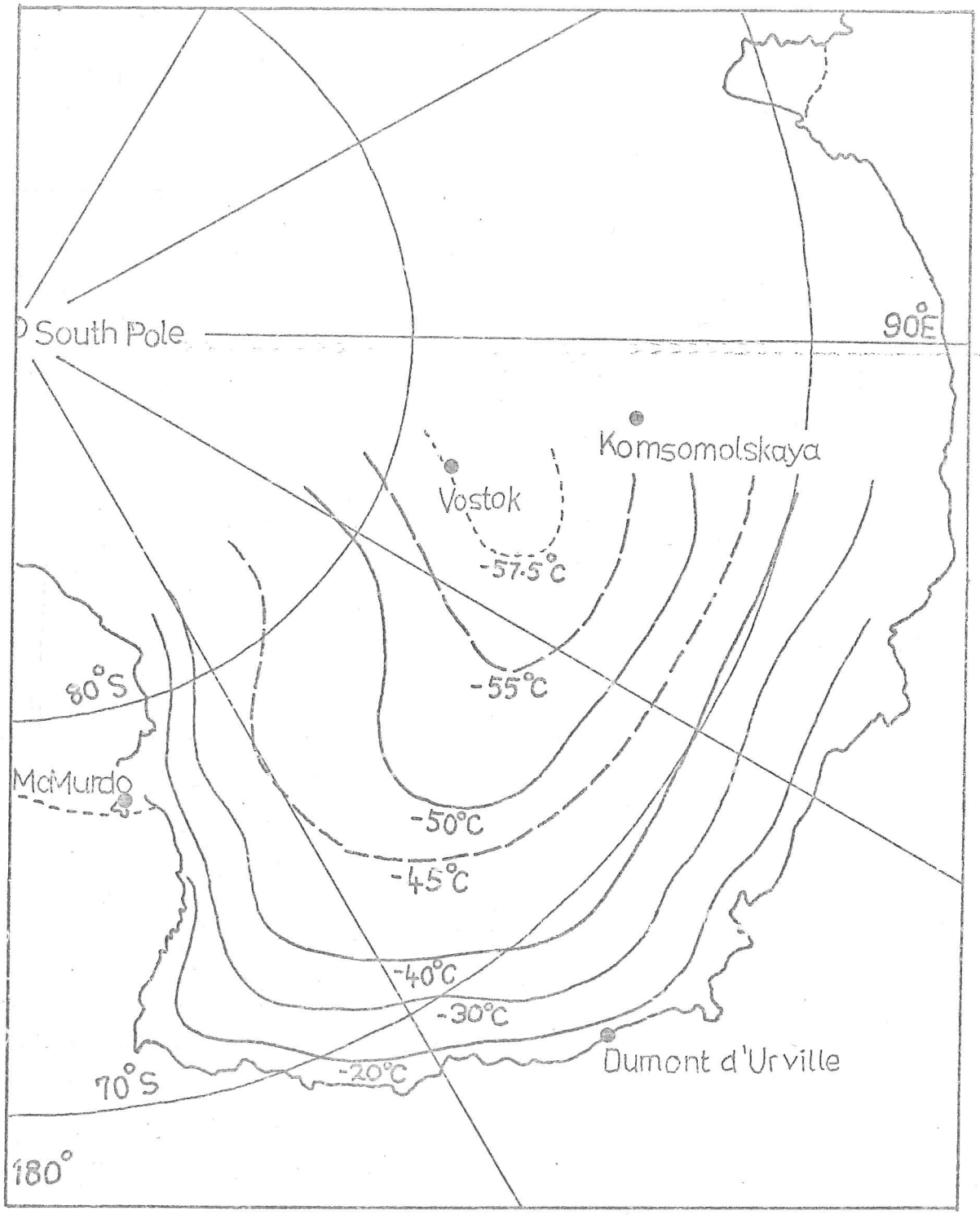

Fig.3.6. Ice surface temperatures in East Antarctica (after Budd, Jenssen and Radok (1971).

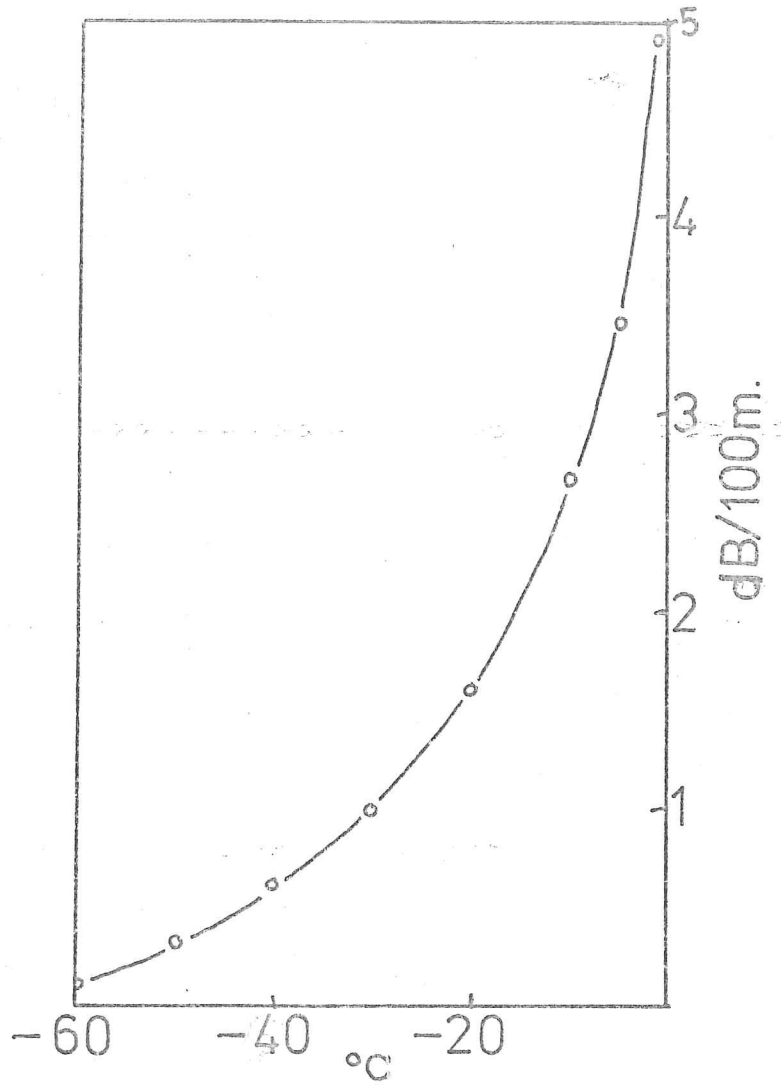

Fig.3.7. Dielectric absorption of electromagnetic waves at 150 MHz, found by Westphal (1963) for tunnel sample from Greenland.

Ice Thickness	Mean absorption temperature	2-way absorption
4000 m	$-30^{o}C$	80 dB
3000 m	$-30^{o}C$	60 dB
4000 m	$-20^{o}C$	128 dB
3000 m	$-20^{o}C$	96 dB

It is quite possible, then, for the temperature effect to dominate that of sheer depth, and we can see that the resultant contrast can be quite large: the absorption expected in 3000 metres of '-20^{o}' ice should exceed by 16 dB that in 4000 metres of '-30^{o}' ice. The temperatures used are weighted means over the ice column, taking into account the relation between temperature and absorption. They represent reasonable values for the East Antarctic Plateau (Campbell, Unpublished).

A detailed comparison of the echo strength map with the relevant strength-determining parameters (including aircraft terrain clearance) was not carried out. The echo strengths are not accurate to better than $\pm$ 5 dB, and the temperature profiles in the ice are not sufficiently well known to allow detailed evaluation of the observed strengths. Looking ahead to Section 2 of this Chapter, there are indications that the basal temperature gradients in this area are higher than has been deduced by Budd, Jenssen and Radok (1971), and that calculated profiles may therefore not be reliable.

(3.1.2) High echo strengths near 'Dome C'

Looking back to Fig.3.2, a further feature of interest is the extension of strong echoes from the centre of outflow of ice ('Dome C') into the area designated 'X' in the figure. Surface

temperature contours have a similar form to those of the surface elevation in this area: that is, there is no extension of low temperatures corresponding to that of the strong echoes. Nor is a decrease evident in the ice thickness (in fact, some of the deepest ice encountered occurs in this region: the trend is towards the deep subglacial trough mentioned in the fieldwork account in Chapter 2).

We must look for the cause of the strong echoes either in a drastically altered temperature profile (which is not reflected in the surface temperature), or in a higher reflection coefficient at the base of the ice, or both.

A typical experimental situation in this part of the ice sheet would be one where the aircraft was flying at an altitude of 5,000 metres above sea level, the bedrock was approximately at sea level, and the ice 4,000 metres thick. In this situation the attenuation due to geometrical spreading of the wavefronts is given by the formula:

$$A_g = \frac{\lambda^2 . g^2}{64\pi^2 . (h+d/n)^2}$$

where λ is the radio wavelength (in air), = 5 metres

g is the antenna gain (+5 dB),

h is the aircraft's terrain clearance,

d is the ice thickness,

n is the refractive index of ice ($\simeq$ 1.8).

Putting in the given values for the various parameters, we have:

$$A_g = -74 \text{ dB}.$$

For a similar situation, where h=2,000 metres, and d=3,000 metres, the attenuation is little different at -75 dB.

If the system performance (the ratio of the transmitted power, P_t, to the smallest detectable received signal power) is 170 dB, this allows a total attenuation due to absorption and reflection losses of 95 dB before the mean signal level is lost. (There may still be peaks which rise above this level and are detectable, due to focusing or random phase additions of reflections from the rough bedrock surface).

Temperature profiles and absorption losses have been calculated by Campbell for stations along the French IAGP traverse from Dumont d'Urville towards the centre of the ice sheet. For a characteristic situation we look at a station high on the Plateau, with ice thickness of 3260 metres, an assumed geothermal flux giving rise to a temperature gradient in ice of 0.024 deg/m, surface temperature of -54.5°C, and surface accumulation of 6 mm water equivalent per year. The basal temperature is calculated to be -2.5°C, and the total dielectric absorption for a one-way passage is 38 dB. The absorption over two-way passage through the ice is therefore a factor of 76 dB, leaving a residual sensitivity of about 19 dB. (The reflection loss on each passage through the ice surface is about 0.3 dB, and has been ignored).

The bottom surface of this column is at the pressure melting point, with a calculated melt of about 75 microns of ice per year. With a non-uniform bedrock surface, we can expect differential basal stresses to give rise to some areas of melting and some where re-freezing takes place.

In areas where no melting occurs we can expect a reflection coefficient of between -10 and -20 dB, giving +9 to -1 dB for the residual strength as seen (or not seen) in the receiver, and the same should be true of re-frozen areas. Where melting occurs, the reflection coefficient will lie between this value and that (close to -0 dB) corresponding to a boundary with deep water. The exact value will depend on the thickness of the film of melt-water, and also on its salinity. Where irregularities in the bedrock surface allow the formation of pools of more than a few centimetres' depth with appreciable salinity the reflection coefficient will approach unity, yielding residual echo strengths up to 19 dB above the noise level. In such an area we expect to see large contrasts between reflections from melting and frozen regions.

For a position at 350 km along the traverse, with an ice thickness of 3980 metres, geothermal gradient of 0.032 deg/C metre, surface temperature of -42°C, surface accumulation of 200 mm/year and horizontal surface velocity of 9.7 metres per year, the absorption reaches 45 dB for a one-way passage. Here, the two-way absorption is such (90 dB) that we could not expect to see reflections at all, except from a highly-reflecting surface such as that of liquid water. Reflections from rock would be lost in noise, unless strongly focused by the bedrock surface undulations.

It can be seen from the strength, temperature and depth maps of Figs.3.2,5,6 that, apart from the high contrasts sometimes seen in adjacent echoes, many reflections can be seen in areas where we might expect the absorption to be too great in conjunction with the low reflection coefficient from an ice-rock boundary. These observations, accompanied by the anomalous reflections

described in Section (3.2), lead to the conclusion that considerable areas of the base of the East Antarctic Ice Sheet are in fact at the pressure melting point.

This is the result of the examination of recorded echo characteristics, whose balance between qualitative and quantitative form and status has been described. We feel that the results and conclusions drawn are representative of the data available. However, we have not yet made great use of the detailed qualitative information available in the records, by means of which individual anomalous echoes may be identified, described and related. Section (3.2) deals with an investigation into several instances of anomalous reflections, making use of this aspect of the recording technique.

(3.2) Subglacial lakes in East Antarctica

Since the determination of the continental nature of the Earth's crust in the Antarctic, it has been generally considered that the ice-sheet as a whole is grounded, rather than floating, in contrast to the sea-ice cover of the Arctic oceanic basin.

The existence of liquid water beneath the ice of East Antarctica was first postulated by Robin, Swithinbank and Smith (1968). During the 1967-68 season of SPRI-NSF radio echo sounding, an isolated echo was observed in deep ice near Sovetskaya Station. The depth was such that, with a reflection coefficient at the base of the ice corresponding to a normal ice-rock boundary, no echo could be expected: the idea of a pocket of water was invoked to explain the observation, as being the most likely source of

an abnormally strong reflection.

In spite of this, basal melting has not been thought to occur widely in East Antarctica (in contrast to West Antarctica, where it has been accepted for many years that basal melting took place, particularly since Gow (1968) encountered water at the bottom of the deep drill hole at Byrd Station). This conclusion was supported by computed model studies of the ice sheet, performed by Budd, Jenssen and Radok (1971). Using interpolated values of ice depth, surface elevation, accumulation, temperature and slope, and an assumed value for the geothermal flux, they calculated temperature-depth profiles and velocity distributions for the entire ice sheet, basing their calculations on the assumption of a steady state regime. Their estimate for the basal temperature in the central region of the ice sheet, East of Vostok Station range from $-15^{\circ}C$ to $-30^{\circ}C$. Though a further calculation was performed using a geothermal flux increased by 50% from the previous value, which did suggest the possibility of extensive basal melting, the low temperature model has been generally accepted as representing the closest approach to the real conditions.

This acceptance has been implied in a proposal, put forward by Zeller, Saunders and Angino (1973) to use the Antarctic ice sheet as a secure, international depository for radioactive wastes from nuclear power installations. Their argument is based on the temperature estimates of Budd, Jenssen and Radok, and they estimate that a canister of waste arriving at the bedrock might be expected to remain embedded for at least 10^5 years. Since the alternative methods of disposing of nuclear wastes involve high, in some cases prohibitive costs, this appeared to be an

extremely attractive proposal. However, its viability rests entirely on the validity of the assumed value for the geothermal flux. It is also necessary to the proposal that the ice sheet should in fact be in a steady state, and in formulating the argument, the authors have relied on calculations which rely on this situation as a premise.

The questions of temperature and stability of the ice sheet have been taken up by Weertman (1973), but without direct evidence of basal temperatures, the argument remained academic.

We shall go on to present evidence which we believe bears directly on this problem, and which should draw our attention to the stability of the ice sheet even in the absence of the disturbing influence of such heat-producing wastes.

During the 1971/72 survey, several instances of unusual echoes were observed, which are best accounted for in terms of pockets of melt-water, providing clear evidence that the temperature regime at the base of the ice is not as has been generally accepted (Oswald and Robin, 1973).

Apart from the survey of recorded echo intensity discussed in Section 1 of this chapter, the film records have also been scanned by eye for variations in other echo parameters such as the amplitude of fading, the fading length, and the length (in delay time) of the echo 'tail'. The records generally are of high visual quality, and these characteristics may be distinguished, and contrasted from area to area.

We must first give an indication of the magnitudes of these aspects of the echoes found over the majority of the survey area, before going on to point out anomalous observations and how they differ from the main body of data.

(3.2.1) Fading amplitude (observed)

The amplitude of fading observed in these records can generally be placed in one of two categories: high- and low-contrast fading. (These terms are used in preference to 'strong/weak' or 'deep/shallow' fading, as these are ambiguous). Low-contrast fading is expected to occur only for reflecting surfaces whose vertical scale of roughness is small compared with the radio wavelength. As the roughness scale approaches and then exceeds $\lambda/4\pi$ (Harrison, 1972), the contrast of fading will increase to the point where total destructive interference may occur (there are present differences of at least 180° in the phases of different reflections), and the echo momentarily disappears at intervals. Above this level of relief, the echo power distribution tends to the invariant shape described in Section (1.2.5), characterised by a width of about 15 dB. Though we cannot derive a reliable observed distribution from the 'z-mod' records, we may judge whether the fading amplitude is of THIS order, or much less.

The fading observed over the great majority of the 1971/72 survey belongs to the high-contrast class, indicating that the vertical scale of roughness is comparable with the radio wavelength in ice ($\lambda_i \simeq 3$ metres). We define a quantity ϕ_o, given by:

$$\phi_o = \frac{4\pi\alpha_o}{\lambda}$$

where α_o is the r.m.s. vertical deviation of the rough surface from its mean plane. ϕ_o describes the phase difference introduced by α_o in a reflected wave, for normal incidence and reflection.

(3.2.2) Fading Lengths

It is more difficult to characterise the horizontal scale of variations of the echo strength (the 'fading length'). For our present purposes, we define a minimum fading length for the 'first return'*, in terms of the geometry of the echo-sounding configuration, involving the length of the rectangular pulse, p:

$$\tau_{p\,min} = \frac{\lambda}{8}\sqrt{\frac{h_a+d/h}{p_{air}}} \simeq \frac{\lambda}{8}\sqrt{\frac{h}{p_{ice}}}$$

Fig. 8 shows the geometry of the situation, from which the above formula was derived, using the approximations

$$\cos\theta_{e_0} \simeq 1 - \theta_{e_0}^2/2 \quad \text{AND} \quad \sin\theta_{e_0} \simeq \theta_{e_0}$$

This figure is calculated on the basis that, if all the reflected power were to occur at this limiting angle, using a one-dimensional model, the power maxima of the fading pattern would be separated by a distance $\frac{\lambda}{4}\sqrt{h/p}$, and we define the 'fading length' for this situation as (separation of maxima)/2. (This simple case would give rise to sinusoidal fading: in more complex cases we shall use a different approach to the 'fading length'. It is perhaps doubtful whether, except in such a simple case as this, a single figure describing the fading is of much value.)

If reflections are distributed evenly over the angular interval from θ_{e_0} to 0, from a 2-dimensional surface, we expect the average fading length to increase by a factor of approximately $2\sqrt{2}$. (This figure may be arrived at by an inspection of the geometry).

* By the 'first return' is meant the echo for the delay when the trailing edge of the pulse has just returned from vertically below the observer.

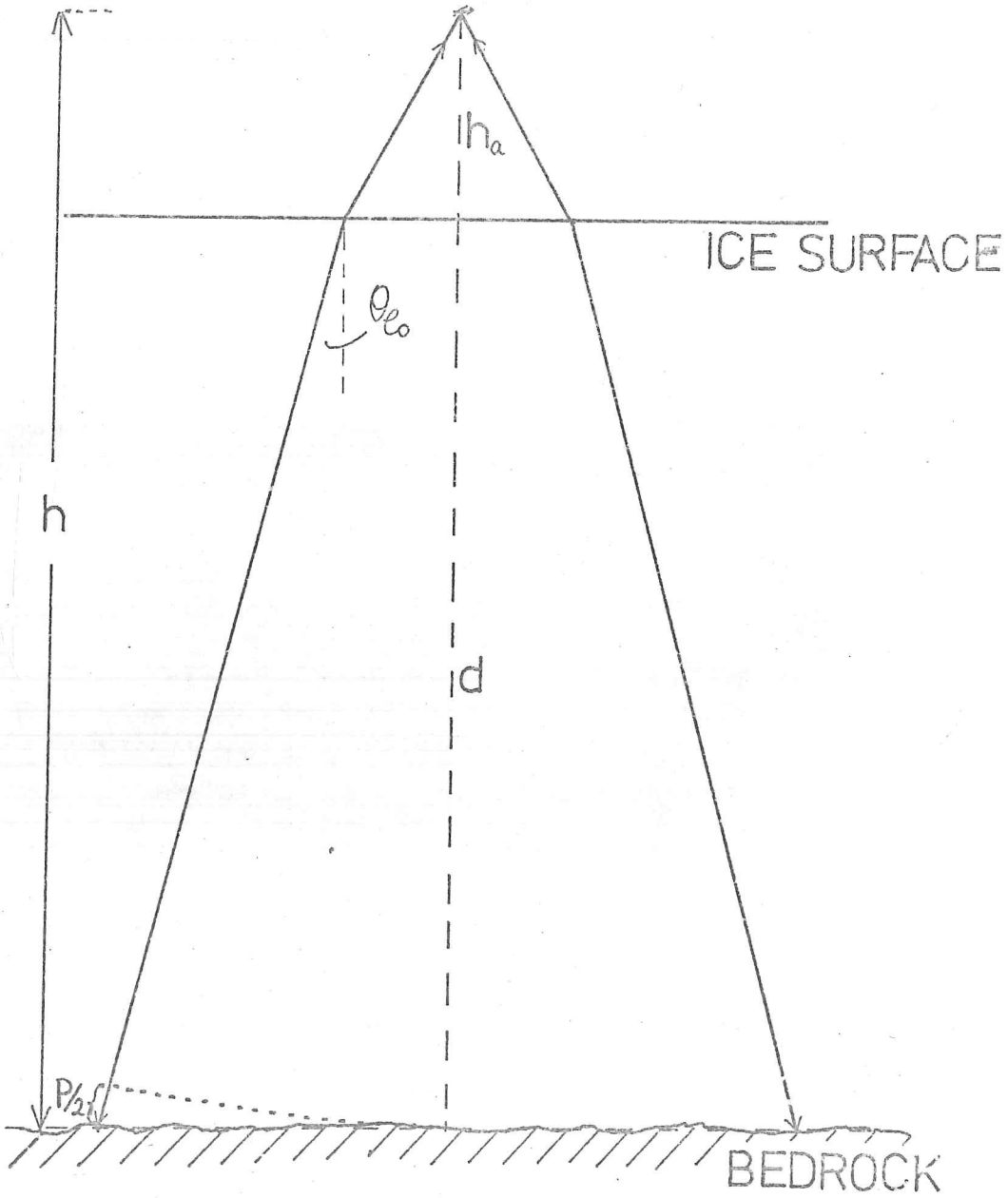

Fig.3.8. Simple one-dimensional geometry indicating the illuminated area for the 'first return'.

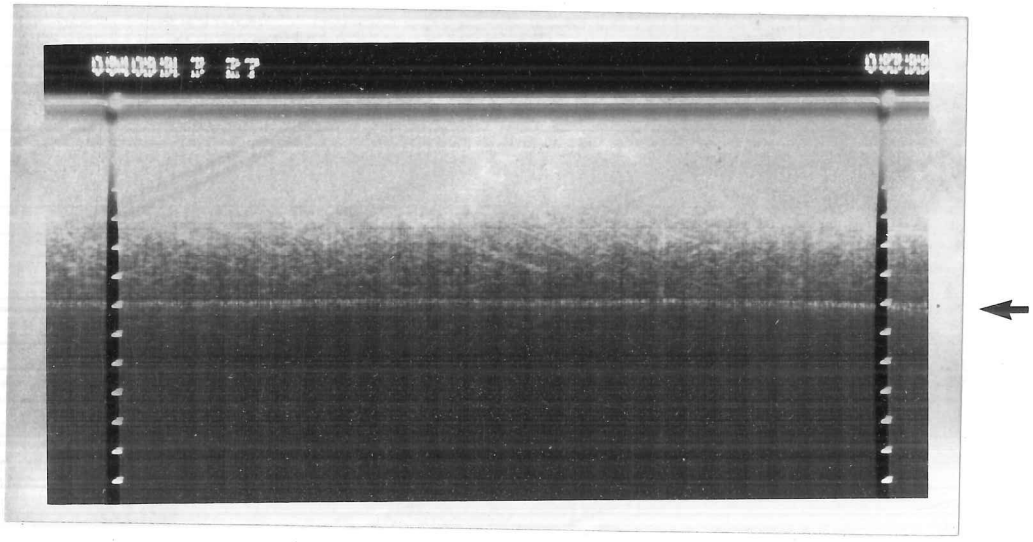

Fig.3.9. An example of a bedrock echo displaying typical fading.

The pulse length used throughout the 1971/72 season was 170 metres. Inserting this figure in (3.5), we derive a value of approximately 5 metres for τ_{Pmin} after conversion to the 2-dimensional, even-distribution model.

With the present recording system, the c.r.t. spot size, and positional irregularities in the film movement are of the same order of magnitude as the recorded minimum separation of power maxima. This makes it hard to evaluate short fading lengths: however, we commonly observe separations between power maxima of between 10 and 50 metres, and it therefore appears that the fading is generally longer than the minimum. (Fig.3.9).

If the local slopes obtaining in the bedrock surface generally exceed the value of θ_{e_0}, we should expect the fading length to remain substantially constant at the minimum value. Since this is not observed to be the case, with the fading length frequently exceeding the minimum value, we deduce that the local slopes do not generally exceed θ_{e_0}.

Given that θ_{e_0} in this case is approximately 10° we may derive a lower limit for the characteristic horizontal size, T, of the irregularities. Knowing that α_0 is greater than $\lambda/4\pi$, we deduce that T is at least of the order of λ. With this result we may assume that reflections from the bedrock may largely be described in the terms of geometrical optics, and that diffraction effects need not be taken into account for the surfaces generally encountered in the Antarctic survey.

(3.2.3) Echo extension due to wide-angle reflections

The echo tail is a further source of information on the distribution of slopes in the surface. A portion of the spherical

transmitted wavefront, travelling at an angle θ to the vertical, can be specularly reflected back to the antenna only if slopes of angle θ to the horizontal exist in the rough surface. (The picture is more complex if diffraction effects, as opposed to geometrical-optical effects, play an important role. However, we have shown that this is unlikely.) From the maximum delay at which significant power is seen to be returned to the receiver, and from the fall-off of power with increasing delay, we may examine the angular distribution of facets of the reflecting surface.

In the present case, the echo tail is generally not 'very long' compared with the transmitted pulse, extending the echo to twice or three times this length at most, at which point the echo power is reduced by 10–20 dB below its maximum.

When the sounding is carried out from the air, the added delay time of high-angle reflections is exaggerated by the effect of refraction at the ice-air interface. Without refraction, the additional range associated with reflections from facets at a tangential gradient β is given by:

$$\delta = \left(\sec\left(\tan^{-1}\beta\right) - 1\right)h$$

If refraction is taken into account, the added 'in ice' range is:

$$\delta_r = d\left(\sqrt{1+\beta^2} + 1\right) - \frac{h}{n}\left(\sqrt{1+\beta'^2} - 1\right)$$

where β' is given by $\sin\beta' = n.\ \sin\beta$ and n is the refractive index of ice. Combining 3.5 and 3.6 , we have, for $\sin^2\left(\tan^{-1}\beta\right) \ll 1$, n = 1.8

$$\delta_r \simeq \frac{d\beta^2}{2} + 0.9h\beta^2$$

For a typical case where the echo extension is equal to the transmitted pulse length, the added range is equivalent to about 85 metres of ice depth (remembering the two-way passage through the ice).

Entering our usual figures for terrain clearance, ice thickness etc., we have

$$\delta \simeq 3200\beta^2$$

From this argument we deduce that the gradients of facets in most of the bedrock surfaces encountered during the survey range up to about 1/6. This is compatible with the result derived from considering the fading lengths, where we deduced that the slopes were generally less than 10°. This result also supports our argument that diffraction effects are not important in determining the angular spectrum of reflections from the bedrock surface.

We have deduced, from qualitative observations of the echoes, that ϕ_o is greater than unity. Without detailed information about the variance and autocorrelation function of the received power, we cannot define this quantity more accurately. We have more accurate information only on the slopes of the surface.

For the majority of the area covered by this survey, we consider that the bedrock surface can be characterised as follows:

(1) The r.m.s. slope is less than 10°

(2) The r.m.s. vertical deviation in the roughness is greater than about .3 metres.

(3) The horizontal size of irregularities is greater than about 2 metres.

(3.2.4) Observation and interpretation of some unusual echo characteristics

However, these characteristics were not invariable. In several locations (at least seventeen have been noted) the echo is seen to take on a markedly different form. The mean strength, as indicated by the exposure of the record film, increases abruptly, and the character of the fading changes: contrasts are no longer easily observable in the echo trace, and any existing changes occur over distances of 200 metres or more. Examples of these unusual echoes are shown in Fig.3.10. Their positions are mapped in Fig.3.11.

The low-contrast fading and long fading lengths are charcteristic of smooth reflecting planes, whose extent varies, from site to site, between 1 and 15 km. The vertical scale of undulations can be said to be less than.5 metres, and the horizontal scale 200 metres or more. The change from a rough to a smooth reflector may be expected to increase the maximum echo power to some extent (not more than 2-3 dB for rough surfaces of the type described, and the present sounding configuration), but cannot account for the changes of 10-20 dB observed. We believe that this must be accounted for in terms of a change of the power reflection coefficient of the surface.

Since the reflection coefficient of an ice-rock boundary lies in the region 10-20 dB, this implies that the smooth surface is almost a total reflector. This can only be achieved if the underlying material has a high permittivity, and in the context of the base of an ice sheet, water seems the obvious choice. Its relative permittivity is approximately 80: the skin depth will

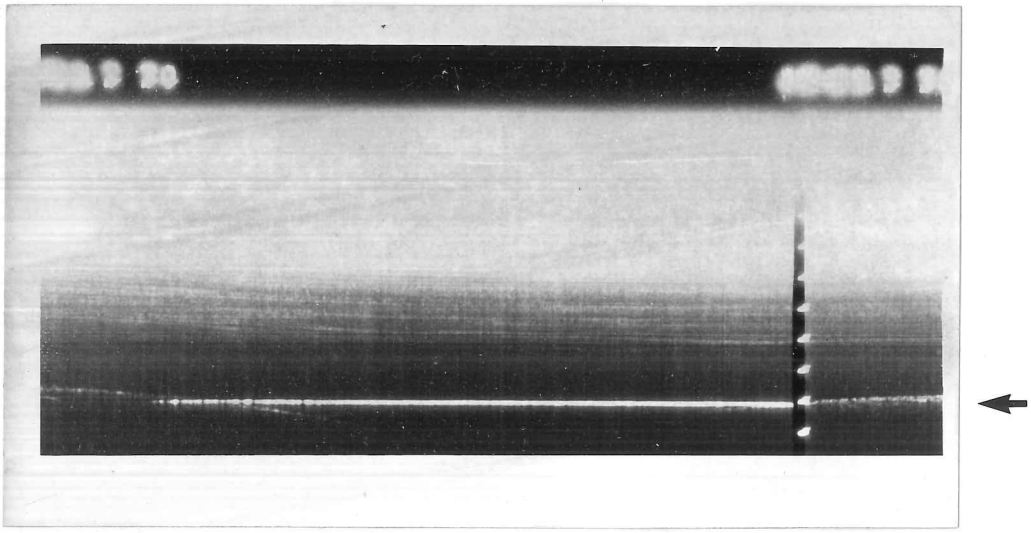

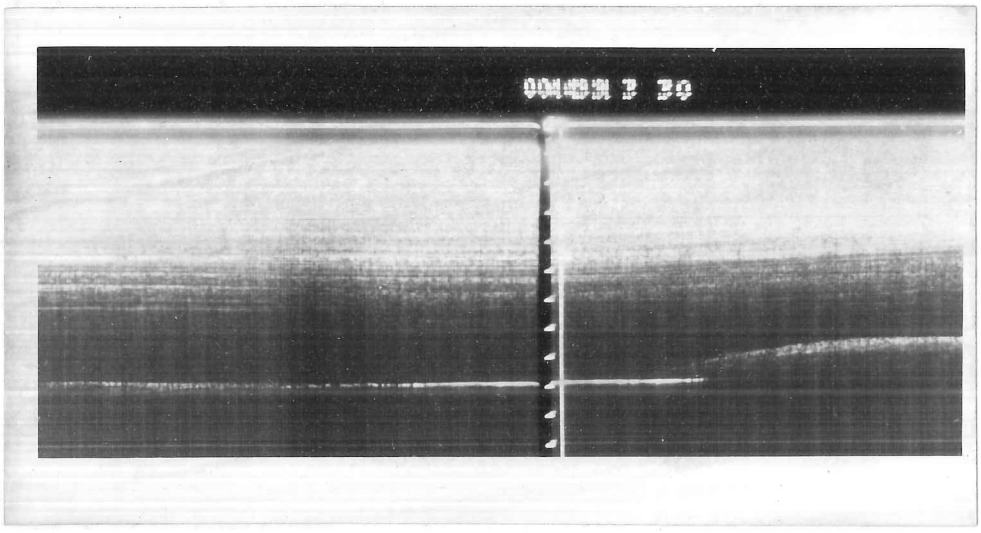

Fig.3.10. Two examples of'lake' echoes.

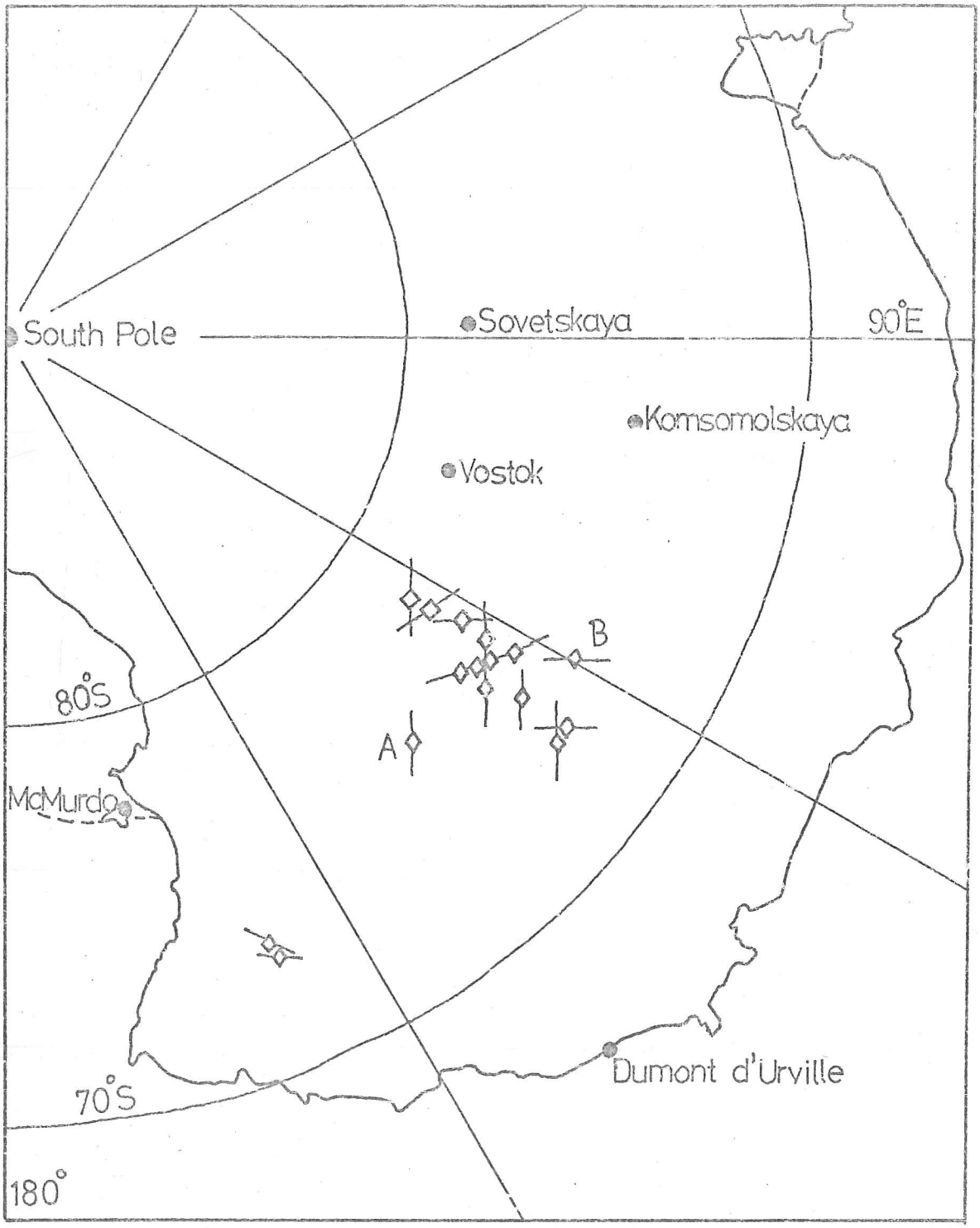

Fig.3.11. Positions of observed 'lake' echoes. The transverse lines indicate the direction of the flight line along which the echo was observed.

vary strongly with its degree of purity, but for water which has been in contact with rocks for a long period we may expect it to be small (of the order of a few cm).

The larger-scale topographical nature of the profile at these points lends weight to their interpretation as water pockets. The rock is seen to slope upwards away from the smooth surface, giving a distinct visual impression of a liquid-filled basin.

The smooth surfaces are close to horizontal, with gradients mostly less than 1:150, though one example exhibits a gradient of about 1:50 (Fig.3.12). Though it might seem that non-zero gradients are incompatible with a fluid-ice interface, this is not the case, since the pressure gradient due to the finite surface slope of the ice must be compensated in the fluid (under low-flow conditions) by a gradient in the fluid surface.

For a fluid of density ρ_f, underlying ice of density ρ_i along any horizontal axis, a gradient of β_s in the ice surface must be balanced by a gradient of β_f in the fluid surface, such that

$$(\beta_s - \beta_f)\rho_i + \beta_f \rho_f = 0$$

For an ice-water interface, $\rho_f/\rho_i \simeq 1.1$, and

$$\beta_f \simeq -10\beta_s$$

Thus any existing surface slope will be reflected in the lower surface, exaggerated by a factor of 10 and in the opposite sense. In order to obtain a gradient of 1:50, with surface slopes being generally less than 1:500, a fluid with density close to that of ice must be present.

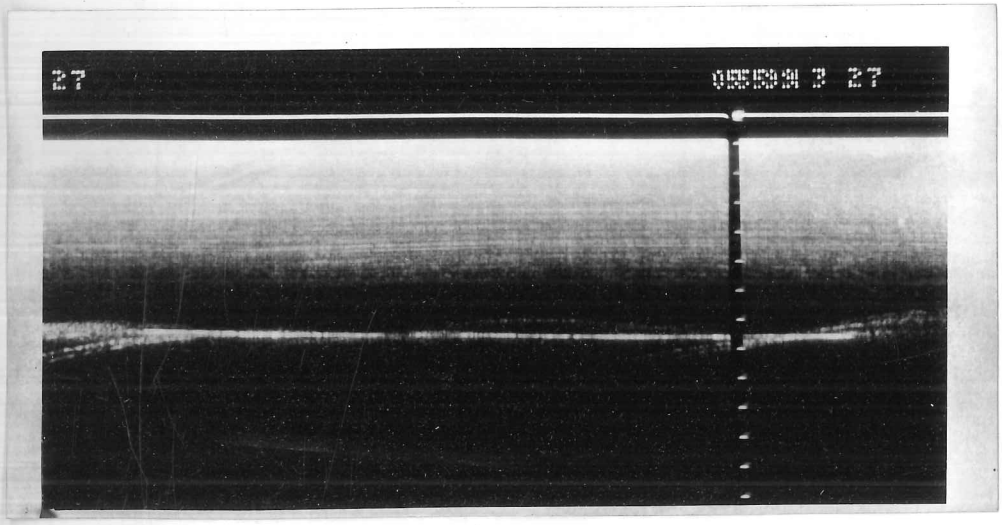

Fig.3.12. A 'lake' echo with an interface gradient of approximately 1 : 50.

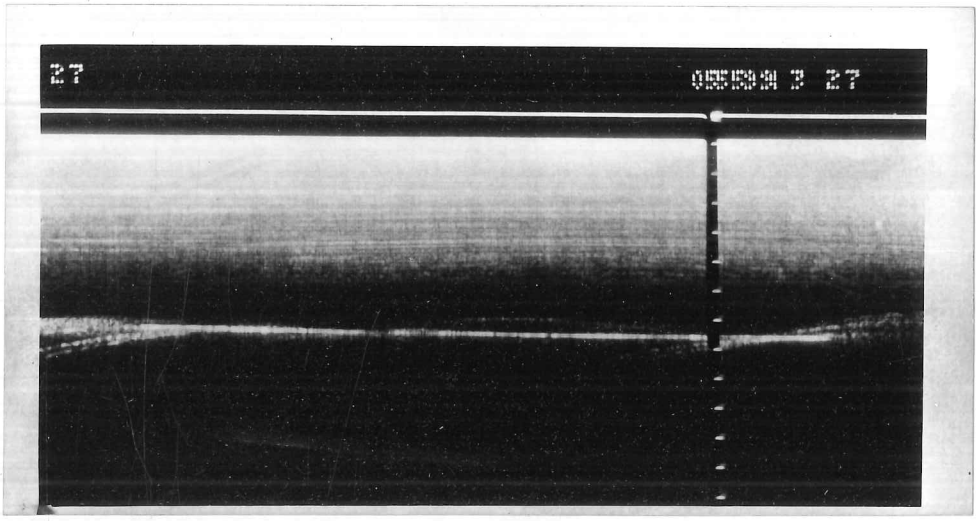

Fig.3.12. A 'lake' echo with an interface gradient of approximately 1 : 50.

The gradients in most cases are too small to be accurately measured from the radio-echo film. However, in the two steepest locations, we find gradients of 1:(50±10) and 1:(70±10) respectively. We cannot measure the surface gradient directly from the film, but we obtain values of approximately 1:1000 for each site, from the most recent contour map (SPRI publication, 1974), on which we will allow an error of ±50%. Using the above formula, we obtain values for the fluid density of

$$\rho_e = (970 \pm 40)\ kg/m^2 \text{ AND } \rho_e = (990 \pm 40)\ kg/m^2$$

respectively, using an ice density of 920 kg/m^3.

Both of these figures are close to the density of water, and strongly support the diagnosis of lakes lying beneath the ice. The two sites used are designated A and B in Fig.3.11, where the other sites are denoted by diamond marks.

The corollary of this point is that, in order to contain a pocket of water, the bedrock must include an opposing slope of gradient ten times that of the ice surface, and contoured in such a way that the water cannot escape. This is not, of course, a prohibitive condition, but does emphasise that the formation of large lakes is a contingent rather than a necessary feature of the existence of sub-glacial melt-water. We can therefore expect much larger areas where pressure melting takes place without the water standing to form such lakes.

Weertman (1972) concludes that in the interior regions of ice sheets, basal water is most likely to exist and flow in the form of a 'modified sheet'. That is, irregularities in the bedrock give rise to non-uniform hydrostatic pressures, and the sheet is punctured at points of high pressure. Points of contact between ice and rock will also arise due to the ice movement, since a film of water cannot sustain any shear stress.

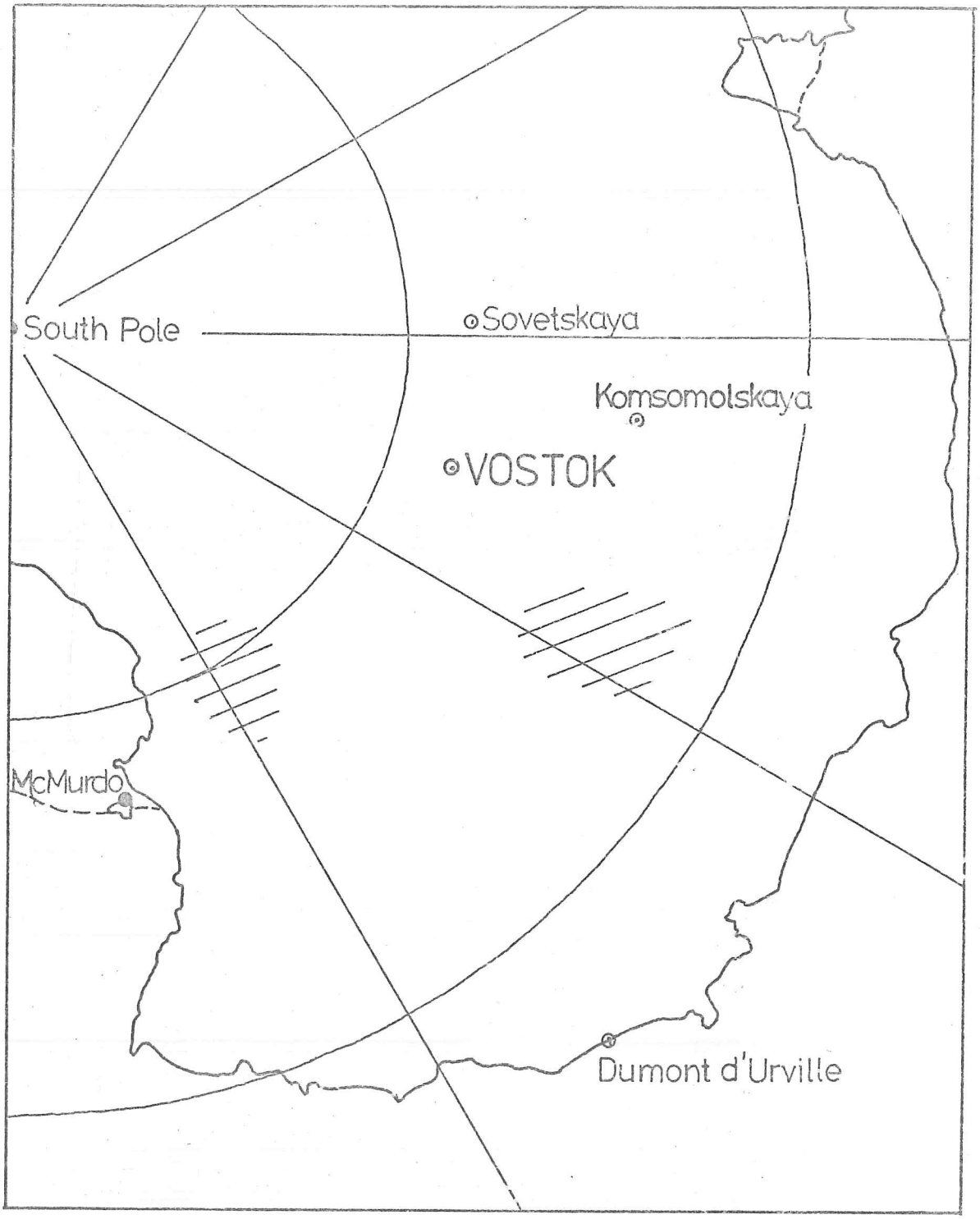

Fig.3.13. Indicating areas where echoes with the characteristics of 'pools' of water are frequently observed.

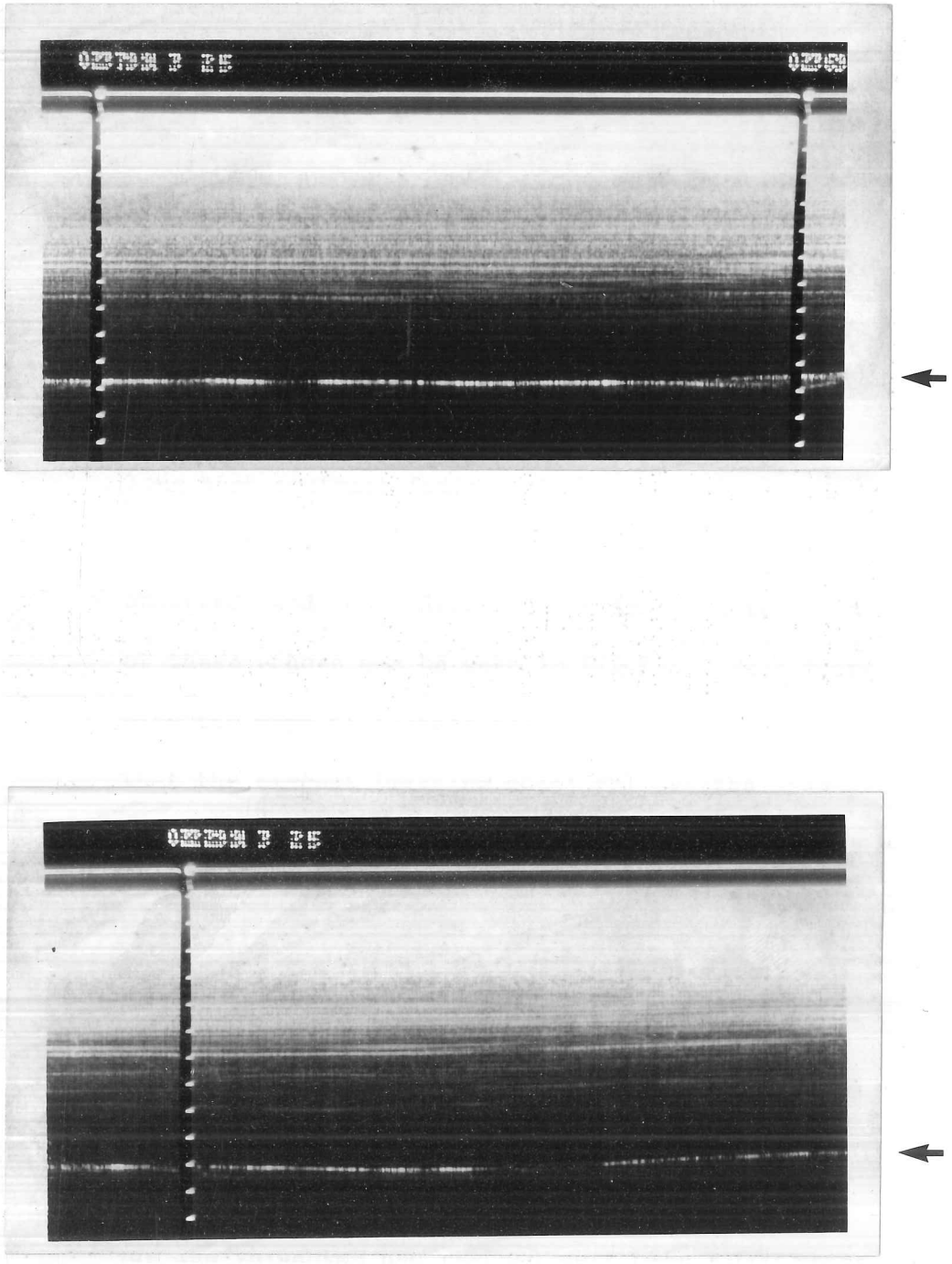

Fig.3.14. Two examples of echoes with the characteristics of intermittent 'pools' of water.

In such areas we cannot expect to find the characteristic long fading lengths associated with extended lakes. The detailed form of the water sheet will be determined by that of the bedrock irregularities. Though, if the size of the irregularities is as we have suggested, we may expect many pools to be formed with widths greater than the normal fading length, the pattern should be expected to have a limiting form similar to that produced by dry bedrock. The differences to be expected are that the mean strength of the reflections will be increased, and the occurence of 'pools' of, say 100 metres' width will appear as anomalously long high-contrast fading.

Areas with just such echo characteristics have been observed, and their distribution is indicated in Fig.3.13. Examples of these echoes can be seen in Fig.3.14. We compare these positions with the maps of surface and bedrock topography. It can be seen that the biggest 'melting zone' follows the deep trench running North-West from the centre of outflow of ice and sub-glacial highland North-East of Vostok Station, which was mentioned in Chapter 2 and, with reference to the anomalously high echo strength, in Section (3.1.2). The extent of this trench is not yet known, though some sounding in this direction has been carried out in the 1974/75 season, whose results await analysis, and further flights are planned. At the North-Western extremity of the 71/72 survey the ice thickness had reached well over 4,000 metres, and the trough a depth of 1200 metres below sea-level, deepening towards the coast.

The results of seismic soundings between this area and the coast give an incomplete and somewhat confusing picture of the large-scale topography. The relief contains large contrasts, including

the Golitsyn Mountains, which rise to over 500 metres above sea level, and the Schmidt Valley which reaches more than 1000metres below. It is an open question whether the deep inland valleys communicate with the sea, but it is an important one: the effect on the ice sheet of the sub-glacial meltwater, and any analysis of melt rates or drainage patterns must depend on whether the water is sealed off by the ice or whether it follows a hitherto unsuspected drainage path to the sea.

The immediate implication of the existence of melt-water is that temperature gradients must be higher in these areas than has been generally supposed. This may be due to a greater geothermal flux than would be expected, or to an increased rate of basal heating due to sliding and shear strain.

(3.2.5) Conclusions

In summary, the existence of the lakes and their identification as pockets of water has established that parts, at least, of the base of the ice sheet are at the pressure-melting point. There is no reason to suppose that the phenomenon of basal melting is confined to such areas as have suitable topography for the formation of extensive lakes. We expect it to occur over much wider areas, and the observed echo characteristics suggest that water does indeed exist over the areas indicated.

The fact that reflections at large angles to the vertical are not frequently seen in association with these echoes suggests that any channels are incised downwards into the rock, with relatively flat upper surfaces. This would agree with Nye's (1969) model of channelled water flow, and would indicate that in

Weertman's model, the water sheet is interstitial between a fairly flat ice under-surface, over-riding the rough bedrock. In this case, the description of the water layer as of 'channelled' or 'sheet' form will depend on whether the bedrock irregularities consist of random undulations, and if so, on their degree of orientational anisotropy. Since melt rates are very low, and erosion by water flow correspondingly slight, we suspect that Weertman's description is probably more apt for this situation.

If we accept that basal melting does occur over widespread areas of the East Antarctic ice sheet, this fact should be taken into account in calculations of the dynamics and stability of the ice sheet. The position is further complicated by the possibility of drainage connections between the melt zones and the sea, allowing an unseen ablation path. Hughes (1973) has pointed out two sources of instability in an ice sheet, arising respectively from the surge phenomenon, as observed in some mountain glaciers, and from an externally-triggered perturbation to the mass-balance of the ice sheet. The occurence of widespread basal melting is relevant to both these mechanisms, since the resistance to surging arises from the basal friction which is, of course, drastically modified by the presence of a water sheet, and the mass-balance depends on the available modes of ablation. We may also expect the first effect to be self-reinforcing, since an increase in lubrication will increase sliding velocities, and shear stresses at points of ice-rock contact, causing greater basal heating, and a consequent increase in the melt rate (that is, until the lubrication and rates of sliding are suchthat the motion is no longer limited by basal friction but by lateral shear in the ice surrounding the melt zone). See also Weertman (1966).

We return now to the question of the dumping of radio-active wastes in the ice-sheet. We have seen substantial evidence of the existence of meltwater beneath the ice sheet, and have mentioned how this may affect its dynamics. The viability of the suggestion must be questioned both as a result of the possibility of drainage between the central regions of the ice sheet and the sea, and also because of the uncertain effect on the extent of melting caused by the introduction of a further heat source in the ice. (The authors have suggested that the additional heat could amount to 1% of the frictional heating over the areas where the wastes were introduced).

We believe that, though this suggestion has by now effectively been dropped, its original apparent force arose from the inappropriate application of the results of a model study. Budd, Jenssen and Radok state in their report that the object of the study was to test the validity of the assumptions on which it was based. This should not have been confused with a suggestion that the results represented a 'best estimate' of the real situation.

CHAPTER 4: A simplified theory for the shape and strength of the echo pulse

A completely general theory of rough-surface reflections, covering all types of surface, and all conditions of sounding, is necessarily very complex. Harrison (1972) and Berry (1973), among others, have attempted to give such a theory, but inevitably the results are divided into separate regimes, where different processes are dominant and which are separated by shadowy transitional regions. It is difficult in such theoretical attempts to select the most important cases for special treatment.

Since we now have some indications of the form of surface with which we are generally dealing, we shall take a more pragmatic approach in the interests of making intelligible deductions from real observations.

(4.1) Limitations on the type of surface under investigation

Two general characteristics of the echoes observed in the Antarctic and, as will be seen in the next chapter, in Devon Island, are that the tail of the echo is a sharply-decreasing function of delay time, and that the maximum level of the echo exhibits high-contrast fading. The implications of the short echo tail are that the gradients of facets in the rough surfaces are limited to values which do not give rise to reflections at extended delays, and that diffraction effects due to abrupt changes in the phase or amplitude of the reflected wave do not make a significant contribution to the echo. That of the high-contrast fading is that the reflecting surface is 'deeply-modulated', that is, that the phase of reflections of plane waves from the surface will

vary along a surface parallel with the incident wave-fronts, by at least a phase angle of one radian. (Harrison, Berry).

In order to develop a useful treatment of the echo form, we shall make the initial assumption that the bedrock has a smoothly undulating surface, with out spikes or ripples of similar dimensions to the radio wavelength. We thereby exclude 'diffraction effects', and base our calculations on treatment of the reflections by the methods of geometrical optics.

This model greatly simplifies calculations involving linear statistics of the reflected intensity (in particular its mean level and angular distribution). It is not adequate for a full description in terms of non-linear statistics such as the variance or auto-correlation function, when results are dependent on the behaviour of the echo over distances of the order of the radio wavelength, and diffraction effects must be taken into account.

It is not necessary yet to assume any particular form for the surface beyond the above assumption. However, for the sake of concrete results, we shall consider the 'Gaussian random surface' employed by previous authors, where the roughness may be described by a random function $\zeta(x,y)$, which gives the displacement at any point (x,y), vertically from a mean horizontal plane. ζ is normally distributed about zero, with standard deviation α_0, and the horizontal autocorrelation function is given by

$$B_\zeta(\sigma,\tau) = \exp\left(-\frac{\sigma^2+\tau^2}{T^2}\right) \times \alpha_0^2 \qquad (4.1)$$

where σ and τ are displacements along the x and y axes.

The distribution of slopes of such a surface in one dimension has been derived by Beckmann and Spizzichino (1963) as

$$p(\beta_x) = \frac{T(1+\beta^2)}{2\alpha_0\sqrt{\pi}} \exp\left(-\frac{\beta_x^2 T^2}{4\alpha_0^2}\right) \qquad (4.2)$$

where $\beta_x = \left(\frac{d}{dx}(\zeta(x))\right)$

For surfaces whose slopes do not generally exceed 0.5, and β_0 is the r.m.s. value of the tangential slope, the distribution is approximately normal, and may be written:

$$p(\beta_x) \simeq \frac{1}{\sqrt{2\pi}\,\beta_0} \exp\left(-\beta_x^2/2\beta_0^2\right) \qquad (4.3)$$

In two dimensions, we have, assuming an isotropic surface, the normalised autocorrelation function:

$$\rho_s(\mu) = \exp\left(-\mu^2/T^2\right) \quad \text{where } \mu^2 = \sigma^2 + \tau^2 \qquad (4.4)$$

The tangential gradient is equal to the 'normal derivative' at any point, so that;

$$\beta^2 = \left(\frac{\partial s}{\partial x}\right)^2 + \left(\frac{\partial s}{\partial y}\right)^2 = \beta_x^2 + \beta_y^2 \qquad (4.5)$$

Taking cross-sections of the surface along axes X and Y, we obtain one-dimensional Gaussian surfaces, giving again, for the partial gradients in these directions:

$$p(\beta_x) = p\left(\frac{\partial s}{\partial x}\right) = \frac{1}{\sqrt{2\pi}\,\beta_0} \exp\left(-\beta_x^2/2\beta_0^2\right) \qquad (4.6)$$

and:

$$p(\beta_y) = p\left(\frac{\partial s}{\partial y}\right) = \frac{1}{\sqrt{2\pi}\,\beta_0} \exp\left(-\beta_y^2/2\beta_0^2\right) \qquad (4.7)$$

The probability of the occurence of a normal surface gradient of β is given by:

$$p(\beta) = \int_{S(\beta^2=\beta_x^2+\beta_y^2)} p(\beta_x)\,p(\beta_y)\,dS = \int_0^{2\pi} p(\beta_x)\,p(\beta_y)\,d\phi.\beta \qquad (4.8)$$

where β_x and β_y are related by 5 and ϕ is given by:

$$\tan\phi = \beta_y/\beta_x \tag{4.9}$$

For an isotropic surface, we have

$$p(\beta_x)\,p(\beta_y) = \frac{1}{2\pi\beta_0^2}\exp\left(-\beta^2/2\beta_0^2\right) \tag{4.10}$$

and

$$p(\beta) = \beta/\beta_0^2 \exp\left(-\beta^2/2\beta_0^2\right) \tag{4.11}$$

with

$$\int_0^\infty p(\beta)\,d\beta = 1 \tag{4.12}$$

WHERE $\sqrt{2}\beta_0$ is equal to the r.m.s. slope.

For a two-dimensional surface, then, a Gaussian distribution of vertical displacements results in a Rayleigh distribution of slopes. We are here in disagreement with Berry, who obtains a Gaussian distribution of slopes in two dimensions, since he derives the probability of linear gradients in the surface, without reference to the direction of the normal at the point of measurement. This is not realistic in the context of the reflection geometry, since any facet of the surface gives rise to a single reflection, whose direction depends on that of the normal, rather than on the gradient of any line which may be drawn in the surface. It is possible that, under the erosion due to ice movement, the probability of low surface gradients may be enhanced over that given by a Gaussian random surface, and we shall continue to bear in mind the case of a surface whose distribution of slopes, rather than of displacements, is Gaussian.

Schloss (1966), describes the roughness of lunar and terrestrial terrain, and deduces a Gaussian distribution, measuring slopes along Cartesian axes. For our purpose it is certainly of more use to consider the distribution of normal slopes which would in this case conform to a Rayleigh probability density.

In the following work we shall assume that the roughness does not give rise to shadowing of one facet by another, or to multiple reflections.

(4.2) Echo sounder characteristics and sounding situation

We shall consider a sounder operating with a carrier frequency near 60 MHz, such that the wavelength in ice is 3 metres. This is similar to the wavelengths employed by both Harrison and Berry. The major difference will be that we shall deal with a rectangular pulse envelope, as opposed to the Gaussian pulse shape used by these authors. This is closer to the real situation for all but the shortest pulses obtainable with a given apparatus, and allows a considerable simplification of the analysis for the 'geometrical-optical' case (to be known as the 'Newtonian' case, since the radiation is treated essentially as a stream of perfectly elastic particles).

The essential difference between the two pulse shapes is that the rectangular pulse possesses a plateau whose duration is long compared with that of the leading and trailing edges. We consider the existence of the pulse edges as a perturbation of a continuous wave, rather than as an intrinsic part of the pulse. In the real situation, the pulse is, of course, not exactly rectangular, but has finite rise- and fall-times, and we shall

indicate the importance of such departures in the text. We shall assume that the bandwidth of radar receiver and recording c.r.t. are such that the form of the received pulse is not distorted in the recording process.

We shall assume throughout that transmission and reception are performed by the same antenna, so that all received reflections occur along the local normal to the reflecting surface. This greatly simplifies the geometry of the situation, and also avoids any variation of the reflection coefficient as a result of changes in the angle of incidence.

We consider a sounding geometry as shown in Fig. 4.1. The height h is assumed to be much greater than the vertical displacements of the roughness, and we shall not in general include the effects of refraction at a boundary between the sounder and the bedrock. In most cases this may be accounted for by a simple apparent-depth correction, and is not important for the theory of reflections.

(4.3) Reflection of continuous spherical waves from a 'Newtonian' surface

It is shown in Appendix 1 that the mean angular distribution of continuous waves received at the point of transmission, after reflection from a Newtonian surface, is given by

$$\langle P(\theta) \rangle \delta\theta = \frac{P_t . g}{4\pi h^2} . \frac{A}{4} . \frac{\rho(\theta)}{\sec^2\theta} . \delta\theta \qquad (4.13)$$

where P_t is the power transmitted, G is the gain of the antenna, A is its effective receiving area, and R is the reflection coefficient at the surface. If $\rho(\theta)$ is small for angles greater than 30°, the term in $\sec\theta$ may be ignored, and the power received between θ_1 and θ_2 is given by

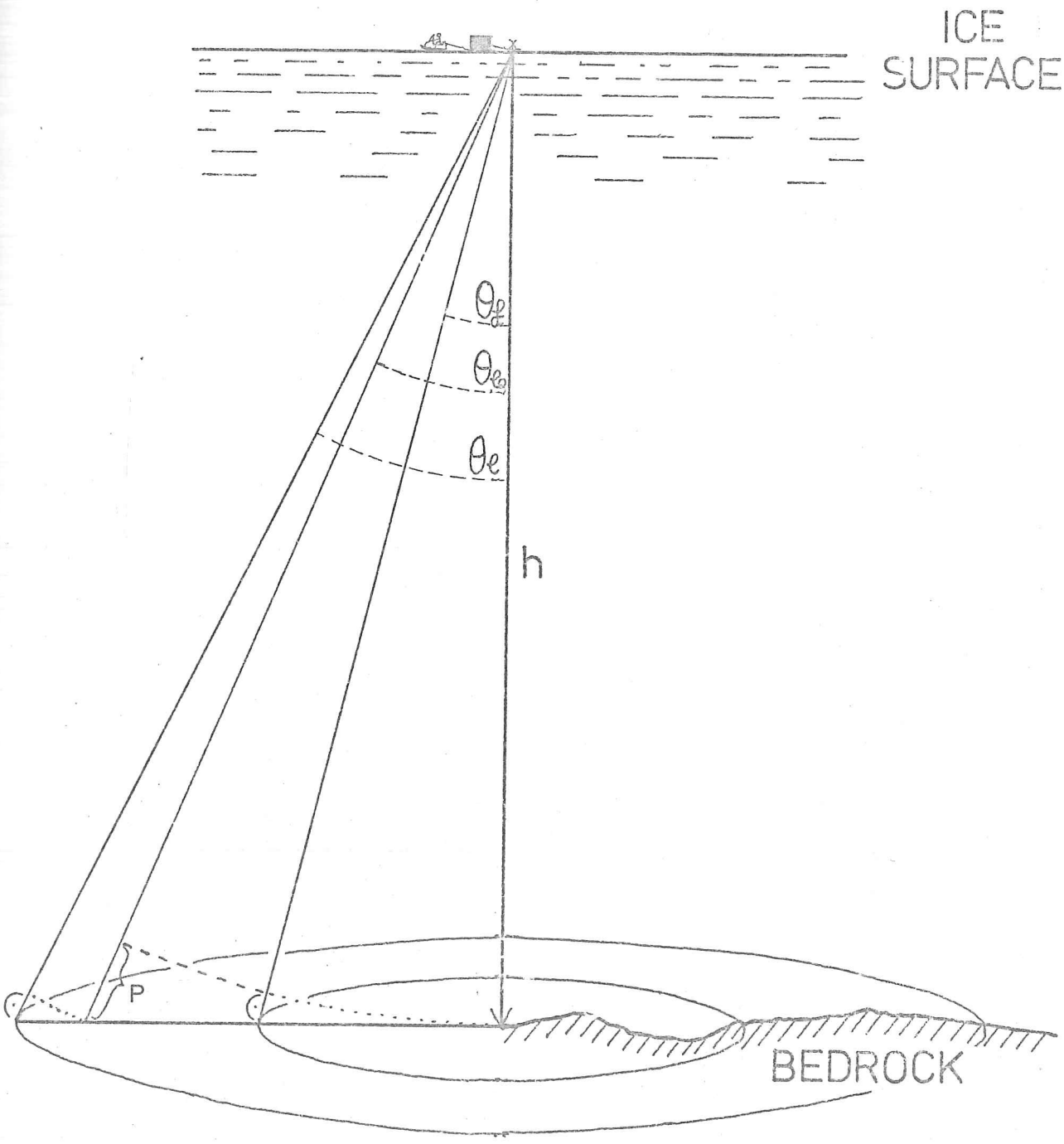

Fig.4.1. The sounding geometry for the oversnow sounding situation, illustrating the angles θ_{e_0}, and θ_e and θ_f for a subsequent time delay.

$$\langle P \rangle_{\theta_1}^{\theta_2} = \int_{\theta_1}^{\theta_2} p(\theta)\, d\theta \cdot \frac{P_t g^2 \lambda^2}{64\pi^2 h^2} \qquad (4.14)$$

For continuous waves, the total power received is given by this integral between limits 0 and $\pi/2$, and is

$$\frac{P_t g^2 \lambda^2}{64\pi^2 h^2}$$

This is equal to the power to be expected after reflection from a polished plane surface of the same material, and will be denoted by P_o.

(4.4) Reflection of a rectangular pulse of spherical waves from a 'Newtonian' surface

Continuous waves are not useful for a depth-sounding radar, and the usual form of modulation consists of an approximately rectangular pulse envelope. Other authors have used a Gaussian envelope, which offers some analytical elegance, but is less realistic and less well suited to these calculations.

The effect of pulse-modulation of the continuous wave is essentially to modify the limits over which the integral (14) is to be performed. In the case of continuous waves the entire surface is illuminated simultaneously: for a pulse the illuminated area has the form of a disc or annulus, depending on the time delay after transmission of the pulse. The geometry of the pulse and surface is shown in Fig. 4.1. for the situations when only the leading edge of the pulse has returned from the surface, and when the trailing edge also contributes to the observed echo. The angles θ_c and θ_f, which describe the positions on the surface of the pulse edges, are given by

$$\theta_e = \sec^{-1}\left(ct/2h\right) \quad \text{for} \quad t > \frac{2h}{c} \tag{4.15}$$

and $$\theta_f = \sec^{-1}\left(\frac{ct-P}{2h}\right) \quad \text{for} \quad t > \frac{2h+P}{c} \tag{4.16}$$

where t is the delay time, measured after the transmission of the leading edge of the pulse and P is the total pulse length. The two time conditions will be denoted by (I) and (II), since we shall continually refer to the two situations.

We can now calculate the mean power received at any instant from a surface with a given distribution of slopes:

$$\langle P(t) \rangle = \int_0^{\theta_e} P_0 \cdot \rho(\theta)\, d\theta \qquad \text{for (I)} \tag{4.17}$$

and $$\langle P(t) \rangle = \int_{\theta_f}^{\theta_e} P_0 \cdot \rho(\theta)\, d\theta \qquad \text{for (II)} \tag{4.18}$$

The power in situation (I) can be seen to be an increasing function of t, regardless of the form of the distribution of slopes in the surface. The initial variation in (II) depends on the relative probability of slopes occurring at the angles corresponding to the leading and trailing edges. In the case of a Gaussian distribution the probability is a maximum for zero slope, so that the mean power for (II) is always a decreasing function of delay time. For a Rayleigh distribution, the probability is zero for zero slope, so that the mean power must continue to rise until incremental area included by the leading edge is balanced by the decremental area excluded by the trailing edge. In the case of a Gaussian distribution of slopes, the maximum echo

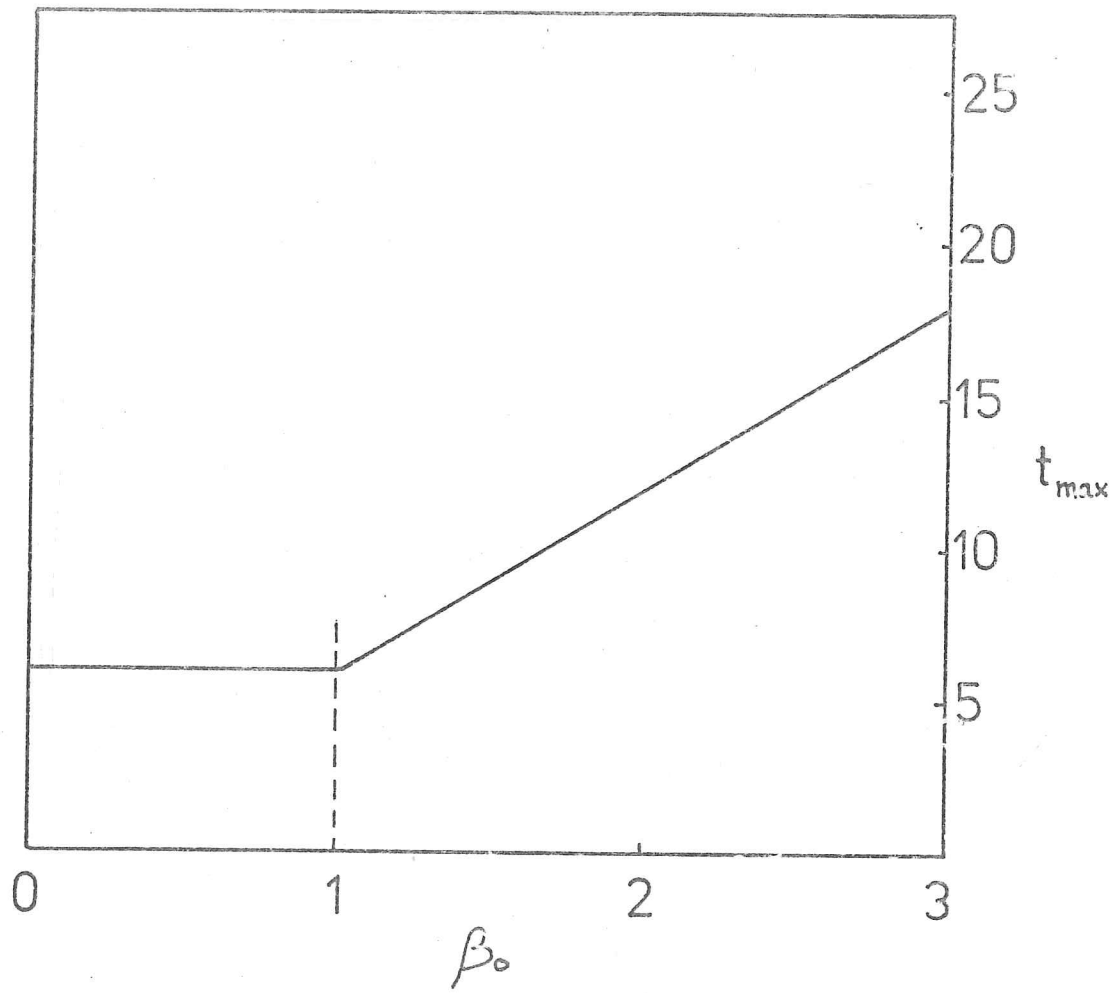

Fig.4.2. Approximate relation between the delay of the maximum level of the mean received pulse and the one-dimensional r.m.s. slope, .

power will occur for a constant time delay given by

$$ct_{max} = 2h + p \qquad (4.19)$$

In cases where the slopes have a Rayleigh distribution, and a large r.m.s. slope, the maximum will be retarded beyond this point, its position being defined by the condition:

$$p(\theta_e)\left(\frac{\partial\theta_e}{\partial t}\right) - p(\theta_g)\left(\frac{\partial\theta_g}{\partial t}\right) = 0$$

We are only interested in solutions where t_{max} is greater than $\frac{2h+p}{c}$, and we find that this only occurs for $\beta_0 \gtrsim 1$ if p is much less than the altitude of the observer. The delay time of the echo maximum is shown as a function of the r.m.s. slope in Fig.4.2. This result is only approximate, since for high values of β_0 (i.e. values greater than unity), our analysis of the angular spectrum breaks down.

For surfaces with slopes less than 30^0, we may replace θ by β in equation (18), so that for case (I),

$$\langle P(t) \rangle = \int_0^{\beta_e} p(\beta)\, d\beta \qquad (4.20)$$

and for case (II)

$$\langle P(t) \rangle = \int_{\beta_g}^{\beta_e} p(\beta)\, d\beta \qquad (4.21)$$

where

$$\beta_e^2 = \frac{c^2t^2}{4h^2} - 1$$

and

$$\beta_g^2 = \frac{(ct-p)^2}{4h^2} - 1$$

Figs.4.3. and 4.4 show the mean received pulse shapes to be expected from surfaces with, respectively, Rayleigh and

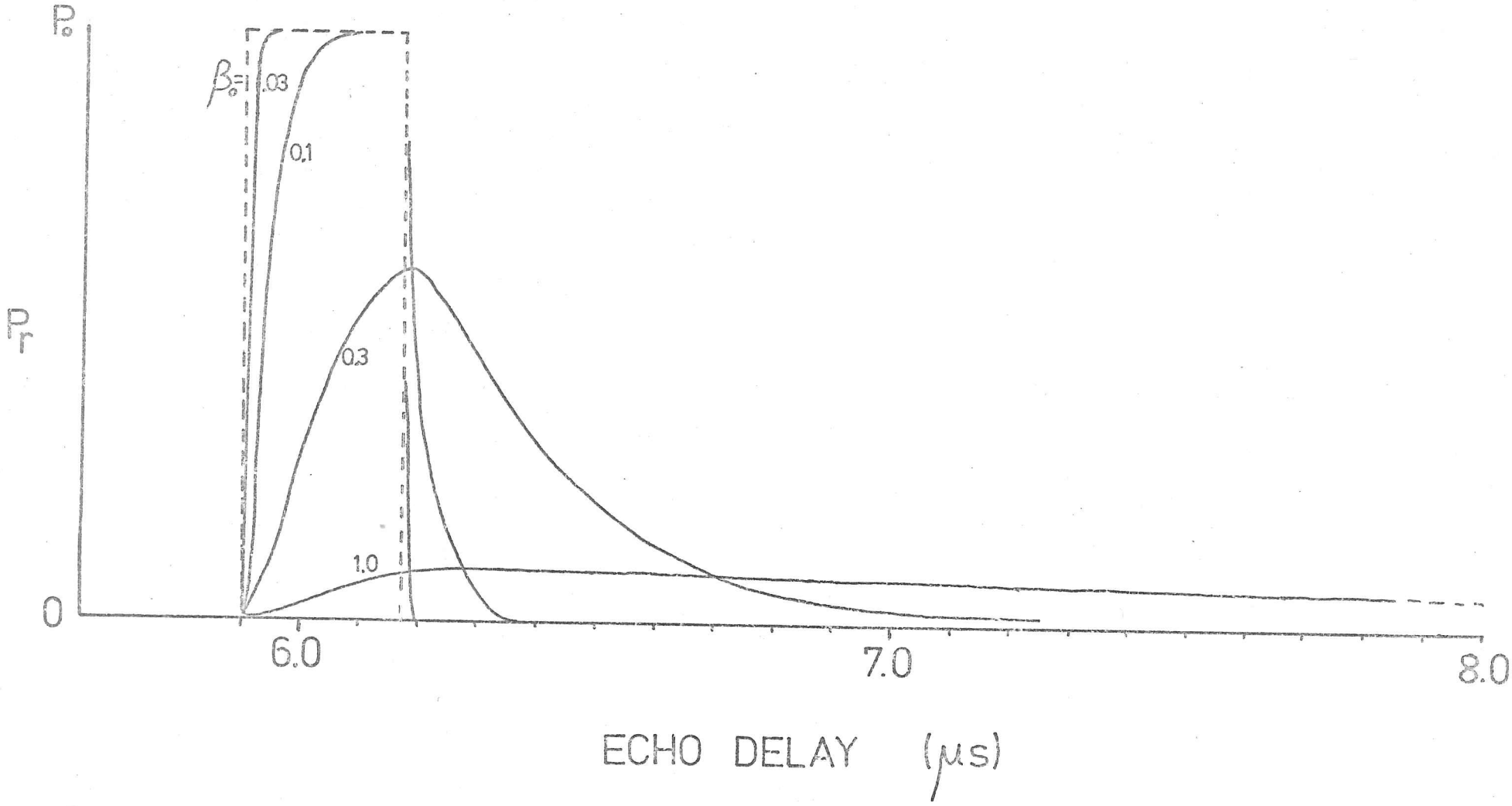

Fig.4.3. Expected pulse shapes for reflection of a rectangular pulse from surfaces with Rayleigh slope distributions.

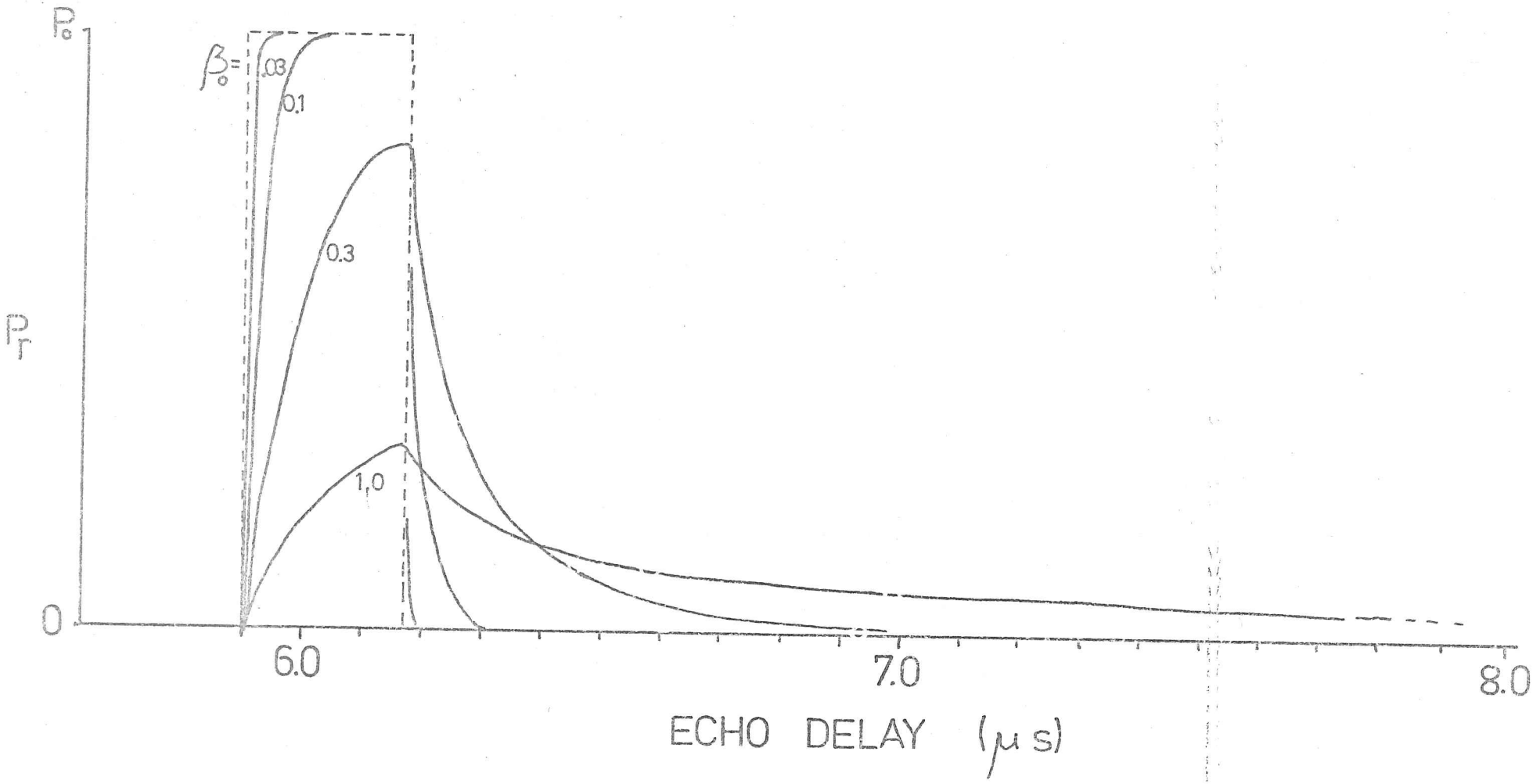

Fig.4.4. As for Fig.4.3., but for surfaces with Gaussian slope distributions.

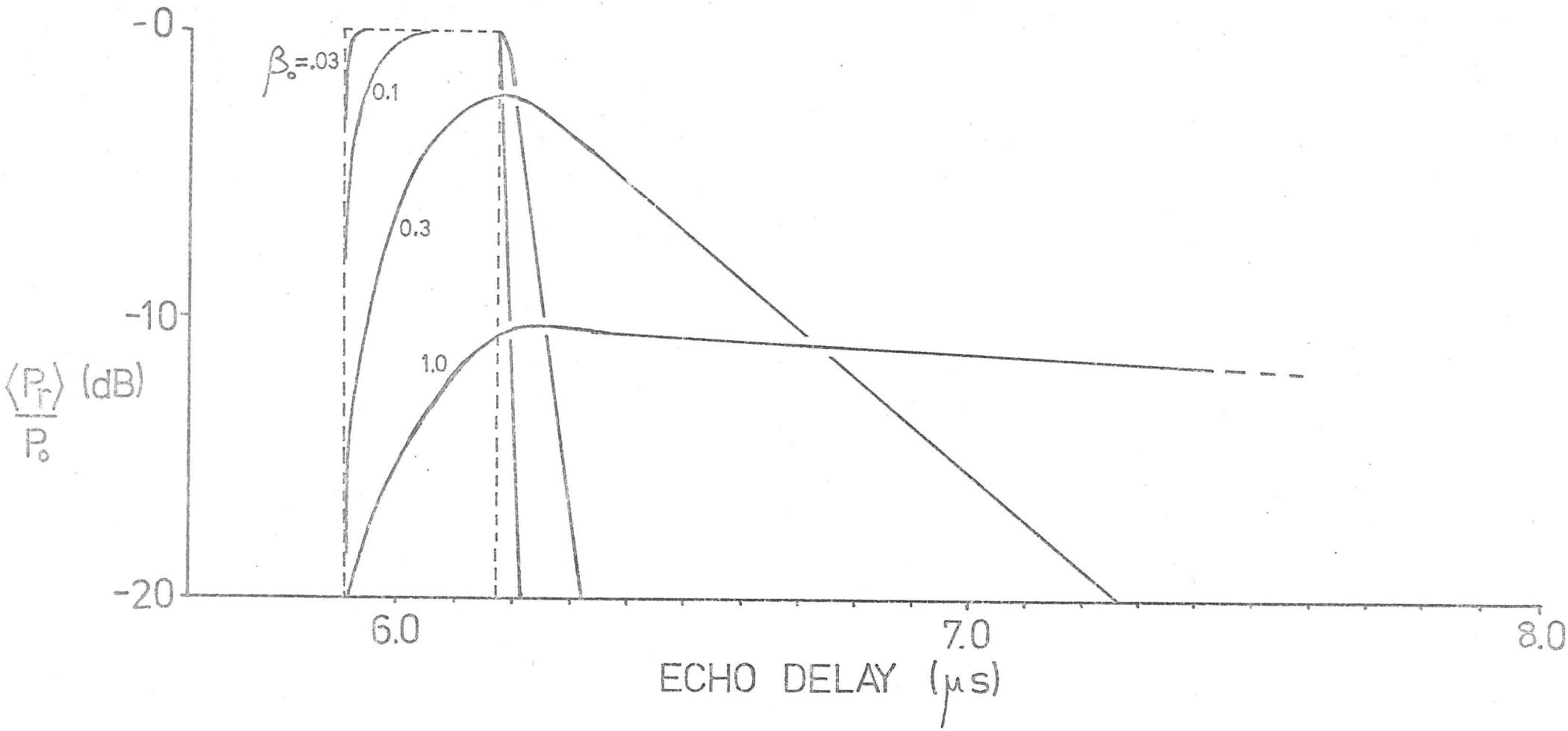

Fig.4.5. Expected mean pulse shapes for a rectangular transmitted pulse reflected from a surface with a Rayleigh distribution of slopes and various values of .

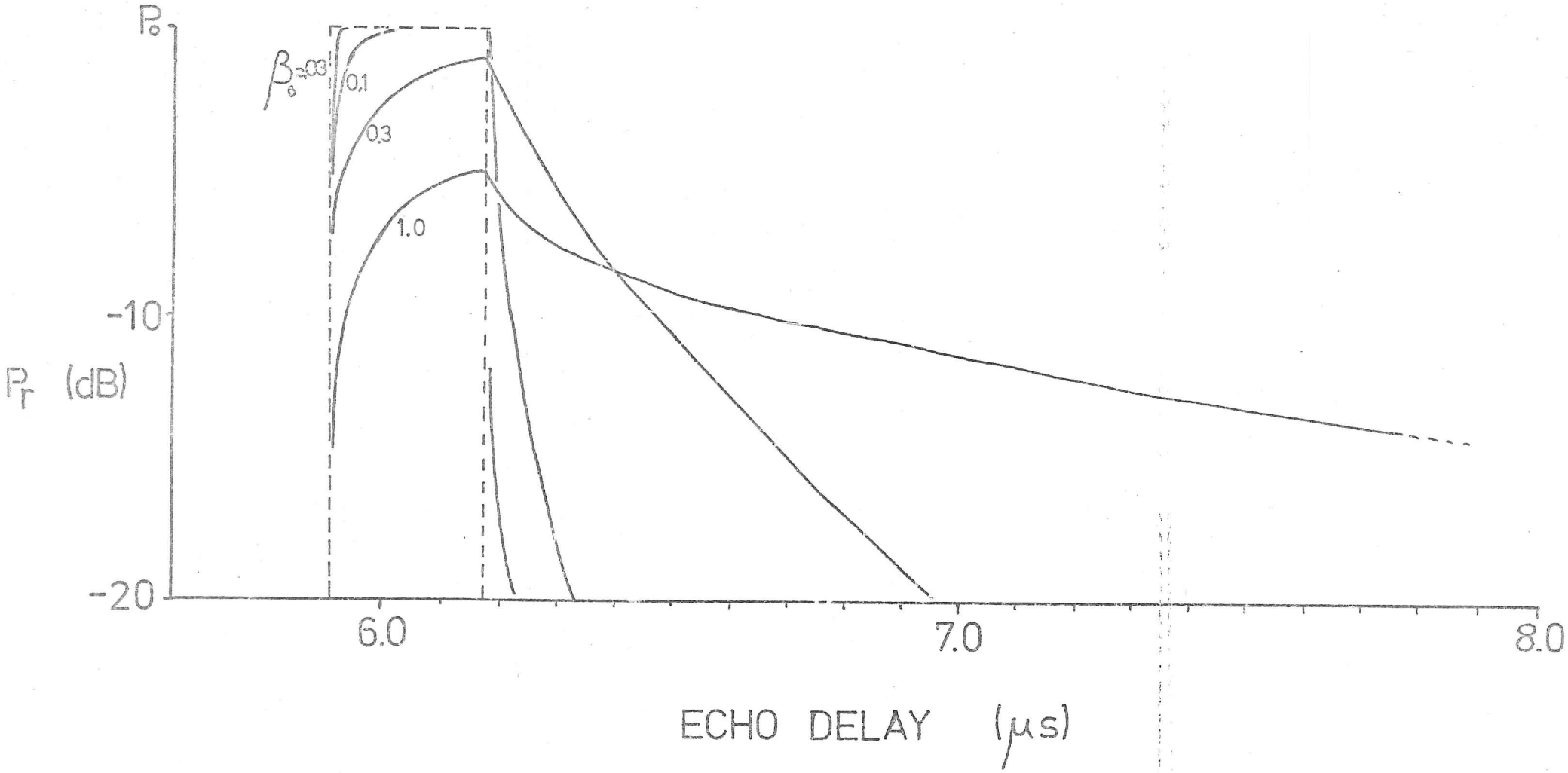

Fig.4.6. As for Fig.4.5., but for a surface with a gaussian distribution of slopes.

Gaussian distributions of slopes, and various values of the r.m.s. slope, for an ice depth of 500 metres, and pulse length of 43 metres, (250 nanoseconds). For the Rayleigh distribution, the maximum of the mean power is reduced below P_o by 0.6 dB for an r.m.s. slope of $\tan^{-1}(0.2)$, and by 2.3 dB for $\langle\beta^2\rangle^{1/2}=\tan^{-1}(0.3)$. For the Gaussian distribution the deficit is less for a given value of $\langle\beta^2\rangle^{1/2}$. The mean shapes, expressed in dB, can be seen in Figs. 4.5 and 4.6.

For the reverse situation, where the pulse shape is given and the distribution of slopes is to be calculated, we transform 20 and 21 to give, for (I),

$$p(\beta_e)\left(\frac{d\beta_e}{dt}\right) = \frac{1}{P_o}\frac{d}{dt}\left(\langle P(t)\rangle\right) \qquad (4.23)$$

and for (II)

$$p(\beta_e)\left(\frac{d\beta_e}{dt}\right) - p(\beta_f)\left(\frac{d\beta_f}{dt}\right) = \frac{1}{P_o}\frac{d}{dt}\left(\langle P(t)\rangle\right) \qquad (4.24)$$

For low-slope surfaces, it is easier to make measurements fromthe trailing edge of the pulse than from the leading edge, where the smaller increments of power corresponding to reflections at larger angles are superimposed on the reflections from lower angles. In the trailing edge, the loss of power due to the exclusion of echoes from successively higher angles can be seen in isolation from the main part of the echo. This is particularly evident when the echo is displayed on a logarithmic scale, as is necessary to allow a sufficient dynamic range.

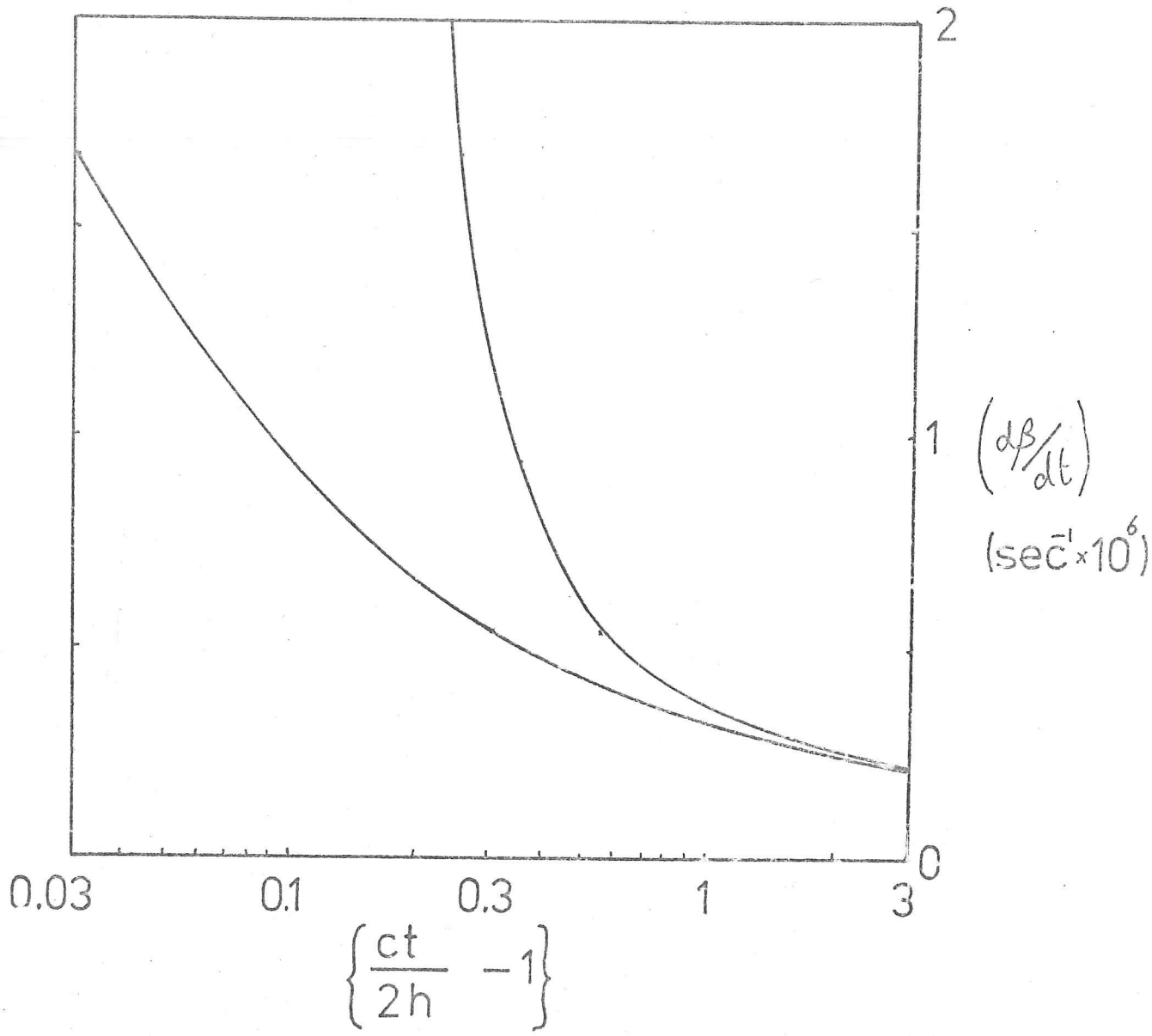

Fig.4.7. Rates of change of the parameters β_e and β_g, plotted as functions of the relative delay, for a transmitted pulse duration of 250 nsec.

For Rayleigh-distributed slopes we have, in case (II), from (24)

$$\beta_e \exp\left(-\beta_e^2/2\beta_0^2\right).\frac{d\beta_e}{dt} - \beta_f \exp\left(-\beta_f^2/2\beta_0^2\right).\frac{d\beta_f}{dt} = \frac{\beta_0^2}{P_0}\frac{d}{dt}\left(\langle P(t)\rangle\right) \quad (4.25)$$

and for a Gaussian distribution,

$$\exp\left(-\beta_e^2/2\beta_0^2\right).\frac{d\beta_e}{dt} - \exp\left(-\beta_f^2/2\beta_0^2\right) = \frac{\beta_0\sqrt{2\pi}}{P_0}\frac{d}{dt}\left(\langle P(t)\rangle\right) \quad (4.26)$$

The values of $(d\beta_e/dt)$ and $(d\beta_f/dt)$ are plotted as functions of time of Fig. 4.7. They are, of course, dependent only on the pulse length and height above the mean horizontal plane.

The calculation is very much simplified for a long pulse, where we may assume that $p(\beta_e)$ is much less than $p(\beta_f)$, and the first terms in (25) and (26) may be neglected.

(4.5) Reflection of a pulse with arbitrary envelope shape, from a 'Newtonian' surface

The situation in section (4.4) is complicated in practice by the finite duration of the leading and trailing edges of the transmitted pulse. For an arbitrary pulse shape given by

$$P(t') = P_{t0}.W(t') \quad (4.27)$$

(where t' is the time lag after the leading edge of the pulse), the received power at any instant is now given by

$$\langle P(t)\rangle = P_0\int_0^\infty W(t')\,p(\beta)\,d\beta \quad (4.28)$$

where $$ct' = ct - 2h\left(1+\beta^2/2\right) \quad \text{FOR SMALL } \beta \quad (4.29)$$

In approximating to the real situation, we shall neglect the finite rise time, since the leading edge of the received

pulse is not to be used for measurement. We shall consider a pulse consisting of a rectangular section, followed by an exponentially-decaying trailing edge, such that

$$W(t') = 1 \qquad \text{for } t' < P/c \qquad (4.30)$$

and

$$W(t') = e^{-\frac{(t'-P/c)}{\tau_s}} \qquad \text{for } t' > P/c \qquad (4.31)$$

We then have

$$\langle p(t) \rangle = P_0 \int_{\beta_s}^{\beta_e} p(\beta)\, d\beta + P_0 \int_0^{\beta_s} p(\beta)\, e^{-\frac{(ct'-P)}{c\tau_s}} d\beta \qquad (4.32)$$

Now, from (29) the second term in (32) becomes

$$\exp\left\{\frac{2h+P-ct}{c\tau_s}\right\} \cdot P_0 \int_0^{\beta_s} p(\beta) \exp\left(\frac{h\beta^2}{c\tau_s}\right) d\beta \qquad (4.33)$$

For a Rayleigh distribution of slopes, with $\beta_0 < 0.4$, the integral becomes

$$\int_0^{\beta_s} \frac{\beta}{\beta_0^2} \exp\left(\beta^2 \left\{\frac{h}{c\tau_s} - \frac{1}{2\beta_0^2}\right\}\right) d\beta \qquad (4.34)$$

giving for the mean power at delay t where $ct > 2h+P$ (case (II)),

$$\langle P(t) \rangle = P_0 \left\{ \exp\left[\frac{1-(ct-P)^2/4h^2}{2\beta_0^2}\right] - \exp\left[\frac{1-c^2t^2/4h^2}{2\beta_0^2}\right] + \frac{\exp\left\{\frac{2h-ct+P}{c\tau_s}\right\}}{1-\frac{2h\beta_0^2}{c\tau_s}} \cdot \left(1 - \exp\left[\frac{\beta_s^2}{2\beta_0^2}\left(1-\frac{2h\beta_0^2}{c\tau_s}\right)\right]\right)\right\} \qquad (4.35)$$

For a Gaussian distribution of slopes the expression is

$$\langle P(t) \rangle = P_0 \left\{ \operatorname{erf}\left[\frac{1-c^2t^2/4h^2}{2\beta_0^2}\right] - \operatorname{erf}\left[\frac{1-(ct-P)^2/4h^2}{2\beta_0^2}\right] + \frac{\sqrt{\pi}\exp\left\{(2h+P-ct)/c\tau_s\right\}}{\sqrt{1-\frac{2h\beta_0^2}{c\tau_s}}} \cdot \operatorname{erf}\left[\beta_s/\beta_0 \cdot \sqrt{1-\frac{2h\beta_0^2}{c\tau_s}}\right] \right. \qquad (4.36)$$

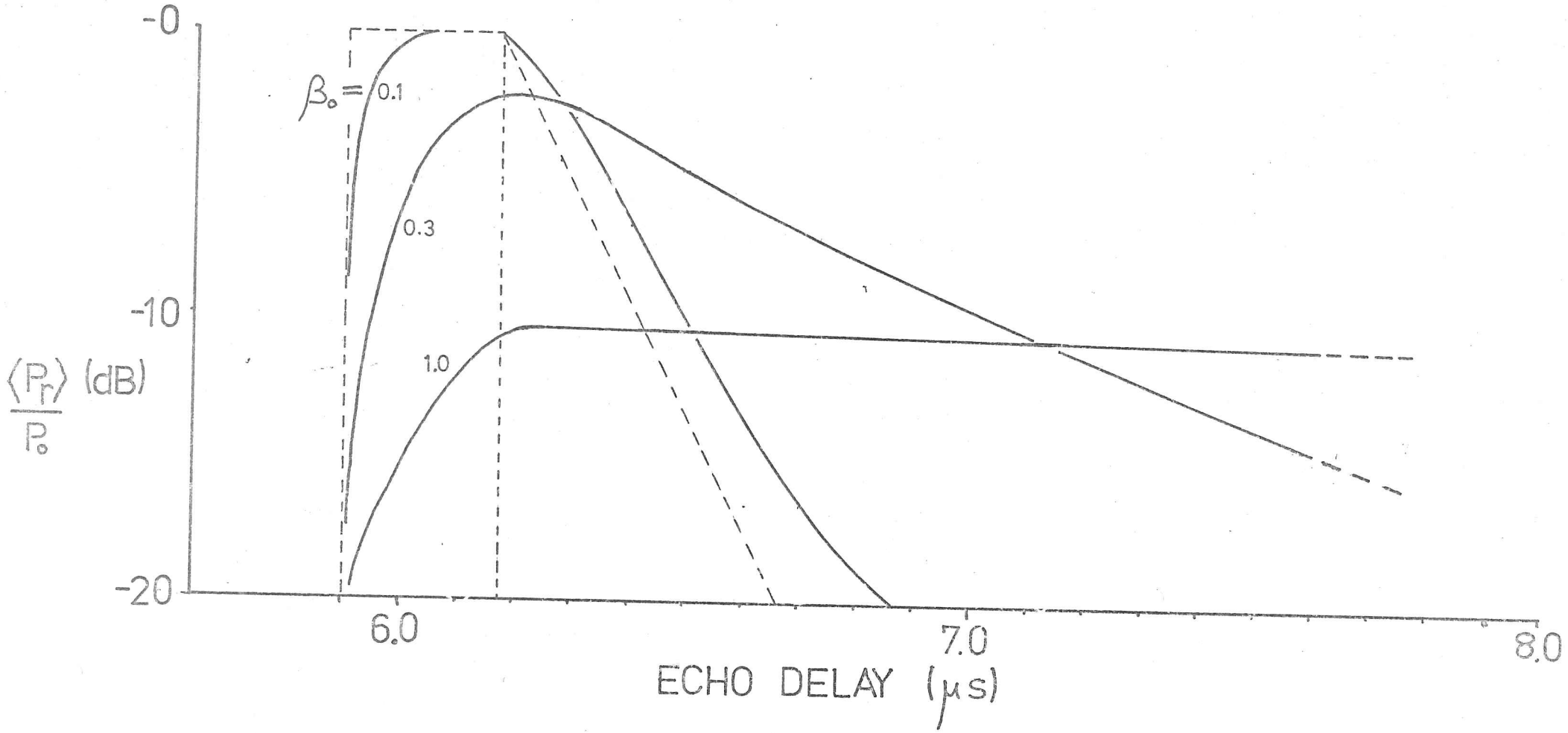

Fig.4.8. Expected pulse shapes as in Fig.4.5, but for a transmitted pulse with exponentially-decaying tail.

The pulse used in work to be described in Chapter 5 may be described by (30) and (31) with $P = 42m$ and $\tau_j = 100ns$. The mean received pulse shape to be expected from surfaces with Rayleigh distributions and r.m.s. slopes of 0.1, 0.3, and 1.0 are shown in Fig. 4.8.

In contrast with section (4.4), the probability distribution of slopes can no longer be expressed simply in terms of the rate of fall of echo power with time in the tail of the echo. The fall-off is now composed of two factors, one corresponding, as before, to the changing area of illumination which gives rise to the echo, the other to the decreasing contribution of areas illuminated by the tail of the transmitted pulse.

Thus from (32), and (29)

$$\frac{d}{dt}\left(P(t)\right) = P_0 \left\{ p(\beta_e)\left(\frac{d\beta_e}{dt}\right) - p(\beta_j)\left(\frac{d\beta_j}{dt}\right) + \exp\left\{\frac{2h+p-ct}{c\tau_j}\right\}\left[p(\beta_j).e^{-\frac{h\beta_j^2}{c\tau_j}}.\left(\frac{d\beta_j}{dt}\right) - \frac{1}{\tau}\int_0^{\beta_j} p(\beta)\, e^{h\beta^2/c\tau}\, d\beta\right] \right. \qquad (4.37)$$

The complexity of this equation, and its degree of dependence on an accurate knowledge of the transmitted pulse shape and accurate measurement of the power gradient, suggest that the best method of estimating the probability distribution will be to compare the observed mean pulse shape with curves derived from equations (35) or (36).

Departures of the transmitted pulse from an ideal shape (whether Gaussian or rectangular) constitute the greatest disadvantage of this method of estimating the distribution of slopes.

Other problems involve the necessity for a strong echo, so that the echo tail is of measurable strength, and for accurate measurement of the power and resolution of gradients within a very small range of time delays near the maximum level of the return. In order to measure the pulse shape accurately a wide frequency bandwidth must be employed both in the radar receiver and the recording apparatus, but these precautions will be useless unless the transmitted envelope is very accurately known.

(4.6) Summary

We shall see in Chapter 5 that the mean shapes of received echoes conform well to the shape outlined in Equation (35). This result supports our initial suggestion that the reflections may be dealt with by the methods of geometrical optics. Within the limitations stated in the last section, the nature of the reflecting boundary may be deduced from the shape of received pulses. This allows us to check the validity of the approximation that the maximum mean power is equal to P_o. We may also verify that, since the position of the maximum is almost constant, this is equal to the mean of the maximum received power levels.

CHAPTER 5: Equipment modifications, and fieldwork in Devon Island

In Chapters 2 and 3, we described fieldwork undertaken in East Antarctica, and subsequent attempts to examine the behaviour of the echoes as recorded in the form of an intensity-modulated profile. It proved impossible to make quantitative deductions from these records due to the uncertainties involved in the recording and retrieval processes.

For more detailed studies to be feasible, quantitative recordings must be made of the strength and shape of the echo pulse, at the time of sounding. Suitable modifications were made to the sounding equipment, and an expedition was organised to Devon Island, part of whose purpose was to develop a technique for detailed investigations of the bedrock surface.

(5.1) Equipment developments

The basic equipment remained much as that used in the Antarctic sounding, using a SPRI Mk IV radio echo sounder, operating at 60 MHz. This was mounted in a sledge-born 'caboose', drawn by one or two motor-sledges, with the antenna mounted on its own skis and towed behind, (Fig.5.1). The prevailing temperature of between -10° and -20°C was not suitable for operation of the sounder, a catalytic heater was used continuously to warm both equipment and operator. Power was derived from two heavy-duty 12-volt accumulators, and the stability of the vehicle was maintained by the combined weight of operator and batteries.

Fig.5.1. The echo-sounding 'train' in the course of the traverse to the West of the base camp.

TABLE 5.1

Characteristics of the radio echo equipment used by the SPRI expedition to Devon Island.

OPERATING FREQUENCIES (MHz)	60	440
RECEIVER BANDWIDTH (MHz)	23	23
PEAK OUTPUT POWER (WATTS)	300	15
ANTENNA GAIN (dB)	+4.5	+10
TRANSMITTED PULSE LENGTH (metres)	46	46

The equipment drew a current of between 5 and 10 amps, depending on the number of recorders being used. Since in the main only one 'z-mod' recording oscilloscope and camera were used, the battery capacity of 120 Ampere-hours gave a maximum continuous operating time of between 16 and 20 hours.

The antenna consisted of a single folded dipole, with a half-wave parasitic reflector mounted 1/4 of a wavelength above it. This was fed through a tunable balun, and provided a calculated forward gain of +4.5 dB, in free space. This was, of course, directed downwards into the ice, and refraction at the surface provides a further 5 dB of gain. (This is due either directly to refraction if the antenna is effectively 'in air', or to increased apparent area due to reduction of the wavelength if the antenna is 'in the ice'. For our purposes the two are equivalent (Ewer. Smith, 1971)).

A summary of the system parameters can be seen in Table (5.1).

(5.1.1) A-scope recording system

The major refinement to the system consisted of the provision for quantitative recording of the echo pulse envelope. As part of the standard echo sounder, an oscilloscope is provided which displays the radar receiver output in 'A-scope' format, so that the operator can monitor the received signals. It was decided that, from a range of possible recording systems including videotape and paper tape loggers, that the simplest, cheapest and, for the purposes of this pilot study, most effective technique would be to photograph the 'A-scope' trace using a Super-8 cine camera. As installed, this could be controlled

either by the proprietary, continuously variable speed control, or by distance-related signals generated by a bicycle wheel towed behind the caboose. In the latter case, a digital dividing unit allowed cine frames to be exposed at intervals of 1,2,5,10 or 50 metres. The recording apparatus is shown in Fig.5.2, and an example of an 'A-frame' in Fig.5.3.

The usual brightness-modulated recording technique was also used, with the addition of a small light-emitting diode close to the c.r.t. screen which caused a mark to appear on the recording film indicating the positions along the survey profile at which A-scope photographs were taken. (These latter will be referred to as 'A-frames'). This allows minute correlation of t the A-frames with the (time-controlled) z-mod films.

The same transmitter and receiver were used throughout these experiments. The exact degree of stability of the output power is not known. However, the antenna was carefully designed, and tuned to the transmitter in situ: we shall assume that the matching was constant, and that the transmitter gave a constant output to within ± 1dB (this is equivalent to assuming stability of the supply voltage to the transmitter of $\pm 10\%$, which is a reasonable figure).

Calibrations were made before each day's work, by connecting the transmitter to the receiver via a step attenuator, and measuring the response to known signal levels. Some discrepancies can be seen between calibrations (Fig.5.4), consisting of a vertical shift between the different curves. The differences arise from a temperature effect in the receiver: the output level of the video amplifier is determined by a chain of diodes, whose forward bias voltage decreases as their temperature rises during operation.

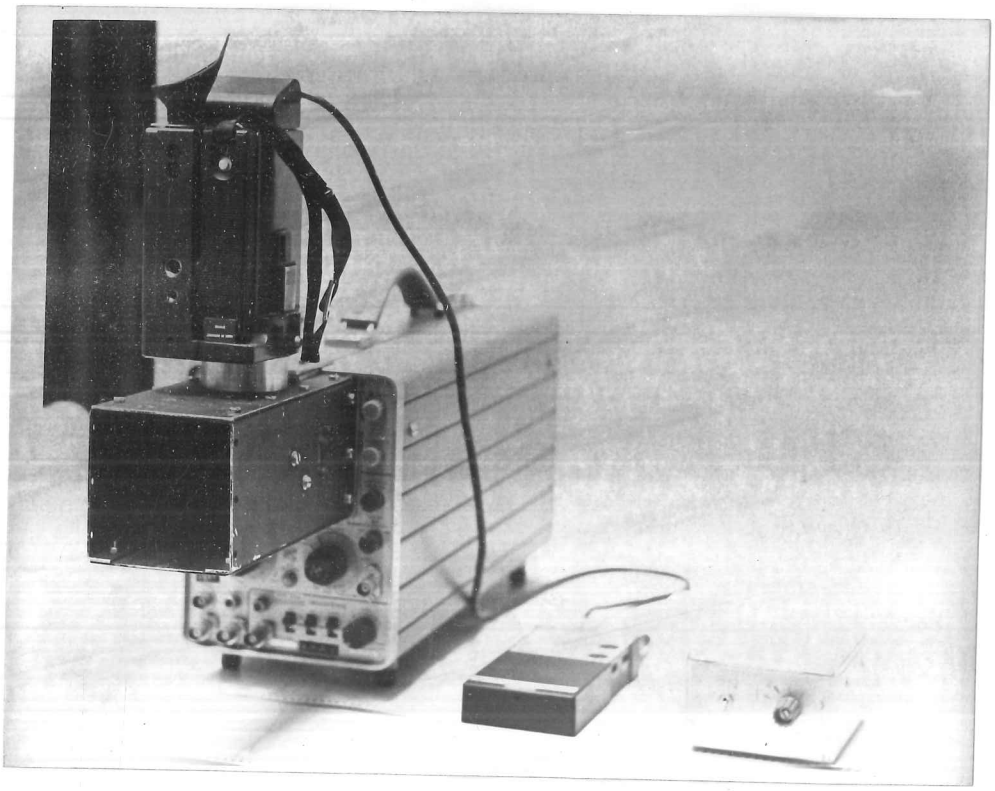

Fig.5.2. The A-frame recording apparatus.

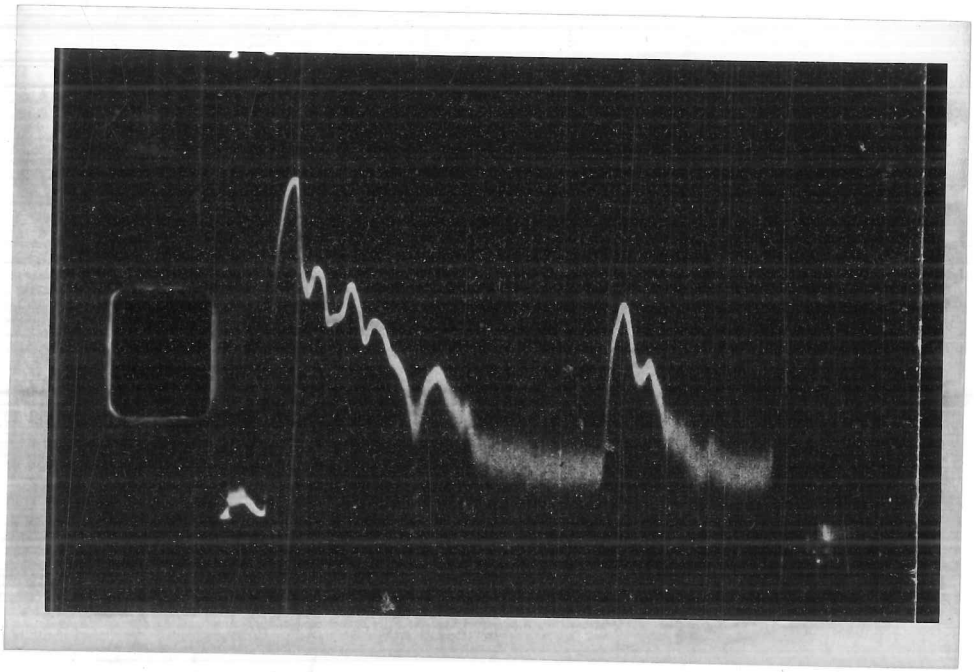

Fig.5.3. A typical A-frame.

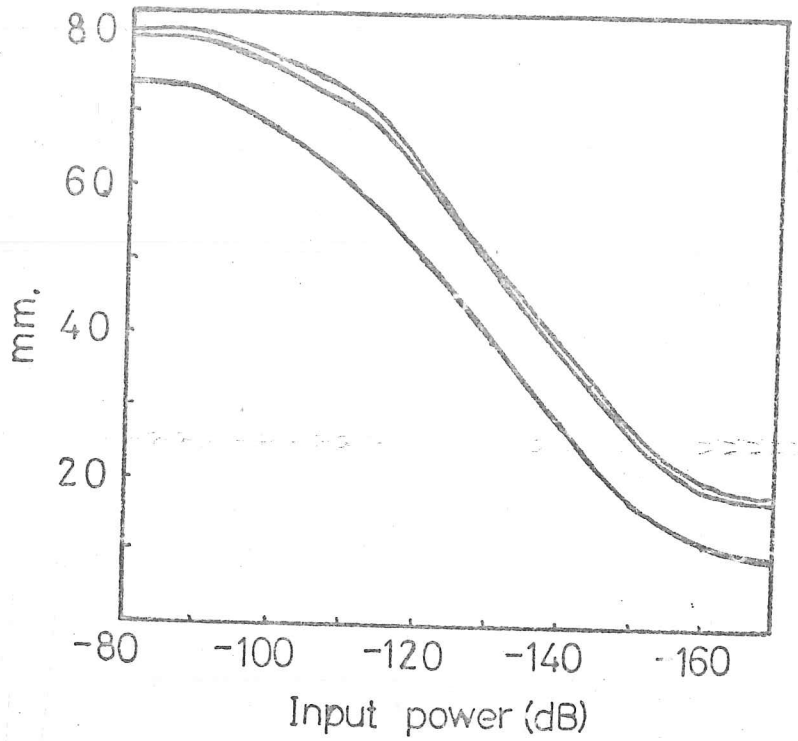

Fig.5.4. Calibration of the receiver system, expressed in terms of millimetres of displacement on the reader screen.

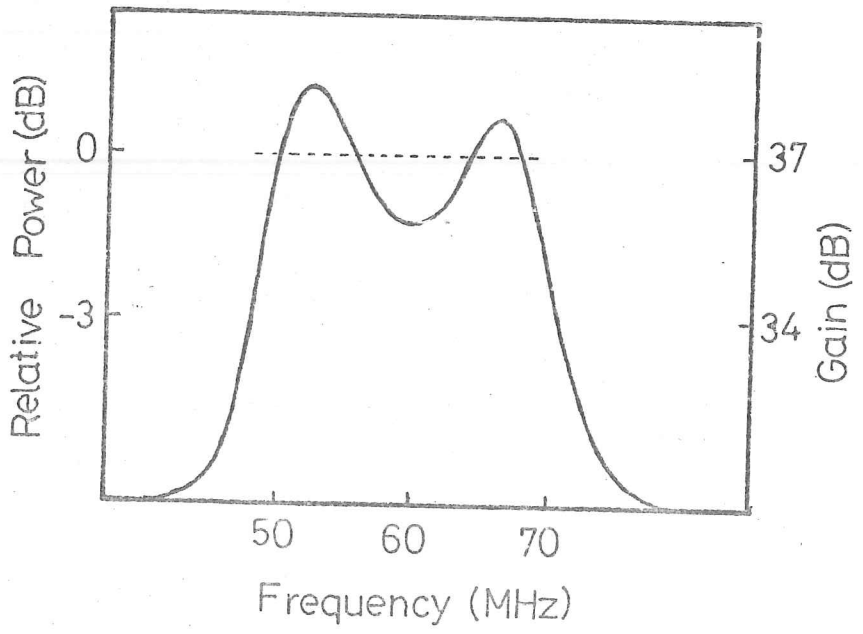

Fig.5.6. Pass-band of the receiver pre-amplifier.

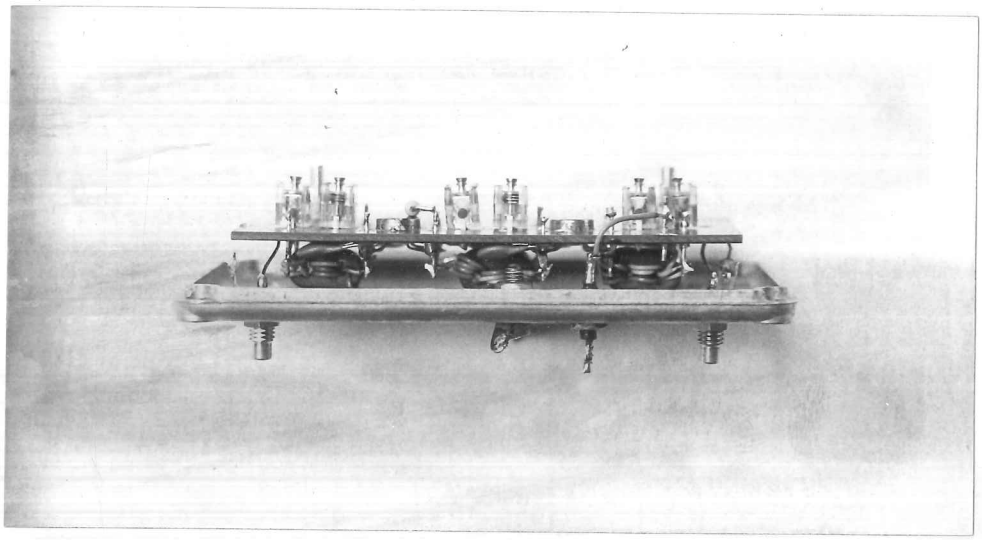

Fig.5.5. The wide-band preamplifier.

In the course of sounding, the output level corresponding to the background noise was found to fall gradually, and we shall use the lowest of the illustrated curves, with a correction for the observed value of noise voltage. A further correction must be applied to allow for 'sky noise'. It was observed that, after a noise level centred at 10mm had been present during calibration, the connection of the antenna resulted in an increase of about 2mm. We therefore take a noise level of 12mm as the standard during operations, and correct to this value.

(5.1.2) Wide-band preamplifier

The requirement to observe as accurately as possible the envelope of the received pulse at all delays made it necessary to build a new filter and pre-amplifier for the receiver. The direct breakthrough signal from transmitter to receiver via the T/R switch had a strength of about 40 dB below that of the transmitted pulse, representing a massive overload to the receiver input. The existing circuit required about 2 microseconds to recover from this overload, which a serious handicap since no echoes could be observed from depths of less than about 200 metres.

A new preamplifier was built, which combined the functions of filtering, with a bandwidth of 20 MHz, and amplification of 35 dB with a very fast recovery time. The circuit was based on a design by Dr. S. Evans, using integrated r.f. amplifiers, coupled by high-frequency ferrite-cored transformers. The premaplifier is shown in Fig.5.5, and its pass-band is illustrated in Fig.5.6.

(5.1.3) 440-MHz radar

A low-powered, phase-sensitive radar, operating at 44 MHz, was built by M. Gorman for the dual purposes of comparison with the results of the 60-MHz sounder, and for wave velccity measurement.

(5.2) Fieldwork in Devon Island

The experiments in Devon Island took place between May 13th and June 26th 1973. The party consisted of, from SPRI, Dr. G. de Q. Robin, A. Clayton, M. Gorman and the author, and Dr. C. S. M. Doake of the British Antarctic Survey. Logistic support was provided by the Canadian Department of Energy, Mines and Resources, through Dr. S. B. Paterson of the Polar Continental Shelf Project.

The expedition had four main objectives:

(a) To sound the ice in the central region of the ice sheet, and deduce a contour map;

(b) To study in detail the form and behaviour of the bedrock echoes; to locate, if possible, a geological boundary which is thought to cross the island beneath the ice; and to develop a procedure for such investigations;

(c) To measure the velocity of the radio waves in ice, through the use of deep boreholes and an interferometric technique;

(d) To measure the surface velocity of the ice with respect to bedrock, by observation of the fading pattern of the echo over a small area, and noting its change in position with respect to the surface over a period of a few weeks.

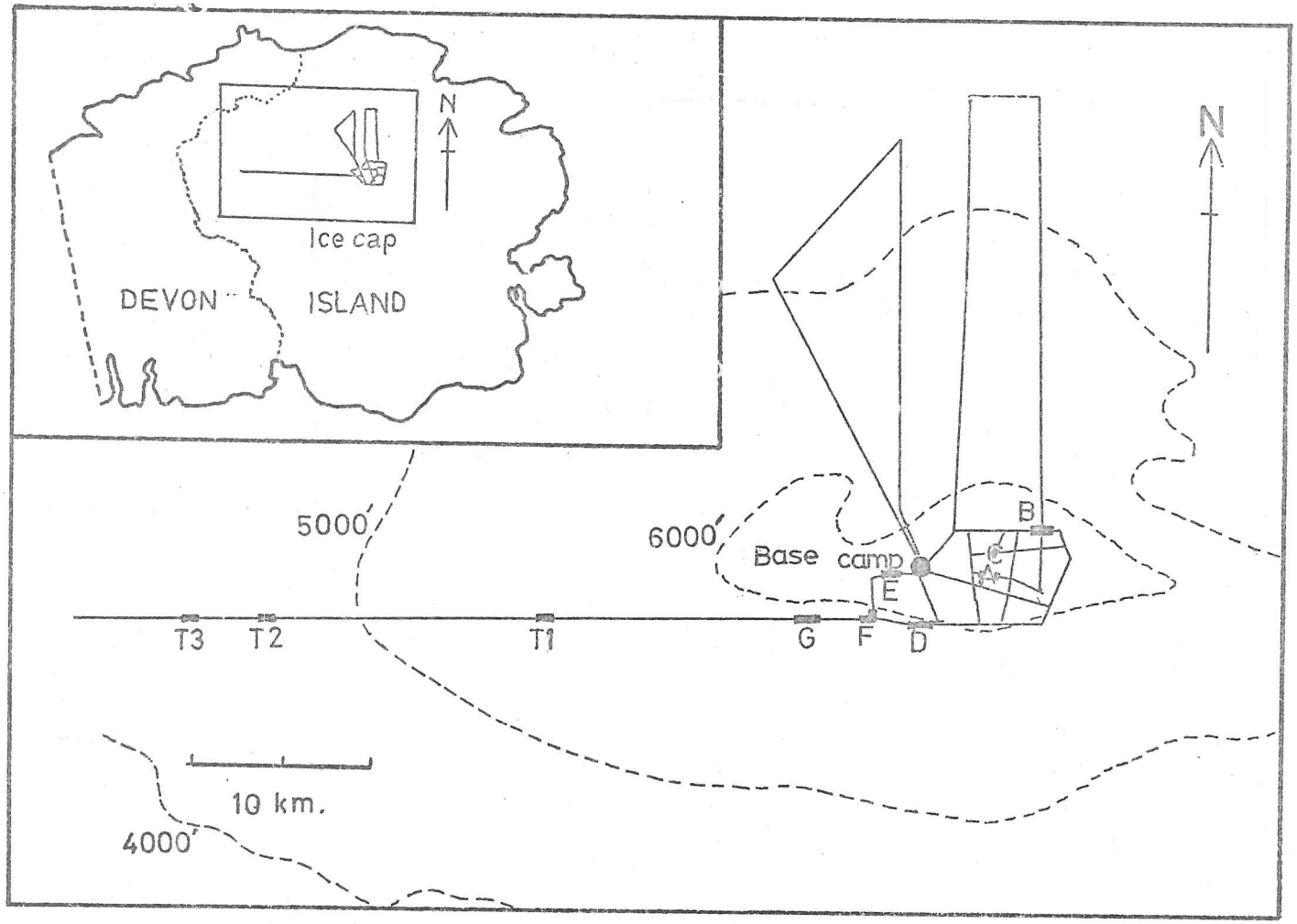

Fig.5.7. Echo sounding paths covered by the SPRI expedition to Devon Island (1973).

Experiments of secondary importance involved reflections from within the ice, caused mainly by density layering, and also a short investigation of the effect on the echo of rotation of the antenna, to throw light on anisotropy of the ice crystal structure.

The main aims were achieved with considerable success.

We are concerned here with part (b) of the programme, which occupied four days' work exclusively, and was carried on concurrently with the great majority of the general depth sounding. We shall describe the analysis of results as it relates to the objective of discovery of changes in the material of the bedrock, after a brief account of the experiments themselves.

The depth sounding was carried out over the paths shown in Fig.5.7. Over most of the distance, A-frames were recorded at intervals of 50 metres, resulting, from the 400 km of sounding track, in some 8,000 frames. At the lettered positions, where the path is more heavily marked, frames were recorded at 1-metre intervals, to give both a quasi-continuous record of the echo strength, and to provide a sufficient population of observations to give accurate values for the mean power, variance and auto-correlation function of the power, over a distance of a few hundred metres. Some of these paths were duplicated using the 440-MHz radar, in order to compare results at the two frequencies. Over a measured path of 300 metres, recordings were made at closely duplicated positions, at intervals of 1 metre, at different frequencies, pulse lengths and input attenuator settings. The arrangement for determining the positions at which the A-frames were recorded is shown in Figs.5.8 and5.9. Despite its ramshackle

Fig.5.8. The 'wheel-and-cord' system by means of which the position of recording of A-frames could be accurately fixed.

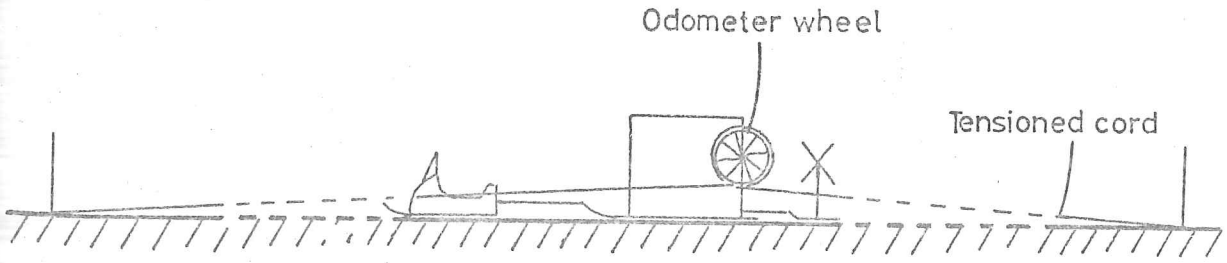

Fig.5.9. A diagrammatic representation of the system in Fig.5.8.

appearance, the system worked remarkably well, giving, for the first set of observations (at 60 MHz) an accuracy over the 300 metres of approximately $\pm 3.10^{-3}$ metres along the track. For the second set (at 440 MHz) the accuracy had deteriorated to about $\pm 10^{-1}$ metre; this was probably the result of adverse conditions such as heavy drifting of snow which caused the sounder to follow a somewhat erratic path. The accuracy across-track was generally about $\pm 10^{-1}$ metre for the 60-MHz set, but probably $\pm$ 1 metre for the 440-MHz set.

The three sets of close-spaced observations labelled T1, T2, and T3 in Fig.5.7 were carried out in the course of an extended traverse towards the Western edge of the ice-cap. It was thought that the geological divide which we have mentioned was most likely to run to the West of the base camp, and that its position might be detected by comparing observations along such a traverse.

The number of A-frames taken at any site varied between 300 and 1000. Over a rough reflecting surface, the echo strength may be expected to vary with a standard deviation of about 10 dB. In order to obtain a value for the mean received power with an expected error of less than $\pm$1 dB, it was necessary to obtain a measurement population of at least 100. (For a random sample from a normally-distributed population, the standard deviation of the mean is related to the standard deviation of the sample members by

$$\sigma_m = \frac{\sigma}{\sqrt{N}}$$

where σ_m is the standard deviation of the mean, σ is the sample standard deviation, and N is the size of the sample.

Though we are not strictly dealing with a normally-distributed population, the relation can be expected to hold approximately for our case.)

Since it is possible that the irregularities of the rough surface are correlated over distances comparable with 100 metres, it is advantageous to extend the samples over as long a path as possible. In practice the length was limited by the requirement that the ice depth should remain constant. Locations were chosen where the general survey had revealed a flat area of bedrock, with a constant ice thickness, (neglecting the small-scale roughness).

(5.3) Analysis of results

(5.3.1) Ice Depths

A detailed contour map of the topography of the ice cap has not been compiled from the SPRI sounding results. However, the sub-ice terrain may be loosely described in terms of a region of high relief towards the Eastern end of the island, reaching elevations of 1200 metres above sea level, which gives way to more gentle relief at lower altitudes towards the West. The change in topography may be related to the change in type of bedrock, which is known to occur on a generally North-South line across the island.

(5.3.2) Echo behaviour

We showed, in Chapter 1, that if we are able to detect changes in the reflection coefficient of the ice-rock interface of ± 2 dB, from measurements of the mean power, this would enable

us to separate rocks whose permittivities differed by about 20%. We shall work towards this as our primary means of detecting variations in the rock.

We saw in Chapter 4 that, in agreement with Harrison (1972) and Berry (1973), the mean value of the maximum level of power in the received pulse is to some extent dependent on the geometrical form of the bedrock surface. However, for a rectangular output pulse (that is an r.f. pulse with a steady maximum level, of a duration long compared with that of the rising and falling edges), this effect is not important unless the r.m.s. slope of the facets of the surface, is close to, or exceeds, the angle θ_{eo}, defined by

$$\theta_{eo} = \sec^{-1}\left(\frac{2h+P}{2h}\right)$$

We must discover, initially, whether or not this limitation is operative for the surfaces in Devon Island. The distinction is closely related to that referred to in Chapter 3, where we discussed the spacing of maxima of the fading pattern, and we shall examine the shape of the echo envelope in order to estimate the value of the r.m.s. slope.

(5.3.2.1) Envelope shape

The power received in the echo fallsoff as the falling edge of the output pulse reaches the surface, and reflections from an increasing range of angles are cut off, (Fig.5.10). We saw again in Chapter 4 that the average angular distribution of received power differs from the distribution of slopes in the reflecting surface mainly as a result of the scattering of waves from the surface due to diffraction effects. Broadly speaking,

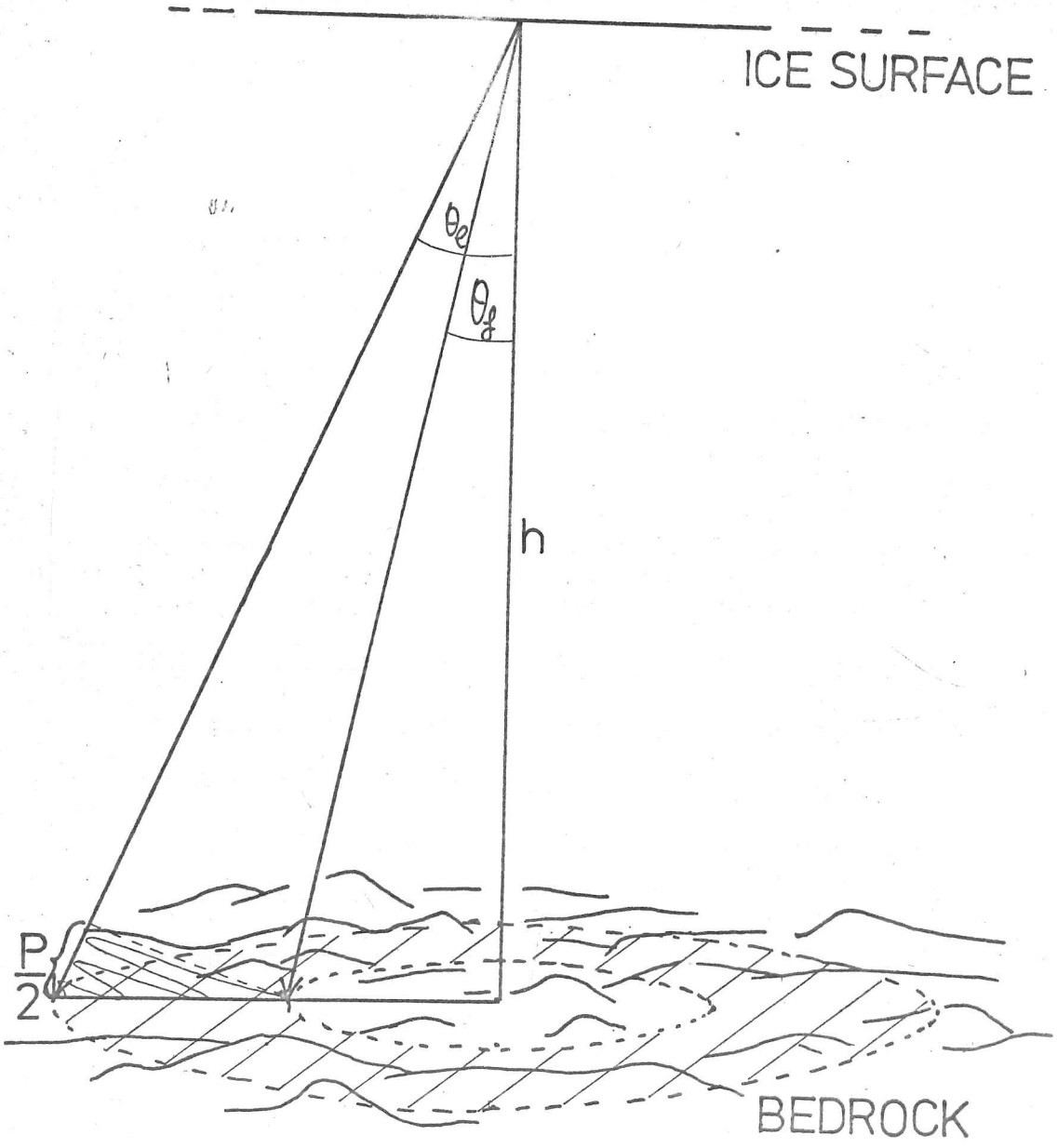

Fig.5.10. The annular area, illuminated by the pulse after the falling edge has reached the rough surface, which contributes to simultaneous returns.

the effect of diffraction would be to introduce an almost isotropic component in the reflected wave, which would be observed as a shallowly-sloping, extended tail to the echoes. Such a tail is not apparent in the recorded traces, and we shall assume that diffraction plays a minor role in defining the angular distribution of received power.

Some examples of echo traces can be seen in Fig.5.11, taken from different parts of the ice sheet. The shape of the transmitter pulse, when applied to a standard 50-ohm load, can be seen for comparison. In interpreting these records, it is important to remember that a logarithmic characteristic was used, and that the power of a signal at the lower edge of the scale may be less than that of one at the upper edge by a factor of 10^6. The echoes are re-plotted in Fig.5.12 on a linear scale. The gradient of the echo tail at any delay is proportional to the frequency of occurrence of facets at the angle θ_f corresponding to the trailing edge of the output pulse at that delay (see Chapter 4). By measuring the gradient of the linear traces we may estimate the distribution of slopes in the surface at any point, and obtain an average value for an area. The usefulness of this technique is limited for small slopes, since the differential delay for angles of less than 10^0 is less than 2% of the total delay for the first return. For ice of 500 metres depth, this represents only 100 nano seconds, and is not sufficient to allow an accurate measurement of the power gradient. Since the trailing edge of the pulse is also of this order of duration, the significance of the gradient, if accurately measured, would not be clear. We can therefore only use the

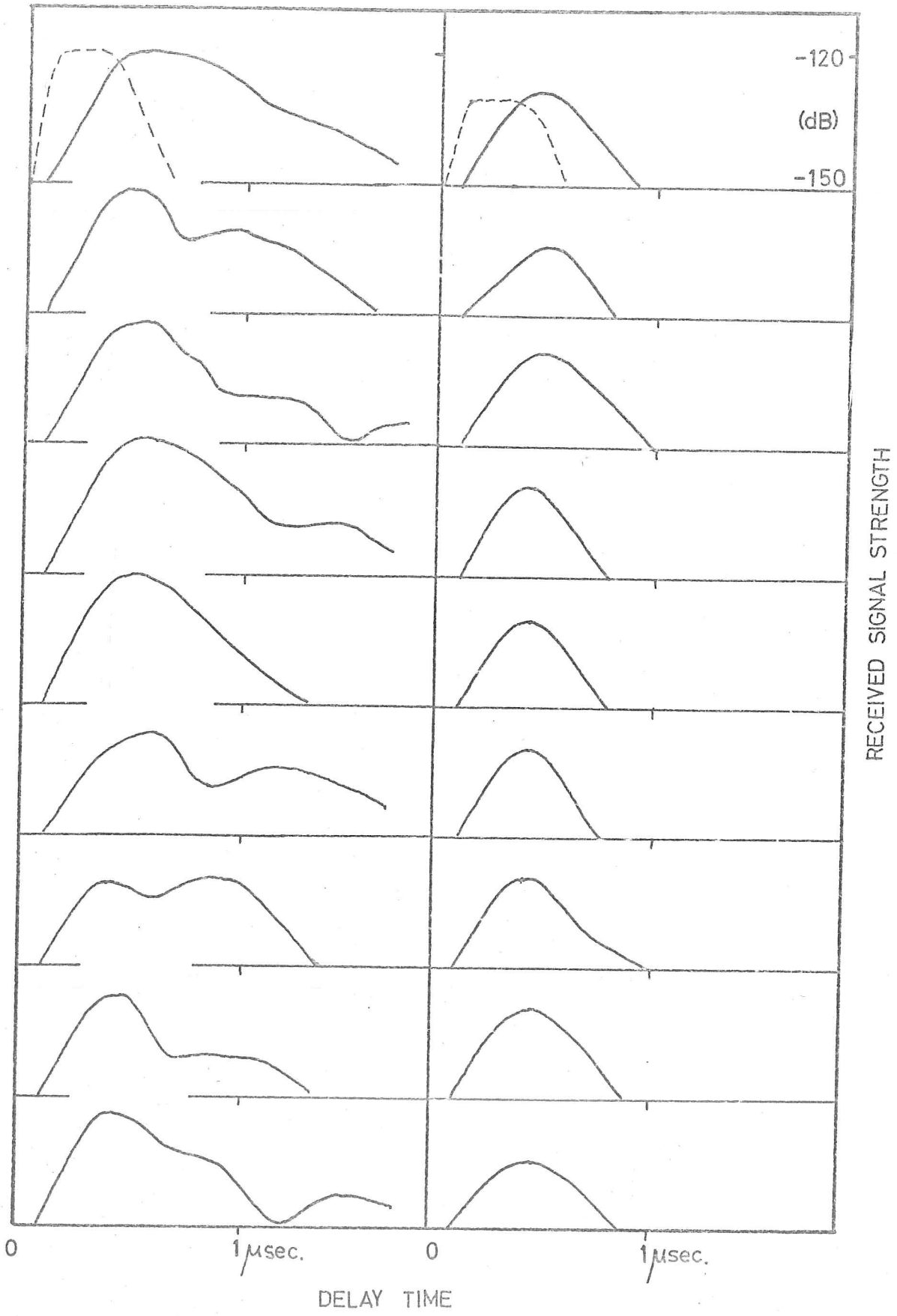

Fig.5.11. Echo envelopes received from regions at opposite ends of the 'Western traverse', with the power expressed in dB referred to the transmitted power.

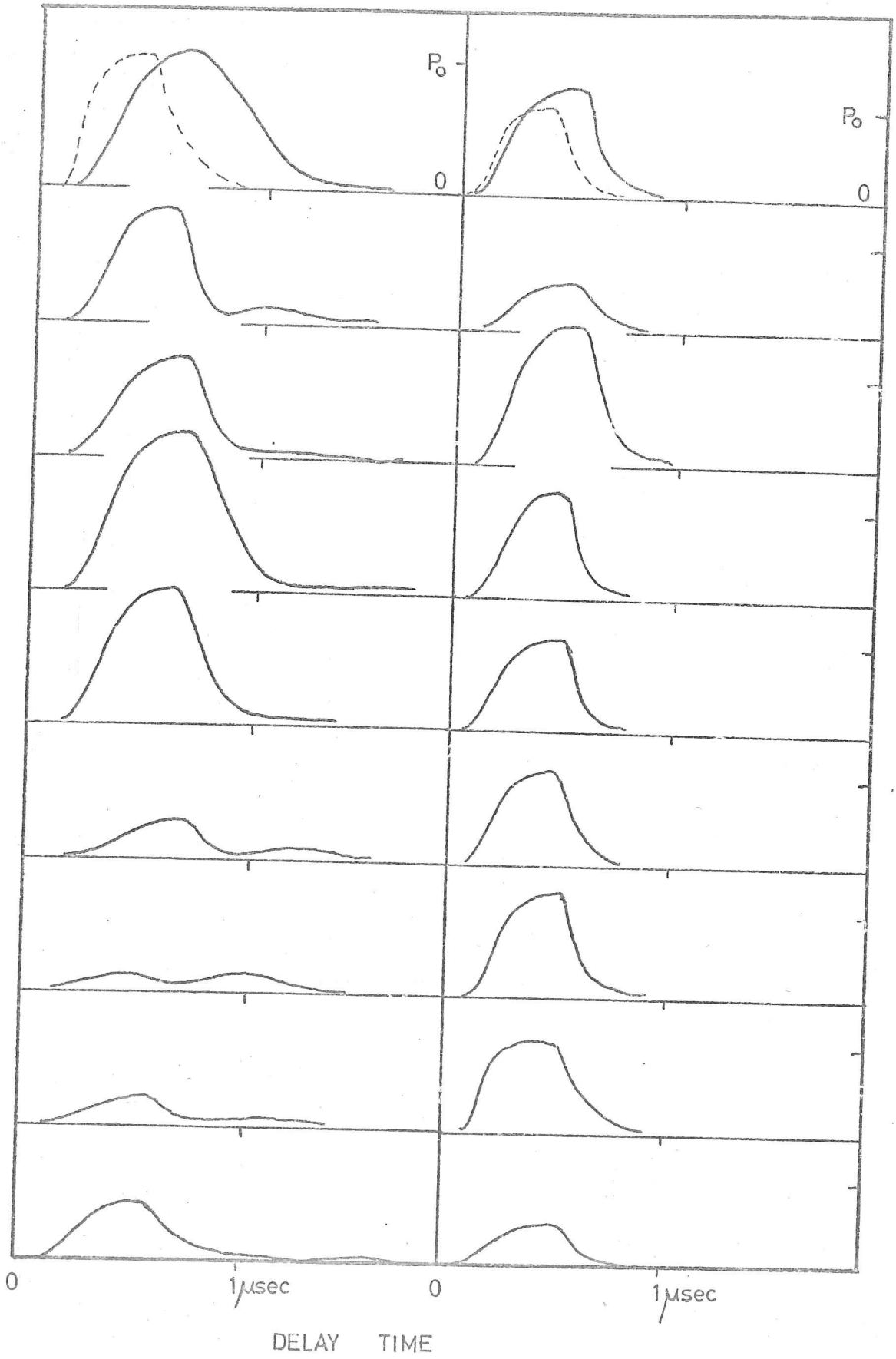

Fig.5.12. The envelopes of Fig.5.11, re-plotted on a linear power scale.

method with any confidence for investigation of the limiting form of the distribution above slopes of about 1:6, rather than for a complete description. The difficulty is illustrated when we analyse the shapes of the echo traces of Fig.5.11. Though the nominal pulse length (-3 dB) is 250 nanoseconds, its duration, including rising and falling edges, is closer to 400 nanoseconds for the purposes of our logarithmic receiver. The exact position of the start of the falling edge of the received pulse is not easy to locate, and the shape of the derived probability distribution for small angles is critically dependent on it. However, the resulting distribution is much less sensitive for angles above 10^{0}-15^{0}. The two sets of traces, which were obtained at the Eastern and Western ends, respectively, of the extended Western traverse have mean shapes as shown in Fig.5.13. By assuming a Rayleigh distribution of slopes, which is justified by the observed FORM of the echo ENVELOPE, we use the maximum rate of change of the power to deduce values of $0.15 \pm .5$ and $.23 \pm .3$ for the r.m.s. slopes describing the surfaces in the two regions. These are less than the angle θ_c, which, for ice of depth 500 metres and a nominal pulse length of 42 metres, has a nominal (and minimum) value of 17^{o}, equivalent to a slope of 0.31. In both cases the estimated frequency of occurence of gradients greater than 0.3 is small. There is no evidence of a diffracted component in the received pulse, and we shall assume that the roughness of the bedrock is correlated, in general, over distances greater than the radio wavelength (2.8 metres).

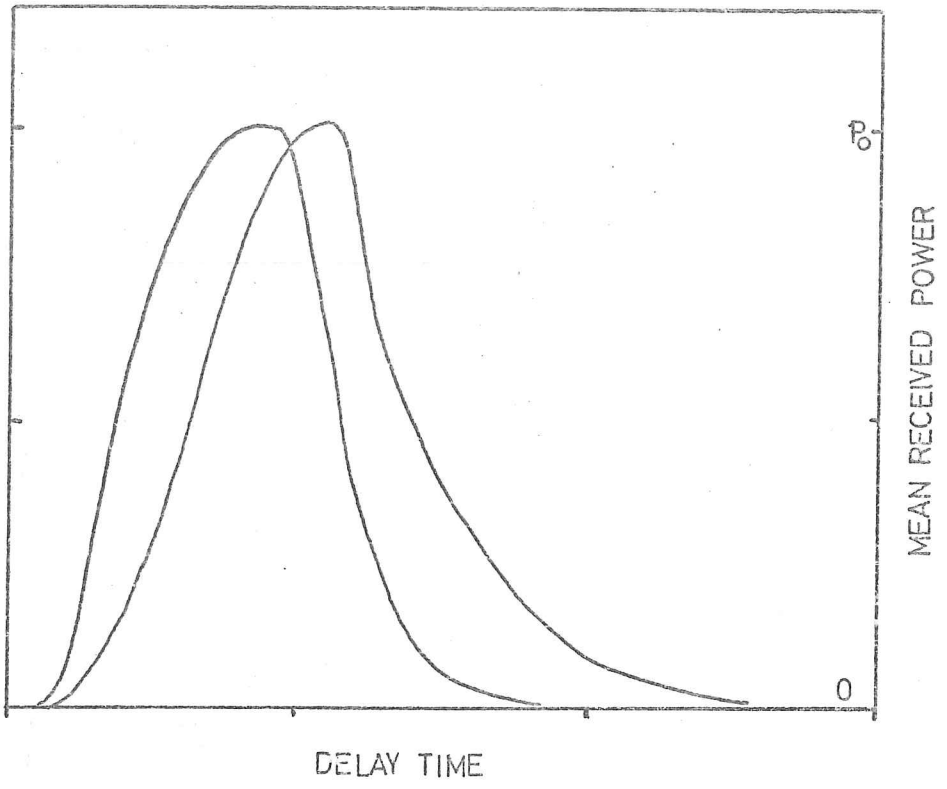

Fig.5.13. Mean shapes for the envelopes shown in Fig.5.12.

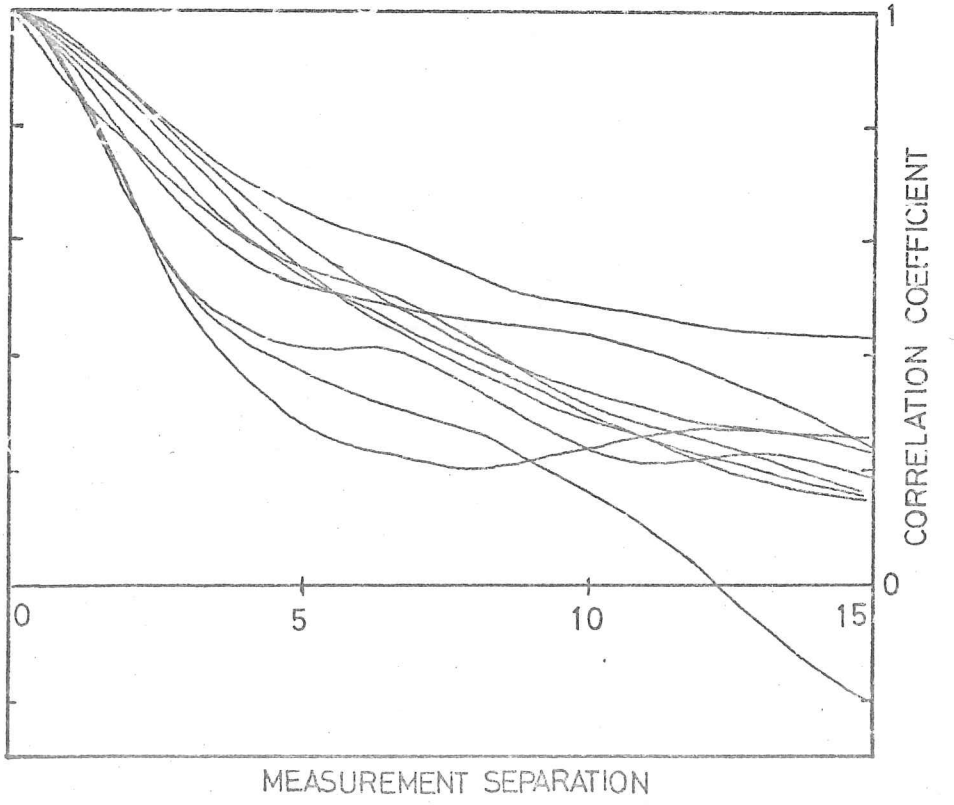

Fig.5.14. Autocorrelation functions for the close-spaced sets of A-frames.

Taking these derived characteristics of the surface into account, we shall assume that the mean level of the maximum received echo power is closely equal to P_o, which is the value expected from a smooth plane reflector at the same range, and was defined in Chapter 4. This greatly simplifies the analysis of the results, since we may calculate relative values for the reflection coefficient at the bedrock without reference to the local roughness characteristics.

The comparison of the r.m.s. slope with θ_{eo} is similar to Harrison's (1972) comparison of $\frac{T}{2\phi_o}$ with $\frac{\lambda}{4\pi}\sqrt{\frac{z_o}{P}}$. Remembering that $z_o = h$, that Harrison uses the pulse half-length rather than the full nominal length, and that $\phi_o = \frac{4\pi\alpha_o}{\lambda}$ condition is more stringent, by a factor of $\sqrt{2}$, than our form

$$\langle \beta^2 \rangle < P/h$$

His treatment deals with Gaussian-shaped transmitted pulses, and he considers the signal corresponding to the 'return' of the centre of the transmitted pulse, rather than the maximum received levels. Within his restriction, these will be approximately equal, and he also deduces that $\langle P \rangle = P_o$.

In Berry's (1973) terminology, this is not a 'long-tailed' echo, where the time delay at which one-half of the echo energy has been received is much longer than the pulse length (cf. Berry's expression (7.7)). We are dealing with his 'geometrical-optical' case, where the echo is almost entirely incoherent. Though he deduces a considerably reduced maximum mean power, this is because of his use of a short, Gaussian pulse, rather than our comparatively long, 'quasi-rectangular' envelope. It is important to recognise the distinction between the terms 'long-tailed' and 'incoherent'.

Confusion has arisen in the past because, though for an echo to possess a 'long tail' implies a degree of incoherence, the reverse is not necessarily the case: an echo, as in our case, may be entirely incoherent, and display all the high-contrast fading associated with high relief in the reflecting surface, without being extended out of proportion to the transmitted pulse. As a comment on Berry's treatment of the 'Fraunhofer case', we would point out that his conclusion that the echo power is given by the coherent component alone is based, besides the condition that h shall be very large, on the assumption that, as in the 'long-wave limit', the vertical extent of the irregularities is very small compared with the wavelength. The essential 'Fraunhofer' condition, where h is much greater than the dimensions of diffracting irregularities, may also be fulfilled where $\phi_0 > 1$ and the echo is entirely incoherent. We shall see that in this case the importance, for our purposes, of the Fraunhofer condition, is that the source-receiver is well outside the range of focusing of curved reflectors in the surface, and necessarily illuminates many reflecting facets simultaneously.

(5.3.2.2) Extent of variation of power

The variance of the received power, expressed as a fraction of the mean power, depends primarily on the vertical dimensions of the irregularities in the reflecting surface. Though the dependence is discussed in detail in Chapter 6, we shall use some of the results here, along with those of other authors, for the purposes of the Devon Island analysis.

If the horizontal dimensions of the irregularities are such that many independent reflections are received

simultaneously, the 'normalised variance v_p'' as defined above, approaches unity rapidly as the value of the r.m.s. vertical excursion of the surface, increases towards and passes the radio wavelength.

However, where the irregularities are of large horizontal extent, the value of v_p' may exceed unity for such values of α_0. In this case the effect of focusing increases the variation of the power beyond what might be expected from the addition of reflections of purely random phase. We can see that, if the illumunated area is of the same order of magnitude as that of 'individual irregularities', the auto-correlation of the surface will have some ordering effect on the reflections. Looked at another way, the curved reflectors give rise to 'caustics' along which a powerful reflection is observed, and troughs where the reflection is weak. If a large number of caustic patterns are randomly superimposed, the variations are averaged, and the variance decreases to that corresponding merely to random phase additions. For any given surface and sounding conditions, the caustics are limited near the surface and the sounder will only observe a significant effect if the sounding path passes through centres of curvature of the reflecting facets. In this case, the variance is only limited by the size of the individual reflectors, and by the wave-length which limits the 'sharpness' of the caustic, (see Chapter 6).

Values of v_p' have been calculated for the sets of close-spaced measurements, and are shown in Table (5.2). All except the value for run 'T3' exceed unity. (It may be noted that these figures differ from those given in Oswald (1975)

TABLE 5.2.

Values of the normalised variance V'_p found for the sets of close-spaced A-frames.

SET	A	B	C	D	E	F	G	T1	T2	T3
V'_p	1.4	1.8	1.1	1.3	1.5	1.2	1.1	1.3	1.0	0.8

for the same data. The difference arises from the use of a revised calibration curve: the main effect is a general reduction in calculated values of the power variance and also, as we shall see later, of the mean power. Horizontal auto-correlation functions for the echoes remain almost unchanged.) It is clear that we are dealing with surfaces whose vertical deviations are at least of the same order of magnitude as the radio wavelength. When v_p' is close to, but less than unity, we may deduce two possible values for ϕ_o, corresponding respectively to surfaces whose centres of curvature lie between the sounder and the surface, and those with very long radii of curvature. These are given by the formulae (Harrison, 1972):

for small radii of curvature, $v_p' = 1 - e^{-2\phi^2}$, and

for large radii of curvature, $v_p' = 2\phi_o^2 . (2\lambda h / \pi T^2)^2$

$= 2 . (8 \alpha_o h / T^2)^2$.

Though we cannot evaluate the second case without knowledge of T, the first case which, considering the surface slopes which we have calculated, is the more likely situation, gives the value for $v_p'=.8$ of $\phi_o = 0.9$. This corresponds to a value of α_o of about 20 cm.

We deduce that for these areas the parameter ϕ_c is close to or greater than unity, and that in some areas a degree of focusing takes place, giving rise to a power variance greater than unity.

(5.3.2.3) Horizontal variation

Our main analysis of the spatial frequency of fading of the echo will be made in Chapter 7.

We observe that the autocorrelation functions (Fig.5.14) fall to the value 1/e after a separation of greater than 4 metres. Harrison deduces a relation between the power fading length, τ_p, corresponding to the above separation, and the r.m.s. surface slope such that

$$\tau_p \simeq \frac{\lambda}{4\pi\beta_0}.$$

We obtain the result that for these areas $\beta_0 < 0.06$

Though this result is not in agreement with that calculated from the average received pulse shape, it represents a more favourable situation for the purposes of the study of the mean received power, and we shall leave the comparison of the two techniques of analysis to the relevant chapters.

(5.4) Mean signal strength levels

(5.4.1) Results for close-spaced observations

Fig.5.15 shows the mean strength of reflections for each of the 10 sets of close-spaced observations. Correction has been made for the geometrical (inverse-square) attenuation, the gain of the antenna and the added gain due to refraction, of + 5 dB (Ewen Smith, 1971). The figures represent residual attenuation due to absorption in the ice, and losses on reflection at the ice-rock interface. The correction applied for geometrical losses has the form:

$$G = \mathrm{Log}_{10}\left\{\frac{\lambda^2_{(air)}}{64\pi^2 h^2}\right\}$$

Seven of the ten points lie close to a straight line, with a correlation coefficient of .99. The regression line has a gradient of 2.25 dB/100 metres, with an intercept at zero

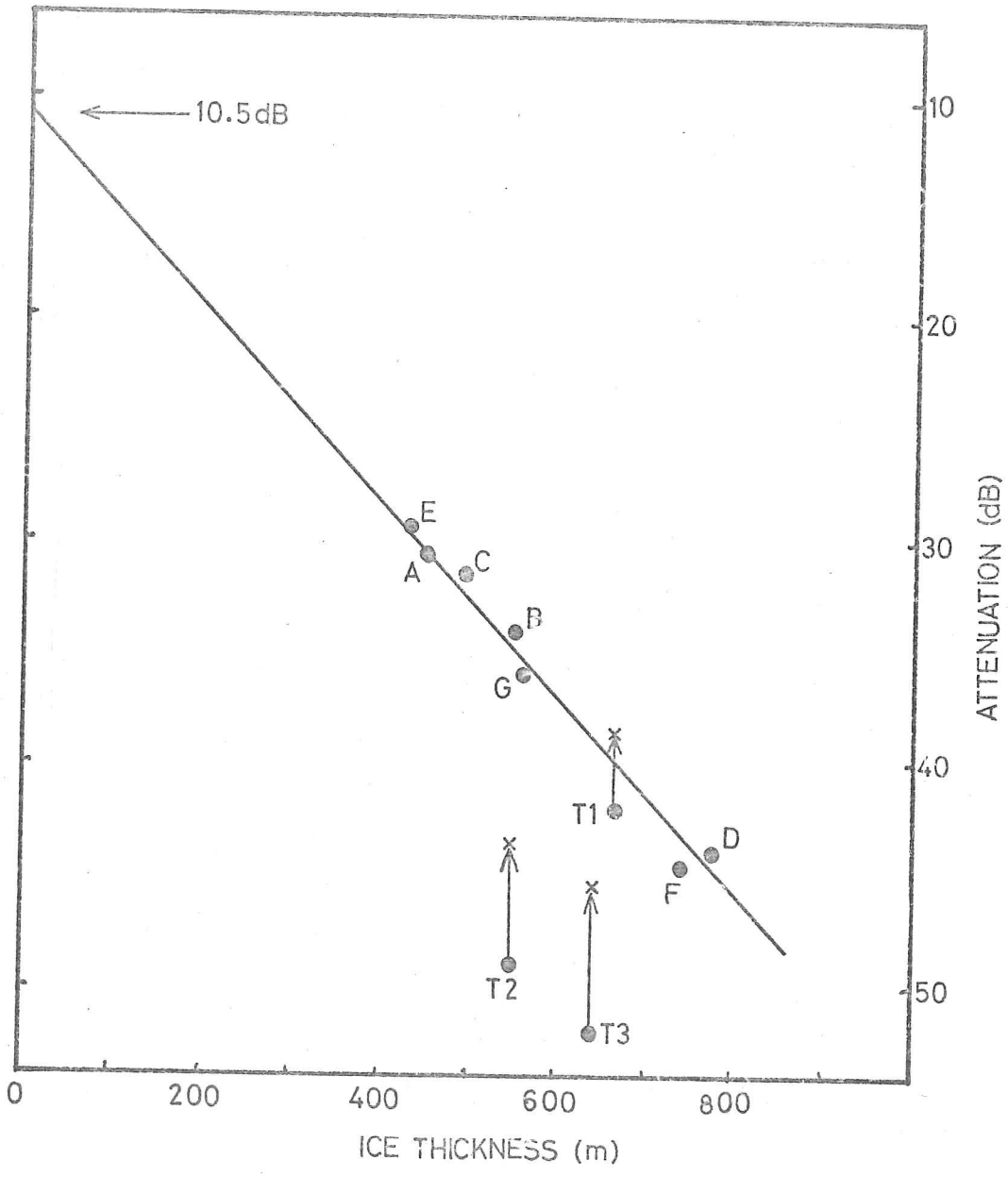

Fig.5.15. Mean power levels for the sets of close-spaced A-frames, expressed interms of the total attenuation due to dielectric absorption and reflection losses, as a function of the ice thickness.

depth of -10.5 dB. The standard error of estimate for the regression is ±0.5 dB. Remembering that a systematic error of ± 1 dB is inherent in the calibration of the strength measurement, we allow for an uncertainty of ± 1.5 dB in any estimate and in the zero-depth intercept. If we first assume that the absorption of radio power in the ice is constant throughout the ice thickness, the intercept corresponds to an estimate of the reflection coefficient at the base of the ice. The value of -10 dB, as extrapolated from the linear regression, is just within the probable range of values given in Chapter 1.

The above assumption is equivalent to that of constant temperature in the ice mass, and is an obvious over-simplification. Because of the geothermal heat flux, and the heating effect of strain in the lower levels of the ice, the temperature of such an absorption shows a corresponding increase.

The shape of the temperature profile at the centre of an ice cap is given theoretically by Robin (1955) in the form:

$$\theta_H - \theta_h = \left(\frac{d\theta}{dh}\right)_{base} \times \frac{\sqrt{\pi}}{2} \sqrt{\frac{2Hk}{\dot{a}}} \left\{ erf\left(\sqrt{\frac{\dot{a}}{2Hk}} \cdot H\right) - erf\left(\sqrt{\frac{\dot{a}}{2Hk}} \cdot h\right) \right\}$$

where θ_H is the ice surface temperature, θ_h is the temperature at a height h above the base of the ice, $\left(\frac{d\theta}{dh}\right)_{base}$ is the temperature gradient at the base of the ice, H is the ice depth, k the thermal diffusivity of ice and $\dot{a}$ the rate of accumulation. We assume values of $3.10^{-7} m^2\ sec^{-1}$ for k, and $3^{\circ}C/100$ metres for $\left(\frac{d\theta_h}{dh}\right)_{base}$. By letting h equal zero, we derive the total temperature difference between base and surface of the ice.

The mass balance of the Devon Island ice cap is extremely variable, both from area to area and from year to

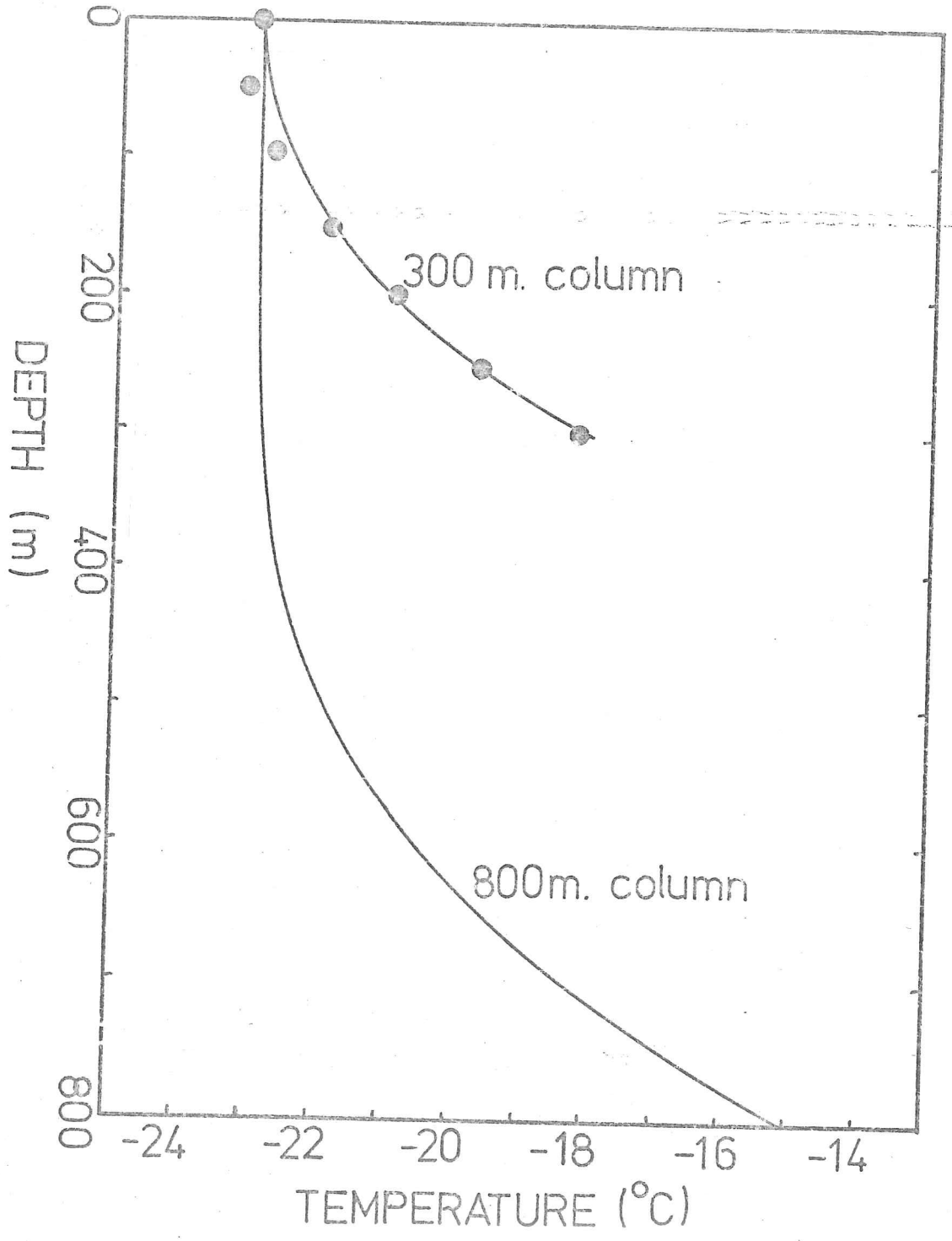

Fig.5.16. Profiles of temperature vs. depth calculated from Robin's (1955) model for 800- and 300-metre-thick ice. The dots represent experimental values found by Paterson in Devon Island for 300-metre ice.

year. (Koerner, 1970). It appears that in fact the average mass balance for the whole ice sheet is negative, with the great majority of the ablation occurring at altitudes below 1200 metres. At altitudes above 1400 metres the balance may vary from year to year between zero and +500 kg/m^2/year, and an average value of +200 kg/m^2/year is reasonable for the areas with which we are concerned. Fig.5.16 shows calculated temperature profiles for depths of 300 and 800 metres and a surface temperature of -23°C. The profile for 300 metres follows very closely the observed profile obtained by Paterson for a 300-metre borehole to bedrock near the ice-cap summit (Fig.5.16), and we may therefore place some confidence in the profile for deeper ice, though the flow rates of the ice will be greater the further we depart from the borehole, and the given formula will be less applicable. The transition from a depth of 300 metres to 800 metres, with the same surface temperature effectively involves the introduction of 100 metres of ice at the higher, bedrock temperature, and 400 metres at the surface temperature. From Westphal's graph (Fig.3.7), we expect the absorption at -17°C (i.e. at bedrock) to be 2 dB/100 metres, and at the surface temperature of -23°C, 1.4 dB/100 metres. We should therefore expect the slope of the graph of echo strength vs. depth to be given by:

$$dP/dh = (4(1.4)+2)/5 = 1.52 \text{ dB/100 metres.}$$

The observed regression line suggests strongly, therefore, that the absorption in Devon Island is greater than would be predicted by Westphal's graph. This may indicate our use of an incorrect temperature profile, but may also simply indicate

a difference between the ice in Devon Island and the Greenland ice sample from which Westphal's results were derived.

Returning to the question of the total absorption in the ice column, and the reflection at the base of the ice, we extrapolate the regression to zero depth as follows:

The gradient of the regression at any depth may be seen from the calculated temperature profiles to be the result of a combination of the absorption coefficient at the surface and at bedrock. Between 300 and 800 metres the combination was taken as having a weighting of 1:4 in favour of the surface ice. However, at less than 300 metres' total depth the temperature approaches a linear function of depth, and we take a simple average of the surface and bedrock temperatures in arriving at the absorption in a 300 metres column. We assume that the discrepancy between our absorption and the figure predicted by Westphal is due to a non-temperature-dependent impurity effect, and deduce the absorption coefficient, at the mean column temperature of $-21^{\circ}C$, from a version of Westphal's curve shifted vertically by 0.7 dB/100 m. Once again, we arrive at a figure of 2.2 dB/100 metres. (The figure is similar to the previous value since, though the absorption weighting is different, the exaggeration of the absorption close to the bedrock is reduced, which cancels the effect of the weighting). We therefore retain the figure of -10.5 dB for the reflection coefficient at the ice-rock interface.

We have so far mentioned only seven of the ten points shown in Fig. 5.15. These seven represent the sets of observations (A,B,C,D,E,F,) made around the summit of the ice cap,

which lies towards the Eastern end of the island. The other three points were obtained during the traverse to the West of the base camp, at a somewhat lower altitude and nearer the Western edge of the ice cap (T1, T2, T3).

These points lie outside the range of the regression for the first eight points. They exhibit strengths respectively 2, 14 and 13 dB below the values to be expected from the trend of these points, which is a difference of about five times the standard error of estimate, for set T1.

We explain the discrepancy as a combination of two effects:

A) Differential dielectric absorption due to higher general temperatures in the ice.

B) A discrepancy in the power reflection coefficient at the bedrock surface.

Dealing with (A) first, a rise in the surface temperature of the ice, and a corresponding rise throughout its volume results from the lower surface elevation as the Western edge of the ice cap is approached. The elevation in the region of the summit is about 1900 metres, falling to about 1400 metres where the Western sets of measurements were made (altitudes measured by aneroid altimeter). Set T1 was made at an altitude of 1600 metres. Ice surface temperature measurements are not available in this area. Loewe (1970) indicates that where the surface of an ice sheet is sufficiently cold that there is little heat transport by melting and refreezing in the upper layers, the firn is generally in thermal equilibrium with the mean annual air temperature. Though some such melting does occur in Devon Island, we shall assume that

the variation of surface temperature parallels that of the air, and calculate the probable value from a standard 'lapse rate' (the meteorological term for variation of air temperature with altitude). The lapse rate should lie between 7.5° and 10°C per 1000 metres, depending on the degree of saturation of the air and the temperature. (Barry and Chorley, 1968). For temperatures as low as -20°C, however, there is little difference between the values for saturated and for dry air, and we take the figure of 10°C per 1000 metres as the upper limit, though 9°C per km. might be a closer approximation. We would therefore predict, for a difference in elevation of 500 metres, a temperature change of about 5°C. The ice surface temperature in the area of the Western sets of observations should therefore be not higher than -18°C, and for an ice column of 500 metres depth, the mean absorption temperature should be approximately -15°C, as opposed to -20°C for the Eastern sets. Though we believe the absolute absorption in Devon Island to be higher than that predicted by Westphal, we assume that the variation with temperature is similar to his finding, in which case we may expect an additional 0.5 dB/100 metres of ice path, or 1 dB per 100 metres of additional range (remembering the two-way transit of the waves).

For T2, then, up to 5.5 dB of the deficit in power may result from the higher temperature of the ice in this region, and for T3 up to 6.5 dB. There remain, therefore, 8.5 dB and 6.5 dB which cannot be accounted for in this way. For T1, the difference in elevation of 300 metres, a deficit of 3.5 dB may be expected, bringing this point in line with the seven eastern sets.

The simplest explanation for the extra reduction in strength lies in a reduction of the reflection coefficient at the bedrock surface. We have estimated a value for the reflection coefficient for the Eastern sets of -10.5 dB. It is not easy to estimate the uncertainty in this figure, since our calculation of the likely temperature profile rests almost entirely on theoretical considerations, with experimental confirmation only under ideal conditions (that is, very close to the centre of outflow of the ice). However, this value is at the upper end of the predictable range of reflection coefficients, and it is at least plausible that any change in the bedrock material would result in a reduction. The value of -10 dB would indicate a rock permittivity of approximately 10, which at radio frequencies may easily be attained. It is more probable in the case of igneous rocks, and less likely in the case of dry (or frozen) sedimentary rocks.

A value of between -19 dB and -17 dB is implied for the Western reflection coefficient, corresponding to a rock permittivity of about 5. This is less likely for igneous rocks, but may well correspond to dry sandstone (Keller, 1966). These values of the rock permittivity would agree with maps of the Canadian Geological Survey, which indicate the dominance of very old igneous rocks (granitic gneiss etc.) towards the Eastern end of the island, which are overlain towards the West by much younger sedimentary rocks of the Cambrian and Ordovician periods. Though we cannot expect to define exactly the geological type of the bedrock in this way, we may at least suggest a correspondence between the apparent change in reflection coefficient and the known change in the subglacial rock.

(5.4.2) Results for 50-metre-spaced observations on the Western traverse

Having shown the change of the apparent reflection coefficient on travelling from East to West over the Devon Ice Cap, and suggested its correspondence with a geological boundary which is known to pass beneath the ice in this area, we may attempt to locate the change by measuring the mean strength of echoes recorded at 50-metre intervals along the entire traverse.

Fig. 5.17 shows the strengths obtained in the course of sounding. Each point consists of an average of ten measurements, giving the average strength over each 500 metres of path. This may be compared with Fig. 5.18, which shows the ice depth on a suitable scale. We see that, allowing for some scatter which is probably due to the large-scale curvature and focusing effect of the surface, the strength at first corresponds closely with the ice depth. However, the strength having risen as expected from cairns 'C' D'' to G', an abrupt fall is observed which is maintained over 3000 metres, with no commensurate increase in the ice depth. The strength then rises to near its previously expected value, between cairns I' and K', before falling away again. After cairn M' the points are more erratic than previously. (The 'cairns' represent positions along the traverse where snow cairns were built to mark the path of the outward journey and to assist in maintaining a straight Westerly direction).

The close-spaced sets of measurements which we have mentioned were made near cairns E', N', and O', respectively. T1 lies in the section before any anomalous reduction of the received power: T2 and T3 lie in the later section, where the

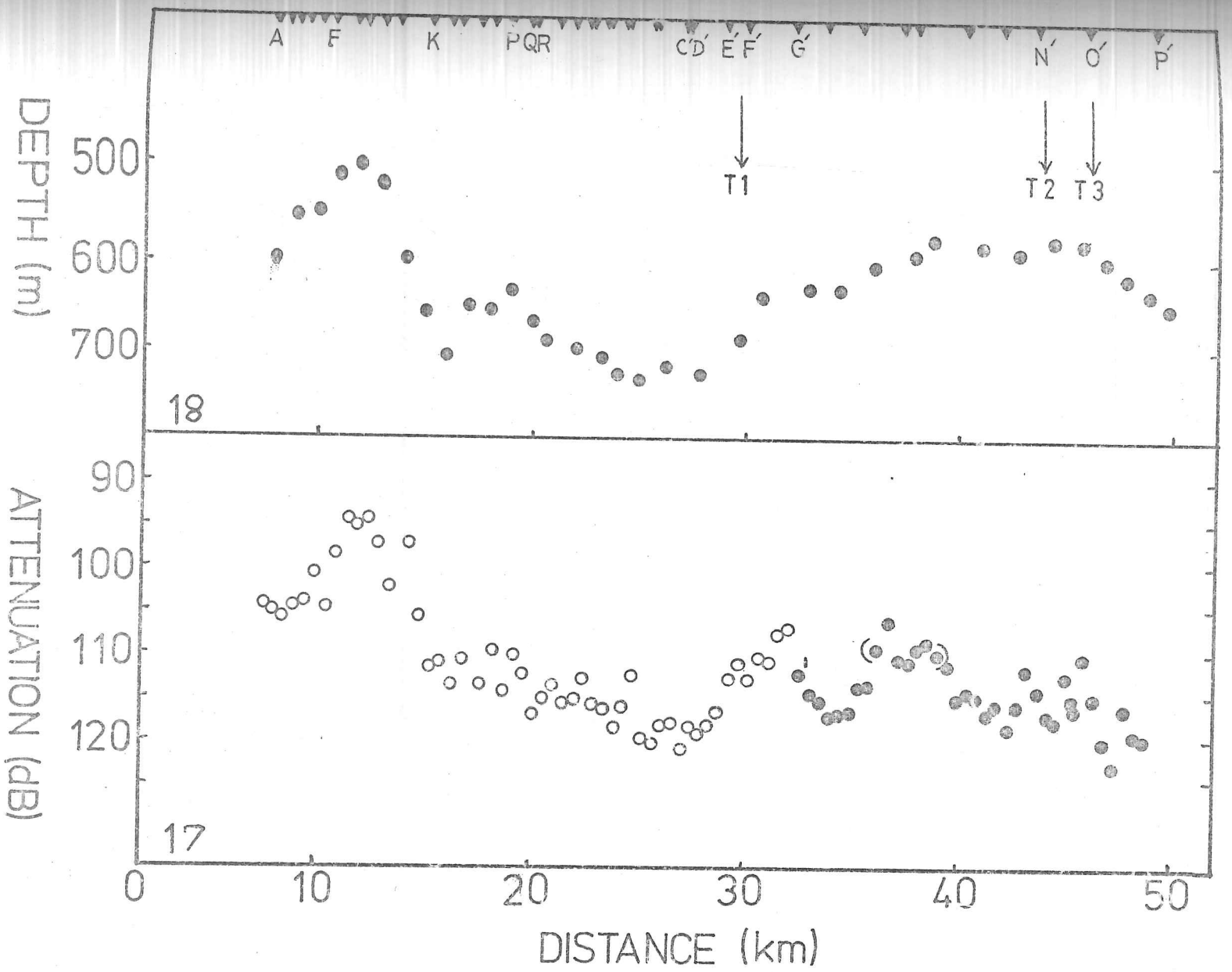

Figs.5.17 and 5.18. Total attenuation, and ice thickness, plotted against distance along the Western traverse.

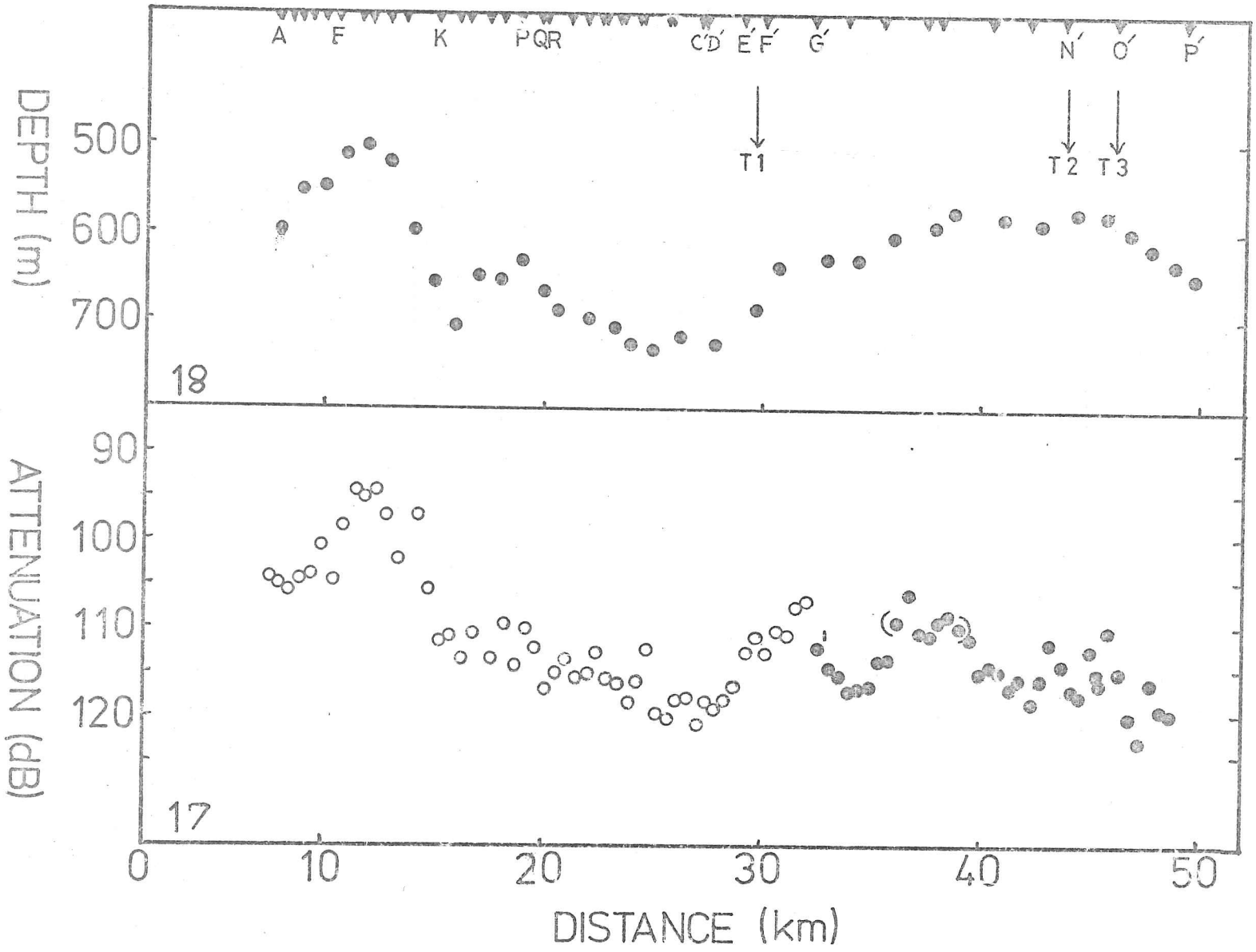

Figs.5.17 and 5.18. Total attenuation, and ice thickness, plotted against distance along the Western traverse.

500-metre means are somewhat erratic but still considerably reduced.

The form of the graph in Fig.5.17 indicates that the strength reductions observed towards the West are not due to a gradual increase in ice temperature, with an attendant increase in dielectric absorption, but to localised changes in the bedrock reflection coefficient. Comparing the variation of strength with the bedrock topography (shown in Fig.5.19), the later increases in strength correspond in most cases with slight prominences in a surface of generally low relief (points a,b,c,d) which contrasts with that of the Eastern part of the traverse. We conclude, remembering the arguments of the previous section, that the granitic bedrock of the Eastern part of the island gives way, some 32 km. West of the base camp, to a superimposed layer of sediment with some protrusions of the older rock (possibly exposed as a result of ice erosion).

These conclusions are supported by a statistical analysis of the observed strength, expressed in decibels referred to the transmitted power as a function of depth. We plot the echo power vs. ice depth in Fig.5.20. Points derived after G' are solid circles. We initially separate the points on either side of G', and make the null hypothesis that they belong to the same normally-distributed population. The correlation coefficient for the whole population is found to be 0.6 which, in view of the large number of points, is highly significant. The standard error of estimate for a single value of the ordinate is $\pm$ 5 dB. The standard error for the mean of n values would be $5/\sqrt{n}$, so that for the group

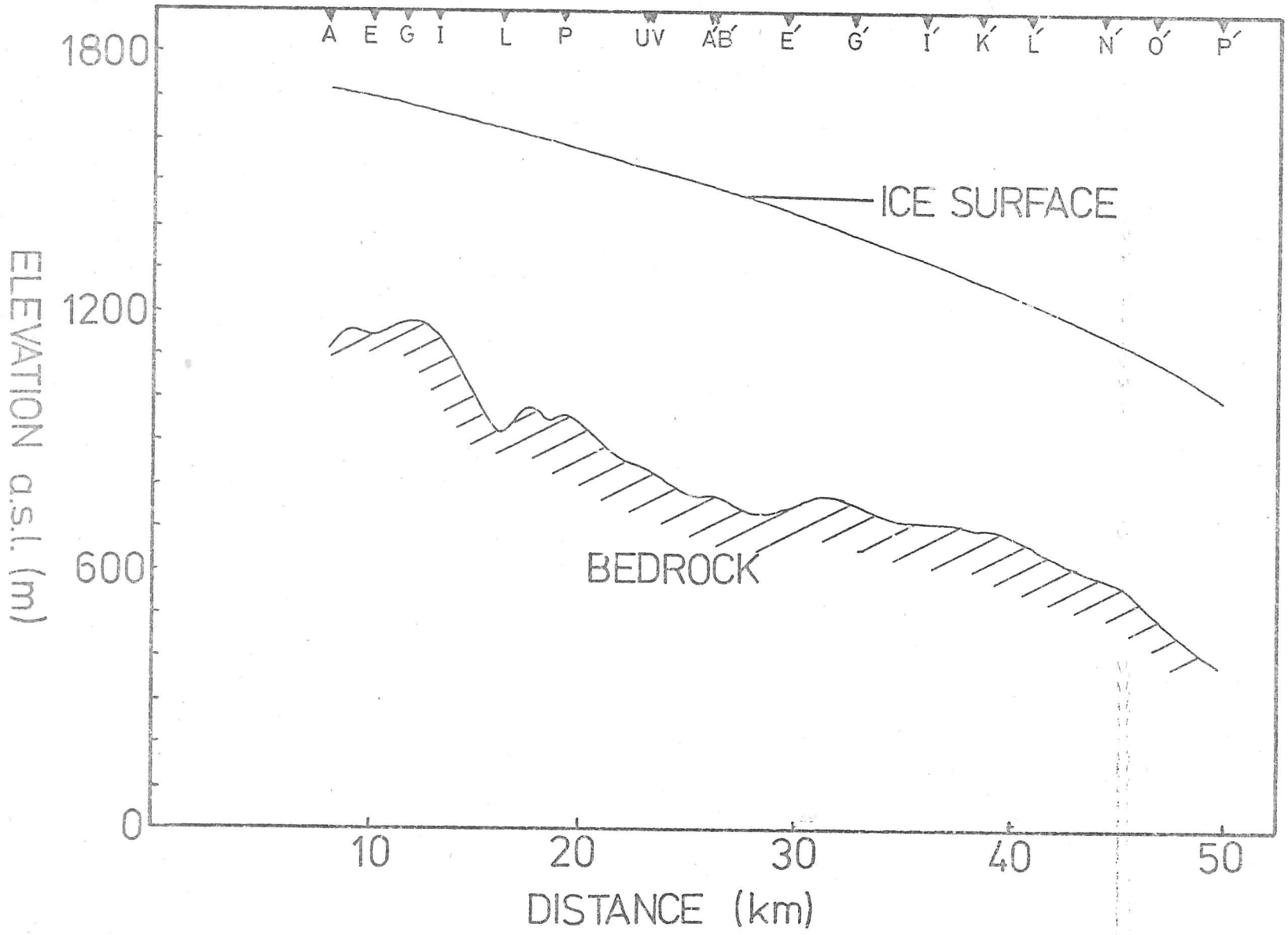

Fig.5.19. The ice surface and bedrock topography along the Western traverse.

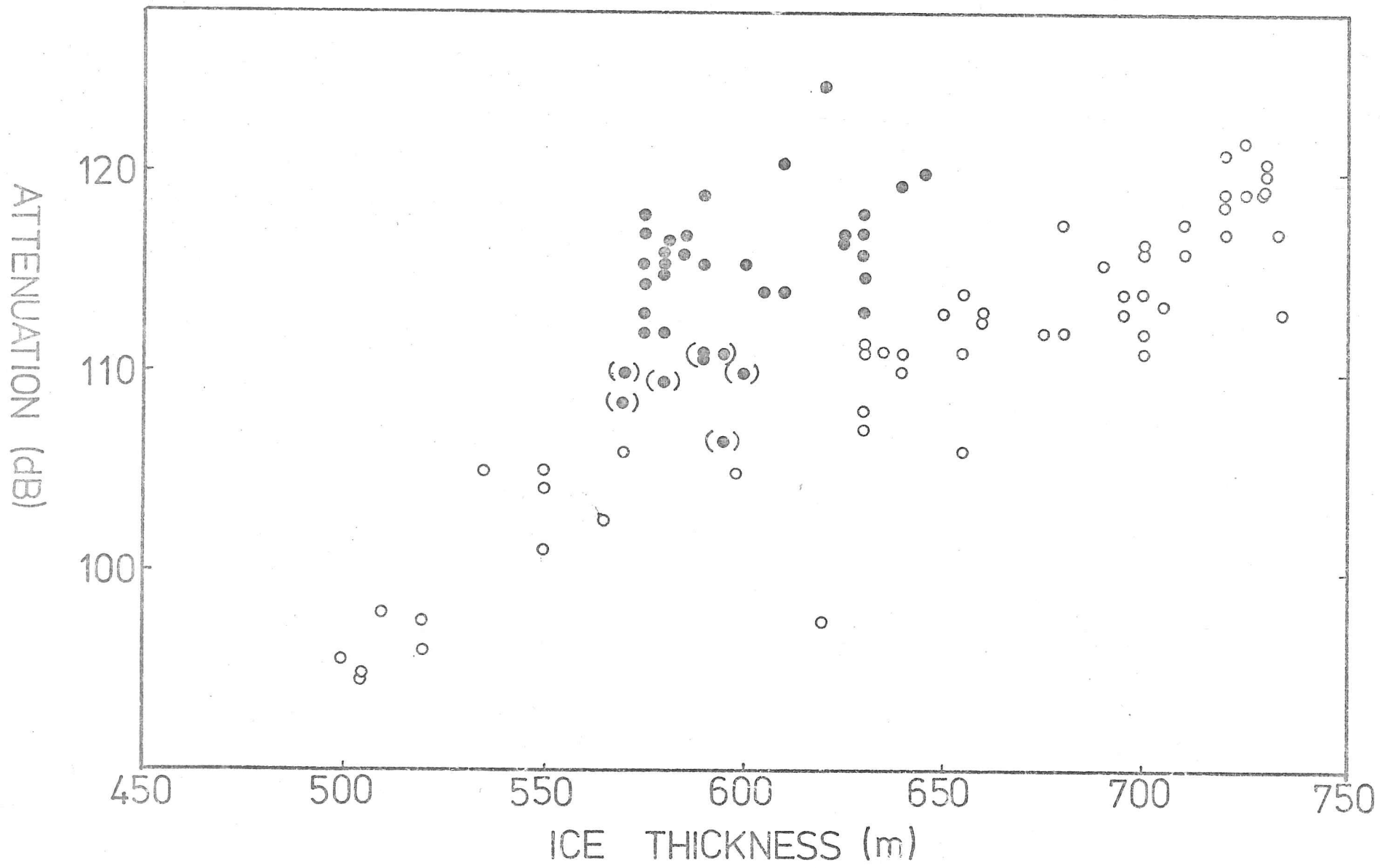

Fig.5.20. Echo attenuation vs. ice depth for the Western traverse. Solid points refer to positions West of cairn G'.

of 36 solid points, we would expect the mean ordinate to lie within 0.83 dB of the estimate from the whole population.

The relevant statistical parameters for the whole population are as follows:

Mean ordinate = -112.5 dB (referred to Tx pulse power)

Mean depth = 627.4 metres.

Regression coefficient = 6.2 dB/100 metres.

The mean depth for the numbered group of points is 596.4 metres, and we deduce an estimate for the mean ordinate of the group of $-112.5 + 6.2(627.4-596.4)/100$, or -110.6 dB.

The mean ordinate for the group is in face -114.7 dB, showing a divergence of 4 dB, or five standard errors away from the estimated value. This is a highly significant deviation, and we must conclude that the two sets are samples of different populations, confirming the visual impression given by the comparison of depth and strength profiles.

On the strength of the previous arguments we shall perform a further separation of points, placing the bracketed solid points in the first group, since we believe that they represent a return to the Eastern type of bedrock. In deriving regression coefficients for the two groups some distortion would otherwise be introduced.

Naming the revised groups 1 (Eastern) and 2 (Western - type reflecting surface), we find the following statistics:

Mean ordinate (1) = -110.8 dB, mean depth (1) = 642 metres

Mean ordinate (2) = -116.0 dB, mean depth (2) = 599 metres

Correlation coefficient (1) = 0.93

Regression coefficient (1) = 9.0 dB/100 metres

Correlation coefficient (2) = 0.39

Regression coefficient (2) = 5.0 dB/100 metres

The correlation coefficient of Group 1 is significant at well below the 1% level: that of Group 2 is significant at about the 5% level (that is, we could expect such a distribution of points to occur in a sample from a completely uncorrelated bivariate population in about 1 in 20 instances). This rather poor correlation may probably be explained in terms of further intrusions of the Eastern type of rock through the Western sediment, causing greater scatter of the observed power levels.

A further discrepancy may also be seen between the regression coefficients of the two groups. We allow in each case for geometrical attenuation of 1.5 dB/100 metres, corresponding to the inverse-square law at about 600 metres' depth. Dividing the remaining gradient by 2, we are left with apparent dielectric absorption of 3.75 and 1.75 dB/100 metres respectively. Neither of these figures agree with the gradient deduced from the mean power levels of the close-spaced observations, lying respectively 1.5 dB above and 0.5 dB below.

We are seeing here the effect of increasing temperature towards the West, combined with the trends of ice depth for the two groups. The trend for Group 1 is for increasing ice thickness towards the West, and the temperature effect therefore tends to reinforce that of the increased length. The opposite is true for Group 2, whose decreasing ice thickness is counteracted, in terms of the total absorption, by increasing temperature.

The surface gradient for Group 1 is, on average, -0.014, and the average ice thickness gradient is 0.0075. For an increase of depth of 100 metres, with a lapse rate

(remembering our earlier assumptions concerning the ice surface temperature and temperature profile) of 10°C/100 metres, we expect a surface temperature change of 1.9°C, and an accompanying increase in absorption over a 2-way path through 650 metres of ice of 2.6 dB. Subtracting this figure from the regression gradient, along with the geometrical attenuation, we are left with a figure for dielectric absorption, corrected to the temperatures at the summit of the ice-cap, of 2.45 dB, which is very close to that obtained for the close-spaced observations.

Returning to Group 2, we have a surface gradient of -0.02, and a thickness gradient of -0.004. For a change of depth of 100 metres, we expect a temperature change of 5°C. The absorption increase over 2x 600 metres would be 6 dB, implying a corrected absorption of 1.75+(6/2) = 4.75 dB/100 metres. This is unexpectedly high, and once again we attribute it to unaccounted intrusions of strongly reflective rock towards the Western end of Group 2, where we would expect the temperature effect to dominate that of decreasing depth. The poor correlation of the Group 2 points and the projected geological situation allow us to disregard the high corrected gradient as an indicator of the true dielectric absorption.

(5.5) Summary

This chapter contains the central experimental results, and the main conclusion of this thesis; namely, that by observing the mean level of the maximum power in the received pulse, it is possible to detect changes in the bedrock of glaciers by means of radio echo sounding. We have been able

to locate a geological boundary whose presence beneath the ice was suspected, but whose position was not known, and to outline the statistical characteristics of the roughness of the bedrock surface.

Having previously shown the possibility of detecting the occurence of basal melting in the Antarctic, we are now able to make detailed analyses of the echoes, and to relate them intelligibly to the form of the reflecting surface. From the point of view of work in very deep ice, it is important that the results depend basically on the behaviour of the maximum of the echo, rather than on the shape of its tail. The latter was sufficiently difficult to analyse in the case of the very strong echoes observed in Devon Island, but comparing the A-scope photographs in Figs. 5.3 and 2.13 (taken in Devon Island and the Antarctic respectively) the problem can be seen to increase with the ice depth. Modification of the system to provide sufficient echo power and an expanded view of the echo might retrieve the situation. However, for the purposes of a large-scale survey we would favour the continuous measurement of the maximum echo power, given sufficiently long pulse to satisfy the conditions under which our simple analysis is valid.

Chapter 6. The distribution of the received power.

Deviations of the power from its mean value arise for three physically separable causes. Though the three may all be taken into account by a comprehensive theory of the diffraction of waves by the surface, the phenomenon of fading may be more easily understood by dealing with them separately. The solution by diffraction theory (Bramley and Young (1967)) necessarily involves large computing resources, and it will be of value to build up an analytical view for our Newtonian surfaces.

We separate the causes of fading as follows:

(a) Pulse spreading. This refers to the matter of Chapter 4, in which we considered the shape of the received pulse as a function of the slopes in the reflecting surface, and of the shape of the transmitted pulse envelope. As the surface slopes increase, the pulse is widened and its maximum level reduced below the power expected for continuous transmitted waves. We deduced, however, that for the surfaces encountered and pulse lengths used in the Antarctic and in Devon Island, the reduction was neglgible. We shall use the observed maximum as representative of the power for continuous waves at the point of observation.

(b) Focusing. The curved facets of the reflecting surface result in convergence or divergence of the reflected 'rays', giving rise to variations in the energy flux at the receiver.

(c) Interference. When more than one reflection is received simultaneously, interference occurs between the waves which constitute each reflection. The resultant intensity varies as the changing position of the observer affects the phase relationships of the components of the received echo. Though the strength of each component may vary only slowly with the observer's position, this interference will give rise to relatively rapid fluctuations in the total intensity.

Causes (b) and (c) are to some extent mutually exclusive. We shall see that the maximum focusing effect is apparent when the observer's height above the surface is close to the inverse of the r.m.s. curvature of the roughness. In this situation, however, more than one reflection will be received for only a small fraction of observer positions, and interference will be a minor effect.

We wish to describe the extent of variation of the received intensity in terms of the shape of the power distribution, and the 'normalised power variance', defined as

$$V_p' = \frac{\langle P^2 \rangle - \langle P \rangle^2}{\langle P \rangle^2} \qquad (6.1)$$

where the angular brackets denote a spatial mean. The mean received power is given, as in Chapter 4, by

$$\langle P \rangle = P_o = \frac{P_T . A . g}{64\pi^2 h^2} = A . I_o \qquad (6.2)$$

where I_o is the mean received intensity.

(6.1) Distribution of intensity for a single reflection.

We use the surface model referred to in Chapter 4, where the vertical displacement from a horizontal plane was described by a random function $\zeta(x,y)$, with mean value zero. The distribution of ζ is given by

$$p(\zeta) = \frac{1}{\sqrt{2\pi}\,\alpha_0} \exp\left(-\zeta^2/2\alpha_0^2\right) \qquad (6.3)$$

and the autocorrelation function by;

$$\rho_\zeta(\sigma,\tau) = \exp -\left(\frac{\sigma^2+\tau^2}{T^2}\right) \qquad (6.4)$$

A small element $\delta x\,\delta y$ of the surface at (x,y) reflects power to a positon (ξ,η) where

$$\xi = x - h\frac{\partial\zeta}{\partial x}\ ,\ \eta = y - h\frac{\partial\zeta}{\partial y} \quad \text{(Fig.6.1)} \qquad (6.5)$$

The observer is at height h above the surface.

The power reflected to a receiver of area L^2 is proportional to the area $\Delta x\,\Delta y$ from which specular reflections may be received, and we have

$$L = \left|\int_{x=x_0}^{x=x_0+\Delta x} d\xi\right| = \left|\int_{y=y_0}^{y=y_0+\Delta y} d\eta\right|$$

$$= \left|\int_{x_0}^{x_0+\Delta x} dx\left(1-h\frac{\partial^2\zeta}{\partial x^2}\right)\right| = \left|\int_{y_0}^{y_0+\Delta} dy\left(1-h\frac{\partial^2\zeta}{\partial y^2}\right)\right| \qquad (6.6)$$

We define the parameters γ_x and γ_y, so that

$$\gamma_x = h\frac{\partial^2\zeta}{\partial x^2}\ ,\ \gamma_y = h\frac{\partial^2\zeta}{\partial y^2} \qquad (6.7)$$

The 'one dimensional mean square' value of γ_x and γ_y is γ_0 and is defined in Appendix 3 .

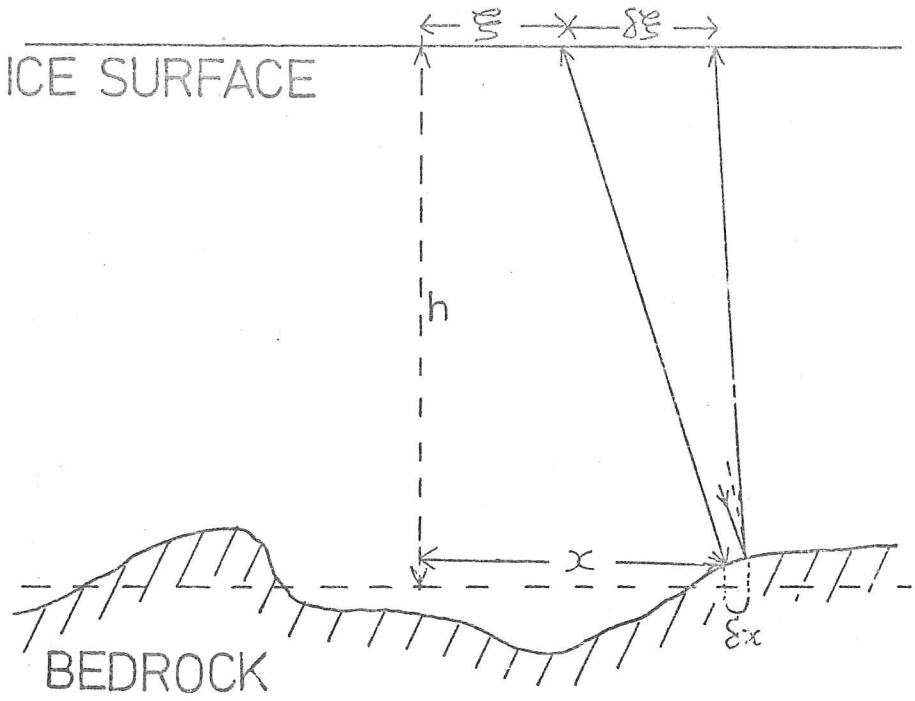

Fig.6.1. The geometry, in one dimension, of specular reflections from the rough bedrock surface, with exaggerated vertical scale of roughness.

Thus

$$L = \left| \int_{x_0}^{x_0+\Delta x} dx\,(1-\gamma_x) \right| = \left| \int_{y_0}^{y_0+\Delta y} dy\,(1-\gamma_y) \right| \qquad (6.8)$$

We expand γ_x and γ_y by Taylor's theorem about the point (x_0, y_0) where

$$\xi = x_0 - h\left(\frac{\partial \xi}{\partial x}\right)_{x_0,y_0} \text{ and } \eta = y_0 - h\left(\frac{\partial \xi}{\partial y}\right)_{x_0,y_0} \qquad (6.9)$$

so that

$$L = \left| \int_{x_0}^{x_0+\Delta x} \left(1 - \gamma_x(x_0,y_0) - (x-x_0)\gamma_x'(x_0,y_0) - \frac{(x-x_0)^2}{2}\gamma_x''(x_0,y_0) - \cdots\right) dx \right| \qquad (6.10)$$

Changing the variable, we have

$$L = \left| \int_0^{\Delta x} \left(1 - \gamma_x - x_1\gamma_x' - \frac{x_1^2}{2}\gamma_x'' - \cdots\right) dx \right| \qquad (6.11)$$

where $x_1 = x - x_0$, and so

$$L = \left| \Delta x\,(1-\gamma_x) - \frac{\Delta x^2}{2}\cdot\gamma_x' - \cdots \right| \qquad (6.12)$$

Restricting ourselves to a single reflection, we look for a solution where $\Delta x < T$. Under the condition that $(1-\gamma_x) \gg T.\gamma_x'$ (which, since γ_x' is of the order of γ_x/T, is equivalent to $\gamma_x \ll 1$) we have

$$L = \Delta x\,(1-\gamma_x) \qquad (6.13)$$

Similarly

$$L = \Delta y\,(1-\gamma_y)$$

In this case the intensity at a point at (ξ, η) is

$$I = I_0 \left\{ \lim_{L \to 0} \frac{\Delta x \Delta y}{L^2} \right\} = \frac{I_0}{(1-\gamma_x)(1-\gamma_y)} \qquad (6.14)$$

and since γ is small,

$$I = I_0 (1 + \gamma_x + \gamma_y) \qquad (6.15)$$

For $\gamma_x \gg 1$, we solve a quadratic in Δx to find that, for a small receiver where $4L\gamma_x' < \gamma_x^2$ (that is, the receiver is not so large in extent that it receives reflections continuing from one 'facet' to another),

$$\Delta x = \frac{L}{\gamma_x} \qquad (6.16)$$

For small values of γ_x, γ_y, the distribution of the received power reflects directly the distribution of curvatures, and is given approximately by

$$p(I) \simeq \frac{1}{2\sqrt{\pi}\,\gamma_0 I_0} \exp\left\{ - \frac{(I-I_0)^2}{4\gamma_0^2 I_0^2} \right\} \qquad (6.17)$$

For higher values of γ_0, the expression becomes very much more complex, and the probability density is extended in the direction of higher values of intensity. It is important to note that in all cases the distribution is sharply cut off as I tends to zero. We shall see that, for the relatively long wavelengths with which we deal in radio echo sounding, the 'Newtonian' surface model breaks

down in calculating the distribution of intensity as approaches unity, and a detailed examination on this basis would be out of place.

For surfaces where there is a finite probability that γ exceeds unity, this model predicts the occurence of singularities in the point intensity, and therefore an infinite value for the power variance. That this is not observed in practice is due to two effects, one of which is included in the 'Newtonian' surface model: for a receiver of finite area, the intensity is averaged over that area, and the singularities smoothed out. This is important in geometrical optics, where the sensor is generally very large compared with the wavelength of the radiation. However, where the dimensions of the receiver are comparable with the wavelength (as in radio echo sounding techniques). the smoothing of singularities is the result of diffraction effects, rather than those of geometrical optics.

The surface gives rise to an array of 'caustics', which are the loci in three dimensions of the centres of curvature of lines in the surface drawn in the plane of the local normal. (The 'loci of foci'). For vanishingly short wavelengths, the caustics are infinitely sharp, and therefore infinitely intense. However, for finite wavelengths the focusing is subject to diffraction as in any optical system involving finite apertures. For a reflecting area of width Δx , a diffraction pattern will be set up with a characteristic width Δw given by

$$\Delta w = h \cdot \frac{\lambda}{\Delta x} \qquad (6.18)$$

In this situation the width of the reflecting area may be estimated from that of the first Fresnel zone. For a region where $\gamma_x = 1$ and $\xi = x - h\frac{\partial \zeta}{\partial x}$, this is defined in terms of the third derivative of the surface displacement:

$$\frac{\lambda}{2} = \left| \frac{1}{6} \Delta x^3 . \zeta_x''' \right| \qquad (6.19)$$

The intensity of the caustic is proportional to $\Delta x / \Delta W$, and therefore, from (6.18), to $\frac{\Delta x^2}{h\lambda}$. Thus

$$I \propto \zeta_x'''^{-2/3} \times h^{-1} \times \lambda^{-1/3} \qquad (6.20)$$

It is shown in Appendix 3 that ζ_x''' is of the order of α_0 / T^3. For the maximum focusing effect, we suggest a constant proportionality between the observer's height and the r.m.s. curvature of the surface, so that $\gamma_0 = \text{const.}$, and $h \propto \frac{T^2}{\alpha_0} . \zeta_x'''$, then, is of the order of $\alpha_0^{-1/2} . h^{-3/2}$, and we expect the mean value of the intensity and its mean square to be given by

$$\langle I_c \rangle \propto \left(\frac{\alpha_0}{\lambda} \right)^{1/3} \quad \text{and} \quad \langle I_c^2 \rangle \propto \left(\frac{\alpha_0}{\lambda} \right)^{2/3} \qquad (6.21)$$

When focusing gives rise to intense caustics, we expect the mean square value of the received power to be largely determined by their contribution. Thus for the maximum focusing variance, we expect, for large $\frac{\alpha_0}{\lambda}$,

that the power variance will be proportional to $(\alpha_0/\lambda)^{2/3}$.

For low values of γ_0, the mean square intensity is given by

$$\langle I^2 \rangle = I_0^2 \langle (1+\gamma_x+\gamma_y)^2 \rangle = I_0^2 (1+2\langle \gamma^2 \rangle) \qquad (6.22)$$

and the mean intensity is equal to I_0, so that

$$V_D' = \tfrac{8}{3}\gamma_0^2 \quad \text{(Appendix 3)} \qquad (6.23)$$

In situations where only one reflection is received at the majority of observer positions, we expect the normalised variance of the received power to increase as a function of γ_0, from zero when $\gamma_0 = 0$. The relation for small values of γ_0 is given by (23). For surfaces where γ_0 approaches unity, the distribution and variance are not well described by this model. However, it enables us to have some physical insight into the reflection process, and we estimate that the variance for $\gamma_0 \simeq 1$ will be proportional to the 2/3 power of (α_0/λ) or ϕ_0.

As the height of the observer increases so that $\gamma_0 > 1$, the intensity of caustics falls off, and the probability of observing more than one reflection increases. The variance may therefore be expected to fall as the caustics are smoothed out, and interleaved with those from neighbouring facets.

The average number of separate reflections received at any observer position is uniquely defined, for 'Newtonian' surfaces by the parameter γ_0, and is calculated in Appendix 2. The result is illustrated in Fig.6.2., and has the expected limiting forms:

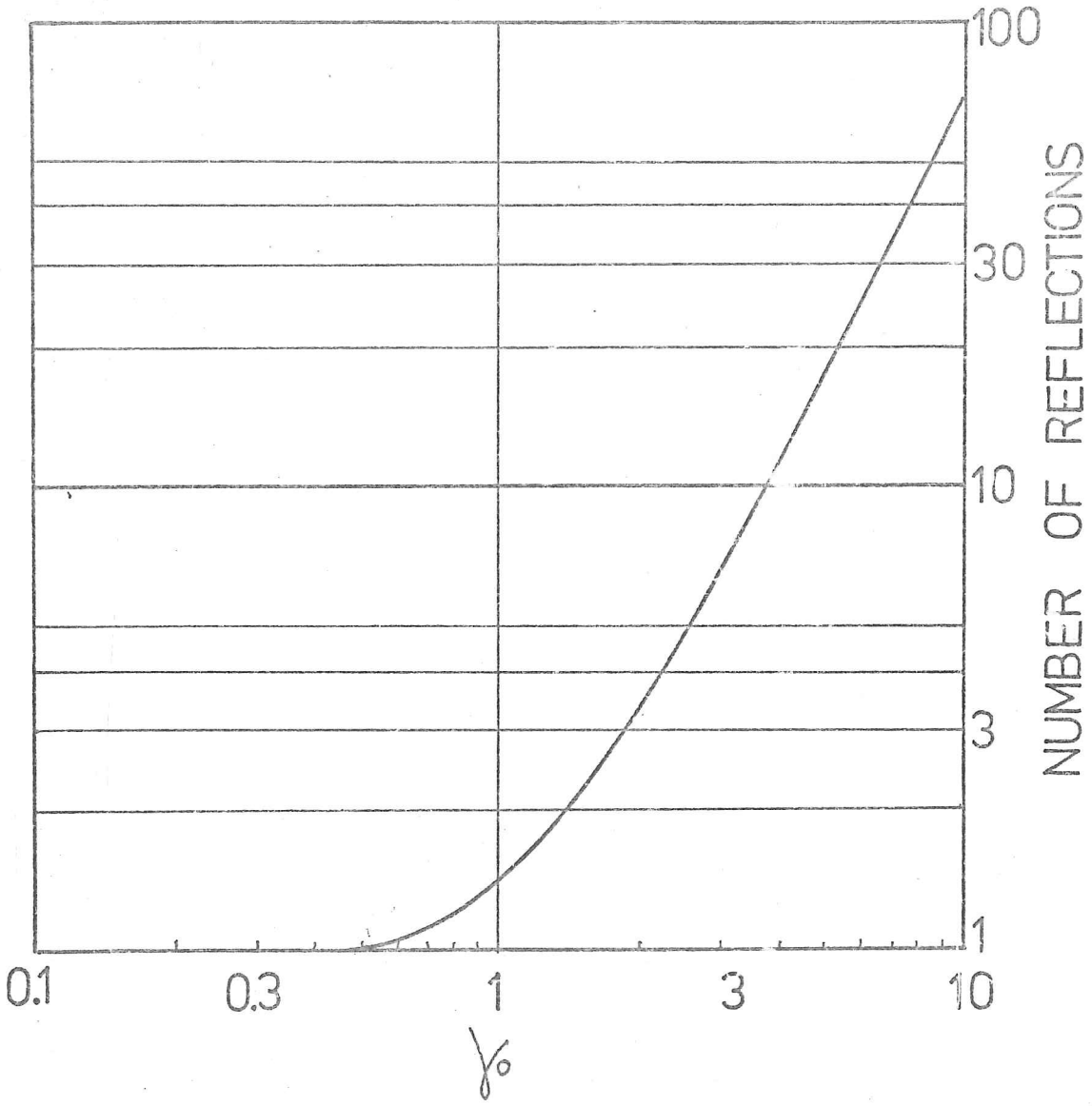

Fig.6.2. The number of separate reflections to be expected from the rough surface, as a function of γ_0 .

for $\gamma_0 \longrightarrow 0 \ , \ n \longrightarrow 1$ (6.24)

and for $\gamma_0 \longrightarrow \infty, \ n \longrightarrow \gamma_0^2/\pi$ (6.25)

(6.2) Distribution of echo intensity for many reflections.

We have seen that the variance of the received power reaches a maximum for $\gamma_0 = 1$, and that thereafter it falls off due to smoothing and interleaving of caustics. However, when more than one reflection is received, the mechanism of interference begins to contribute to the variation. The 'separateness' of the reflections implies a discontiuity in phase between each pair, which is dependent on the position of the observer.

For a large number (that is, greater than 4 or 5), of reflections, the received power maybe described as the sum of a number of vectors of random phase and amplitude. Beckmann and Spizzichino (1963) show that the resultant amplitude of such a sum is distributed according to

$$p(R) = \frac{2R}{R_0^2} \exp\left\{-R^2/R_0^2\right\} \qquad (6.26)$$

We may transform this expression by means of the relation

$$I = R^2$$

to obtain the distribution of intensity:

$$p(I) = \frac{1}{I_o} \exp\left\{-I/I_o\right\} \qquad (6.27)$$

where, of course, $I_o = R_o^2$.

Under these conditions, then, the intensity has an exponential distribution, whose probability density reaches a maximum for $I = 0$. We contrast this with the distribution at low levels of intensity for variations due to focusing, where the density was sharply cut off as $I \longrightarrow 0$. The power distribution on each side of the variance maximum near $\gamma_o = 1$ may be expected to tend to these shapes; that is, Gaussian for $\gamma_o \to 0$ and exponential for $\gamma_o \to \infty$. We may therefore distinguish between the different fading regimes by examining the intensity distribution at low levels.

We note that, when the power is measured in decibels, referred to the mean power level, we derive the distribution

$$p(dB) = \frac{k}{10} \exp\left\{\frac{k.dB}{10}\right\} . \exp\left\{-\exp\left[\frac{k.dB}{10}\right]\right\} \qquad (6.28)$$

where k is $\mathrm{Log}_e 10$,

(6.3) Existing computed solutions for V_p'.

Bramley and Young (1967) have computed values of V_p' using a series solution arising from Kirchhoff diffraction theory, which is adapted by Harrison(1972). They give results for several different values of ϕ_o , as a function of a dimensionless parameter $Z = \frac{2\lambda z_o}{\pi T^2}$.

In Bramley and Young's model, plane waves were diffracted on transmission through a 'deeply-modulated, random-phase screen'. The observer was at a distance z_o from the screen. In relating their solutions to the radio echo sounding situation, where spherical waves are reflected from the screen, we note that ϕ_o is now defined as $\frac{4\pi\alpha_o}{\lambda}$, whereas in their model it was $\frac{2\pi\alpha_o}{\lambda}$. The change in geometry of ray paths leads us to replace z_o by $h/2$, in which case events which would have been apparent at z_o for the plane wave case, now occur at height h, the height of our observer above the surface.

It is shown in Appendix 3 that γ_o, the '1-d' r.m.s. value of γ is related to α_o and T by

$$\gamma_o^2 = \frac{12\alpha_o^2 h^2}{T^4} \qquad (6.29)$$

It is evident that the parameter Z is closely related to γ_o. In fact, we have

$$\gamma_o^2 = 3/4 \cdot \phi_o^2 Z^2 \qquad (6.30)$$

and we transform the curves derived by Bramley and Young (shown in Fig.6.3) so that the abscissa Z is replaced by γ_o. Since the curves are drawn for constant values of ϕ_o, this involves a simple shift along the horizontal axis, defined for each curve by the value of ϕ_o. The result of this transformation is shown in Fig.6.4.

It is immediately obvious that the maxima of the curves occur for coincident values of γ_o, and that this value is unity. This is in full agreement with our

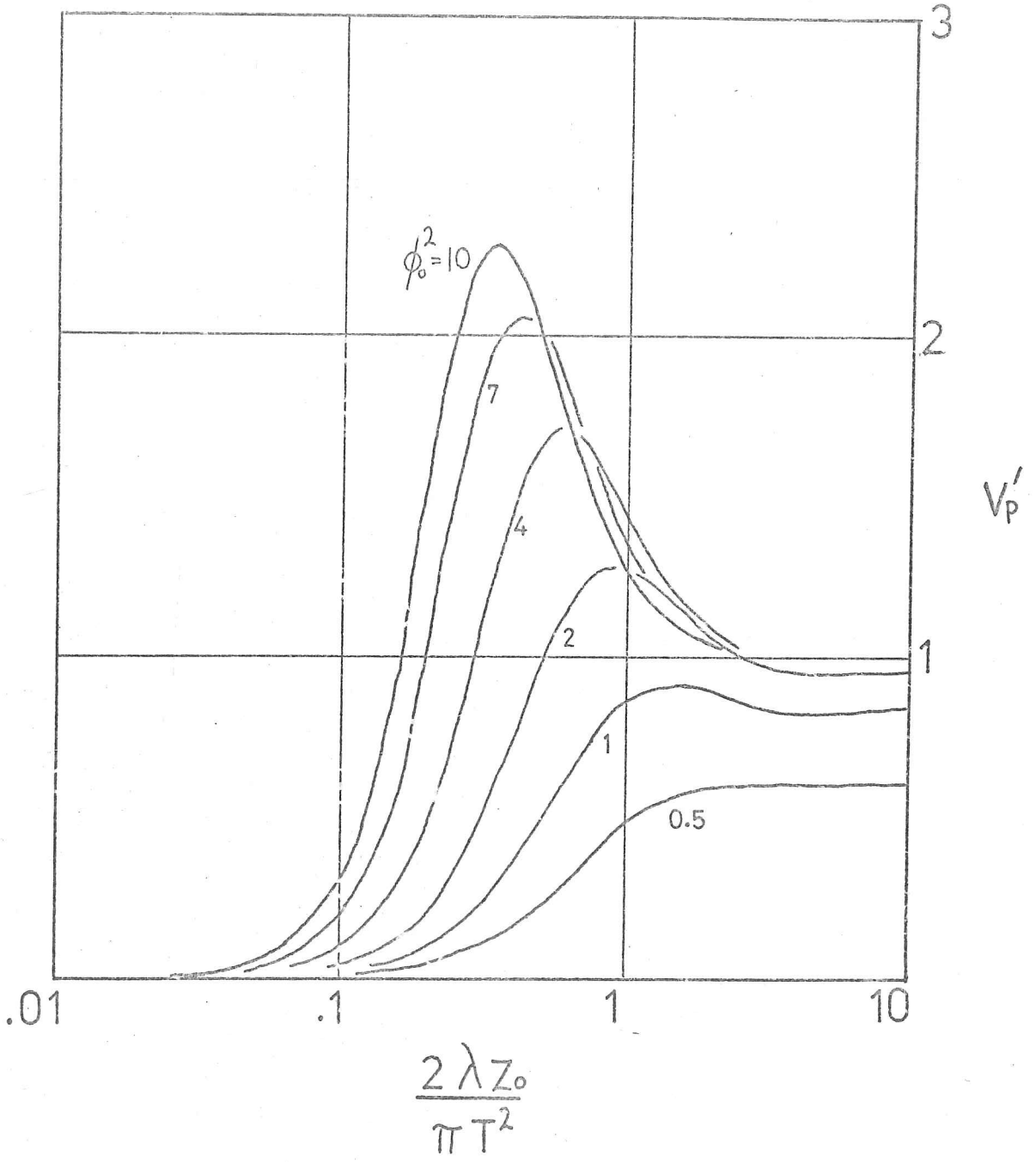

Fig.6.3. Curves derived by Bramley and Young, showing the variation of V_p' with the dimensionless parameter Z for various values of ϕ_0^2.

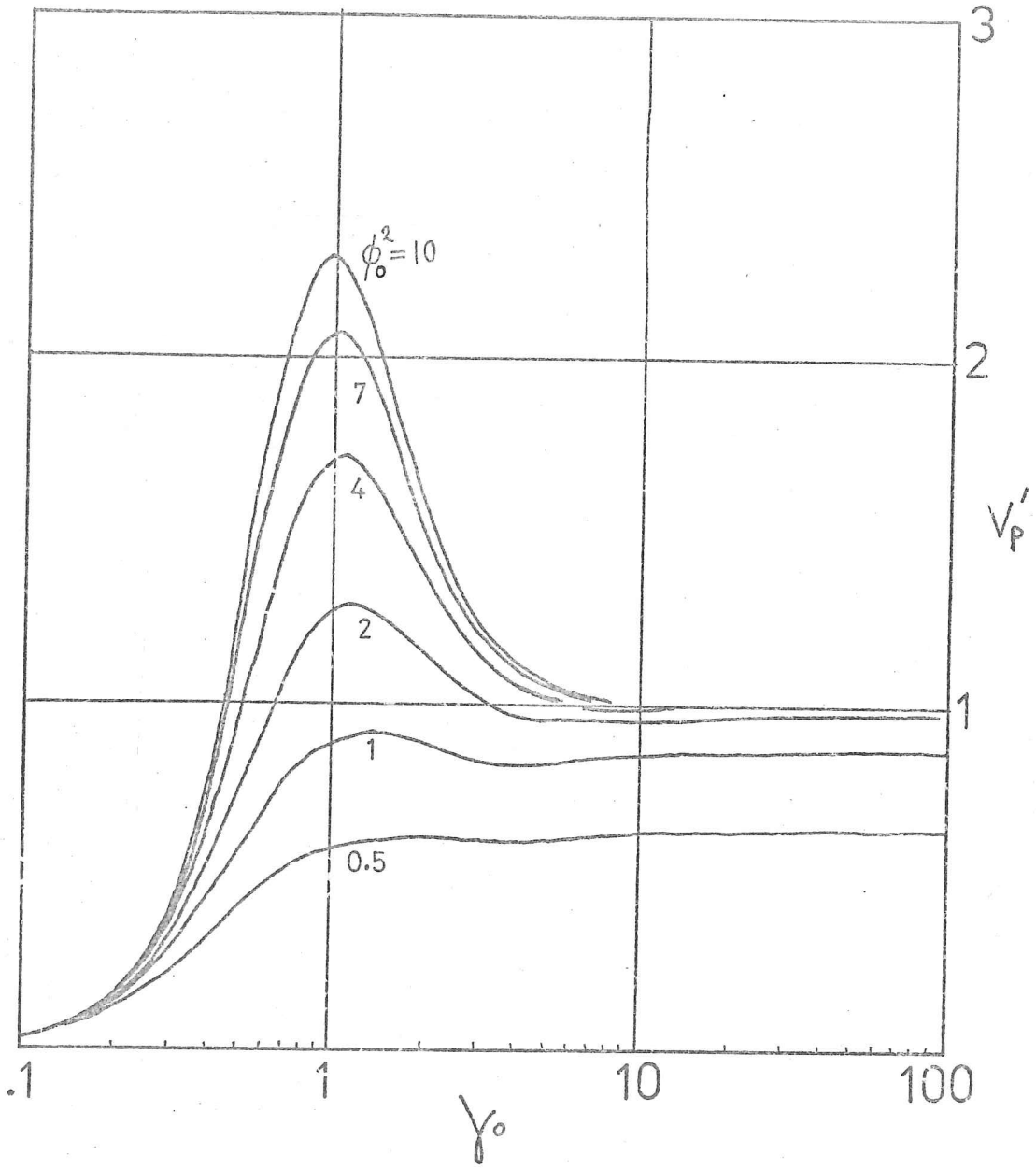

Fig.6.4. The curves of Fig.6.3. shown as functions of the '1-d. r.m.s. curvature, γ_0 '.

analysis of the reflection geometry. The form of the curves is as expected, with the variance for low values of γ_0 being proportional to γ_0, as in equation . For large values of γ_0 and ϕ_0, the variance tends to unity, as predicted by the exponential distribution .

(6.4) Deduction of unique surface parameters α_0 and T .

The curves of Fig.6.4 do not in themselves allow us to deduce unique values for α_0 and T . For any value of V_p', there is a range of possible values of α_0 and γ_0 : for $V_p' < 1$ the whole range of α_0 and γ_0 give possible solutions; for V_p' the possible solutions arise for $\alpha_0 > \frac{\lambda}{4\pi}$ and two separate ranges of γ_0 which may be distinguished by examination of the intensity distribution. since they refer to the different causes of fading; for $V_p' = 1$ no information is available relating α_0 and γ_0 since the variance tends to this same value for all values of $\alpha_0 > \frac{\lambda}{4\pi}$ and large γ_0 . However, if $V_p' \neq 1$, we may draw sets of curves of α_0 vs. γ_0 for constant V_p' . since our transformation of the variance curves has placed them in an intelligible relation to each other. (Fig. 6.5)

We now remember that the values of α_0 and γ_0 are also related in terms of the r.m.s. slope of the surface, which may be determined either by the methods of Chapter 4, or from the spatial rate of fading as will be described in Chapter 7. On the same axes as the curves of α_0 vs γ_0 for constant V_p' , we draw sets of curves of α_0 vs γ_0 for

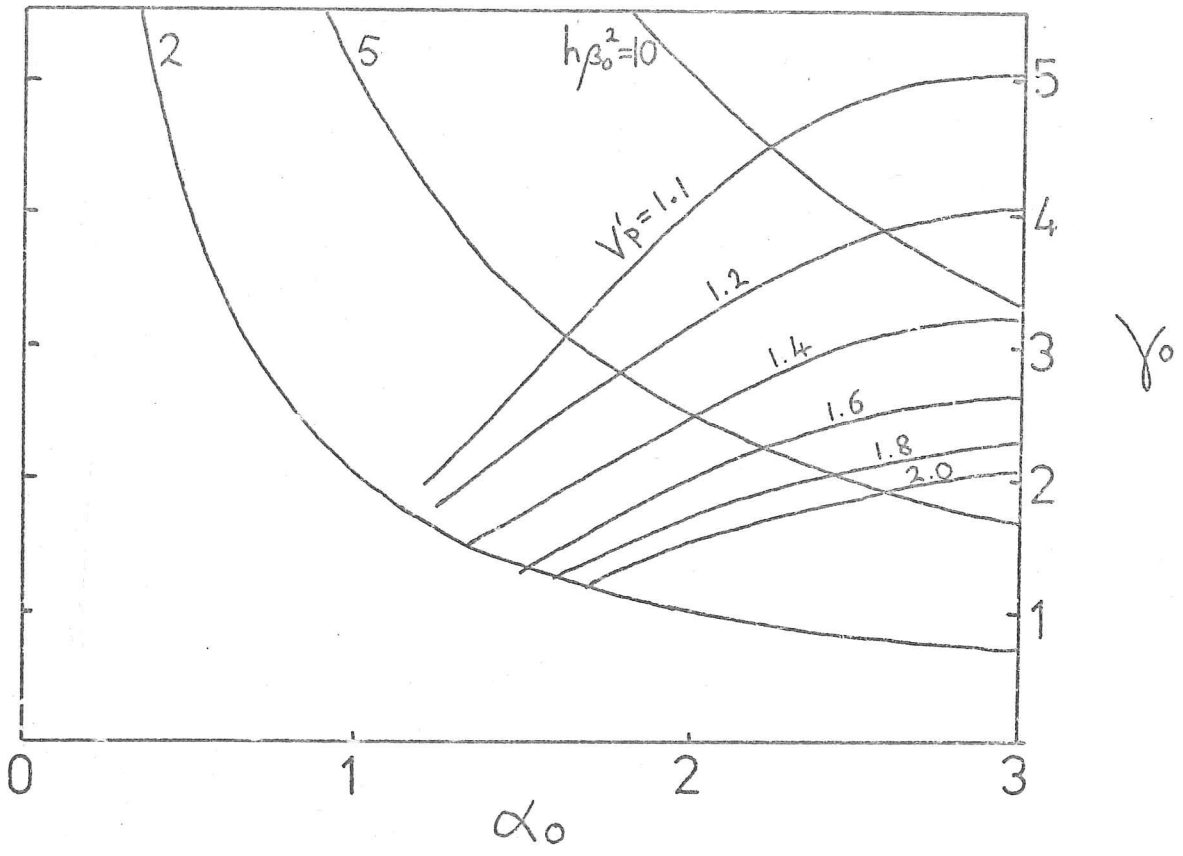

Fig.6.5 . Curves of γ_0 vs. α_0 for various constant values of V_P' and $h\beta_0^2$, for $\gamma_0 > 1$.

constant values of β_0 . By selecting curves of α_0 vs. γ_0 for the determined values of β_0 and V_p' , we define a single point of intersection which gives us unique values for α_0 and γ_0 , and hence for T . Thus, within the assumption of an isotropic Gaussian rough surface, a knowledge of the extent and rate of variation of the received power may lead to estimates for the absolute values of vertical and horizontal scales of the surface roughness.

(6.5) Summary.

We have shown that a large measure of understanding of the phenomenon of fading may be gained, for the case of radio echo sounding, by considering a 'Newtonian' model of the surface. Though this model is not quantitatively reliable for calculation of the power distribution in general, it has enabled us to interpret the results computed from a general diffraction theory in a way which considerably improves their usefulness, and allows us to make reasonable extrapolations of the computed curves. It therefore does not substitute for the diffraction theory, but is necessary for a physical understanding where diffraction processes merge with geometrical optics.

Chapter 7. Spatial frequency of intensity variations.

In Chapter 6, we examined the extent of variation of the power received in the course of radio echo sounding, without reference to the spatial rate of fading of the echo. This subject has been dealt with by the methods of Kirchhoff diffraction theory, by Bramley and Young (1967), Harrison (1972), Berry (1967), among others. Much of the early work arose from the study of fading of signals received in investigations of the ionosphere, where the phase of radio waves is modulated as they penetrate the medium of the ionosphere. In our case, of course, the phase modulation arises from the roughness of the reflecting surface, but the problems are essentially similar. It is natural in the case of reflections from a rough surface to consider the effect of curved facets in the surface in determining the behaviour of the echoes. This viewpoint has considerably helped our physical interpretation of results in Chapter 6, and we shall continue to consult this model in the present Chapter.

We stated in Chapter 6 that the variation of echo intensity arises from three sources. One of these arises from the finite length of the transmitted pulse. Since, however, we have concluded that for a sufficiently long pulse the maximum echo power at any position is close to that which we would expect for continuous waves, we shall neglect this effect, and consider only the fading to be expected for continuous waves. The fading of the echo tail has been shown by Berry to be largely a unique function of the echo delay time at which it is measured. Its importance relates only to the degree of horizontal anisotropy of the surface, which we shall discuss later in this chapter.

There are various ways of characterising the spatial rate of the fading. Most authors have attempted a description in terms of a single number. Bramley and Young used a universal criterion, taking the spacing of observations for which the autocorrelation coefficient of the calculated echo intensity fell below the value 1/e. Harrison uses a similar criterion. Berry, however, uses the more direct method of calculating the probable number of times that the echo intensity crosses a given datum level.

This approach is acceptable when, as is often the case, the fading is essentially the result of a single physical mechanism, which gives rise to an autocorrelation function which decreases monotonically with the spacing of measurements. However, we have indicated that more than one mechanism is available. In the situation where the fading is due to the interference of a large number of randomly-phased reflections, the usefulness of this classification is not in doubt, since the since the autocorrelation function is well-defined, and may be expected to decrease monotonically. On the other hand, when we are dealing with a combination of interference and focusing effects, or with a surface which gives rise to reflections with a degree of correlation of phase over long distances, it may be inadequate.

(7.1) Fading rate for 'distant observer'.

The simplest case for the study of fading rates is that where the observer is at a large distance from the surface as compared with the r.m.s. radius of curvature of the surface. (in the notation of Chapter 6, that is, when γ_0 is greater

than 4 or 5, and a 'large number' of reflections are received simultaneously. In this case the fading is almost entirely the result of interference between these reflections. The intensity should have the exponential distribution deduced in Chapter 6, with the probability density reaching a maximum as I_r (the received intensity) tends to zero.

Berry's calculation of the fading rate, which was referred to above, concerns this case specifically, since his argument makes use of the condition that there should be a large number of reflecting facets within the reflecting zone at any one time. He considers the number of times that the echo amplitude passes through a given level within unit horizontal distance. He calculates that the maximum crossing rate occurs when the datum is set at $1/\sqrt{2}$ of the r.m.s. amplitude. (When we consider the intensity of the echo, this will refer to 1/2 of the mean value). For a 'completely incoherent echo', that is, one where the components of the total echo are uncorrelated in phase, he finds that the maximum crossing rate is given in terms of a 'modified delay time', $\bar{t}$, by

$$N = \frac{4.24}{\lambda}\left(\frac{c\bar{t}}{h}\right)^{1/2} = \frac{4.24}{\lambda}\left\{\frac{c}{h}\,\frac{\int_0^\infty t'\,\varphi(t')\,W(t-t')\,dt'}{\int_0^\infty \varphi(t')\,W(t-t')\,dt'}\right\}^{1/2} \qquad (7.1)$$

where

$$\varphi(t') = \frac{cT^2}{4\alpha_0^2 h}\cdot \operatorname{exch}\left\{-t'\cdot\frac{cT^2}{4\alpha_0^2 h}\right\},$$ AND $W(t)$ IS THE PULSE POWER ENVELOPE.

Berry calculates that, for a Gaussian transmitted pulse, and a surface such that the tail of the echo is very long compared with the transmitted pulse length, the crossing rate is uniquely dtermined by the delay time for which it is

measured. He concludes that the fading rate is not useful as a source of information on the form of the rough surface.

However, we note that this conclusion is dependent on the use of a Gaussian form for the transmitted pulse envelope. The relevant characteristic of the Gaussian form is that the leading and trailing edges of the pulse are defined in terms of the total pulse length: they cannot be short as compared with the total length. The approximation which Berry makes in order to calculate $\bar{t}$ requires physically that the echo extension should be long compared with the trailing edge of the transmitted pulse, which in the case of a Gaussian pulse is equivalent to the condition that it should be long as compared with the total pulse length.

Using a rectangular pulse, we are not subject to the same restriction, and we may use the same approximation, provided that the echo tail is long compared with the trailing edge of the transmitted pulse. (We remember that in Chapter 4 we found that the simple measurement of the distribution of slopes in the rough surface depended on the same condition).

We calculate the 'modified delay time' for a rectangular pulse where

$$W(t-t') = 0 \quad \text{for} \quad (t-t') < 0$$

$$W(t-t') = 1 \quad \text{for} \quad 0 \leq (t-t') \leq P/c \qquad (7.2)$$

$$\text{and } W(t-t') = 0 \quad \text{for} \quad P/c < (t-t')$$

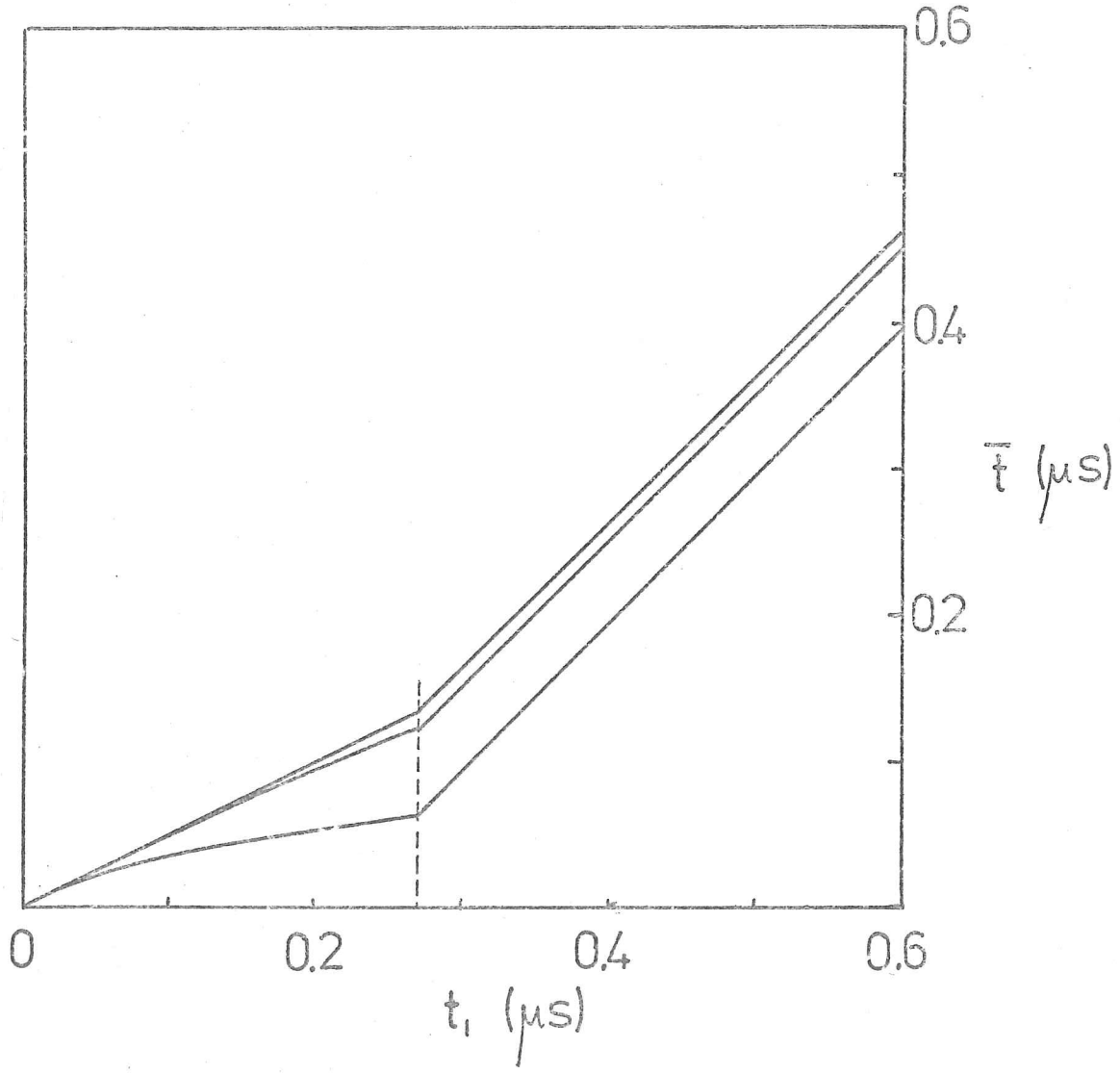

Fig.7.1. The function $\bar{t}$, expressed in terms of the 'relative delay time', t_1.

We find that for $(t-t')<0$, $\bar{t}=0$.

For $0\leq(t-t')\leq P/c$, which corresponds with 'case (I)' in Chapter 4, we have

$$\bar{t}=\frac{1/\alpha-(t_1+1/\alpha)e^{-\alpha t_1}}{1-e^{-\alpha t_1}} \quad , \text{where } \alpha=\frac{cT^2}{4\alpha_0^2 h} \text{ and } t_1=t-t' \qquad (7.3)$$

and for $P/c<(t-t')$, (case (II)),

$$\bar{t}=\frac{(t_1-P/c+1/\alpha)e^{-\alpha(t_1-P/c)}-(t_1+1/\alpha)e^{-\alpha t_1}}{e^{-\alpha(t_1-P/c)}-e^{-\alpha t_1}} \qquad (7.4)$$

$\bar{t}\,(t_1)$ is illustrated in Fig.7.1.

These expressions are equal when $t_1=P/c$. Though we found that, for a rough surface with normally-distributed vertical displacements (and therefore Rayleigh-distributed normal slopes), the echo maximum may occur a short time after this delay, we shall assume that the surface slopes are sufficiently low for this not to occur.

It is obvious from (7.3) and (7.4) that the crossing rate is dependent on the form of the surface for the case of a rectangular pulse: in particular, it is dependent on the r.m.s. slope of the surface. The range of r.m.s. slopes for which this dependence is useful is a function of the length of the rectangular pulse and the altitude of the observer. This range of values of $\sqrt{2}\beta_0$ is closely related to that for which $\langle P\rangle = P_0$. In Fig.7.2., we have plotted N and $\langle P\rangle/P_0$ as functions of β_0 for a Gaussian surface, and this correspondence is clear.

In using this method of calculating the value of β_0 we measure, of course, the crossing-rate for the echo intensity, rather than for the echo amplitude. This should not, however, affect

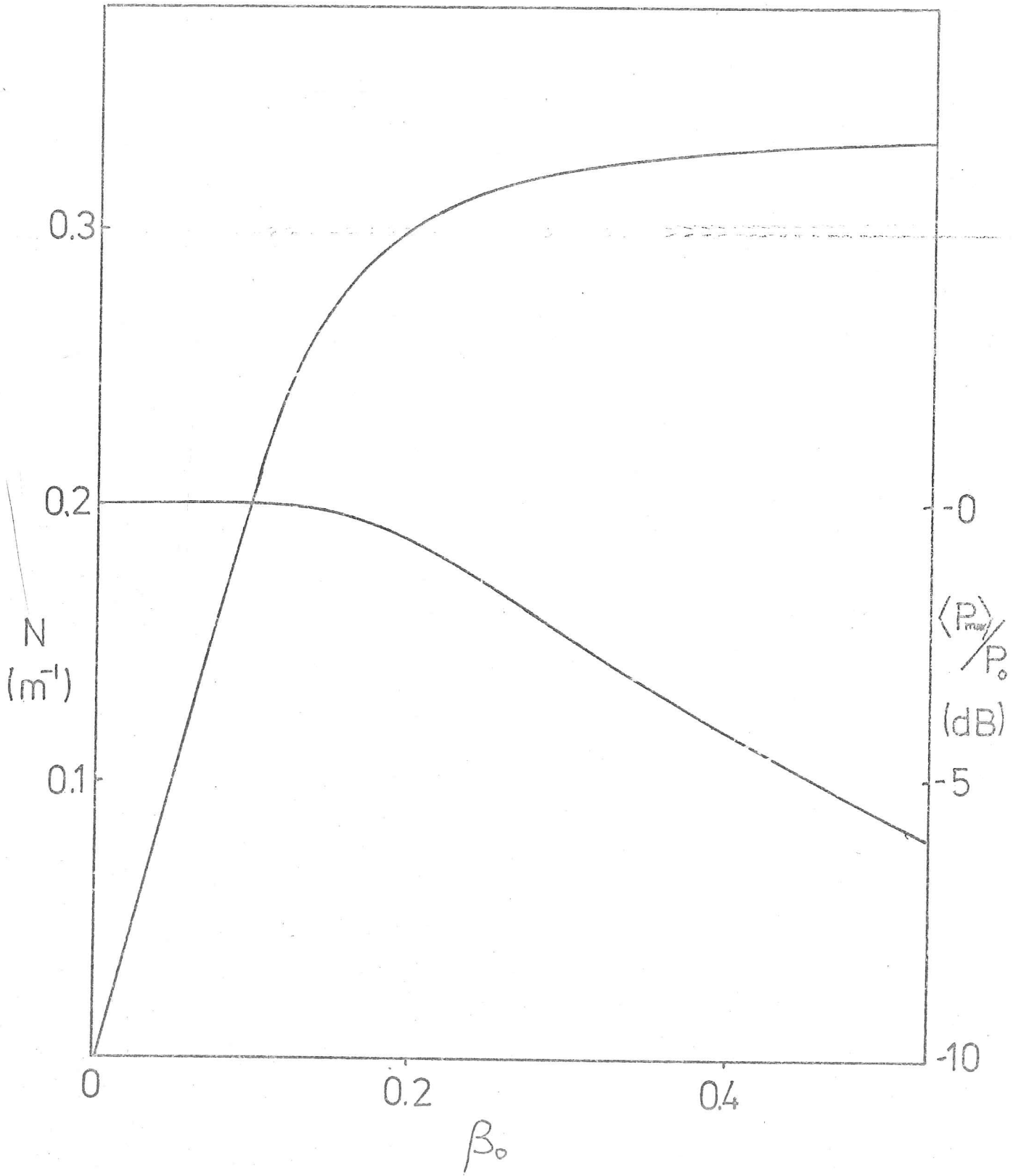

Fig.7.2. The 'crossing rate', N , and mean received power level, plotted as functions of the 'one-dimensional r.m.s. slope' β_0 . The pulse length is 46 metres.

the crossing rate, since we are not dealing with the complex amplitude, but merely with its modulus.

An alternative approach to the fading in this situation where γ_0 is large is that adopted by Bramley and Young, and later by Harrison, in considering the autocorrelation function (strictly the 'normalised autocorration function' of the received echo power). In the present case they find that the form of this function may be calculated analytically, and give the result, initially deduced by Mercier (1962);

$$\rho_I(\sigma,\tau) = \frac{\exp(2\phi_0^2 \rho_s(\sigma,\tau)) - 1}{\exp(2\phi_0^2) - 1} \qquad (7.5)$$

where $\rho_s(\sigma,\tau)$ is the autocorrelation fuction of the surface roughness. For large values of ϕ_0, this is essentially a function only of the r.m.s. surface slope, in the case where the surface has a Gaussian autocorrelation function. and we have FOR THE FADING LENGTH:

$$\tau_p = \frac{\lambda}{4\pi\beta_0} \qquad (7.6)$$

as found by Harrison.

Thus when the distribution of echo intensity is found to have an exponential form, we may use either of these techniques to estimate the value of the r.m.s. slope in the rough reflecting surface. For the purpose of obtaining unique values of and T, we face the dilemma that in this limit, the variance of the echo power tends rapidly to unity as γ_0 becomes large, and the curves derived in Chapter 6 become inapplicable. In the case where the distribution has the correct form, but the variance is still appreciably greater than unity, we may

still make an estimate of the slopes from these methods, though the rigour of the calculation will be doubtful.

(7.2) Fading for the observer close to the rough surface.

We now consider the case where the observer is so close to the surface that no caustics are encountered, and the focusing effect may be regarded as a linear function of the curvature of the surface. ($\gamma_x + \gamma_y$)

In this case the echo intensity at any position (x,y) is given by

$$I \simeq I_0(1 + \gamma_x + \gamma_y) \qquad (7.7)$$

and the autocorrelation of the intensity is equal to that of the curvature ($\rho_\gamma(\sigma,\tau)$). It is shown in Appendix that this is equal to

$$\left(1 - 2\mu^2/T^2 + \tfrac{1}{2}\cdot\mu^4/T^4\right)e^{-\mu^2/T^2} \quad \text{WHERE } \mu^2 = \sigma^2 + \tau^2 \qquad (7.8)$$

for a surface with a Gaussian autocorrelation function, and we therefore have the same result as Bramley and Young for this situation.

We have seen that in this situation the distribution of intensity tends sharply to zero as I_r tends to zero, so that when this is the case the value of T may be deduced directly from the autocorrelation function of the intensity, with the assumption of a Gaussian surface.

In this case the extension of the obseved echo due to the reception of reflections from a large range of angles will be absent, leaving no means of estimating the r.m.s. slope of

this type of surface directly.

However, in this limit the power variance tends to a unique function of the r.m.s. curvature (see Chapter 6, equation (23)). We may therefore calculate directly the value of γ_0, so that, having found T from the autocorrelation function, α_0 may be derived from the equation:

$$\gamma_0^2 = \frac{12\alpha_0^2 h^2}{T^4} \qquad (7.9)$$

(7.3) Fading rates for intermediate observer positions.

We have so far covered the situations where the observer is atsuch a height above the surface that γ_0 is either less than about o.5, or greater than about 4. In the intermediate range of γ_0 no analytical solution is available or accessible, and we must turn to computed solutions. The series solution for the Kirchhoff diffraction theory for rough surfaces, used by Bramley and Young, was mentioned in Chapter6. They obtained autocorrelation functions for various surfaces, with the restriction that the roughness was isotropic in the horizontal plane, and normally distributed in the vertical, with a Gaussian autocorrelation function.

Bramley and Young concluded that the 'autocorrelation length'of the received intensity was not a single-valued function of that of the rough surface, even for a simple Gaussian surface. In the region of $\gamma_0 = 1$, the'relative fading length' τ_p/T at first falls as the caustics intersect more frequently with

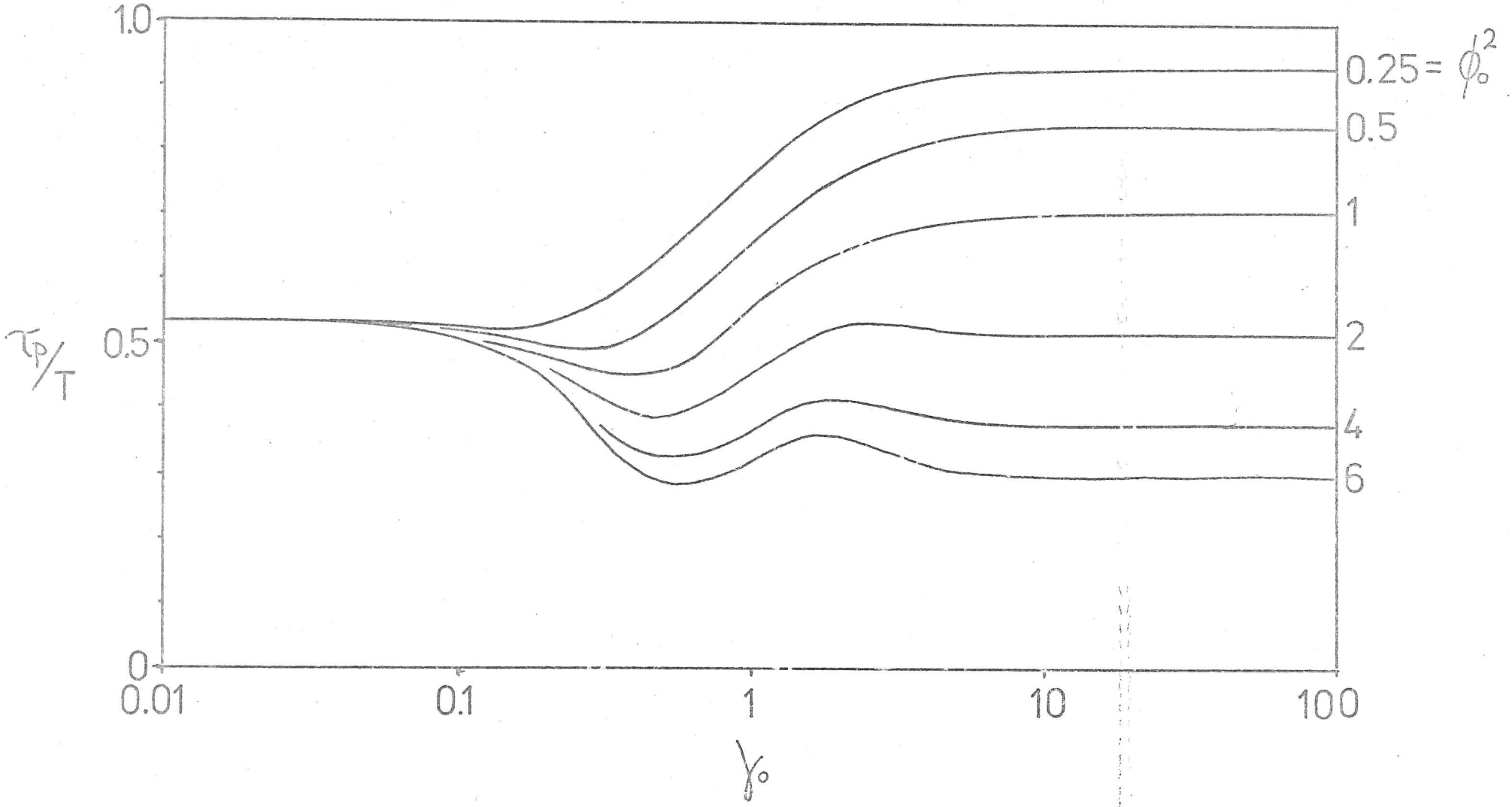

Fig.7.3 Bramley and Young's curves of $\tau_p/_T$ vs Z , tranformed to read in terms of γ_o .

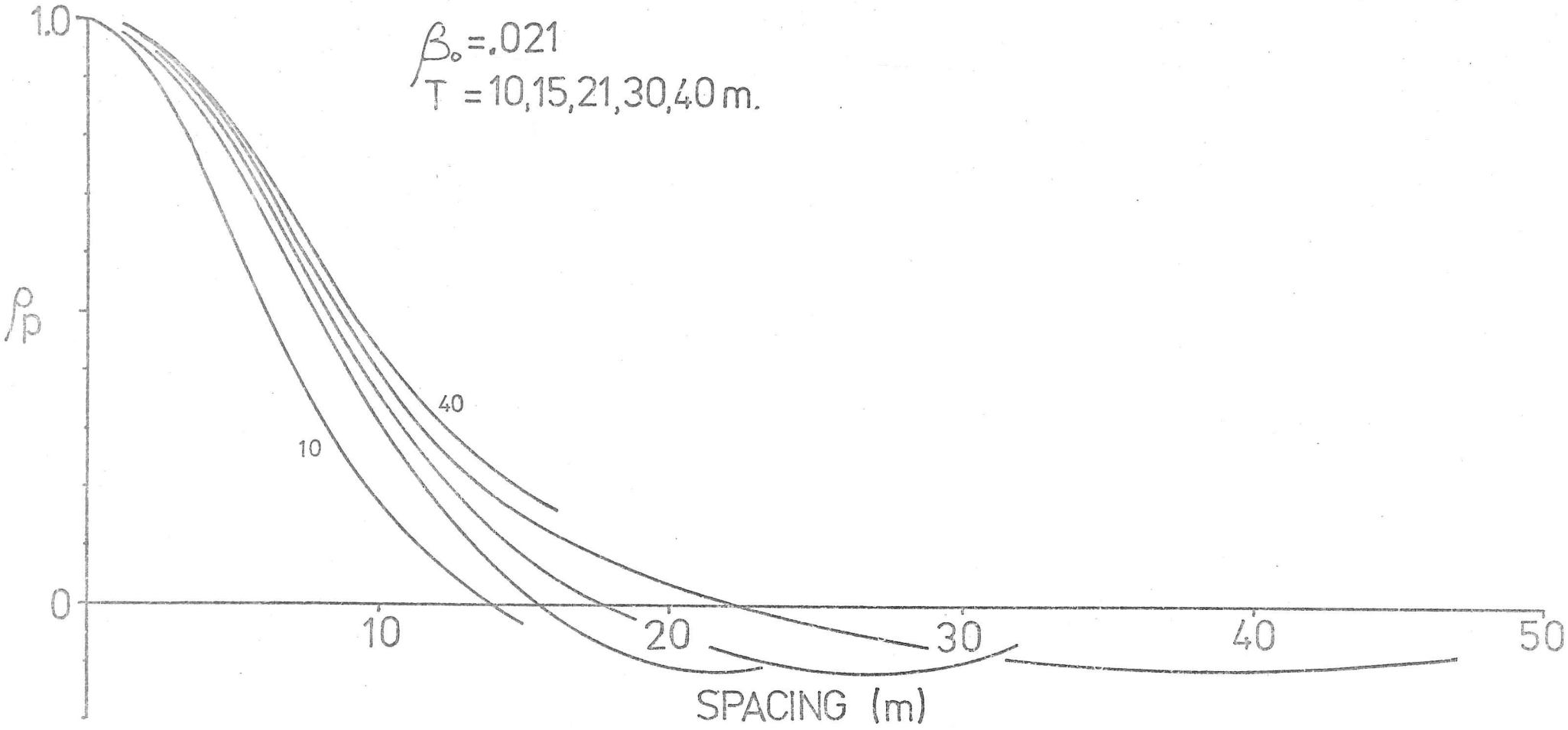

Fig.7.4.a. Autocorrelation functions for the echo power received from a Gaussian surface with the indicated values of β_o and T , from the results of Bramley and Young.

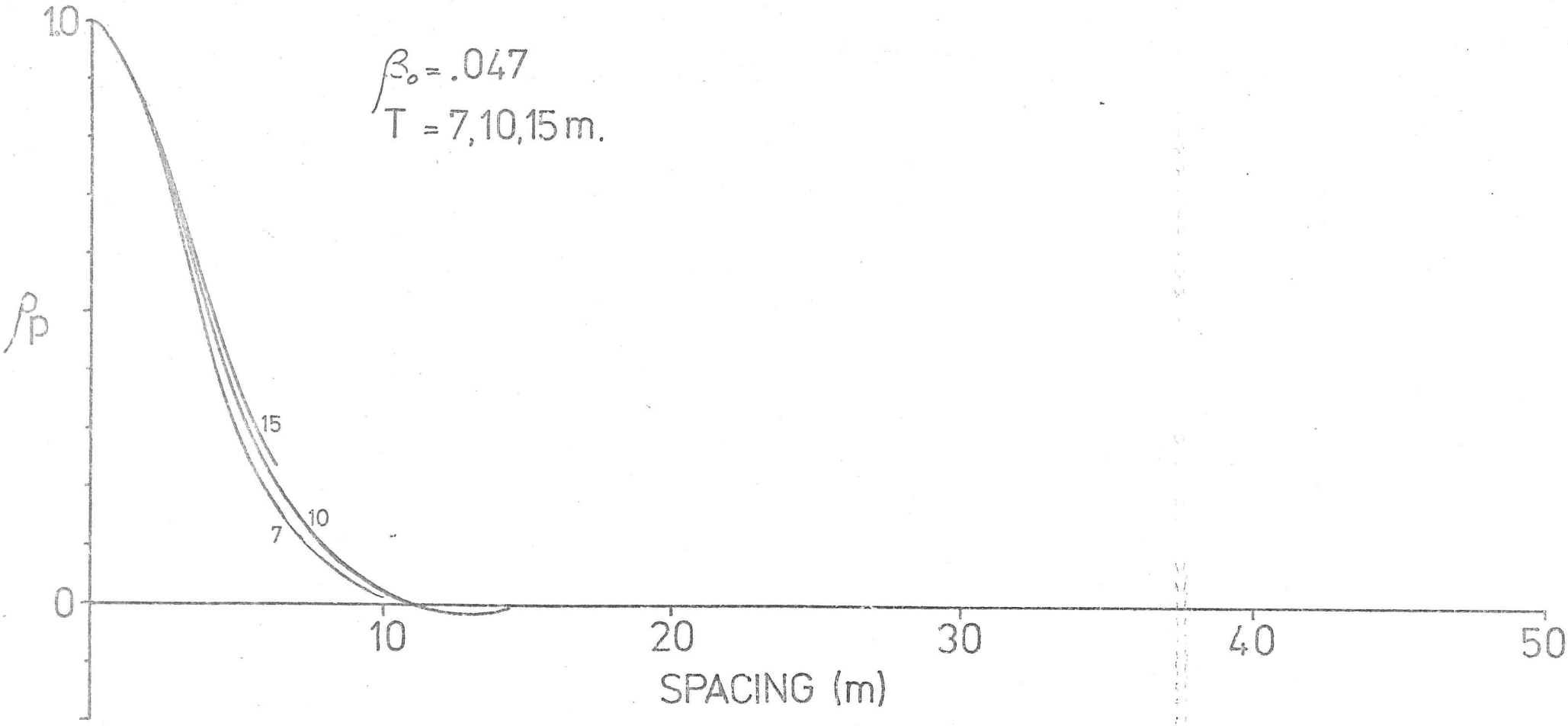

Fig.7.4.b. Autocorrelation functions for the echo power received from a Gaussian surface with the indicated values of β_o and T , from the results of Bramley and Young.

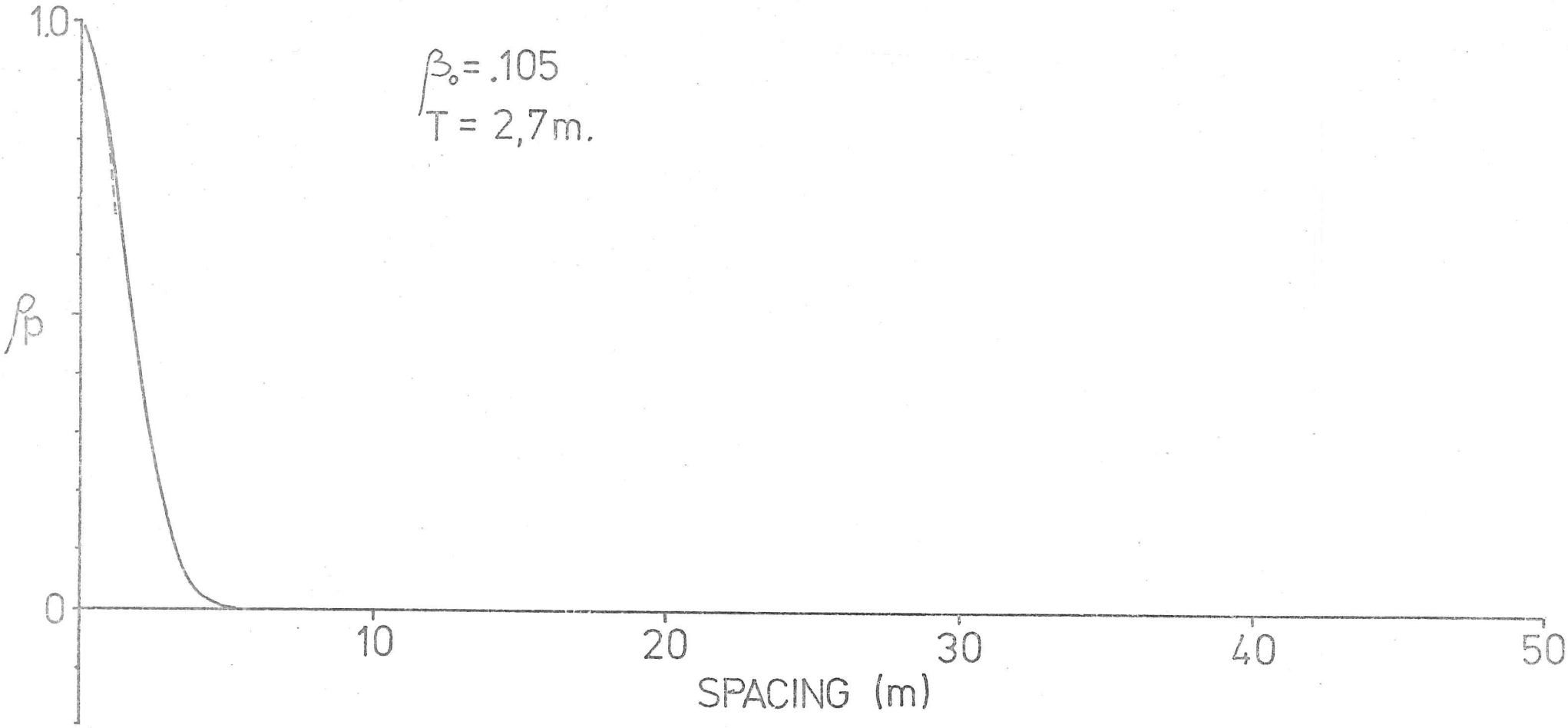

Fig.7.4.c. Autocorrelation functions for the echo power received from a Gaussian surface with the indicated values of β_0 and T, from the results of Bramley and Young.

the sounding path, then rises as they decrease in intensity. Finally, as interference begins to occur, it tends to the value defined in section (7.1) for the case of $\gamma_0 \gg 1$. Fig.7.3 shows the information in Bramley and Young's graph of τ_p/T versus their parameter $Z = \frac{\lambda h}{\pi T^2}$, transformed to read in terms of γ_0. As in the transformation from Fig.6.3 to 6.4, this consists simply of a shift of each curve along the abscissa axis, and once again we observed the coincidence of maxima and minima of the curves after the transformation.

In this situation the best approach is simply to match observed autocorrelation functions with calculated forms, using the variance and distribution of the intensity as guides to the correct fading regime. A range of curves, drawn from Bramley and Young's original calculations, are shown in Figs7.4a,b,etc. The values of ϕ_0^2 are restricted to below 6, and the usefulness of the curves would be greatly enhanced if the series could be extended to higher values. However, this would require the allocation of large computing resources, since the number of terms in the series summation must be increased rapidly as ϕ_0 increases.

(7.4) Summary.

In the case of the 'distant observer', we are able to derive the r.m.s. surface slope directly from two methods arising from the spatial frequency of the fading. These are to be used in preference to the method using the shape of the received pulse envelope, since they are less dependent on the shape of the transmitted pulse, and on the characteristics and

situation of the sounder. (They do not require a very strong received pulse, since it is only necessary to measure the maximum level of the echo at any position: nor is it necessary to measure accurately the shape of the received pulse over very short time intervals.) They do not, however, include the potential for deducing the complete form of the distribution of slopes, as does the 'envelope' technique: this is the only direct method of checking the validity of the assumption of a Gaussian random surface.

For the case where the observer is close to the rough surface, we have been able to calculate in a simple way the autocorrelation function of the received intensity, in relation to that of the surface. We note the statistical point that for an isotropic surface the one-dimensional gradients are anisotropically distributed, the autocorrelation function being truncated in the direction in which the gradient is defined.

Where the observer's height is such that γ_0 lies between 0.5 and about 4, numerical solutions must be used to provide model autocorrelation functions with which observed functions may be compared.

It was mentioned in section (7.1) that the fading of the tail of the echo might be used to investigate the degree of anisotropy of the rough surface. It is clear from the geometry of the situation that the fading resulting from reflections fore-and-aft of the observer along the sounding path will give rise to more rapid fading of the echo than those to either side, in the case where interference is the dominant mechanism in

producing the fading. We suggest that, by using a very short transmitted pulse, the fading rate for reflections at different vertical angles may be separated. The fading rate would then be a function of the vertical angle, and also of the distribution in the horizontal plane of reflectors observed at that angle. In view of the forms of glacially eroded, exposed terrain, the assumption of anisotropy of the surface, though convenient, is perhaps not realistic. It would be of great interest to check the extent of validity of this assumption before proceeding with extensive modelling of echo statistics.

Chapter 8. Further analysis of results from Devon Island, and conclusions.

(8.1) Observed distributions of the received echo power.

The distributions of the echo power received for the ten sets of closely-spaced measurements in Devon Island (Chapter 5)are shown in Figs.8.1a,b,c. The power is expressed in dB, and in each case the histogram may be compared with the expected form for the distribution for fading caused entirely by interference. This curve is characterised by coincidence of the mode with the value in dB of the mean real power, by an abrupt cut-off in the direction of increasing power, and a more gentle fall-off as P tends to zero.

In only one of the ten cases is the observed distribution very close to this theoretical shape. The value of the parameter , which describes the 'goodness of fit' of the histogram, is found to be 5 for the case of set T3. This, for a histogram with seventeen degrees of freedom, implies a 'very good fit' in terms of a 'null hypothesis'.

For the other sets, the value of varies between 20 and 93. For sets F and G, we find values of 29 and 20 respectively, which implies that deviations from the curve are less significant than the '5% level'. In these cases, we conclude that, though some focusing is taking place, the fading is dominated by the effect of interference.

For sets B,C and E, the modes of the histograms occur for power levels lower than the mean value. This is a feature of the focusing regime, where the intensity is automatically negatively correlated with the frequency, in terms of observer positions, at which it may be observed.

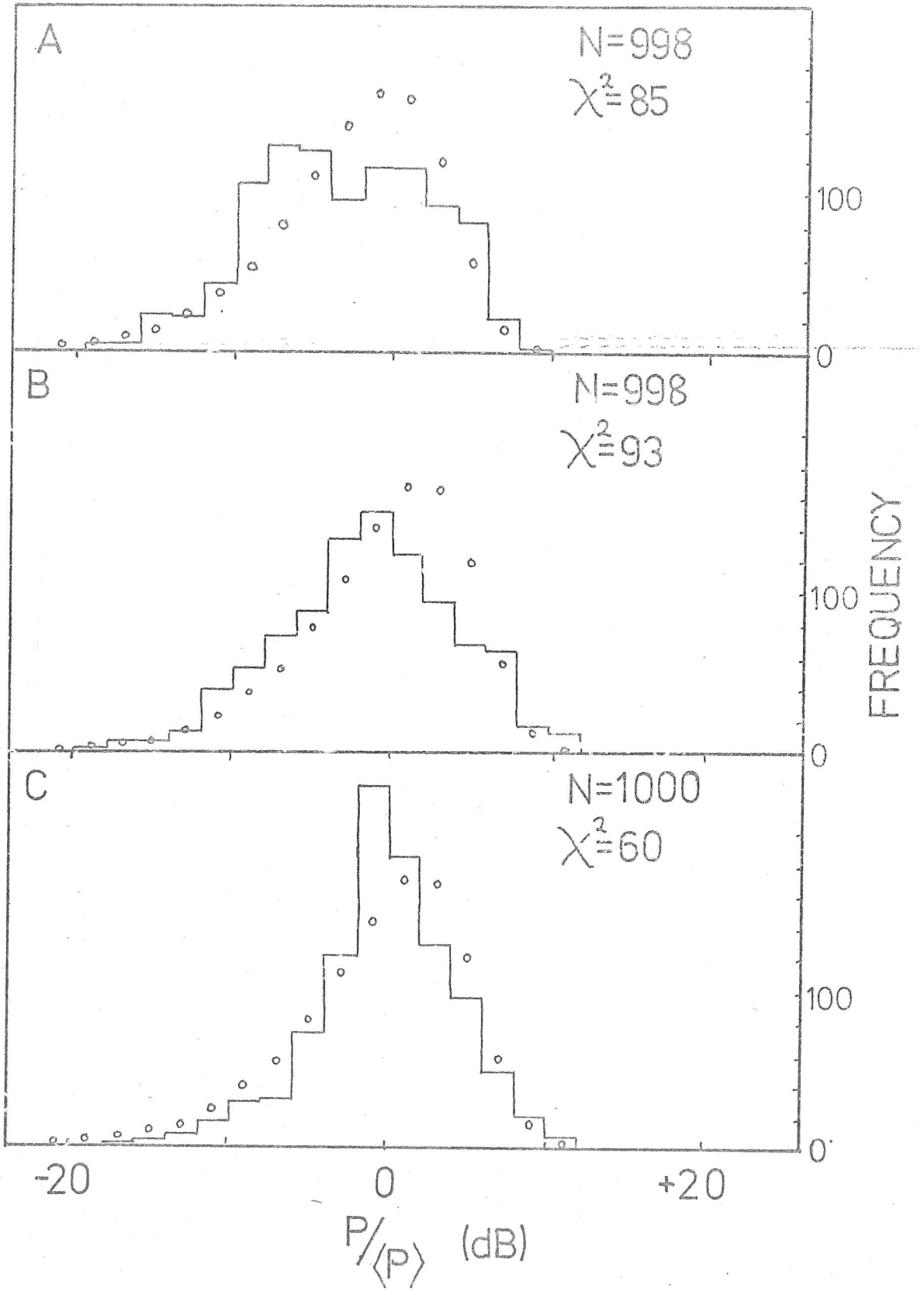

Fig.8.1a. Distributions of the received power for sets A,B and C.

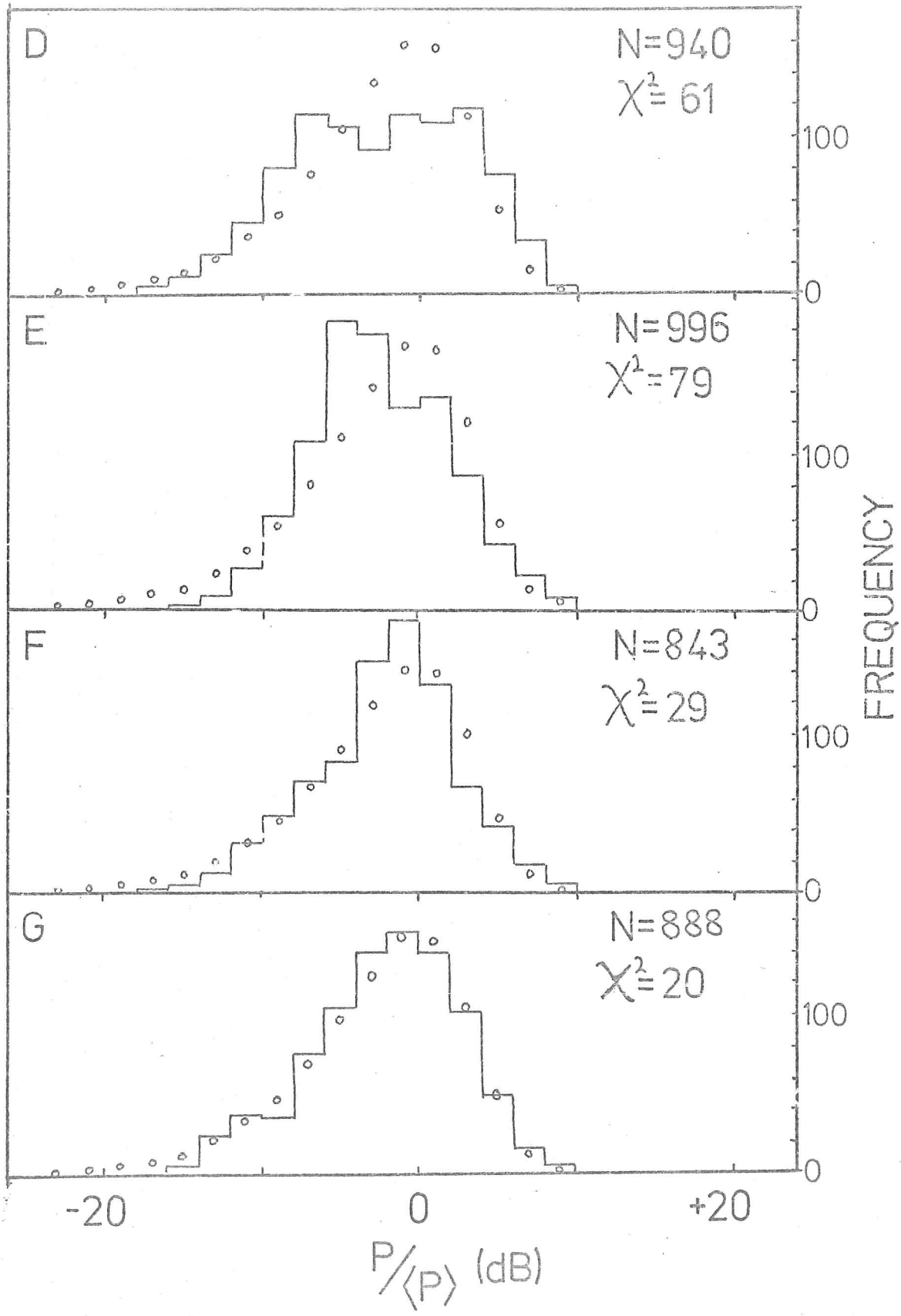

Fig.8.1b. Distributions of received power for sets D,E,F and G.

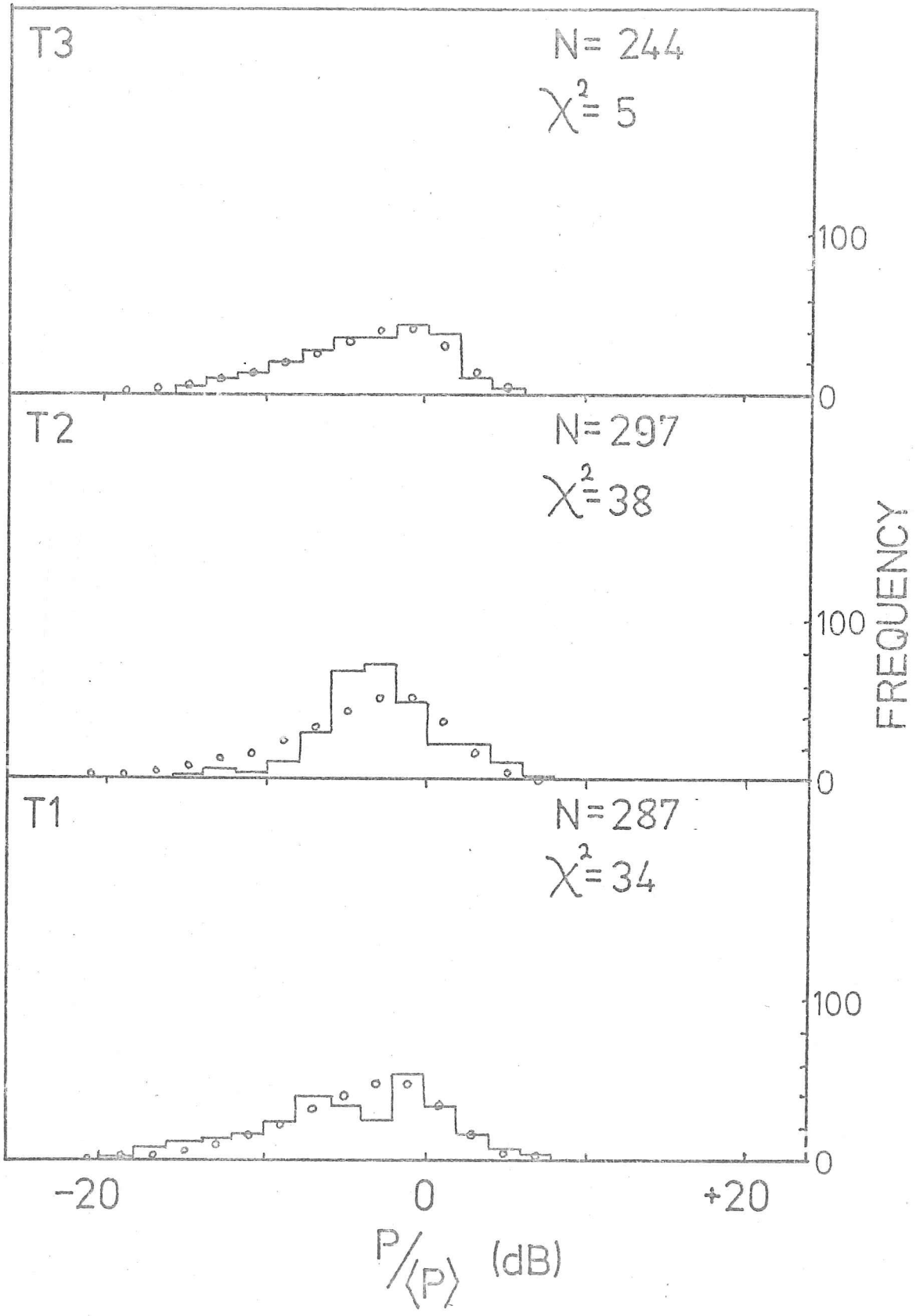

Fig.8.1c. Distributions of received power for sets T1,T2 and T3.

Sets A and D exhibit very similar distributions, which are fairly symmetrical, and are flattened in comparison with the predicted curve. In both cases the distribution is apparently double-peaked, and we suspect that this may be caused either by a separation into regions where different processes dominate the fading, or by the existence of bedrock with different reflection coefficients.

(8.2) Observed autocorrelation functions of received power.

The autocorrelation functions calculated for the sets of close spaced observations are shown in Figs.8.2a,b,c. It is not, of course, simple to fit these curves to the smooth shapes described in Chapter 7. Quantitatively, little can be said, other than to give the spacing at which the correlation coefficient falls below 1/e. This can be seen to lie between 4 metres (T2) and 22 metres (B). For those sets where the autocorrelation has a form indicating the dominance of inter ference in the fading (for a Gaussian surface, the autocorrelation would approach a Gaussian form), we may interpret the 'fading length' in terms of the r.m.s. slope. Where a focusing regime is indicated, the autocorrelation length of the surface roughness may be inferred directly.

We suggest tentatively that for sets F and G, the r.m.s. slope is given, according to equation (7.6), as 0.03 and 0.02 respectively. These values are lower than those suggested by measurements of the received pulse envelope. The discrepancy may lie either in our allowance for the shape of the transmitted pulse, or in our interpretation of the autocorrelation function.

The dilemma imposed by the ambiguity of the autocorrelation

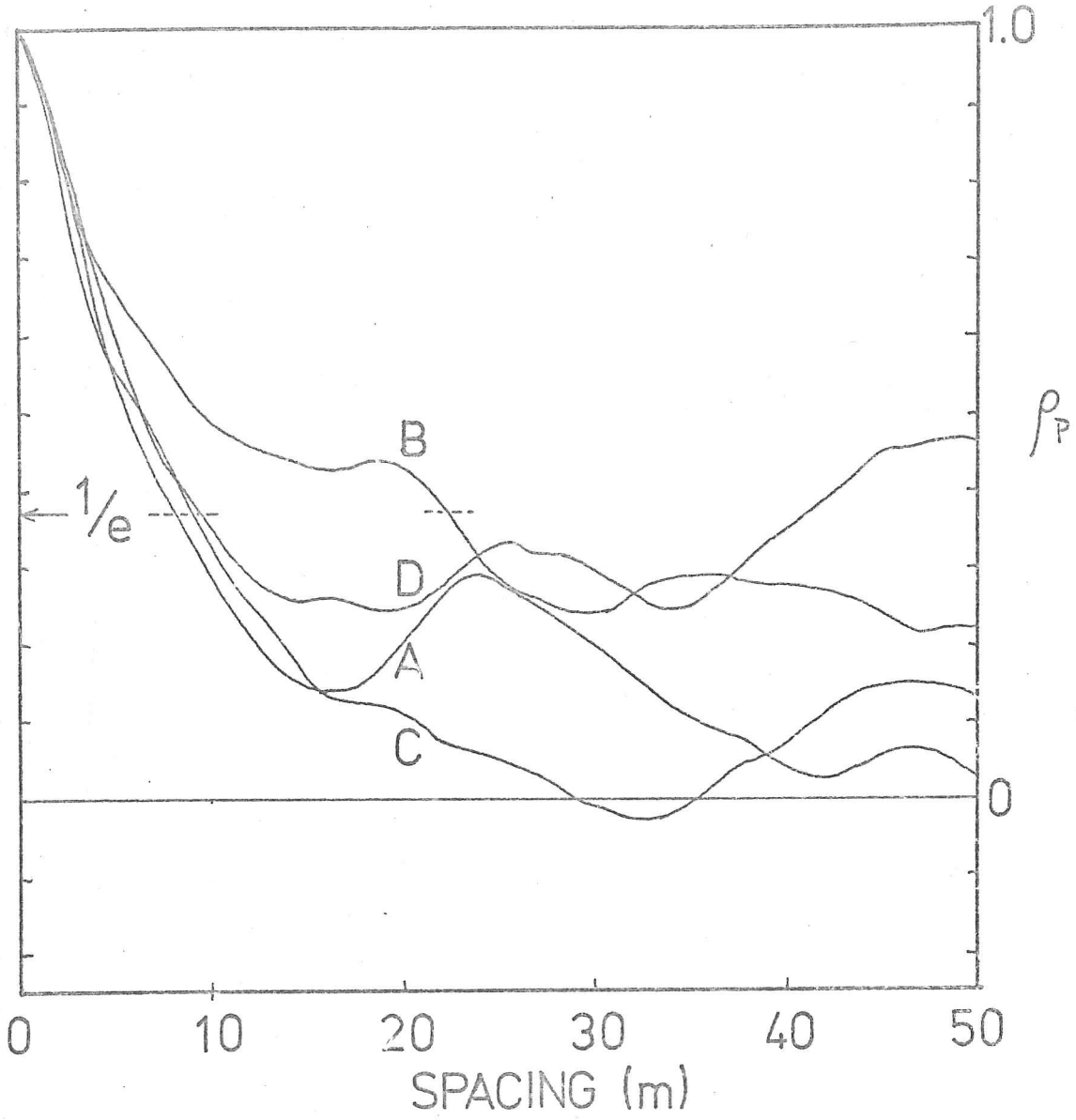

Fig.8.2a. Autocorrelation functions for the power received in sets A,B,C and D.

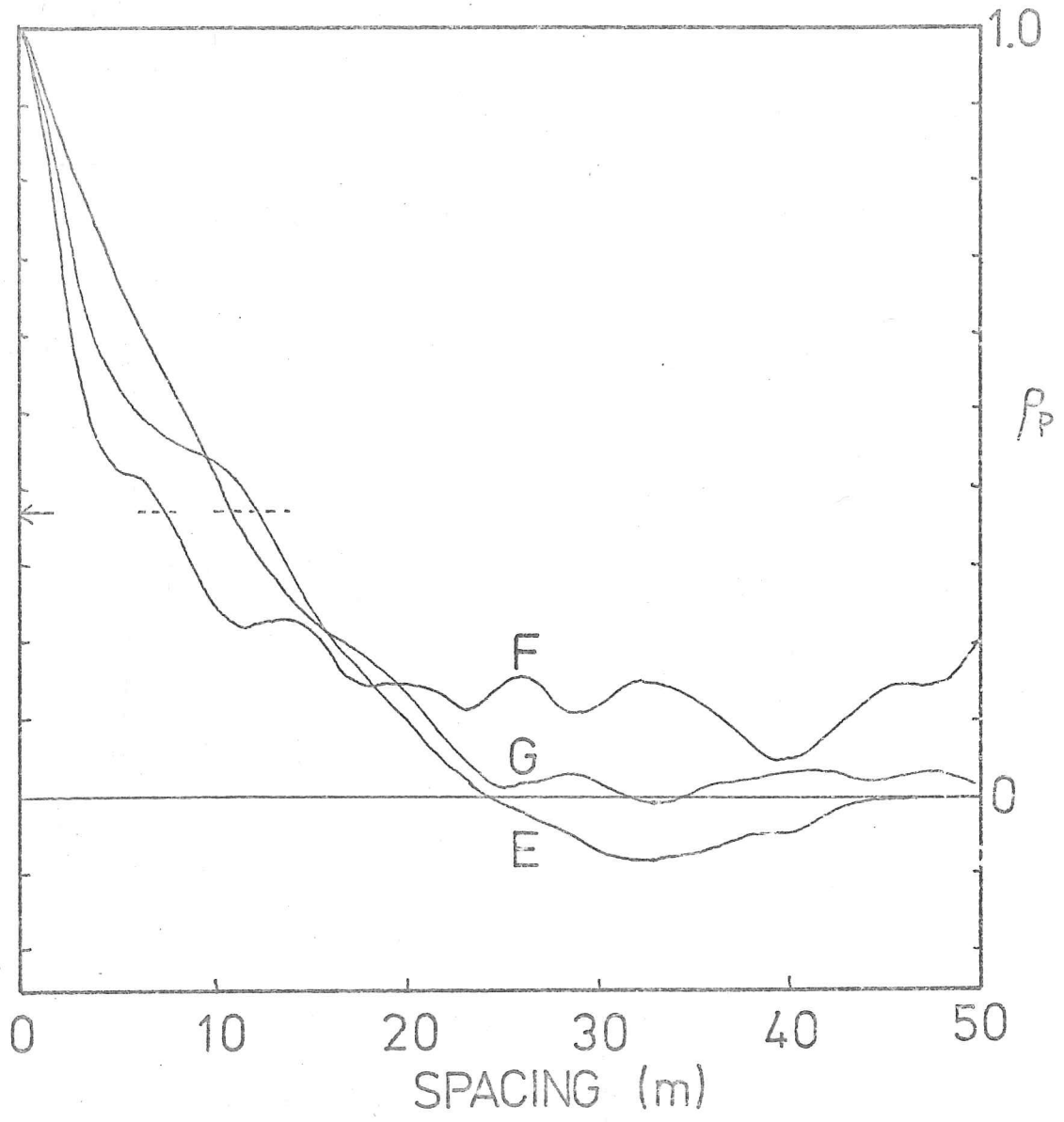

Fig.8.2b. Autocorrelation functions for the power received in sets E,F and G.

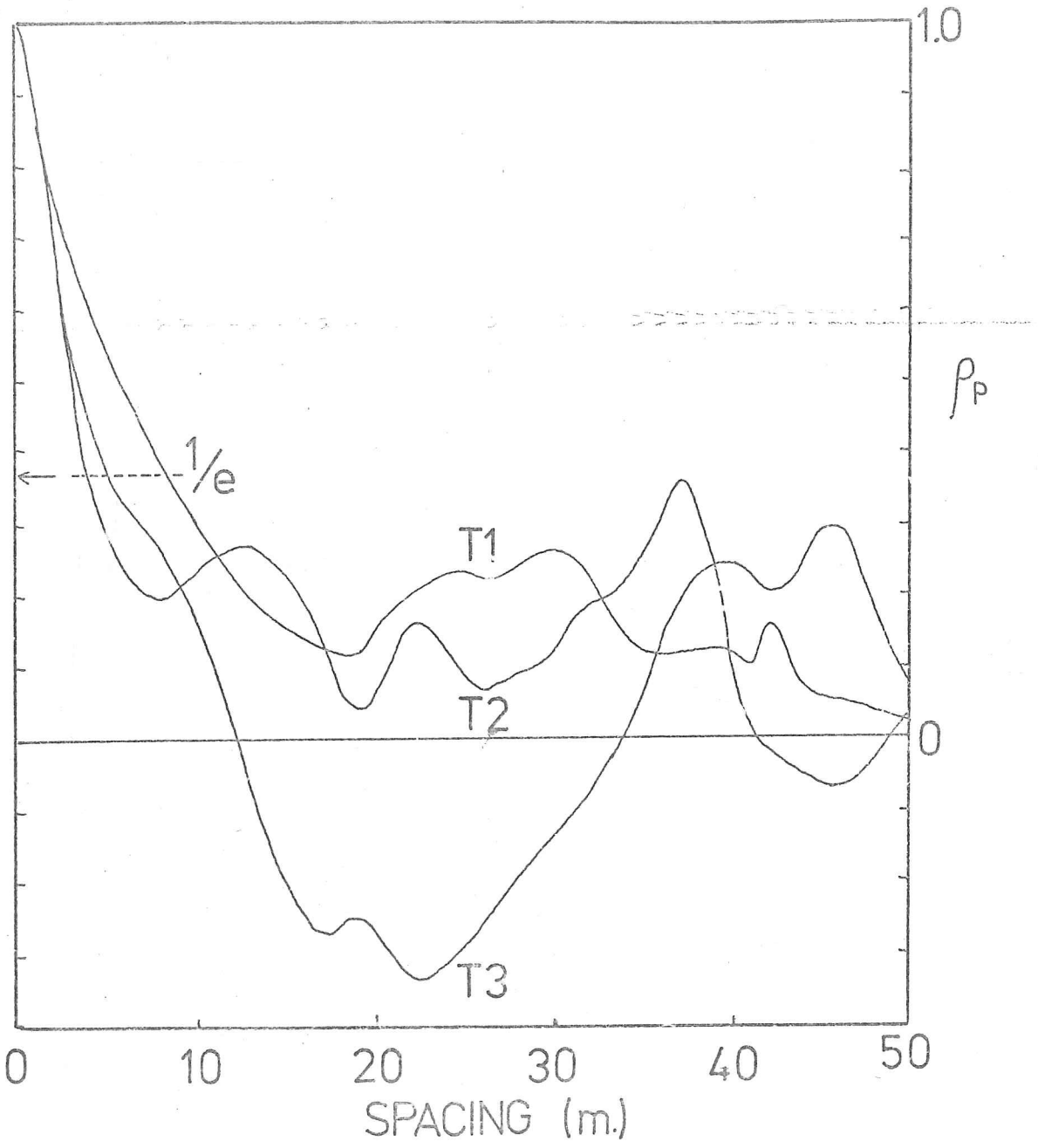

Fig.8.2c. Autocorrelation functions for the power received in sets T1, T2 and T3.

function is emphasised by the case of set T3. In the last section it appeared that this set gave the closest approach to fading due entirely to interference. However, for a surface with a Gaussian autocorrelation function, we should not expect the autocorrelation of the received power to fall below zero for any separation. Thus we are driven to question the form of the surface autocorrelation function, upon which most specific calculations of the echo behaviour have been based.

The form of the autocorrelation function exhibited by, in particular, set D, finds no parallel either in the limiting forms for focusing or interference regimes for a Gaussian surface.

These observations indicate that, the mechanisms of echo fading having been studied in some detail, experiments should be performed in order to determine the nature of subglacial surfaces beyond the convenient assumption of the Gaussian form.

(8.3) Suggested developments.

In connection with the comments of the last section, two techniques are suggested by means of which the form of the subglacial surface may be investigated.

The first makes simple use of the matter of Chapter 4, where it was shown that, with an exact knowledge of the shape of the transmitted pulse envelope, and with a sufficiently broad receiver bandwidth, the distribution of slopes in the reflecting surface might be determined from measurements of the trailing edge of the received pulse envelope. A surface whose vertical displacements from a mean horizontal plane are normally distributed, with a Gaussian autocorrelation function, should give rise to normal slopes with a 'Rayleigh' distribution.

Other distributions, representing, for instance, spiky surfaces, stepped surfaces, or dimpled surfaces, could be distinguished (Berry,(1973)). An important part of the technique would be to use a long, rectangular transmitted pulse, whose leading and trailing edges were as sharp as possible, so that reflections from facets of low slope would not be masked by the trailing edge of a reflection from vertically below the observer.

The second technique would involve ensuring that the observed fading was caused by interference, rather than focusing of the reflected waves. This is possible for any given surface by increasing the altitude of the observer until γ_0 is much greater than unity. It is thought that, since fading in Devon Island appears to have been caused by an inconvenient mixture of focusing and interference, this may not be a problem in airborne work over the very deep ice of the Antarctic ice cap. In this case the autocorrelation function of the received power will reflect that of the reflecting surface, its scale being determined by the slopes, rather than the horizontal or vertical scales of roughness of the surface. In deep ice, this method is perhaps to be preferred, from purely practical considerations, since it is necessary only to observe the maximum level of the echo.

Under these conditions, it would not be possible to deduce unique values for the vertical and horizontal scales of the roughness. In fact, without the assumption that the surface may reasonably be described as 'Gaussian', the validity of using single figures for these 'scales of roughness' is questionable. We believe that the distribution of slopes offers a more flexible way of describing the surface, without being tied to any particular model. It is experimentally more accessible than the 'scales of roughness' , and seems better

adapted for studies of the processes of strain, sliding and erosion at the bases of glaciers.

We return now to the subject of the mean intensity of the received echoes. The most important implication of this work concerns the length of the transmitted pulse. This should be sufficient for the received power to be equivalent to the level to be expected were the transmitter to radiate continuous waves. This involves an assumption (or a preliminary survey) to provide a value for the r.m.s. slope of the surface. On the basis of experience in Devon Island, we suggest that the transmitted pulse length should be not less than

$$p \simeq 0.1.h$$

where (neglecting the effect of refraction at the ice-air interface), h is the altitude of the observer above the reflecting plane, and p is the pulse length (both figures in metres).

We believe that the use of such a pulse has enabled us to locate a subglacial geological boundary in Devon Island, and that similar results should be obtainable elsewhere. The use of close-spaced observations is important for accurate determinations of the mean echo intensity. Profiling of the intensity at longer intervals has proved to be of value in locating accurately the boundaries between surfaces with different reflecting powers.

Appendix 1. Relation of the angular distribution of the received echo power to that of the facets of the rough surface.

We consider a rough surface such that the scattering of radio waves may be treated by the geometry of specular optical reflection. We assume that the surface is horizontally isotropic, and that the r.m.s. slope is sufficiently low that the effects of shadowing and multiple reflection are negligible.

Consider elements of the surface inclined at between θ and $\theta + \delta\theta$ to the vertical, and with random azimuthal orientation. Such facets reflect power, incident vertically, into a solid angle

$$2\pi . 2\delta\theta . \sin 2\theta$$

For power incident close to the vertical, the solid angle occupied by reflections will be close to this value.

These reflections can only be received at the point of transmission if they originate within an annulus on the rough surface defined by the vertical polar angles θ and $\theta + \delta\theta$. The power incident on this annulus is

$$\frac{P_T . g}{4\pi r^2} . r\delta\theta . 2\pi r \sin\theta = \frac{1}{2} P_T g . \sin\theta \delta\theta$$

of which a fraction $p(\theta)\delta\theta$ is distributed over an area

$$4\pi r^2 . 2\sin\theta \delta\theta$$

which includes the observer.

Thus the power received by the observer at the angle θ is

$$\delta\theta . P_r(\theta) = \frac{P_T . g . A}{16\pi r^2} . p(\theta) . \delta\theta$$

and for surfaces including only low slopes, we may approximate:

$$P_r(\theta)\delta\theta = \frac{P_T g^2 \lambda^2}{64\pi^2 h^2} . p(\theta)\delta\theta$$

Appendix 2. The average number of separate received reflections.

When radiation from a point source is reflected from a perfectly plane surface, a single reflection can be seen by an observer at the point of transmission. Each element of the surface, of area $\delta x\,\delta y$, reflectes power over an area $4\delta x\,\delta y$ at the height of the source/observer. For a rough surface, the area into which an element reflects power is given by:

$$\delta A = \langle 4\delta x\,\delta y \cdot |1-\gamma_x||1-\gamma_y| \rangle$$

where $\gamma_x = h.\frac{\partial^2 \zeta}{\partial x^2}$ and $\gamma_y = h.\frac{\partial^2 \zeta}{\partial y^2}$ where $\zeta(x,y)$ is the vertical displacement of the surface from its mean plane.

On replacing the smooth by the rough surface, many reflections may be received by the observer, from different facets of the rough surface, and the average number of such reflections is given by the ratio of the integral of the above reflection area over the surface, to the integral for the plane surface. This is equal to the mean area (at the height of the observer) over which an element of area 0.25 units reflects its incident power.

Thus if n is the average number of received reflections, we have :

$$n = \int\int_{-\infty}^{\infty} |1-\gamma_x|.|1-\gamma_y|\, p(\gamma_x)\, p(\gamma_y)\, d\gamma_x\, d\gamma_y$$

The second derivatives of the surface displacement are normally distributed, as are the first derivatives (we assume a 'Gaussian' surface), and we have

$$p(\gamma) = \frac{1}{\sqrt{2\pi}\,\gamma_0}\, e^{-\gamma^2/2\gamma_0^2}$$

where γ_0 is the r.m.s. value of the one-dimensional curvature.

We now split the above integral, so that

$$n = \int_{-\infty}^{1} d\gamma_x \int_{-\infty}^{1} d\gamma_y \, (1-\gamma_x)(1-\gamma_y)\, p(\gamma_x) p(\gamma_y)$$

$$+ \int_{1}^{\infty} d\gamma_x \int_{1}^{\infty} d\gamma_y \, (\gamma_x - 1)(\gamma_y - 1)\, p(\gamma_x) p(\gamma_y)$$

$$+ \int_{-\infty}^{1} d\gamma_x \int_{1}^{\infty} d\gamma_y \, (1-\gamma_x)(\gamma_y - 1)\, p(\gamma_x) p(\gamma_y)$$

$$+ \int_{1}^{\infty} d\gamma_x \int_{-\infty}^{1} d\gamma_y \, (\gamma_x - 1)(1-\gamma_y)\, p(\gamma_x) p(\gamma_y)$$

in which we have two basic integrals:

$$I_1 = \int_{-\infty}^{1} (1-\gamma)\, p(\gamma)\, d\gamma$$

and $$I_2 = \int_{1}^{\infty} (1-\gamma)\, p(\gamma)\, d\gamma$$

These may be solved simply to give

$$I_1 = \frac{1}{2}\left\{1 + \operatorname{erf}\left(\frac{1}{\sqrt{2}}\gamma_0\right) + \sqrt{\frac{2}{\pi}} \cdot \gamma_0 \cdot e^{-\frac{1}{2}\gamma_0^2}\right\}$$

and $$I_2 = \frac{1}{2}\left\{1 - \operatorname{erf}\left(\frac{1}{\sqrt{2}}\gamma_0\right) - \sqrt{\frac{2}{\pi}} \cdot \gamma_0 \cdot e^{-\frac{1}{2}\gamma_0^2}\right\}$$

Combining terms from these results we have, from

$$n = \left\{\operatorname{erf}\left(\tfrac{1}{\sqrt{2}}\gamma_0\right) + \sqrt{\frac{2}{\pi}}\, \gamma_0 \operatorname{exh}\left(-\frac{1}{2\gamma_0^2}\right)\right\}^2$$

This expression has the correct limiting forms such that

for $\gamma_0 \to 0$, $n \to 1$,

and for $\gamma_0 \to \infty$, $n \to \frac{2}{\pi}\gamma_0^2$

Appendix 3. Autocorrelation functions, and variances for derivatives of the rough surface.

Once again, we consider the Gaussian rough surface whose vertical displacements are normally distributed with r.m.s. value α_0, and whose horizontal autocorrelation function is given by:

$$\rho_\zeta(\sigma,\tau) = e^{-\frac{\sigma^2+\tau^2}{T^2}}$$

Beckmann and Spizzichino (1963) state the result that, for a one-dimensional normal process, the derivative is also normally distributed, with mean value zero and r.m.s. value given by

$$\beta_0^2 = \alpha_0^2 \left[\frac{d^2}{d\sigma^2}\rho_\zeta(\sigma)\right]_{\sigma=0} = \frac{2\alpha_0^2}{T^2}$$

A profile of our isotropic Gaussian surface in one direction yields such a normal process (as a function of distance), and we define gradients along the x- and y-axes:

$$\beta_x = \frac{\partial\zeta}{\partial x} \quad , \quad \beta_y = \frac{\partial\zeta}{\partial y}$$

The autocorrelation function of the gradients may be calculated as follows: we define

$$\rho_{\beta_x}(\sigma,\tau) = \frac{\langle \beta_x(x,y)\,\beta_x(x+\sigma,y+\tau)\rangle}{\langle \beta_x^2\rangle}$$

$$= \frac{T^2}{2\alpha_0^2}\langle \beta_x(x,y)\,\beta_x(x+\sigma,y+\tau)\rangle$$

Now,

$$\beta_x(x,y) = \lim_{\delta x\to 0}\frac{(\zeta(x+\delta x,y)-\zeta(x,y))}{\delta x}$$

and

$$\beta_x(x+\sigma,y+\tau) = \lim_{\delta x\to 0}\frac{(\zeta(x+\sigma+\delta x,y+\tau)-\zeta(x+\sigma,y+\tau))}{\delta x}$$

and we have, in the limit $\delta x \to 0$

$$\rho_{\beta_x}(\sigma,\tau) = \frac{T^2}{2\alpha_0^2 \delta x^2} \Big\langle \zeta(x+\delta x, y)\zeta(x+\sigma+\delta x, y+\tau) + \zeta(x,y)\zeta(x+\sigma, y+\tau) - \zeta(x+\delta x, y)\zeta(x+\sigma, y+\tau) - \zeta(x+\sigma+\delta x, y+\tau)\zeta(x,y) \Big\rangle$$

$$= \frac{T^2}{2\delta x^2}\left\{2\rho_\zeta(\sigma,\tau) - \rho_\zeta(\sigma-\delta x,\tau) - \rho_\zeta(\sigma+\delta x,\tau)\right\}$$

$$= \frac{T^2 e^{-\frac{\sigma^2+\tau^2}{T^2}}}{2\delta x^2}\left\{2 - \left(\exp\left[\frac{-2\sigma\delta x + \delta x^2}{T^2}\right] + \exp\left[\frac{2\sigma\delta x + \delta x^2}{T^2}\right]\right)\right\}$$

As $\delta x \to 0$,

$$\exp\left\{-\frac{2\sigma\delta x + \delta x^2}{T^2}\right\} \to 1 - \frac{2\sigma\delta x}{T^2} + \frac{\delta x^2}{T^2} + \frac{2\sigma^2\delta x^2}{T^4}$$

and reduces to

$$\rho_{\beta_x}(\sigma,\tau) = e^{-\frac{\sigma^2+\tau^2}{T^2}}\left(1 - 2\sigma^2/T^2\right)$$

We have, therefore, the result that the autocorrelation function of gradients along a given axis is azimuthally anisotropic.

By an identical method we may calculate the autocorrelation function of the one-dimensional curvature, deriving the result

$$\rho_{\gamma_x}(\sigma,\tau) = e^{-\frac{\sigma^2+\tau^2}{T^2}}\left(1 - \frac{4\sigma^2}{T^2} + \frac{4\sigma^4}{3T^4}\right)$$

The r.m.s. value of the one-dimensional curvature, γ_0, is given, by analogy with , by

$$\gamma_0^2 = \beta_0^2\left[\frac{\partial^2}{\partial\sigma^2}\rho_{\beta_x}(\sigma)\right]_0$$

and has the value

$$\gamma_0 = \frac{\sqrt{6}\,\beta_0}{T}$$

As a result of the anisotropy of the autocorrelation function of the gradients, the parameter γ_0 cannot be used as a true r.m.s. value over the surface. In order to determine the mean square curvature, we use an autocorrelation function in terms of μ, where

$$\mu^2 = \sigma^2 + \tau^2$$

and we average the value of σ for constant μ over all directions of μ, obtaining $\langle \sigma^2 \rangle = \mu^2/2$. From this autocorrelation function we obtain the value of $\frac{4\beta_0^2}{T^2}$ for the mean square curvature in one dimension, giving for the mean square two-dimensional curvature:

$$\langle \gamma^2 \rangle = \frac{4}{3} \gamma_0^2$$

In the same way as for the gradients and curvatures, we deduce that the third derivative of the roughness function is described by

$$\left\langle \left(\frac{\partial^3 \zeta}{\partial x^3} \right)^2 \right\rangle \propto \frac{\alpha_0^2}{T^6}$$

REFERENCES

ADAMS,R.D.,1970. Dispersion-wave studies in Antarctica. (Review) In: Adie,R.J.(Ed.) Antarctic Geology and Geophysics. Symposium on Antarctic Geology and Solid Earth Geophysics, Oslo,1970.

BARRY,R.G. and CHORLEY,R.J. Atmosphere, Weather and Climate. Methuen, 1968.

BECKMANN,P. and SPIZZICHINO,A.,1963. The Scattering of Electromagnetic Waves from Rough Surfaces. Pergamon Press, London.

BENTLEY,C.R.,1964. The Structure of Antarctica and its Ice Cover. In: Odishaw,H. (Ed.) Research in Geophysics, MIT Press.

BENTLEY,C.R.,1971. Seismic Evidence for Moraine within the Basal Antarctic Ice Sheet. Antarctic Research Series, Vol.16.

BERRY,M.V.,1973. The Statistical Properties of Echoes Diffracted from Rough Surfaces. Philosophical Transactions of the Royal Society of London. Ser.A, Vol.273, No.1237.

BOOKER,H.G., RATCLIFFE,J.A. and SHINN,D.H.,1950. Diffraction from an Irregular Screen with Applications to Ionospheric Problems. Phil. Trans. Roy. Soc. A.,Vol. 242, p.599-607.

BRAMLEY,E.N. and YOUNG,M.,1967. Diffraction by a Deeply-Modulated, Random-Phase Screen. Proceedings of the Institution of Electrical Engineers. Vol.114, No.5.

BUDD,W.F., JENSSEN,D., and RADOK,U., 1971. Derived Physical Characteristics of the Antarctic Ice Sheet. Mark 1. University of Melbourne, Department of Meteorology, Publication No.18.

CAMPBELL,J.A.,1973. Unpublished communication to G.deQ.Robin, Scott Polar Research Institute, Cambridge University.

CAMPBELL,M.J. and ULRICHS,J.,1969. Electrical Properties of Rocks and their Significance for Lunar Radar Observations. Journal of Geophysical Research. Vol.74, No.25.

DEWART,G. and TOKSÖZ,M.N.,1965. Crustal Structure in East Antarctica from Surface Wave Dispersion. Geophysical Journal of the Royal Astronomical Society. Vol.10,No.2.

DREWRY,D.J.,1973. Sub-Ice Relief and Geology of East Antarctica. Ph.D.Thesis, University of Cambridge.

EVANS,S.,1966. Radio Glaciology. Cambridge Research.

EVANS,S., and SMITH,B.M.E., 1969. A Radio Equipment for Depth-Sounding in Polar Ice Sheets. Journal of Scientific Instruments, Journal of Physics E. Series 2, Vol.2.

EVANS,S.,GUDMANSEN,P.,SWITHINBANK,C.W.M.,HATTERSLEY-SMITH,G., and ROBIN,G.deQ., 1969. Glacier Sounding in the Polar Regions: a Symposium. Geographical Journal. Vol.135,Part 4.

EVANS,S.,and SMITH,B.M.E., 1970. Radio Echo Exploration of the Antarctic Ice Sheet, 1969-70. Polar Record. Vol.15, No.96.

EVANS,S., DREWRY,D,J. and ROBIN,G.deQ., 1972. Radio Echo Sounding in Antarctica, 1971-72. Polar Record. Vol.16, No.101.

EVANS,S. and ROBIN,G.deQ.,1972. Ice Thickness Measurements by Radio Echo Sounding. Antarctic Journal of the United States. Vol.7, No.4.

EVISON,F.F., INGHAM,C.E., ORR,R.H., and LeFORT,J.H., 1960. Thickness of the Earth's Crust in Antarctica and the Surrounding Oceans. Geophysical Journal of the Royal Astronomical Society. Vol.3. No.3.

GOW,A.J., UEDA,H.T., and GARFIELD,D.E.,1968. Preliminary Results of First Core Hole to Bedrock. Science. Vol.161. No.3845.

GRUSHINSKY,N.P.,1970. Gravity Determinations in Antarctica. In: Adie,R.J. (Ed.) Antarctic Geology and Geophysics. Symposium on Antarctic Geology and Solid Earth Geophysics, Oslo.

GRUSHINSKY,N.P. and LAZAREV,G.E., 1970. Project of a Gravimetric Network and Gravity Survey in Antarctica. In: Adie,R.J. (Ed.) Antarctic Geology an Geophysics. Symposium on Antarctic Geology and Solid Earth Geophysics, Oslo.

HARRISON,C.H., 1971. Radio Echo Records cannot be used as Evidence for Convection in the Antarctic Ice Sheet. Science Vol.173. No.3994.

HARRISON,C.H., 1971. Radio Echo Sounding: Focusing effects in Wavy Strata. Geophysical Journal of the Royal Astronomical Society. Vol.24, No.4.

HARRISON,C.H.,1972. Radio Propagation Effects in Glaciers. Ph.D.Thesis, University of Cambridge.

HUGHES,T.,1973. Is the West Antarctic Ice Sheet Disintegrating ? ISCAP Bulletin No.2, Institute of Polar Studies, The Ohio State University.

KELLER,G.V.,1966. Electrical Properties of Rocks and Minerals. In: Clark,S.P. (Ed.) Handbook of Physical Constants. Geological Society of America.

KOERNER,R.M.,1970. The Mass Balance of th Devon Island Ice Cap, Northwest Territories, Canada. 1961-66. Journal of Glaciology. Vol.9. No.57.

KOGAN,A.L., and MOROZOV,Ye.Ye.,1969. Geological Interpretation of Ground Magnetic Measurements along an Inland Traverse. Informatsionyy Byulleten Sovetskoy Antarkticheskoy Ekspeditsii. (IBSAE). No.75.

KOZMINSKAYA,I.P. and RIZNICHENKO,Y.V.,1964. Seismic Studies of the Earth's crust in Eurasia. In: Odishaw,H.,(Ed.), Research in Geophysics, MIT Press.

LOEWE,F.,1970. Screen Temperatures and 10 metre Temperatures. Journal of Glaciology. Vol.9. No.56.

NYE,J.F.,1969. Water at the Bed of a Glacier. In:International Association of Scientific Hydrology. Commision of Snow and Ice. Symposium on the Hydrology of Glaciers.

OSWALD,G.K.A., and ROBIN,G.deQ., 1973. Lakes Beneath the Antarctic Ice Sheet. Nature. Vol.245. No.5423.

OSWALD,G.K.A., 1975. Investigation of Sub-Ice Bedrock Characteristics by Radio Echo Sounding. Journal of Glaciology. (In press)

PAKISER,L.C., and STEINHART,J.S., 1964. Explosion Seismology in the Western Hemisphere. In: Odishaw,H. (Ed.), Research in Geophysics. MIT Press.

ROBIN,G.deQ.,1955. Ice Movement and Temperature Distribution in Glaciers and Ice Sheets. Journal of Glaciology. Vol.2. No.18.

ROBIN,G.deQ.,EVANS,S., and BAILEY,J.T.,1969. Interpretation of Radio Echo Sounding in Polar Ice Sheets. Phil. Trans. Roy. Soc. A. Vol.265. No.1166.

ROBIN,G.deQ., SWITHINBANK,C.W.M., and SMITH,B.M.E.,1970. Radio Exploration of the Antarctic Ice Sheet. In: Gow,A.J. (Ed.) International Symposium on Antarctic Glaciological Exploration (ISAGE) 1968. Gentbrugge, International Association of Scientific Hydrology, Publ. No.86.

ROBIN,G.deQ.,1975. Velocity of Radio Waves in Ice by Means of a Bore-Hole Interferometric Technique. Journal of Glaciology. (In press)

SCHLOSS,M.,1966 Quantifying Terrain Roughness on Lunar and Planetary Terrain. Journal of Spacecraft, Engineering Notes. Vol.3. No.2.

SMITH,B.M.E., 1971. Radio Echo Studies of Glaciers. Ph.D. Thesis, University of Cambridge.

SOLOV'YEV,D.S., and KOGAN,A.L., 1970. Deep Seismic Sounding in Dronning Maud Land. IBSAE No.77.

WEERTMAN,J.,1966. Effect of a Basal Water Layer on the Dimensions of Ice Sheets. Journal of Glaciology. Vol.66. No.44.

WEERTMAN,J.,1972. General Theory of Water Flow at the Base of a Glacier or Ice Sheet. Reviews of Geophysics and Space Physics. Vol.10 No.1.

WEERTMAN,J., SIBERT,J., WEEKS,W,F., and STERNIG,J., 1973. Radioactive Wastes on Ice. Further Discussion. Bulletin of the Atomic Scientists. Vol.29, No.4.

WESTPHAL,W.,1963. Private communication to S.Evans. In: Robin,G.deQ., Evans,S. and Bailey,J.T., 1969 (see above).

ZELLER,E.J., SAUNDERS,D.F., and ANGINO,E.E., 1973. Putting Radioactive Wastes on Ice. Bulletin of the Atomic Scientists. Vol.29. No.1.